Final Report

Grant NAGW-1392
"Research into the Influence of Spatial Variability and Scale on the Parameterization of Hydrological Processes"

Principal Investigator
Eric F. Wood

Water Resources Program
Department of Civil Engineering
Princeton University
Princeton, NJ
08544

Objectives

The understanding of hydrologic responses over a range of scales from less than 0.1 km^2 to 1000 km^2 is one of the most important current problem in hydrology. The stochastic variability in soil parameters, rainfall inputs, vegetation and topography complicates the analysis. The objective of the research was to investigate hydrologic processes over a range of catchment scales. The proposed research improved our understanding of how hydrologic models at various scales are related, which is important in hydrologic model building and is necessary to improve the land surface boundary conditions for meteorology and climatology models. During the last three years, the principal investigator has been studying the influence of spatial variability on land surface water and energy balances, as predicted through coupled hydrologic models. The fundamental research issue addressed during this research was understanding the relationships between hydrologic response and spatial scale. Essentially what role does variability in soil, topography and rainfall play in the transition (or averaging) of micro-scale (point) response to macroscale or regional response? How do we parameterize the effect of spatial variability on the hydrologic response at different scales?

The objectives of the research were as follows:

1. Extend the Representative Elementary Area (REA) concept, first proposed and developed in Wood et al, (1988), to the water balance fluxes of the interstorm period (redistribution, evapotranspiration and baseflow) necessary for the analysis of long-term water balance processes.
2. Derive spatially averaged water balance model equations for spatially variable soil, topography and vegetation, over a range of climates. This is a necessary step in our goal to derive consistent hydrologic results up to GCM grid scales necessary for global climate modeling.
3. Apply the above macroscale water balance equations with remotely sensed data and begin to explore the feasibility of parameterizing the water balance constitutive equations at GCM grid scale.

Background

As stated earlier, the primary objective of the research is to further investigate the effect of spatial variability and scale on the parameterization of hydrologic processes. Specifically the goal is to understand the relationship among parameterizations of the hydrologic response at different scales.

To better understand the current research, let us pose the problem in terms of the following variables: Let $g\{\theta(x), \quad i(x,t)\}$ be a point representation of hydrologic processes dependent upon a spatially varying parameter set $\theta(x)$ and subject to spatially and temporally varying inputs, $i(x,t)$.. The output of $g\{\theta(x), \quad i(x,t)\}$ will be water balance fluxes (runoff, infiltration evaporation and soil moisture redistribution) and can be represented by $o(x,t)$..

The question posed herein is: How does the mathematical structure of the integrated function of $g\{\theta(x), \quad i(x,t)\}$ represented by $G(\theta,I)$, change as we consider the integrated function of $o(x,t)$ defined by

$$O = \int_{t\varepsilon T} \int_{x\varepsilon A} o(x,t)dx\, dt \tag{1}$$

where θ represents the lumped or averaged process parameter and I the averaged inputs. Equation (1) embeds the three issues described in the research tasks given earlier. When the averaging area, A, is less than the REA for the parameterization $g(\bullet)$, then equation (1) investigates how the statistics of $o(x,t)$ change with averaging.

It has been shown by in earlier research by the PI (see Wood, et al.,1986; Wood, et al.,1988; and Beven et al., 1988) that at an area A equal to the REA, the behavior of the statistics of O will qualitatively change; for example the highly variable flux behavior (like mean infiltration) among small catchment areas stabilizes as is shown later.

It is hypothesized that a finite hierarchy of scales exists due to large scale non-stationarities and therefore a set of REA's exists, each governed by a different set of controls. This is the central focus of Objective 1 of this proposal. For A > REA, the relationship between $G(\theta,I)$ and $g\{\theta(x), \quad i(x,t)\}$, and the relationships among the hydrologic responses at higher scales (*i.e.*, $G(\theta,I)$) is the focus of the current research for storm response, and the proposed research for

water balances. Here $o(x,t)$ can be viewed as the point scale fluxes and O as the fluxes at the hillslope, catchment or regional scale depending on the size of A in equation (1). The diagram below conceptualizes the relationships between scales and outputs.

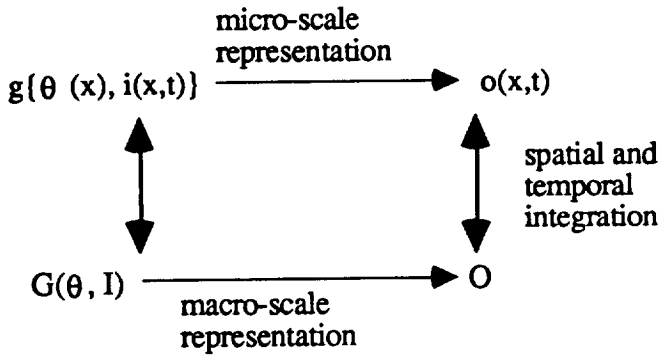

Figure 1: Schematic of the scaling problem.

Current Research Results

Results on comparing $g\{\theta(x),\ i(x,t)\}$ *with* $G(\theta,I)$.

A point water balance equation that relates precipitation, evaporation, runoff and changes in local unsaturated and saturated soil water storage still requires parameterization; i.e. the algebraic form of the water balance equation needs to be specified. At a point, the fully 3-dimensional transient Richards is often used to describe water fluxes and this algebraic form can be described with $g\{\theta(x),\ i(x,t)\}$. As the spatial scale increases, from a point to a catchment, over heterogeneous land surfaces, it is unclear what is the most appropriate model parameterization, conceptually this large scale parameterization can be written as $G(\theta,I)$.

To fully explore how these two fundamentally different parameterizations compare, two different parameterizations were developed and compared: (i) In Paniconi and Wood (1993), a 3-D Richards equation based model was developed and solved using a finite element Gelerkin discretization in space, finite differences in time and linearized using either a Newton or Picard iteraction scheme; (ii) a distributed conceptual water and energy balance model was developed as described in Famiglietti and Wood (1991). Spatial variability in the water balance controls is dominated through variability in topography, soils and vegetation, and represented through a topographic-soil index. Thus the model is an extension of Beven and

Kirkby's TOPMODEL in which local depths to the water table (and therefore surface soil moisture) are related to the local value of a soil-topographic index. The surface soil moisture controls infiltration, runoff and evaporation.

In Troch et al (1993), comparisons were made to evaluate the steady-state assumptions within the TOPMODEL parameterization and to compare the two appraoches with field data collected during a remote sensing field experiment (MAC-HYDRO'90) carried out in the US Agricultural Research Service Mahantango Creek, PA experimental watershed. The 12 day experiment started out dry, had two days of rain followed by a strong drydown. Results show that both the numerical and conceptual model provided reasonable, consistent results. The conceptual model seemed to simulate the behaviour of the shallow water table, which better reflects the underlying steady state assumptions while the numerical model simulated the deeper wells better.

The importance of these results is that the distributed TOPMODEL-based water and energy balance model can provide a parameterization for $g\{\theta(x), \ i(x,t)\}$, i.e. a distributed model that accounts for small scale variability; and through aggregation of the spatial characteristics provide a consistent parameterization for a macro-scale model, i.e. a parameterization $G(\theta,I)$. This forms a framework in which scaling questions concerning the comparisons between the outputs of the two parameterizations (the right hand side of Figure 1) can be explored: $o(x,t) \rightarrow O$.

As an aside, it should be noted that under separate funding for the First ISLSCP Field Experiment (FIFE), the distributed water and energy balance model, refered to above, has been validated using measured surface energy fluxes. This is the first time that a fully coupled, distributed water and energy balance model has been developed and validated in this manner. Such validation is important in the scaling research described here since the basis of the To understand the relationship between a fully distributed (microscale) representation of land surface hydrology and a macroscale representation where the spatial variability is accounted for with a statistical representation, it was necessary to develop a fully 3-D dimensional numerical Richards equation based land surface hydrological model

Results on output averaging: $o(x,t) \rightarrow O$

An early result on the REA concept, Wood, et al. (1988), reported that for storm response fluxes (runoff, infiltration) from areas less than $\cong$ 1000 (30m x 30m) pixels ($\cong$ 1 km^2) the storm runoff volume is highly variable among the

subcatchments. For areas greater than ≡ 1000 pixels, the variability stabilizes; implying an REA of ≡ 1 km^2. This early work was based on topography from the Coweeta catchment in North Carolina and hypothetical storm forcings.

Under the current research, three efforts were pursued in exploring the issues of averaging. The first effort built upon earlier scaling research by the PI and led to the development of a similarity concept for looking at the storm response from catchment areas. These results are developed and reported in Sivalpalan et al (1990) and Wood et al (1990). These papers provide the first attempt at a systematic theoretical framework for understanding the connections between small scale spatial variability and catchment scale water balance fluxes. The early work focused on storm responses.

The second major effort in the current research was to extend our results on scaling of storm responses to analyzing the scale issues for both water and energy fluxes during both storm and inter-storm periods. These analyses were carried out using the high resolution data from the First ISLSCP Field Experiment (FIFE) collected during 1987. For storm response fluxes during summer rain events, we found a similar size REA (1 sq km) as was reported in Wood et al., (1988). This work is reported in Wood et al., (1990). The extension to interstorm period evaporation fluxes required the extension of distributed and lumped models that allowed for the scaling analyses carried out earlier. This model extension is described in Famiglietti and Wood (1991).

The results from the scaling analysis with the land surface energy and water balance model are described in Wood (1992), Famiglietti and Wood (1993) and Wood (1993). In Famiglietti and Wood (1993), it is shown that for the wet 1987 FIFE Intensive Field Campaign (IFC) periods (IFC-1, IFC-2 and IFC-3) the spatially lumped and spatially distributed models give essentially similar catchment scale water and energy fluxes. For the dry October IFC (IFC-4), the lumped model is unable to reproduce the correct mid-day fluxes. During a typical IFC-4 day, the lumped and distributed models predict similar fluxes during the morning, with the lumped model reaching a maximum rate which is held constant until the late afternoon when it then falls (along with the distributed model's prediction of latent heating. The distributed model has a diurnal cycle in its latent heating, with a near noon peak, which compares very well to that latent heating measured by the flux stations.

The difference in behaviour between the lumped and distributed models during IFC-4 is attributed to the non-linearities induced by the dry soils. Since the

distributed model accounts for spatial variabilty in the land surface, there remains aras that have significantly higher values and when aggregated across the site match the observed behaviour. The important implication of these results, is that reported results from other investigators who have analyzed the wetter IFC-1, IFC-2 and IFC-3 conditions and claim that scaling can be done (i.e. spatially constant parameters) are only correct for wet, atmospherically controlled conditions. To understand exactly how soil moisture plays a role in this bias between the lumped and distributed models, Wood (1993) developed some derived distributions for the topographic-soil control for wet and dry conditions. These results explain very clearly when the equivalent parameter, spatially lumped model will fail.

The third area of effort was to try and understand the concept of scaling and the REA scale from remote sensing data. These results are reported on in Wood and Lakshmi (1993) and Wood (1992). These results support the that scaling is effective during wet conditions; more work needs to be carried out for a wider range of climatic conditions.

Papers published under the Grant:

The following papers have either been published or are under the review. Presentations at conferences anmd workshops ar enot included. In addition, the grant supported three PhD students (J.S. Famiglietti, V. Lakshmi, and Claudio Paniconi), partially supported two research visitors (Peter A. Troch and Marco Mancini). The published papers are given below, and are attached.

[1] (with M. Sivapalan and K. Beven), "On Hydrologic Similarity 3. A Dimensionless Flood Frequency Model Using a Generalized Geomorphologic Unit Hydrograph and Partial Area Runoff Generation", in *Water Resources Research*, Vol. 26, No. 1, pages 43-58, January 1990.

[2] (with M. Sivapalan and K. Beven), "Similarity and Scale in Catchment Storm Response", in *Reviews of Geophysics*, Vol. 28, No. 1, February 1990.

[3] (with J.S. Famiglietti), "Evapotranspiration and Runoff from Large Land Areas: Land Surface Hydrology for Atmospheric General Circulation Models", in *Surveys in Geophysics*, Vol. 12, pages 179-204, 1991.

[4] "Heterogeneity and Scaling Land-Atmospheric Water and Energy Fluxes in Climate Systems", presented at the IHP/IAHS George Kovacs Colloquium on Space and Time Variability and Interdependencies in Various Hydrological Processes, July, 1992, UNESCO, Paris. To be published by Cambridge University Press.

[5] (with V. Lakshmi), "Scaling Water and Energy Fluxes in Climate Systems: Three Land-Atmospheric Modeling Experiments", in *Journal of Climate*, Vol. 6, No. 5, May 1993.

[6] (with Troch, Peter A., Marco Mancini, and Claudio Paniconi) "Evaluation of a Distributed Catchment Scale Model Water Balance Model", Water Resources Research, 29(6):1805-1817, June 1993.

[7] (with C. Paniconi), "A Detailed Model for Simulation of Catchment Scale Subsurface Hydrologic Processes", in *Water Resources Research,* Vol. 29, No. 6, pages 1601-1620, June 1993.

[8] (with J.S. Famiglietti), "Effects of Spatial Variability and Scale on Areal-Average Evapotranspiration", submitted to *Water Resources Research*, February, 1993.

[9] "Scaling, Soil Moisture and Evapotranspiration in Runoff Models", *Special Issue on Hydroclimatology, Advances in Water Resources*, accepted, October 1993.

References.

Beven, K, E F Wood and M. Sivapalan, "On Hydrological Heterogeneity: Catchment Morphology and Catchment Response", *J. Hydrology*, 100, pp. 353-375, 1988.

Famiglietti, J. S. and Eric F. Wood, "Evapotranspiration and Runoff from Large Land Areas: Land Surface Hydrology for Atmospheric General Circulation Models", in *Surveys in Geophysics*, Vol. 12, pages 179-204, 1991.

Famiglietti, J. S. and Eric F. Wood, "Effects of Spatial Variability and Scale on Areal-Average Evapotranspiration", submitted to *Water Resources Research*, February, 1993.

Paniconi, Claudio and Eric F. Wood, "A Detailed Model for Simulation of Catchment Scale Subsurface Hydrologic Processes", in *Water Resources Research,* Vol. 29, No. 6, pages 1601-1620, June 1993.

Sivapalan, M., E. F. Wood and K. Beven, "On Hydrologic Similarity 3. A Dimensionless Flood Frequency Model Using a Generalized Geomorphologic Unit Hydrograph and Partial Area Runoff Generation", in *Water Resources Research*, Vol. 26, No. 1, pages 43-58, January 1990.

Troch, Peter A., Marco Mancini, and Claudio Paniconi, Eric F. Wood "Evaluation of a Distributed Catchment Scale Model Water Balance Model", Water Resources Research, 29(6):1805-1817, June 1993.

Wood, Eric F., "Heterogeneity and Scaling Land-Atmospheric Water and Energy Fluxes in Climate Systems", presented at the IHP/IAHS George Kovacs Colloquium on Space and Time Variability and Interdependencies in Various Hydrological Processes, July, 1992, UNESCO, Paris. To be published by Cambridge University Press.

Wood, Eric F., "Scaling, Soil Moisture and Evapotranspiration in Runoff Models", *Special Issue on Hydroclimatology, Advances in Water Resources*, accepted, October 1993.

Wood, E. F., K. Beven, M. Sivapalan and L. Band "Effects of Spatial Variability and Scale with Implication to Hydrologic Modeling", *J. Hydrology*, 102, pp. 29-47, 1988.

Wood, Eric F. and V. Lakshmi, "Scaling Water and Energy Fluxes in Climate Systems: Three Land-Atmospheric Modeling Experiments", in *Journal of Climate*, Vol. 6, No. 5, May 1993.

Wood, E. F., M. Sivapalan and K. Beven "Scale Effects on Infiltration and Runoff Production", in *Conjunctive Water Use*, S.M. Gorelick(ed.), IAHS Publ. 156, pp. 375-390, 1986.

Wood, Eric F., M. Sivapalan and K. Beven, "Similarity and Scale in Catchment Storm Response", in *Reviews of Geophysics*, Vol. 28, No. 1, February 1990.

WATER RESOURCES RESEARCH, VOL. 26, NO. 1, PAGES 43–58, JANUARY 1990

On Hydrologic Similarity
3. A Dimensionless Flood Frequency Model Using a Generalized Geomorphologic Unit Hydrograph and Partial Area Runoff Generation

MURUGESU SIVAPALAN[1] AND ERIC F. WOOD

Water Resources Program, Department of Civil Engineering and Operations Research Princeton University, Princeton, New Jersey

KEITH J. BEVEN

Institute of Environmental and Biological Sciences, University of Lancaster, Lancaster, England

One of the shortcomings of the original theory of the geomorphologic unit hydrograph (GUH) is that it assumes that runoff is generated uniformly from the entire catchment area. It is now recognized that in many catchments much of the runoff during storm events is produced on partial areas which usually form on narrow bands along the stream network. A storm response model that includes runoff generation on partial areas by both Hortonian and Dunne mechanisms was recently developed by the authors. In this paper a methodology for integrating this partial area runoff generation model with the GUH-based runoff routing model is presented; this leads to a generalized GUH. The generalized GUH and the storm response model are then used to estimate physically based flood frequency distributions. In most previous work the initial moisture state of the catchment had been assumed to be constant for all the storms. In this paper we relax this assumption and allow the initial moisture conditions to vary between storms. The resulting flood frequency distributions are cast in a scaled dimensionless framework where issues such as catchment scale and similarity can be conveniently addressed. A number of experiments are performed to study the sensitivity of the flood frequency response to some of the "similarity" parameters identified in this formulation. The results indicate that one of the most important components of the derived flood frequency model relates to the specification of processes within the runoff generation model; specifically the inclusion of both saturation excess (Dunne) and Horton infiltration excess runoff production mechanisms. The dominance of these mechanisms over different return periods of the flood frequency distribution can significantly affect the distributional shape and confidence limits about the distribution. Comparisons with observed flood distributions seem to indicate that such mixed runoff production mechanisms influence flood distribution shape. The sensitivity analysis also indicated that the incorporation of basin and rainfall storm scale also greatly influences the distributional shape of the flood frequency curve.

1. INTRODUCTION

Considerable research effort has been spent in recent years on the estimation of flood frequencies using the derived distribution approach. The first example of such an effort was described by *Eagleson* [1972]. Two more recent examples were presented by *Hebson and Wood* [1982] and *Diaz-Granados et al.* [1984]. The rainfall-runoff models used by the latter are based on versions of the geomorphologic unit hydrograph (GUH) proposed by *Rodriguez-Iturbe and Valdes* [1979].

Despite the simplicity and ease of parameterization of the GUH, a number of significant shortcomings still exist in the use of GUH-based models for the estimation of derived flood frequency. Recently, *Moughamian et al.* [1987] compared the approaches of *Hebson and Wood* [1982] and *Diaz-Granados et al.* [1984]. They found that both models performed poorly in every catchment studied when compared to sample distributions, suggesting that fundamental improvements are needed before they can be applied with any confidence.

The GUH of *Rodriguez-Iturbe and Valdes* [1979] is based on the assumption that rainfall excess is generated uniformly throughout the catchment area. In their application of the GUH to derived flood frequency estimation, both *Hebson and Wood* [1982] and *Diaz-Granados et al.* [1984] assumed two simple models of essentially Hortonian runoff generation to calculate the rainfall excess. In reality, runoff generation on catchments is much more complex. It is now recognized [*Dunne*, 1978] that in many catchments much of the runoff during storm events is produced on variable contributing areas which form narrow bands adjacent to the streams. The failure to incorporate these observed features of the catchment response into the GUH-based models is likely to be a source of major errors in the derived flood frequency estimates.

In all of the examples cited above, the initial moisture condition of the catchment prior to the storm is assumed to be the same for all the storms. This is contrary to the reality in many catchments. *Wood* [1976] extended the flood frequency model of *Eagleson* [1972] in order to study the effects of parameter uncertainties. He found that uncertainty in the parameter that represented the initial moisture state of the

[1]Now at Centre for Water Research, University of Western Australia, Nedlands, Australia.

Paper number 89WR01579.
0043-1397/90/89WR-01579$05.00

catchment could have a substantial effect on the predicted return periods.

In addition, both *Hebson and Wood* [1982] and *Diaz-Granados et al.* [1984] used a lumped representation of the catchment response with spatially homogeneous rainfall based, however, on point rainfall statistics. This inconsistency gives rise to scale-dependent biases in the derived flood frequency distributions. *Wood and Hebson* [1986] overcame this problem by deriving a scale-independent flood frequency curve using an areal rainfall input distribution based upon areal rainfall similarity.

Finally, *Surkan* [1969] has shown that catchments that are topologically similar (based for example on Horton's order ratios) may yet produce different impulse response functions. This is the result of topological randomness whereby networks with different link-node configurations give rise to the same order ratios. For this reason, *Beven* [1986] has argued against generalizing the network for making predictions about specific catchments; instead Beven used a simple routing procedure based on a constant channel wave velocity and network link histogram. More recently, *Gupta et al.* [1986] have presented an approach that utilizes the actual network structure directly for the routing of runoff through use of the so-called "width function." This is a subject of intense current research interest.

1.1. *Scope of the Paper*

This is the third in a sequence of papers whose aim has been to provide a greater understanding of the interrelationships that underlie the storm response of catchments of different scales and physical characteristics by focusing on concepts of similarity. In the first paper, *Wood and Hebson* [1986] developed similarity relationships for flood frequency distributions that are independent of basin scale. They obtained a dimensionless flood frequency curve using the GUH basin response model of *Rodriguez-Iturbe and Valdes* [1979] under the assumptions of spatially homogeneous rainfalls and a simple Hortonian runoff generation model consisting of a constant contributing area during the storm events.

Later, *Sivapalan et al.* [1987] relaxed these assumptions and developed a model of storm runoff generation due to spatially variable rainfalls on heterogeneous catchments taking account of the effects of catchment topography on the within-storm dynamics of runoff contributing areas. This model was also expressed in dimensionless form leading to the identification of five dimensionless catchment similarity parameters and three dimensionless auxiliary variables which govern the scaled storm response.

This paper represents the logical next step toward the development of a physically based flood frequency curve. First, we generalize the existing GUH theory in order to incorporate, in a simple and parsimonious way, runoff generation on partial areas by both the infiltration excess (Hortonian) and saturation excess (Dunne) mechanisms. The generalized GUH is structured in such a way that it can be coupled to the runoff generation model of *Sivapalan et al.* [1987] by means of the topography-soil index which is used to predict the areal distribution of soil moisture deficits and the proportion of contributing areas. This coupling permits the lumped runoff generation model of *Sivapalan et al.* [1987] to be integrated with the generalized GUH in a physically consistent manner.

Second, the runoff generation model of *Sivapalan et al.* [1987] and the generalized GUH are combined together with assumed distributions of rainfall intensity and duration and an assumed distribution of the initial conditions to obtain the flood frequency curve. The scaled dimensionless formulations of *Wood and Hebson* [1986] and of *Sivapalan et al.* [1987] are essentially preserved in the derivations of the catchment storm response. The scaled flood frequency distributions are used to address such issues as catchment scale effects and similarity. The sensitivities of the flood frequency curve to changes of various similarity parameters are also investigated.

1.2. *Outline of the Paper*

The paper begins with a summary of the GUH theory. The outline of the theory, given in section 2.1, is made sufficiently general so as to be able to incorporate partial area runoff generation. This is followed in section 2.2 by the introduction of a runoff generation model based on the topography-soil index. A methodology for combining the partial area runoff generation model with the GUH-based runoff routing model is presented next in sections 2.3 and 2.4; this results in the generalized GUH. The sensitivities of the generalized GUH to two parameters of the partial area generation model are then studied. The results of this study are presented in section 2.5.

Section 3 involves the estimation of the dimensionless flood frequency distribution. In section 3.1 the dimensionless peak discharge is calculated based on the dimensionless S curve derived from the scaled generalized GUH. Sections 3.2 and 3.3 are devoted to the specification of frequency distributions of the scaled rainfall intensities, storm durations, and the initial conditions. Section 3.4 describes the procedure for the estimation of the flood frequency distribution and return period. Section 4 presents results of the sensitivity analyses carried out on the model with respect to a number of similarity parameters.

2. Derivation of a Generalized GUH Based on Partial Area Runoff Generation

2.1. *A Review of the GUH*

Let T_B denote the time of travel of any particle of surface runoff from the location of its generation to the catchment outlet. It is assumed that the time-variant instantaneous unit hydrograph (iuh) at the time τ, $h(t|\tau)$, is given by

$$H(t|\tau) = \frac{d}{dt} P(T_B \leq t|\tau) \tag{1}$$

where $P(\ )$ denotes the probability of the event given in the parentheses. Note that for all particles that are generated at time τ, both T_B and t are measured from the instant τ. The right-hand side of (1) is simply the probability density function (pdf) of T_B.

Let Ω be the highest order of the catchment stream network; $c_i (1 \leq i \leq \Omega)$ denotes a channel state of order i; and $r_i (1 \leq i \leq \Omega)$ denotes an overland flow region or hillslope state of order i. We assume that runoff is generated only on the hillslopes; rainfall falling directly into stream channels is neglected. We can then define a collection $S = \{s\}$ of paths s

which a particle of water may follow from the state r_i where it is generated to the catchment outlet. Thus we have

$$P(T_B \le t|\tau) = \sum_{s \in S} P(T_s \le t) P(s|\tau) \quad (2)$$

where $T_s (s \in S)$ is the travel time along a path s and $P(s|\tau)$ is the probability of the given path s out of all paths S, for given τ. Neglecting the travel time over the hillslopes, any path $s \in S$ necessarily takes a form $s = \langle x_1, x_2, \cdots, x_k \rangle$, where $x_1, x_2, \cdots, x_k \in \{c_i, i = 1, \Omega\}$. For a path $s \in S$ that originates in a hillslope of order i (note that $x_1 = c_i$), $P(s|\tau)$ is given by

$$P(s|\tau) = \Pi_i(\tau) P_{x_1 x_2} P_{x_2 x_3} \cdots P_{x_{k-1} x_k} \quad (3)$$

where $\Pi_i(\tau)$ is the probability that the particle of runoff came from a hillslope of order i and $P_{x_i x_j}$ is the transition probability for the particle between order x_i and x_j. In the general formulation it is equated to the ratio of the number of particles of runoff generated in all the hillslopes of order i to the total number of particles of runoff generated from the entire catchment. The generalized GUH is then obtained by combining (1), (2), and (3). The probabilities $\Pi_i(\tau)$, for $i = 1, \Omega$, in (3) are dependent on the runoff generation model. Their derivation is presented in section 2.3. The assumption neglecting hillslope travel times is reasonable for large catchments or narrow partial areas. The interaction between hillslope and channel travel times over a range of catchment scales is currently being investigated by the authors.

2.2. *Model of Runoff Generation*

The runoff generation model used in this paper is a simplified version of the conceptual model of *Sivapalan et al.* [1987]. It is based on the fundamental assumption that, under quasi-steady conditions, the difference between the local prestorm water table depth z_x at a location x and its catchment-wide average $\bar{z}$ is linearly related to the corresponding difference between $\ln (aT_e/T_x \tan \beta)$, a topography-soil index, and its catchment average λ. This relationship can be expressed as

$$z_x = \bar{z} - \frac{1}{f}\left\{\ln\left(\frac{aT_e}{T_x \tan \beta}\right) - \lambda\right\} \quad (4)$$

In (4), a denotes the area draining through location x per unit contour length, T_x is a local transmissivity parameter, and f is a hydrogeological constant for the catchment and is a measure of the decline of the saturated hydraulic conductivity with depth. For soils for which this decline is exponential, *Beven* [1986] showed that $T_x = K_0/f$, where K_0 is the saturated conductivity of the surface soil layer; λ and T_e are given by

$$\lambda = \frac{1}{A}\int_A \ln\left(\frac{aT_e}{T_x \tan \beta}\right) dA$$

$$\ln T_e = \frac{1}{A}\int_A \ln T_x \, dA$$

Given $\bar{z}$ and the spatial pattern of values of the topography-soil index $\ln (aT_e/T_x \tan \beta)$, equation (4) enables the prediction of the pattern of local initial water table depths for all points in the catchment.

Generation of saturation excess runoff depends on the initial moisture storage deficit S_x at any location x. For simplicity, we neglect the downslope redistribution of moisture within the duration of the storm and assume that saturation excess runoff will be generated wherever the cumulative infiltration $M_g(\tau)$ exceeds S_x. It is assumed further that just before the storm the unsaturated zone moisture profile comes close to the case of complete gravity drainage; i.e., reaches "field capacity." This assumption is consistent with field observations. S_x may then be uniquely predicted from the depth to the water table. This unique functional relationship between z_x and S_x is denoted here by $z_x = \gamma(S_x)$.

The initial contributing area $A_c(0)$ is obtained by using (4) to determine the value of the topography-soil index for which $z_x \le \psi_c$, where ψ_c is the thickness of the capillary fringe and is assumed to be equal to the air-entry value of the matrix head for the soil. The contributing area is thus given by

$$\ln\left(\frac{aT_e}{T_x \tan \beta}\right) \ge \lambda + f\bar{z} - f\psi_c \quad (5)$$

The contributing area A_c expands with time during the storm, and at any time τ after the beginning of the storm, the dynamic contributing area is obtained by determining the locations where $M_g(\tau) \ge S_x$. In terms of the topography-soil index this condition can be expressed as

$$\ln\left(\frac{aT_e}{T_x \tan \beta}\right) \ge \lambda + f\bar{z} - f\gamma[M_g(\tau)] \quad (6)$$

The model presented by *Sivapalan et al.* [1987] assumes that infiltration is controlled by the initial moisture content and saturated hydraulic conductivity of the surface layer and neglects the variation of these quantities with depth. This allows analytical solutions for the infiltration process to be developed. Both the rainfall intensity p and the surface hydraulic conductivity K_0 are assumed to be spatially variable. Rainfall p is assumed to be gamma distributed within the catchment with mean $\bar{p}$ and coefficient of variation C_{vp}. K_0 is assumed to be lognormally distributed with mean $\bar{K}_0$ and coefficient of variation C_{vK}. The model uses quasi-analytical expressions for mean infiltration rate $m_g(\tau)$ and cumulative infiltration volume $M_g(\tau)$. These were derived by *Sivapalan* [1986] based on the *Philip* [1957] infiltration equation and the time compression approximation.

In this paper, a further simplification of the modeling of infiltration excess runoff is effected by approximating the infiltration process by a single lumped equation that uses the average moisture content over the noncontributing areas. This approximation is justified by the results of *Sivapalan et al.* [1987] which show that the variation of surface moisture content in space accounts for a negligible component of total runoff.

Following *Sivapalan et al.* [1987], the model equations are expressed in dimensionless form in terms of five dimensionless similarity parameters and three auxiliary variables. The listing and definition of these eight parameters are presented in Appendix A. For more details, the reader is referred to *Sivapalan et al.* [1987].

2.3. *Derivation of* $\Pi_i(\tau)$

Let A be the area of the entire catchment. We denote by A_i^* the total area of all the hillslopes that drain directly to streams of order i; θ_i denotes the proportion of A_i^* to A, i.e., $\theta_i = A_i^*/A$ and $\Sigma\theta_i = 1$. Expressions for θ_i for a third-order catchment in terms of Horton's order ratios R_A and R_B are presented in Appendix B.

Let $A_c(\tau)$ be the contributing area for the entire catchment defined as the area contributing direct runoff by the saturation excess mechanism. We also define by $A_{c_i}^*(\tau)$ the total contributing area from all the hillslopes which drain directly to streams of order i. Then we can easily establish the following relationship:

$$\frac{A_c(\tau)}{A} = \sum_{i=1}^{\Omega} \theta_i \left(\frac{A_{c_i}^*}{A_i^*}\right) \tag{7}$$

Let $m_g(\tau)$ be the areal mean infiltration rate over the non-contributing area of the catchment, $A - A_c(\tau)$. Here $m_g(\tau)$ is modeled using an average surface moisture content of the soil over the nonponded area. The areal average rainfall intensity, assumed constant in time during the storm event, is denoted by $\bar{p}$. Then the rate of runoff generation at any time τ from the entire catchment is given by

$$q(\tau) = A\left\{\frac{A_c(\tau)}{A}\bar{p} + \left(1 - \frac{A_c(\tau)}{A}\right)[p - m_g(\tau)]\right\} \tag{8}$$

We also make the scale approximation that the averages of rainfall and the infiltration rate taken over, say, all of the hillslopes that drain directly to streams of order i are equal to the catchment-wide means $\bar{p}$ and $m_g(\tau)$, respectively. The mean runoff production rate from all the hillslopes that drain to streams in order i is then given by

$$q_i(\tau) = A_i^*\left\{\frac{A_{c_i}^*(\tau)}{A_i^*}\bar{p} + \left(1 - \frac{A_{c_i}^*(\tau)}{A_i^*}\right)[\bar{p} - m_g(\tau)]\right\} \tag{9}$$

The proportion $\Pi_i(\tau)$ of the number of particles of runoff generated on all the hillslopes that drain to streams of order i, to the total number from the entire catchment is simply q_i/q; thus we have

$$\Pi_i(\tau) = \frac{A_i^*}{A}\left\{\frac{A_{c_i}^*}{A_i^*}\bar{p} + \left(1 - \frac{A_{c_i}^*}{A_i^*}\right)\cdot[\bar{p} - m_g(\tau)]\left[\frac{A_c}{A}\bar{p} + \left(1 - \frac{A_c}{A}\right)[\bar{p} - m_g(\tau)]\right]^{-1}\right\} \tag{10}$$

At this point we approximate $A_{c_i}^*/A_i^*$ in the infiltration excess component of (10) by the corresponding quantity for the entire catchment A_c/A. This is a reasonably good approximation when (1) $A_{c_i}^*/A_i^*$ and A_c/A are much less than 1 and (2) surface runoff generation in natural catchments takes place predominantly by the saturation excess mechanism. Based on *Freeze*'s [1974] and *Dunne*'s [1978] reviews of a large number of field studies and computer simulations, it is apparent that these conditions are met in most catchments, especially in humid areas. With this approximation, equation (10) simplifies to

$$\Pi_i(\tau) = \frac{A_{c_i}^*}{A_c} Q_s(\tau) + \theta_i[1 - Q_s(\tau)] \tag{11}$$

where $Q_s(\tau)$ is the proportion of the total runoff rate from the entire catchment that is generated by the saturation excess mechanism and is defined by

$$Q_s(\tau) = \frac{A_c}{A}\bar{p}\left[\frac{A_c}{A}\bar{p} + \left(1 - \frac{A_c}{A}\right)[\bar{p} - m_g(\tau)]\right]^{-1} \tag{12}$$

Note here that the approximate equation (equation (11)) is exact for the two extreme cases, $Q_s = 0$ (infiltration excess runoff only) and $Q_s = 1$ (saturation excess only). Also, when $Q_s = 0$, $\Pi_i(\tau) = \theta_i$ which then yields the original GUH of *Rodriguez-Iturbe and Valdes* [1979].

To evaluate $\Pi_i(\tau)$, we require expressions for $A_{c_i}^*/A_c$. In section 2.4 we derive expressions for $A_{c_i}^*/A_c$ in terms of A_c/A using geomorphologic principles and the topography-soil index framework of *Beven* [1986] and *Sivapalan et al.* [1987].

2.4. *Derivation of* $A_{c_i}^*/A_c$

To disaggregate A_c into $A_{c_i}^*$ for $i = 1, \cdots, \Omega$, we assume that the catchment area can be broken up into a number of rectangular plane hillslopes which drain directly to streams of different orders i. As outlined in the earlier description of the runoff generation model, the contributing areas are predicted by the topography-soil index $\ln (aT_e/T_x \tan \beta)$. Given the threshold value of this index at saturation, $\ln (aT_e/T_x \tan \beta)_s$, the proportion of contributing area A_c/A can be obtained from the cumulative distribution function of $\ln (aT_e/T_x \tan \beta)$.

The A_c/A versus $\ln (aT_e/T_x \tan \beta)$ relationship for an idealized rectangular plane hillslope was derived by *Beven and Wood* [1983]; applying this relationship to the hillslopes that drain directly to streams of order i and whose combined area as defined above is A_i^*, we have

$$\frac{A_{c_i}^*}{A_i^*} = \left\{1 - \frac{\bar{s}_{g_i}}{\bar{L}_g}\left(\frac{T_x}{T_e}\right)_s \exp\left[\ln\left(\frac{aT_e}{T_x \tan\beta}\right)_s\right]\right\} \tag{13a}$$

$$\frac{a}{\tan\beta} < \frac{\bar{L}_g}{\bar{s}_{g_i}}$$

$$\frac{A_{c_i}^*}{A_i^*} = 0 \qquad \frac{a}{\tan\beta} \geq \frac{\bar{L}_g}{\bar{s}_{g_i}} \tag{13b}$$

where $\bar{s}_{g_i}$ is the mean ground surface slope of the hillslopes in a direction normal to the streams to which they drain and $\bar{L}_g$ is the mean length of the hillslopes in the same direction. *Horton* [1945] and *Morisawa* [1962] have found that $\bar{L}_g$ in most catchments can be approximated by $1/2D$, where D is the drainage density which does not vary greatly with the order of the catchment and can therefore be assumed to be constant. At very large catchment scales where there is significant nonstationarity in landforms, this assumption would not hold.

We now make use of *Horton*'s [1945] law of stream slopes which can be expressed as

$$\bar{s}_i/\bar{s}_{i-1} = R_S \tag{14}$$

where $\bar{s}_i$ is the mean stream slope of ith-order streams. *Strahler* [1950] observed a consistent relationship between the mean slope of a stream and the mean ground slope of the

hillslope draining to it. This relationship can be approximated by

$$\bar{s}_{g_i} = c\bar{s}_i^d \tag{15}$$

where c and d are constants. Combining (14) and (15), we obtain a "law of hillside slopes" which can be expressed as

$$\bar{s}_g/\bar{s}_{g_{i-1}} = R_{SG} \approx R_S^d \tag{16}$$

Substitution of (16) in (13) yields

$$\frac{A_{c_i}^*}{A_i^*} = \left\{1 - \frac{\bar{s}_{g_1} R_{SG}^{i-1}}{\bar{L}_g}\left(\frac{T_x}{T_e}\right)_s \exp\left[\ln\left(\frac{aT_e}{T_x \tan\beta}\right)_s\right]\right\} \qquad \frac{a}{\tan\beta} < \frac{\bar{L}_g}{\bar{s}_{g_1} R_{SG}^{i-1}} \tag{17a}$$

$$\frac{A_{c_i}^*}{A_i^*} = 0 \qquad \frac{a}{\tan\beta} \geq \frac{\bar{L}_g}{\bar{s}_{g_1} R_{SG}^{i-1}} \tag{17b}$$

Now,

$$\frac{A_{c_i}^*}{A_c} = \theta_i \left(\frac{A_{c_i}^*}{A_i^*}\right) \Big/ \left(\frac{A_c}{A}\right) \tag{18}$$

Combining (7), (17), and (18) and eliminating $(a/\tan\beta)$, we can derive expressions for $A_{c_i}^*/A_c$ as a function of A_c/A and the geomorphologic constants θ_i and R_{SG}. The resulting expressions for a third-order catchment are presented in Appendix C.

Both the variables A_c/A and Q_s are outputs from the conceptual runoff generation model described earlier. Also, A_c/A and Q_s are functions of τ and are dependent on the rainfall intensity, soil properties, topography, and the initial moisture conditions. The sensitivities of A_c/A and Q_s to a number of dimensionless similarity parameters and auxiliary variables that represent climatic inputs, catchment properties, and initial conditions were investigated by *Sivapalan et al.* [1987].

2.5. *The Generalized GUH*

We define a dimensionless generalized GUH, denoted by $h^*(t^*|\tau^*)$, as

$$h^*(t^*|\tau^*) = \tau_l h(t|\tau) \tag{19a}$$

$$t^* = t/\tau_l \qquad \tau^* = \tau/\tau_l \qquad t_r^* = t_r/\tau_l \tag{19b}$$

where τ_l and τ_r are two characteristic time scales; τ_r is the mean duration of storms, and τ_l is a characteristic basin lag time defined here as

$$\tau_l = L_\Omega/v \tag{20}$$

where L_Ω is the length of the highest-order stream in the catchment and v is the mean velocity of flow in the stream network. Following *Wood and Hebson* [1986], we use an empirical relationship for τ_l (in hours) in terms of the catchment area A (in square kilometers) as follows:

$$\tau_l = 2.51A^{0.38} \tag{21}$$

TABLE 1. Horton's Order Ratios for Four Selected Catchments

Parameter	Catchment: Santa Paula Creek	Davidson River	North Nashua River	Bald Eagle Creek
Area ratio R_A	6.8	5.8	5.6	3.64
Bifurcation ratio R_B	4.7	4.3	3.9	3.17
Length ratio R_L	1.9	2.1	3.2	3.18

Taken from *Moughamian et al.* [1987] and *Hebson and Wood* [1982].

Following *Rodriguez-Iturbe and Valdes* [1979], $h^*(t^*|\tau^*)$ for a third-order catchment is then given by

$$h^*(t^*|\tau^*) = B\exp(-R_L^2 t^*) + C\exp(-R_L t^*) + (D + Et^*)\exp(-2t^*) \tag{22}$$

The coefficients B, C, D, and E are functions of the order ratios R_A, R_B, R_L, and R_{SG} and the variables A_c/A and Q_s. The functional relationships of B, C, D, E to A_c/A and Q_s are expressed through the probabilities Π_i. The expressions for B, C, D, and E are presented in Appendix D. In the original formulation of *Rodriguez-Iturbe and Valdes* [1979], Π_i are equated to θ_i.

The generalized dimensionless GUH was determined for four different combinations of the parameters R_A, R_B, and R_L and for different values of the variables A_c/A and Q_s. The values of R_A, R_B, and R_L were taken from four catchments analyzed by *Moughamian et al.* [1987] and *Hebson and Wood* [1982]. These are summarized in Table 1. R_{SG} was arbitrarily assumed to be 0.62. The variations of h_p^*, the peak of the dimensionless GUH, with variations of A_c/A and Q_s are presented in Figures 1*a* and 1*b*. They show that partial area runoff generation can have a significant impact on the GUH peak and time to peak in many catchments.

3. Estimation of Dimensionless Flood Frequency

3.1. *Derivation of Dimensionless Peak Discharge*

Henderson [1963] has found that as long as the unit hydrograph peak and the time to peak are preserved, a triangular unit hydrograph is sufficient for the prediction of streamflow response. *Wood and Hebson* [1986] derived the peak discharge Q_p from a catchment due to storm runoff generated at a constant rate q and having duration t_r by utilizing a triangular IUH having peak h_p and time to peak t_p. The resulting expression for Q_p is as follows:

$$Q_p = qh_p t_r\left(1 - \frac{h_p t_r}{4}\right) \qquad h_p t_r \leq 2 \tag{23a}$$

$$Q_p = q \qquad h_p t_r > 2 \tag{23b}$$

In the present paper the rate of runoff generation varies in time even though the generated rainstorms were temporally constant. The results of *Beven* [1986] suggest that the temporal variations in rainfall can influence the shape of the flood frequency curve. This issue will be addressed in the discussions following the results. To capture the effects of the temporal variation in runoff production, the peak dis-

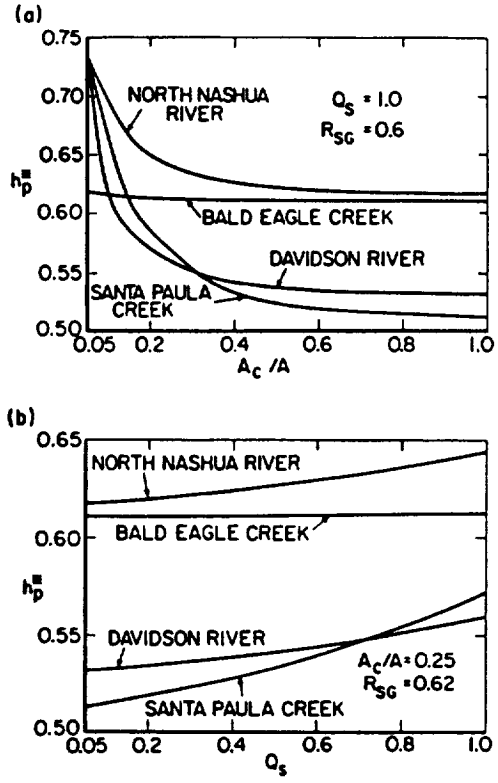

Fig. 1. Variation of h_p^*, the peak of the dimensionless generalized GUH, to (*a*) A_c/A and (*b*) Q_s.

charge is calculated using a dimensionless S^* curve derived from (22). That is,

$$S^*(t^*) = \frac{B}{R_L^2}[1.0 - \exp(-R_L^2 t^*)] + \frac{C}{R_L}[1.0 - \exp(-R_L t^*)] + 0.25(2D + E) \cdot [1.0 - \exp(-2t^*)] - 0.5Et^* \exp(-2t^*) \quad (24)$$

The time-varying runoff production was then convoluted with the dimensionless $S^*(t^*)$ curve to yield the outflow hydrograph from which the peak discharge and time to peak were extracted. As discussed in section 2, generalized GUH is a function of A_c/A and Q_s which are also time variable. For the simulation results presented in this paper, we used time-averaged values, $\bar{A}_c/A$ and $\bar{Q}_s$, in the calculation of h^*.

Relationships between the scaled (or dimensionless) and nonscaled discharge values can be established using the time scales τ_l and τ_r defined earlier and the following transformations. These transformations are similar to the ones used by *Sivapalan et al.* [1987] and are consistent with the definitions presented in Appendix A.

$$Q_p^* = \frac{Q_p \tau_r}{\psi_c(\theta_s - \theta_r)} \quad (25)$$

$$q^* = \frac{q\tau_r}{\psi_c(\theta_s - \theta_r)} \quad (26)$$

The above expressions for the dimensionless peak discharge do not include a base flow component; its treatment is discussed in section 3.3.

3.2. *Frequency Distributions of Inputs*

As in most previous work, we assume that the scaled storm duration is exponentially distributed; in this case it has mean 1. The scaled point rainfall intensities are assumed to be gamma distributed with parameters α and β and coefficient of variation C_v. Following *Wood and Hebson* [1986], we assume that the scaled mean rainfall $\bar{p}^*$ over a catchment of area A is also gamma distributed with parameters α_A and β_A. *Wood and Hebson* [1986] have shown that

$$\alpha_A = \alpha\kappa^{-2}$$

$$\beta_A = \beta\kappa^2 \quad (27)$$

where κ^2 is a geoclimatic scaling parameter defined by

$$\sigma_A^2 = \sigma^2\kappa^2 \quad (28)$$

where σ^2 and σ_A^2 are the variances of point rainfall and areal average rainfall, respectively. The κ^2 can be estimated for any catchment area A using the space correlation of the rainfall intensity process.

The variance of point rainfall intensities within a catchment is also important and has a significant effect on predictions of the rates of runoff generation. The model of *Sivapalan et al.* [1987] requires the coefficient of variation C_{vp} of point rainfall intensities within the catchment. The relationship between C_{vp} and C_v for a catchment of area A is given by

$$\frac{C_{vp}}{C_v} = (1 - \kappa^2)^{1/2} \quad (29)$$

Following *Sivapalan and Wood* [1987], the spatial correlation structure of rainfall is assumed to be of the form

$$\rho_p(r) = a_1 \exp(-b_1^2 r^2) + a_2 \exp(-b_2^2 r^2) \quad (30)$$

where a_1, a_2, b_1, and b_2 are constants with $a_1 + a_2 = 1$. The correlation length is given by

$$\lambda_p \equiv \int_0^\infty \rho_p(r)\, dr = \frac{a_1(\pi)^{1/2}}{b_1} + \frac{a_2(\pi)^{1/2}}{b_2} \quad (31)$$

In this paper we assume $a_1 = 0.7$, $a_2 = 0.3$, and $b_1/b_2 = 3.0$. For such a correlation structure the variation of κ^2 and C_{vp}/C_v with the scaled catchment area $A^* = A/\lambda_p^2$ is presented in Figure 2.

3.3. *Distribution of the Initial Condition*

In the model of *Sivapalan et al.* [1987] the initial moisture state of the catchment is uniquely represented by the auxiliary variable Q^*. Q^* is a dimensionless baseflow parameter which in combination with the topography-soil index parameter ϕ^* and the hydrogeologic parameter ψ_c^* determines the initial contributing areas and the soil moisture in the unsaturated zone (note that the baseflow is inversely proportional to Q^*).

In reality, Q^* can vary between storms (short term) as well as between seasons (long term). Ideally, the distribution of

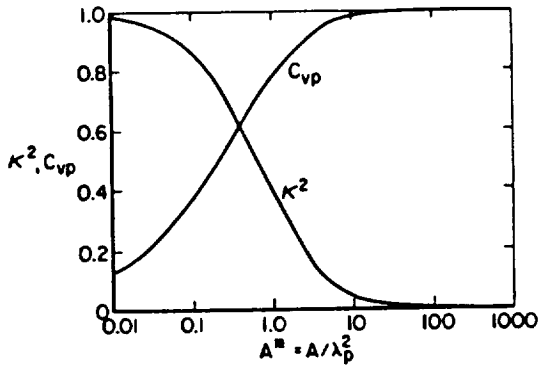

Fig. 2. The variation of κ^2 (the geoclimatic scale parameter) and C_{vp}/C_v with scaled catchment area, $A^* = A/\lambda_p^2$.

Q^* can only be obtained by the modeling of the processes in the interstorm periods. Although this is the long-term objective of much current hydrologic research, in this paper we arbitrarily assume that Q^* belongs to a gamma distribution whose parameters (mean $\bar{Q}^*$ and coefficient of variation C_{vQ}) can be obtained from the analysis of a large number of base flow recession curves of the catchment of interest.

The base flow component of peak discharge can be related to the antecedent moisture conditions which then yields

$$q_b^* = \frac{\bar{K}_0^*}{(1 + c_{vK}^2)^{1/2} f_1} \exp\left(-f_2 \frac{Q^*}{\psi_c^*}\right) \tag{32}$$

where $f_1 = f \exp(\lambda)$ and $f_2 = f\psi_c$. In the present work we have set $f_1 = 400.0$ and $f_2 = 0.40$. Here, f is the parameter that controls the decrease in hydraulic conductivity with depth.

3.4. *Dimensionless Flood Frequency Distribution*

The cumulative distribution function for flood peaks Q_p^* is given by

$$F(Q_p^*) = \int_R f(\bar{p}^*, t_r^*, Q^*)\, d\bar{p}^*\, dt_r^*\, dQ^* \tag{33}$$

where $f(\bar{p}^*, t_r^*, Q^*)$ is the joint probability density function of the point rainfall intensity $\bar{p}^*$, rainfall duration, t_r^*, and base flow parameter Q^*, respectively, and R is the region containing all combinations of $\bar{p}^*$, t_r^*, and Q^* for which flood peaks exceed Q_p^*. It is not feasible to analytically evaluate (33) without recourse to further simplifications. For the purposes of this paper, we decided to numerically evaluate the integral in (33) by Monte Carlo simulation. The variables which are assumed to vary from storm to storm are the scaled mean storm intensity $\bar{p}^*$, scaled storm duration t_r^*, and the scaled initial soil dryness represented by Q^*. As discussed below, the distributional characteristics of these variables are assumed fixed for each analysis, thus representing a stable and stationary climate. Nevertheless, due to the nonlinearities in the storm response, both in the transformation from rainfall to runoff generation and in the relationship between flood peak and basin lag, the derived flood frequency distributions are not scale-independent. The catchment area influences basin lag τ_l and geoclimatic scaling parameter κ^2, both of which are important parameters of the flood response.

Realizations of the random variates are then input into the storm response model which results in the output Q_p^*. When arranged in ascending order, this yields the sample cumulative distribution of flood peaks $\hat{F}(q_p^*)$. For n storm events per year the annual exceedance series flood frequency return periods are obtained from

$$T_E(Q_p^*) = 1/n\hat{F}(Q_p^*) \qquad Q_p^* \geq \hat{F}^{-1}(1/n) \tag{34}$$

In the simulations carried out in this work was have used $n = 20$ storms per year and simulated a total of 4000 storms; this set was repeated 25 times for a total of 4000(25) storm analyses. For many climates, 20 storms per year may be too small. For the object of exploring the effect of catchment characterizations on the shape of the flood frequency curve, 20 is probably sufficient. In section 4 of this paper, further comments are provided on how the results from this analysis can provide insights into the flood frequency characterization in actual catchments.

4. Results and Discussion

A number of experiments were performed with the model to study the sensitivity of the flood frequency response to many of the dimensionless similarity parameters. Some of these parameters (namely, $\bar{p}^*$, $\bar{K}_0^*$, ψ_c^*, $\bar{Q}^*$, and ϕ^*; see Appendix A for their definitions) arose from the runoff generation model and were identified by *Sivapalan et al.* [1987]. The remainder, A^*, ω_r^*, C_{vQ}, and the Horton order ratios (R_A, R_B, R_L, and R_{SG}), were introduced in this paper during the development of the flood frequency model. The parameters were varied, one at a time, from the following arbitrary base values: $\bar{p}^* = 0.657$, $\bar{K}_0^* = 0.657$, $\psi_c^* = 0.05$, $\bar{Q}^*$

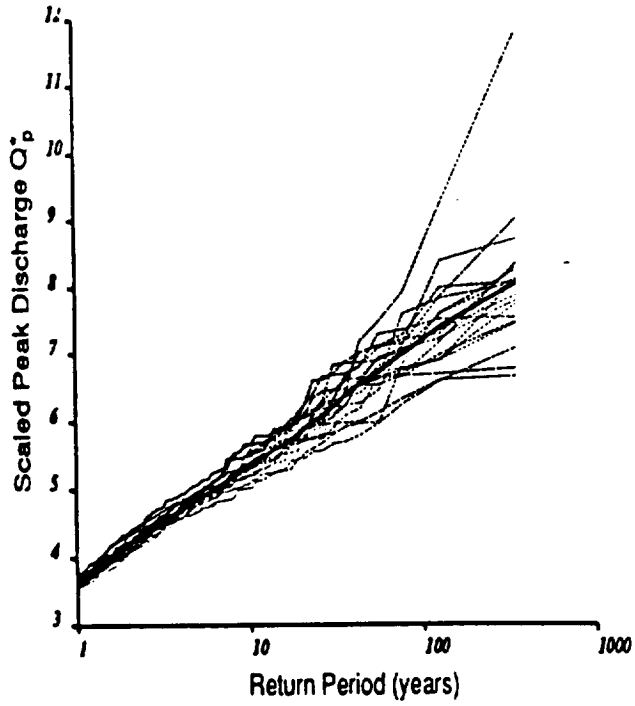

Fig. 3. Variability of the flood frequency distribution over 25 realizations.

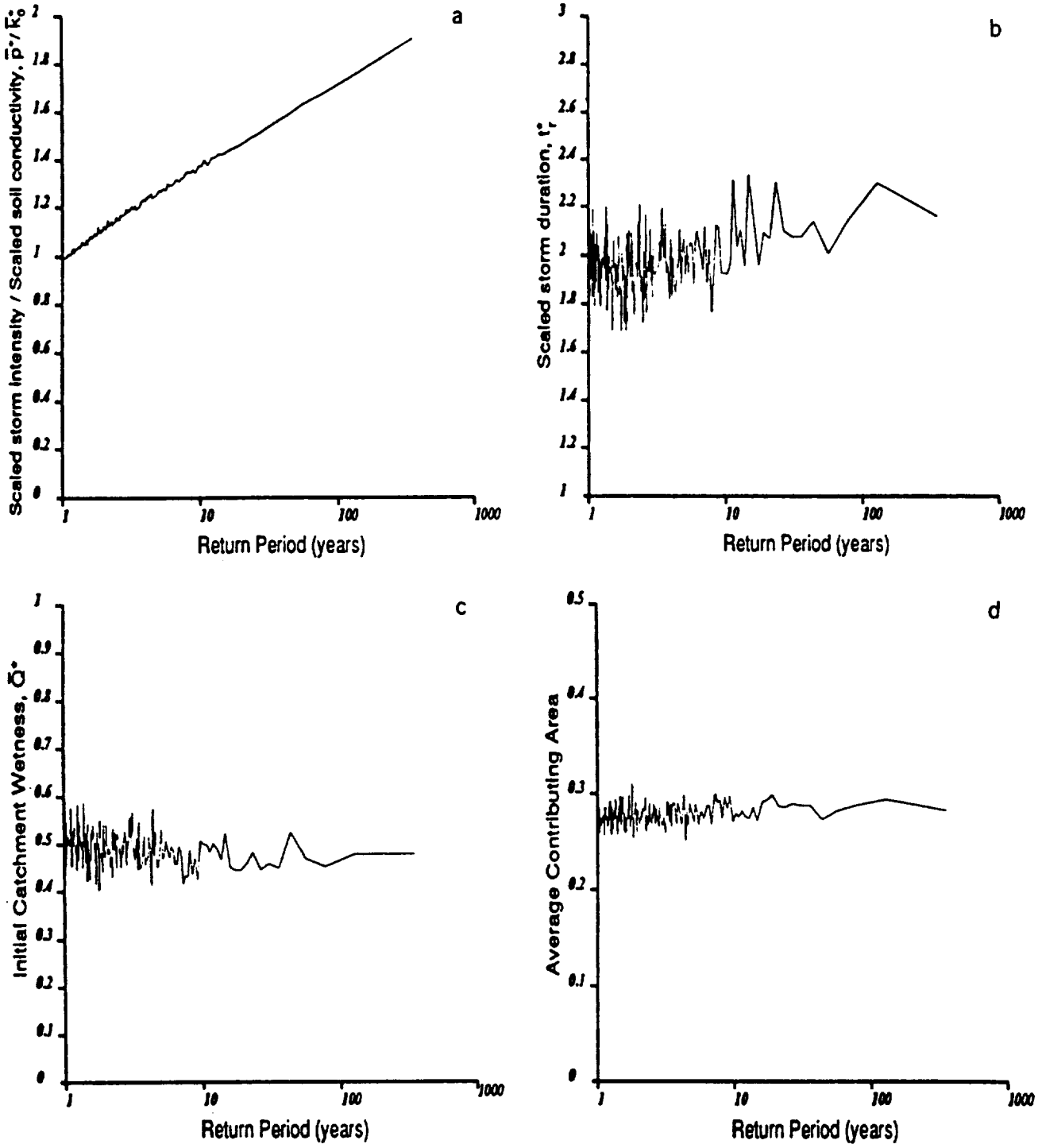

Fig. 4. Value of selected parameters of the runoff generation model corresponding to the flood discharges of Figure 3, plotted against the discharge return period. The parameters were averaged across the 25 realizations at each return period: (*a*) scaled storm intensity divided by scaled soil conductivity $\bar{p}^*/\bar{K}_0^*$, (*b*) scaled storm duration t_r^*, (*c*) initial soil wetness $\bar{Q}^*$, (*d*) average contributing area, and (*e*) fraction of runoff as saturation excess runoff.

$= 0.555$, $\phi^* = 2.34$, $A^* = 9.0$, $\omega_\tau^* = 1.45$, $R_A = 6.8$, $R_B = 4.7$, $R_L = 1.9$, $R_{SG} = 0.62$. The spatial coefficient of variation of the rainstorms, C_v, was set at a value of 2.0 for all storms; for the soil parameter K_0, its C_{vK}, was set equal to 1.0, and for the initial catchment dryness its C_{vQ} was set equal to 1.0. The Brooks-Corey parameter B was set to 0.40, $f_1 = 400.0$ and $f_2 = 0.40$ in all simulations. Results using these parameter values will be referred to as the base case. Figures 3 and 4, presents some results for the base case. In Figure 3 the variability of the derived flood frequency curve for the 25 repetitions is shown. The average flood frequency curve is darkened and is essentially a straight line showing EV-1 behavior; the same as the rainfall-soil input. This can be seen in Figure 4*a* where the average frequency curve for $\bar{p}^*/\bar{K}_0^*$ is presented. To construct this, and all remaining figures in the paper, the 25 repetitions were averaged for

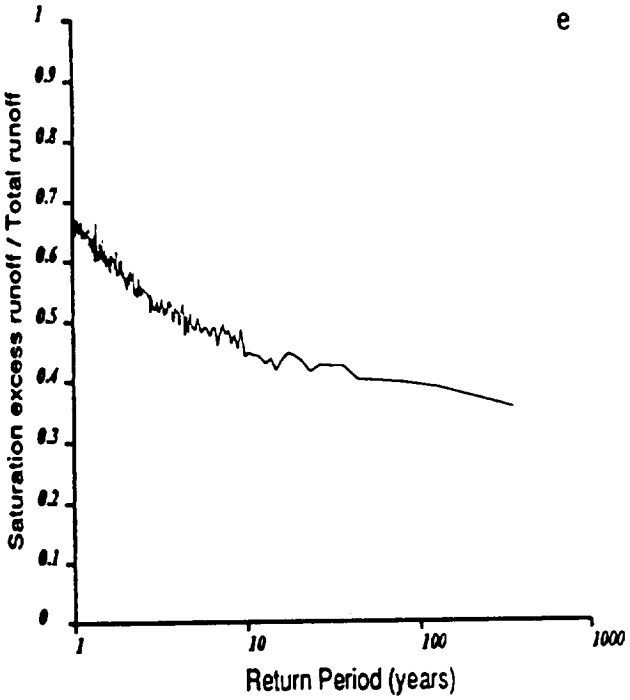

Fig. 4. (continued)

each return period. In Figures 4*b*–4*e* the frequency curves for scaled storm duration t_r^*, initial catchment wetness $\bar{Q}^*$, average contributing area during the storm, and fraction of runoff due to saturated excess runoff mechanism are presented.

These five curves represent the significant hydrologic processes represented in the flood frequency curve. What is extremely surprising is that it appears that the shape of the flood frequency curve is determined from the shape of the rainfall-soil distribution and that variables such as average contributing area, initial catchment wetness, and storm duration are constant across return periods. Further sensitivity analyses carried out later in this paper show a rather more complex situation than that represented here in the base case. Closer inspection of Figure 4 shows that the floods of importance to the base case catchment are heavily influenced by infiltration excess runoff production (Figure 4*e*); so perhaps the base case represents a semiarid climate. In this case it is quite reasonable that initial catchment wetness is independent of return period. Somewhat more surprising is to see that on average storm duration is only slightly related to return period and that contributing area is extremely stable at just under 30%. The constant contributing area and increase in infiltration excess runoff with return period demonstrates that for the base case, catchment topography plays only a minor role in the generation of floods of interest.

A series of sensitivity analyses were performed by varying one parameter at a time from the base case. The purpose of these sensitivities is to explore how fundamental hydrologic processes can influence flood frequency characteristics. Curves of the type presented in Figure 4 are available for each parameter set; essentially, only the flood frequency curves (averaged over the 25 repetitions) will be presented for each sensitivity analysis with selected results of other parameters to bring forth important features.

Mean scaled storm intensity. Two additional runs were made to explore increases and decreases of the mean scaled storm intensity. In the base case the mean scaled storm intensity was set equal to the mean scaled soil hydraulic

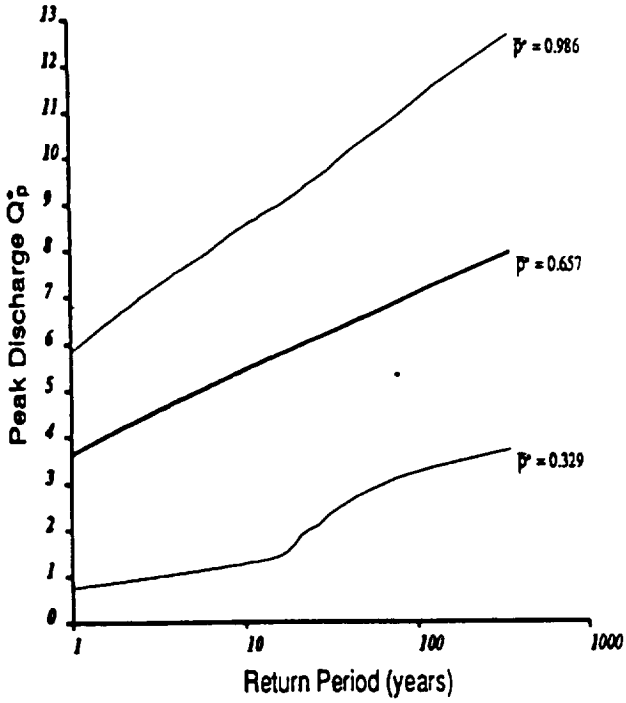

Fig. 5. The sensitivity of the flood frequency distribution to scaled storm intensity $\bar{p}^*$.

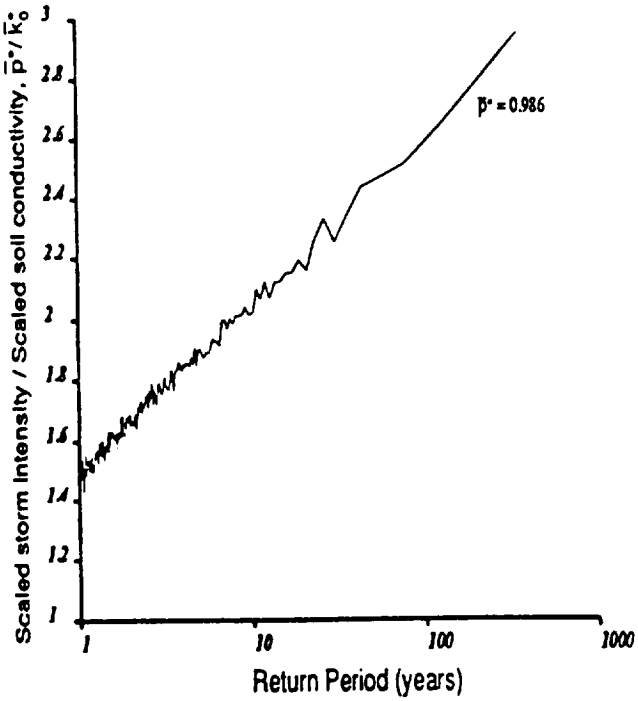

Fig. 6. Values of the scaled storm intensity divided by scaled soil conductivity corresponding to the flood discharges for the sensitivity run of $\bar{p}^* = 0.986$, plotted against the discharge return period (averaged over 25 realizations).

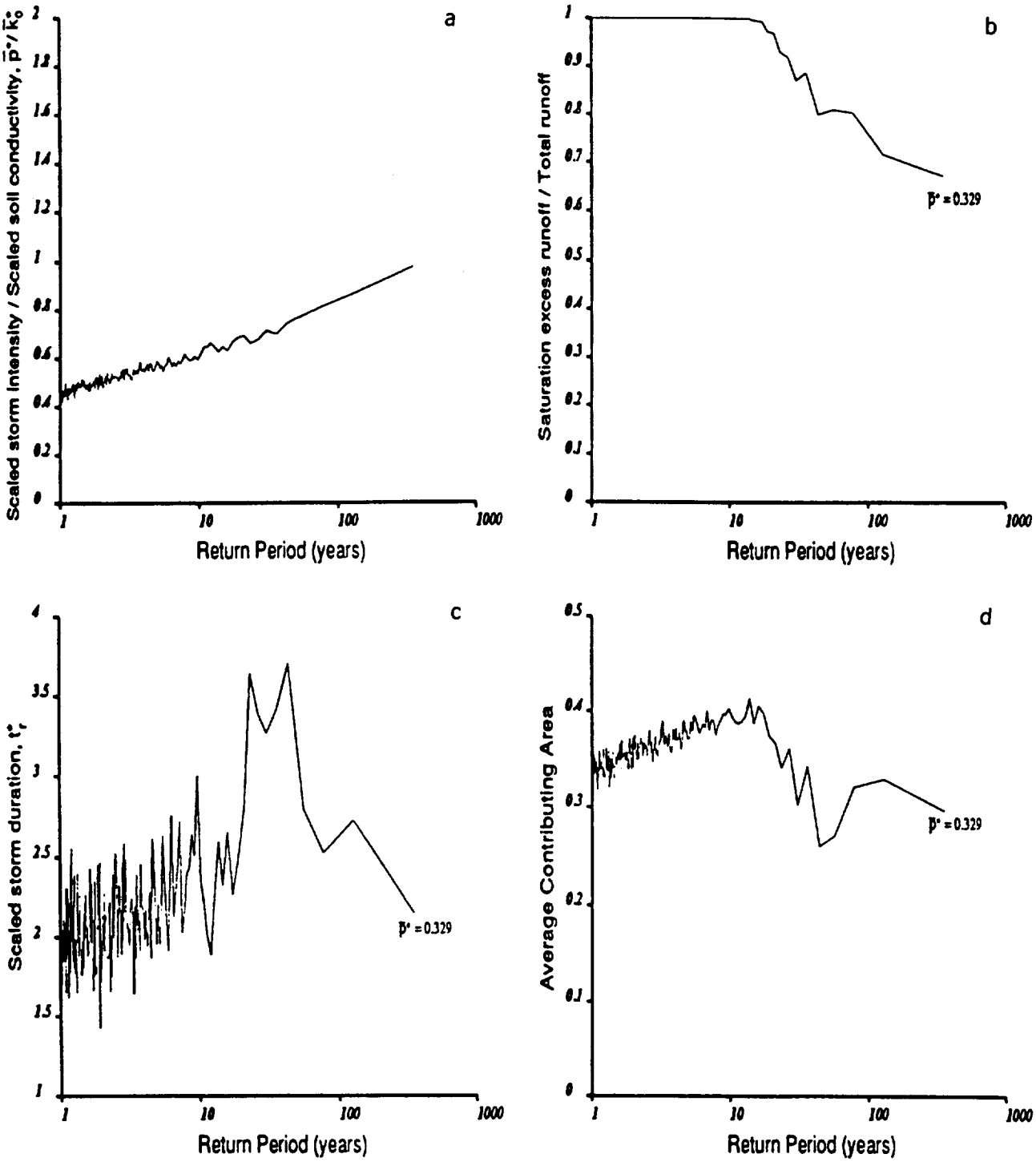

Fig. 7. Value of selected parameters of the runoff generation model corresponding to the flood discharges of the sensitivity run of $\bar{p}^* = 0.329$, plotted against the discharge return period. The parameters were averaged across the 25 realizations at each return period: (*a*) scaled storm intensity divided by scaled soil conductivity $\bar{p}^*/K_0^*$, (*b*) fraction of runoff as saturation excess runoff, (*c*) scaled storm duration t_r^*, (*d*) average contributing area, and (*e*) initial catchment wetness $\bar{Q}^*$.

conductivity. The two additional runs had values 50% larger and smaller than the base case. Figure 5 shows the results. For the case of $\bar{p}^*$ larger than the base case the average flood curve is still linear with the log of the return period but at a steeper slope. This change with respect to the base case is also exactly mimicked in the frequency curve of the rainfall-soil conductivity ratio, as can be seen in Figure 6. This clearly demonstrates the importance of both soil and rainfall characteristics in determining the basic shape of flood frequency curves. This is even more evident in the analysis of the second sensitivity curve in Figure 5.

The second sensitivity curve had $\bar{p}^*$ half of K_0^* and at first inspection the shape is somewhat confusing in that the curve appears to go towards an EV-3 shape. Upon closer inspec-

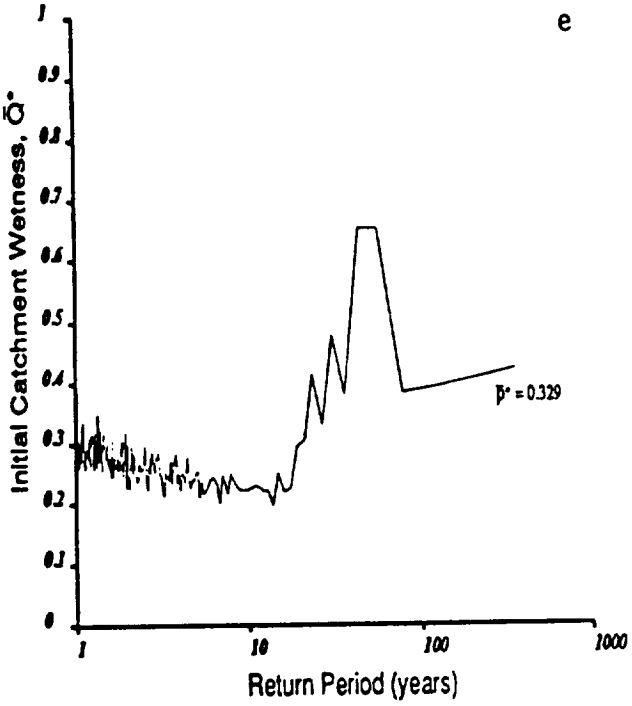

Fig. 7. (continued)

tion, this parameter set provides a catchment where different processes dominate over various parts of the flood frequency curve. For return periods less than about 20 years the flood peaks are completely dominated by saturation excess runoff with a virtual absence of any infiltration excess runoff. At high return periods (greater than 100 years) the flood frequency curve reflects the frequency curve of the rainfall-soil distribution (as shown in Figure 7*a*). The shift in the mechanisms can be clearly seen in Figure 7*b* which shows the fraction of generated runoff due to saturation excess. For low return periods, only saturation excess runoff is generated. For frequencies between 20 and 100 years there is a transition between the two curves. Since the "saturation excess" curve (low return periods) is controlled by catchment topography, there is no real reason why its slope should be the same as the "infiltration excess" flood frequency curve.

Figures 7*c*–7*e* show the frequency curves for scaled storm duration, average contributing area, and initial catchment wetness. From these results it appears that the transition

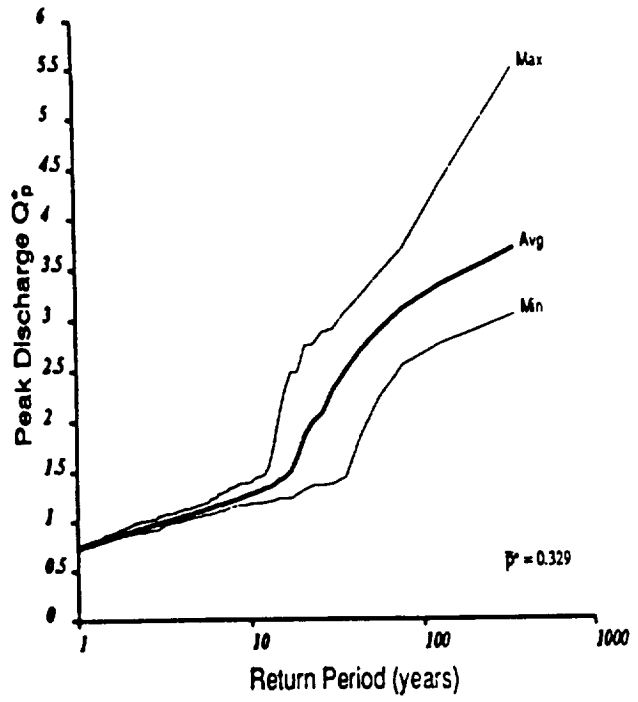

Fig. 8. The envelope, over 25 repetitions, of the flood frequency distribution for the sensitivity run, $\bar{p}^* = 0.329$.

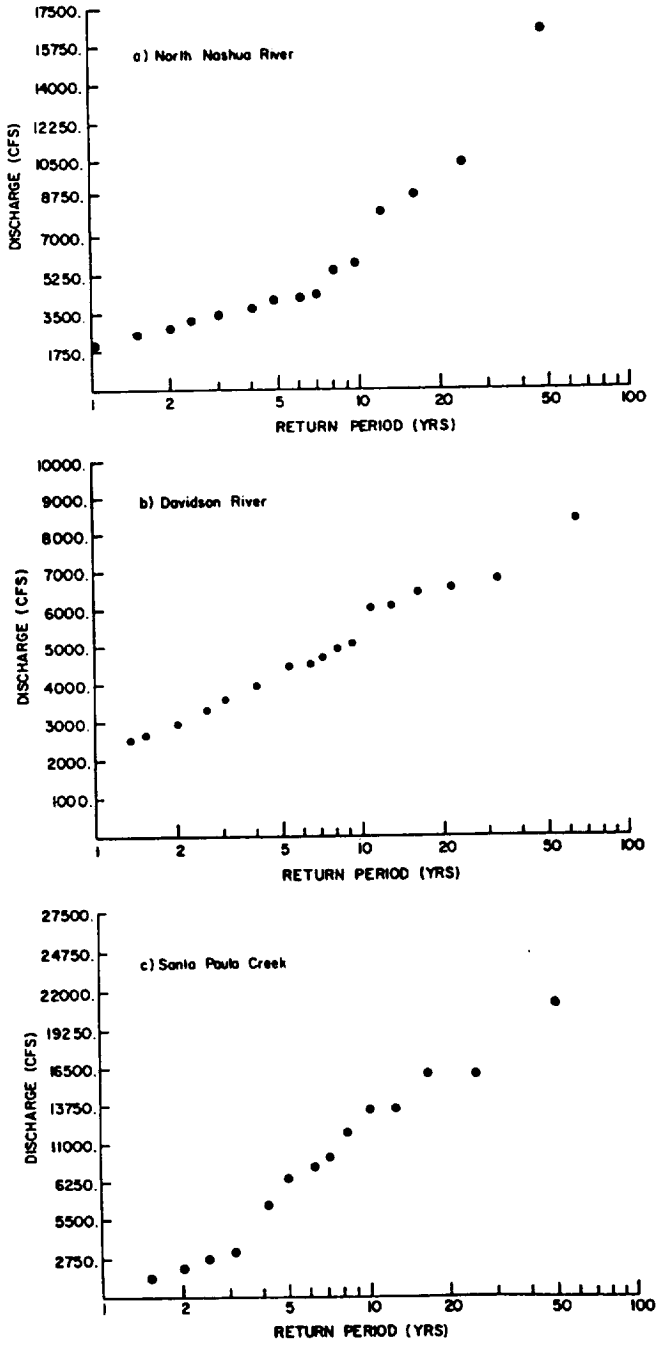

Fig. 9. Flood frequency distributions for three watersheds [after *Moughamian et al.*, [1987]: (*a*) North Nashua River, (*b*) Davidson River, and (*c*) Santa Paula Creek.

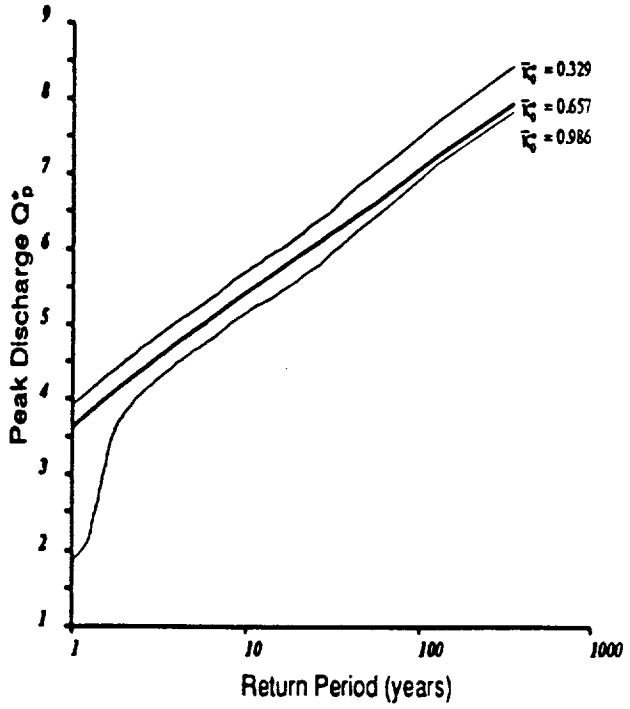

Fig. 10. The sensitivity of the flood frequency distribution to scaled soil conductivity $\bar{K}_0^*$.

from the saturation excess flood curve to the infiltration excess curve is accompanied by storms that are of long duration on a wet catchment. The uncertainty of the occurrence of this combination in actual catchments contributes to the uncertainty as to when this transition would take place.

Figure 8 shows the envelope for the 25 repetitions using $\bar{p}^* = 0.329$. The transition appears to start at a scaled peak discharge of about 1.5, with a stable (topographically controlled) saturation excess curve and a somewhat unstable transition and infiltration excess flood curve. The envelope of Figure 8 covers a significant portion of observed flood data and may help explain why flexible flood frequency curves such as the Wakeby fit data so well.

For actual vegetated catchments, with medium to deep soils having high conductivities (due to forest litter and macropores) when compared to mean storm intensities, such transitions can have an important effect on the flood frequency curve and affect the parameterization of standard flood frequency curves. Figure 9 presents the plotting positions for flood data on three catchments presented by *Moughamian et al.* [1987]; it is left to the reader to see (imagine?) the transition described here. It should be noted here that the location of the transition can vary as is seen in the sensitivity runs for the mean scaled soil conductivity which are presented next.

Mean scaled soil conductivity. In a manner similar to the analyses with mean scaled storm intensity, the mean scaled soil hydraulic conductivity was varied 50% larger and 50% smaller than the base case. Figure 10 presents the three flood frequency curves (again averaged over 25 repetitions.) The results essentially parallel the results for the storm intensity analysis. Two points should be noticed: similar changes in conductivity produce less sensitivity in the scaled peak flood discharge and the transition from saturation excess to infiltration excess occurred at lower return periods for the parameter sets used. In Figure 7*e* there was a hint that as the shift to infiltration excess dominated flood curve occurred, the influence of the catchment soil wetness decreased (be-

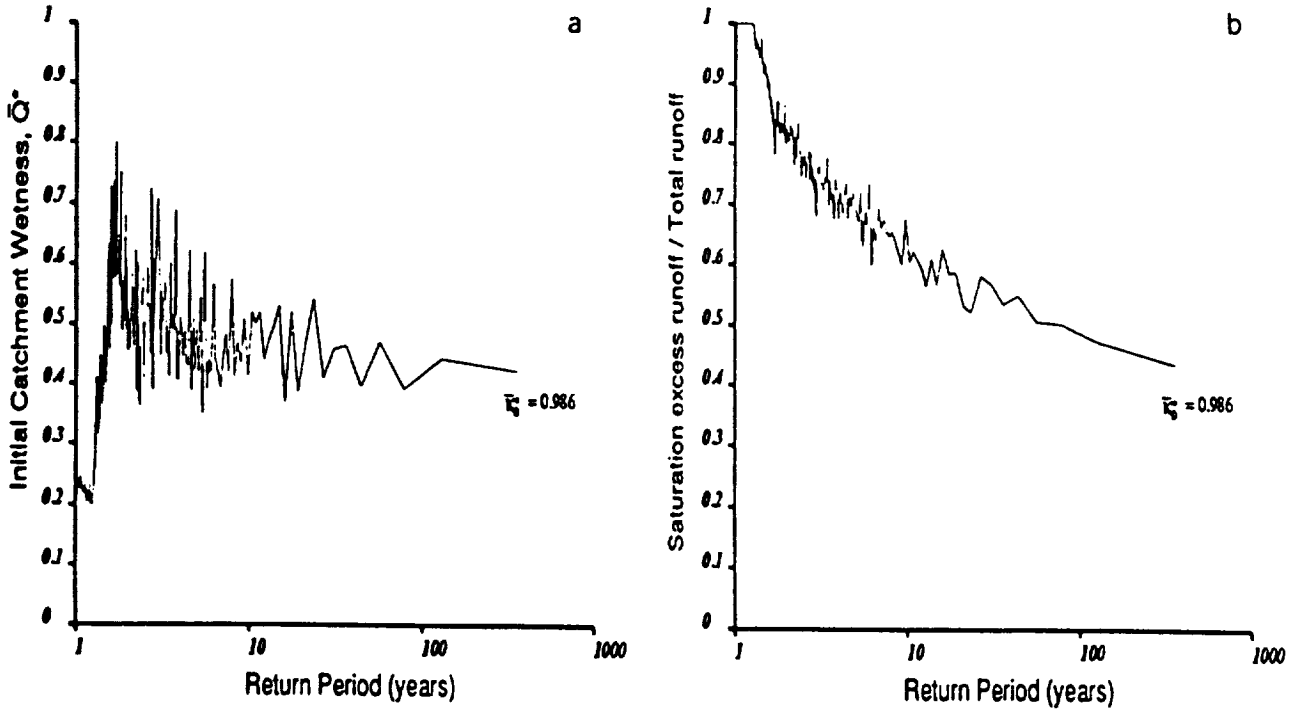

Fig. 11. Value of selected parameters of the runoff generation model corresponding to the flood discharges of the sensitivity run of $\bar{K}_0^* = 0.986$, plotted against the discharge return period. The parameters were averaged across the 25 realizations at each return period: (*a*) initial soil wetness $\bar{Q}^*$ and (*b*) fraction of runoff as saturation excess runoff.

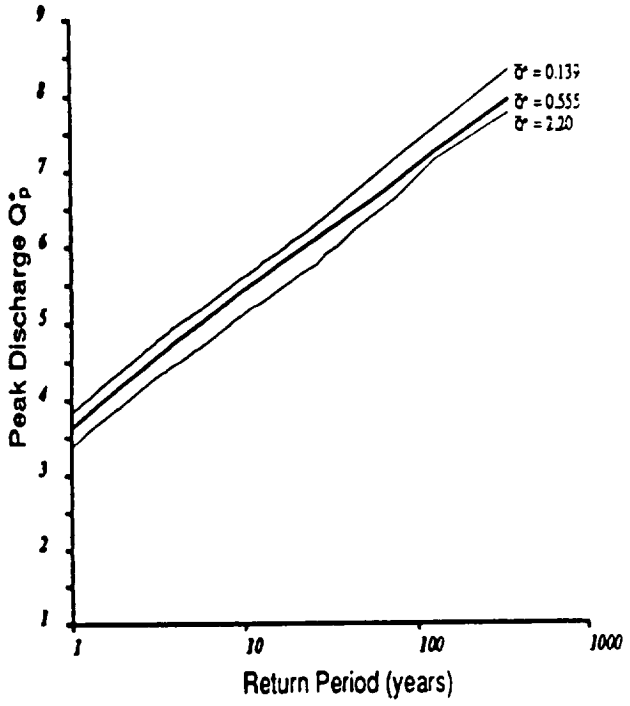

Fig. 12. The sensitivity of the flood frequency distribution to initial soil wetness $\bar{Q}^*$.

came more stable.) Figure 11*a*, which gives the initial catchment wetness for $\bar{K}_0^* = 0.986$, tends to support this. Notice the transition at about the 2- to 5-year return period. Figure 11*b* gives the fraction of runoff due to the saturation excess mechanism for the same case. Notice that this fraction varies from 1.0 at low return periods to about 0.40 at the 200 year return period.

Initial catchment wetness. The third random input in the Monte Carlo simulations was the initial catchment wetness $\bar{Q}^*$. The earlier results showed that for the base case this parameter was stable over all return periods. Therefore one would not expect to see any sensitivity of the flood frequency curve to this parameter. Figure 12 shows this.

Topographic and soil parameters. The flood frequency curve for the base case was infiltration excess dominated. The topographic and soil parameters, ϕ^* and ψ_c^* are important in the saturation excess runoff generation. The hydrogeologic parameter ψ_c^* is a measure of the depth of the soil horizon and thus the depth to the water table. Small ψ_c^* represents a deep soil horizon and a deep water table. The parameter ϕ^* is the fitting parameter for the distribution of ln $(aT_e/T_x \tan \beta)$, the soil-topographic index introduced in section 2.2. Sensitivities from the base case should, therefore, have little influence on the flood frequency curve. Figures 13 and 14 show this. Further work is being done to explore the sensitivity of "saturation excess" dominated catchments to these parameters.

Scaled catchment area. Figure 2 presented the relationship between point rainfall variances within a catchment of area A for a rainfall field having a correlation length λ_p. The ratio A/λ_p^2 was defined as A^*, the scaled catchment area. Large A^* correspond to "large" catchments in so much that the catchment is not well covered by a homogeneous rainfall field and the opposite for small values for A^*. In the base case, A^* was set to 9. Two additional sensitivity runs were performed with A^* set to 1 and 36. Figure 15 presents these results, and it is clear that catchment scale, with respect to the scale of a storm, has a significant impact on the shape of the resulting flood frequency curve. These results support

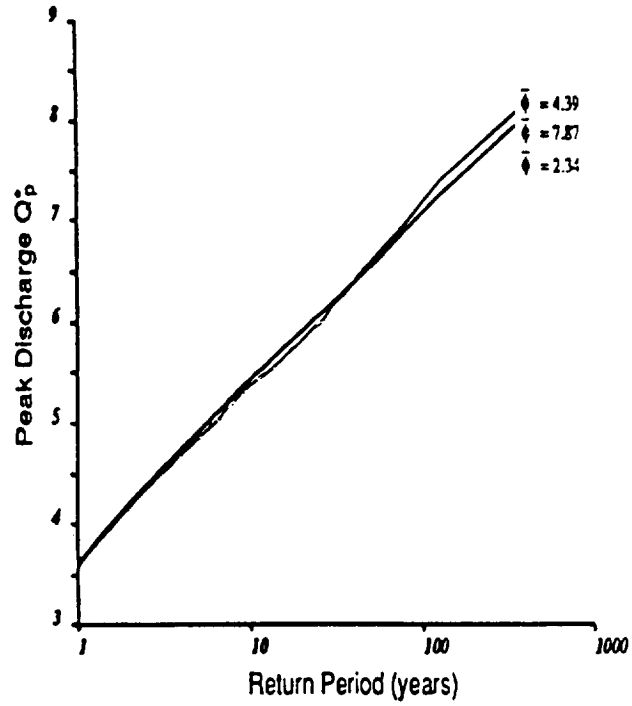

Fig. 13. The sensitivity of the flood frequency distribution to the shape parameter ϕ^* of the distribution of ln $(aT_e/T_x \tan \beta)$.

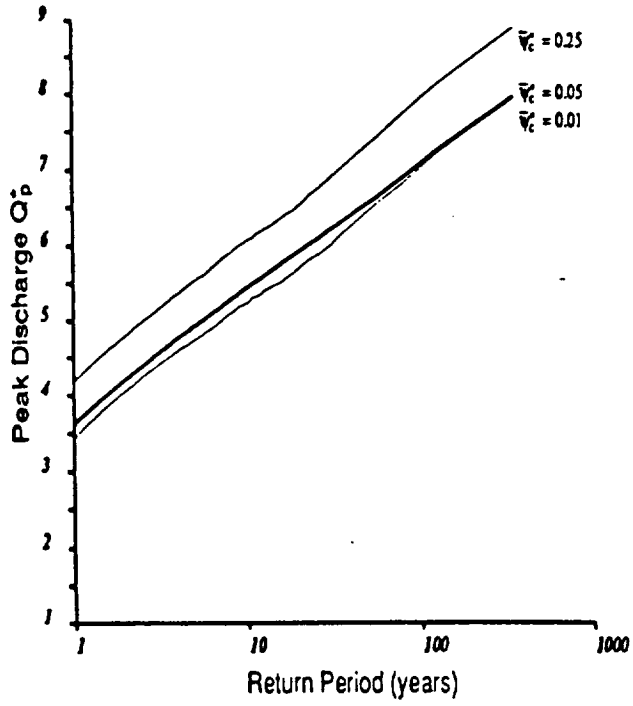

Fig. 14. The sensitivity of the flood frequency distribution to the dimensionless soil parameter ψ_c^*.

the results presented by *Hebson and Wood* [1986], which showed that the interplay between catchment and rainfall scales was critical in the shape of the derived flood frequency curve. In actual catchments the value of A^* would vary as storms of different types occurred. It is clear from these results that the interplay between scales requires further investigation.

5. Conclusions

This paper has described a derived flood frequency model using a generalized GUH and based on partial area runoff generation. The first objective of the work was to obtain a greater understanding of the interrelationships among processes that underlie the storm response of catchments of different scales and physical characteristics as reflected in flood frequency distributions. We attempted to do this here by casting the storm response model using scaled (or dimensionless) parameters and focusing on concepts of hydrologic similarity. Second, we wished to understand why previous derived flood frequency models based on the GUH have performed poorly and to make significant fundamental improvements to these methods.

In this paper, we adopted a derived flood frequency approach with a GUH-based runoff routing model, following on previous work by *Hebson and Wood* [1982], *Diaz-Granados et al.* [1984], and *Wood and Hebson* [1986]. Significant improvements were made to these methods through the following extensions: (1) use of a physically based runoff generation model that incorporates runoff generation on partial areas by both infiltration excess and saturation excess mechanisms, (2) use of a generalized GUH based on partial area generation and consistent with extension 1 above, (3) variability of antecedent moisture conditions between storms, and (4) incorporation of the effects of catchment scale both on the rainfall input distributions and in runoff generation.

It has been known for at least 50 years that the important problem in surface hydrology is determining "what to route" not "how to route." Most of the hydrology literature has focused on the latter topic. Our work demonstrates the importance of the former and the mechanism that generated the direct runoff. For example, the results of the Monte Carlo simulations have shown that for catchments dominated by infiltration excess runoff the flood frequency curve is completely defined by the distribution of the scaled rainfall-soil parameter $\bar{p}^*/K_0^*$, and the scaled catchment area A^*. This emphasizes the need for further research into rainfall distributions, especially the distributions resulting from storms of different types and scales.

For catchments where saturation excess storm production dominates at low flood return periods and infiltration excess dominates at high return periods, the results show that the resulting flood frequency distribution may appear toward an extreme value type 3 (EV-3) curve, implying a limiting flood. Such an interpretation is incorrect, and the flood frequency curve is transitioning to an infiltration excess dominated flood curve. Further research is required to understand the rainfall and catchment characteristics that define the extent of the two mechanisms. The results of the simulation imply that the transition part of the flood frequency curve is produced by long storms of medium intensity on initially wet catchments.

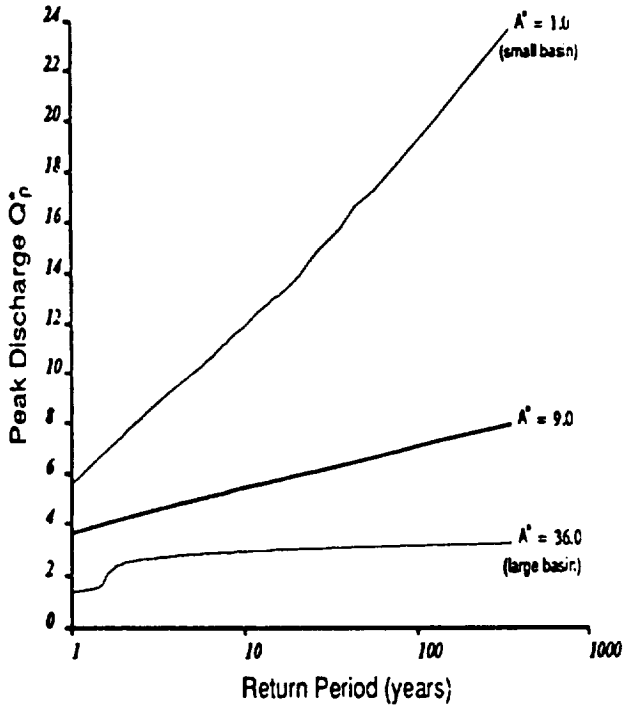

Fig. 15. The sensitivity of the flood frequency distribution to the scaled catchment area A^*.

The analysis of catchment similarity by means of the kinds of sensitivity analyses carried out in this work have yielded valuable insights into the interrelationships between various processes at the catchment scale. These can help in the development of simple physically based models of catchment behavior. The work in this paper can be extended in a number of directions. The first extension would be to augment the rainfall model to include temporal variability as well as the spatial variability that was considered. Further, the Monte Carlo simulations should randomize storm scale (through A^*) and correlate storm scale with storm characteristics to consider cyclonic and convective storms. The second extension is to expand the range of the Monte Carlo simulations by starting the base case where the mixed mechanisms occurred (Figure 8). This would allow one to explore the sensitivities with respect to those soil and catchment parameters which were not interesting for the base case presented here (e.g., Figures 12–14).

Finally, the flood frequency model developed in this paper needs to be applied to some actual catchments before one can be sure that the conclusions made in this paper correctly explain the flood data presented in Figure 9.

Appendix A

Topography. It is assumed that $\ln (aT_e/T_x \tan \beta)$ follows a three-parameter gamma distribution with location parameter μ, scale parameter χ^*, and shape parameter ϕ^* and having mean $\lambda = \mu + \phi^*\chi^*$.

Soil. The soil hydraulic properties are expressed in terms of the Brooks-Corey relationship with parameter θ_r, θ_s, ψ_c, and B [see *Sivapalan et al.*, [1987].

Hydrogeology. $Q(0)$ is the base flow from the catchment at the beginning of the storm and Q_0 and f are catchment hydrogeologic parameters and can be estimated by the

analysis of the baseflow recession curve just prior to the storm.

The following dimensionless parameters can then be defined:

$$\bar{p}^* = \frac{\bar{p}\tau_r}{\psi_c(\theta_s - \theta_r)}$$

$$\bar{K}_0^* = \frac{\bar{K}_0\tau_r}{\psi_c(\theta_s - \theta_r)}$$

$$\psi_c^* = \frac{\psi_c f}{\lambda - \mu}$$

$$Q^* = -\frac{\ln [Q(0)/Q_0]}{\lambda - \mu}$$

$$\phi^*$$

C_{vp}, C_{vK}, and B complete the list of dimensionless similarity parameters.

APPENDIX B

The variables θ_i denote the proportion of the hillslopes that drain directly into streams of order i. The expressions for θ_i in terms of Horton order ratios are

$$\theta_1 = R_B^2/R_A^2 \tag{B1}$$

$$\theta_2 = \frac{R_B}{R_A} - \frac{R_B(R_B^2 + 2R_B - 2)}{R_A^2(2R_B - 1)} \tag{B2}$$

$$\theta_3 = 1 - \frac{R_B}{R_A} - \frac{R_B(R_B^2 - 3R_B + 2)}{R_A^2(2R_B - 1)} \tag{B3}$$

APPENDIX C

For the following A_c/A condition

$$\frac{A_c}{A} \le \theta_2 + \theta_3 - \frac{1}{R_{SG}} \sum_{i=2}^{3} \theta_i R_{SG}^{i-1}$$

The ratios of contributing area for different orders are

$$\frac{A_{c_1}^*}{A_c} = \frac{A_{c_2}^*}{A_c} = 0 \qquad \frac{A_{c_3}^*}{A_c} = 1$$

For the following A_c/A condition

$$\theta_2 + \theta_3 - \frac{1}{R_{SG}} \sum_{i=2}^{3} \theta_i R_{SG}^{i-1} \le \frac{A_c}{A} \le 1 - \sum_{i=1}^{3} \theta_i R_{SG}^{i-1}$$

The ratios of contributing area for different orders are

$$\frac{A_{c_1}^*}{A_c} = 0 \qquad \frac{A_{c_i}^*}{A_c} = \frac{\theta_i}{(A_c/A)} \left\{ 1 - \frac{R_{SG}^{i-1}(\theta_2 + \theta_3 - A_c/A}{\sum_{i=2}^{3} \theta_i R_{SG}^{i-1}} \right\}$$

$$i = 2, 3$$

For the following A_c/A condition

$$\frac{A_c}{A} \ge 1 - \sum_{i=1}^{3} \theta_i R_{SG}^{i-1}$$

The ratios of contributing area for different orders are

$$\frac{A_{c_i}^*}{A_c} = \frac{\theta_i}{(A_c/A)} \left\{ 1 - \frac{R_{SG}^{i-1}(1 - A_c/A)}{\sum_{i=1}^{3} \theta_i R_{SG}^{i-1}} \right\} \qquad i = 1, 2, 3$$

APPENDIX D

The relationships between the parameters for the third order generalized GUH (equation (22)) and Π_i, the number of particles of runoff generated on all hillslopes draining into streams of order i are as follows:

$$B = -\Pi_1 A_1 R_L^2 \tag{D1}$$

$$C = -(\Pi_1 A_2 + \Pi_2 A_5) R_L \tag{D2}$$

$$D = \Pi_1(A_3 R_L^2 - 2A_4) + \Pi_2(A_6 R_L^2 - 2A_7) \tag{D3}$$

$$E = -2(\Pi_1 A_3 + \Pi_2 A_6 + \Pi_3 A_8) R_L^2 \tag{D4}$$

where

$$A_1 = \frac{4(P_{13}R_L - 1)}{(1 - R_L)(2 - R_L^2)^2} \tag{D5a}$$

$$A_2 = \frac{4P_{12}R_L}{(1 - R_L)(2 - R_L)^2} \tag{D5b}$$

$$A_3 = \frac{2(R_L^2 - 2P_{13}R_L)}{R_L(2 - R_L)(R_L^2 - 2)} \tag{D5c}$$

$$A_4 = [8P_{13}R_L^2(2 - R_L^2)(R_L - 2) - (12 - 4R_L - 4R_L^2 + R_L^3)] \cdot (4R_L^3 - 8P_{13}R_L^2)]/[4(R_L^2 - 2)^2(R_L - 2)^2]^{-1} \tag{D5d}$$

$$A_5 = -\frac{4}{(2 - R_L)^2} \qquad A_6 = \frac{2}{R_L(2 - R_L)} \tag{D5e}$$

$$A_7 = \frac{R_L(4 - R_L)}{(R_L - 2)^2} \qquad A_8 = -2/R_L^2 \tag{D5f}$$

and

$$P_{12} = \frac{R_B^2 + 2R_B - 2}{2R_B^2 - R_B}$$

$$P_{13} = \frac{R_B^2 - 3R_B + 2}{2R_B^2 - R_B} \tag{D6}$$

Acknowledgments. The work presented in this paper was supported in part by NASA Grants NAG-5-491 and NAG-1392, and the U.S. Department of the Interior (USGS) grant 14-08-0001-G1138. This research support is gratefully acknowledged.

REFERENCES

Beven, K., Runoff production and flood frequency in catchments of order n: An alternative approach, in *Scale Problems in Hydrol-*

ogy, edited by I. Rodriguez-Iturbe, V. K. Gupta, and E. F. Wood, pp. 107–132, D. Reidel, Hingham, Mass., 1986.

Beven, K., and E. F. Wood, Catchment geomorphology and the dynamics of runoff contributing areas, *J. Hydrol.*, *65*, 139–158, 1983.

Diaz-Granados, M. A., J. B. Valdes, and R. L. Bras, A physically based flood frequency distribution, *Water Resour. Res.*, *20*(7), 995–1002, 1984.

Dunne, T., Field studies of hillslope flow processes, in *Hillslope Hydrology*, edited by M. J. Kirkby, pp. 227–294, Chichester, 1978.

Eagleson, P. S., Dynamics of flood frequency, *Water Resour. Res.*, *8*(4), 878–898, 1972.

Freeze, R. A., Streamflow generation, *Rev. Geophys.*, *12*(4), 627–647, 1974.

Gupta, V. K., E. Waymire, and I. Rodriguez-Iturbe, On scales, gravity and network structure in basin runoff, in *Scale Problems in Hydrology*, edited by I. Rodriguez-Iturbe, V. K. Gupta, and E. F. Wood, pp. 159–184, D. Reidel, Hingham, Mass., 1986.

Hebson, C., and E. F. Wood, A derived flood frequency distribution using Horton order ratios, *Water Resour. Res.*, *18*(5), 1509–1518, 1982.

Hebson, C. S., and E. F. Wood, A study of scale effects in flood frequency response, in *Scale Problems in Hydrology*, edited by I. Rodriguez-Iturbe, V. K. Gupta, and E. F. Wood, pp. 133–158, D. Reidel, Hingham, Mass., 1986.

Henderson, F. M., Some properties of the unit hydrograph, *J. Geophys. Res.*, *68*(16), 4785–4793, 1963.

Horton, R. E., Erosional development of streams and their drainage basins: Hydrophysical approach to quantitative morphology, *Geol. Soc. Am. Bull.*, *56*, 275–370, 1945.

Morisawa, M. E., Quantitative geomorphology of some watersheds in the Appalachian Plateau, *Geol. Soc. Am. Bull.*, *73*, 1025–1046, 1962.

Moughamian, M. S., D. B. McLaughlin, and R. L. Bras, Estimation of flood frequency: An evaluation of two derived distribution procedures, *Water Resour. Res.*, *23*(7), 1309–1319, 1987.

Philip, J. R., Theory of infiltration, 4, Sorptivity and algebraic infiltration equations, *Soil Sci.*, *84*, 257–264, 1957.

Rodriguez-Iturbe, I., and J. B. Valdes, The geomorphologic structure of hydrologic response, *Water Resour. Res.*, *15*(6), 1409–1420, 1979.

Sivapalan, M., Scale problems in rainfall, infiltration, and runoff production, Ph.D. dissertation, 271 pp., Dep. Civ. Eng., Princeton Univ., Princeton, N. J., 1986.

Sivapalan, M., and E. F. Wood, A multidimensional model of nonstationary space-time rainfall at the catchment scale, *Water Resour. Res.*, *23*(7), 1289–1299, 1987.

Sivapalan, M., K. Beven, and E. F. Wood, On hydrologic similarity, 2, A scaled model of storm runoff production, *Water Resour. Res.*, *23*(12), 2266–2278, 1987.

Strahler, A. N., Equilibrium theory of erosional slopes approached by frequency distribution analysis, *Am. J. Sci.*, *248*, 673–696, 800–814, 1950.

Surkan, A. J., Synthetic hydrographs: Effects of network geometry, *Water Resour. Res.*, *5*(1), 112–128, 1969.

Wood, E. F., An analysis of the effects of parameter uncertainty in deterministic hydrologic models, *Water Resour. Res.*, *12*(5), 925–932, 1976.

Wood, E. F., and C. S. Hebson, On hydrologic similarity, 1, Derivation of the dimensionless flood frequency curve, *Water Resour. Res.*, *22*(11), 1549–1554, 1986.

K. J. Beven, Institute of Environmental and Biological Sciences, University of Lancaster, Bailrigg, Lancaster LA1 4YQ, England.

M. Sivapalan, Centre for Water Research, University of Western Australia, Nedlands, Western Australia 6009, Australia.

E. F. Wood, Water Resources Program, Department of Civil Engineering and Operations Research, Princeton University, Princeton, NJ 08544.

(Received January 28, 1988;
revised July 31, 1989;
accepted August 3, 1989.)

SIMILARITY AND SCALE IN CATCHMENT STORM RESPONSE

Eric F. Wood
Water Resources Program
Princeton University
Princeton, New Jersey

Murugesu Sivapalan
Centre for Water Research
University of Western Australia
Nedlands

Keith Beven
Centre for Research
on Environmental Systems
University of Lancaster, Lancaster, England

Abstract. Until recently, very little progress had been made in understanding the relationship between small-scale variability of topography, soil, and rainfalls and the storm response seen at the catchment scale. The work reviewed here represents the first attempt at a systematic theoretical framework for such understanding in the context of surface runoff generation by different processes. The parameterization of hydrological processes over a range of scales is examined, and the concept of the "representative elementary area" (REA) is introduced. The REA is a fundamental scale for catchment modeling at which continuum assumptions can be applied for the spatially variable controls and parameters, and spatial patterns no longer have to be considered explicitly. The investigation of scale leads into the concept of hydrologic similarity in which the effects of the environmental controls on runoff generation and flood frequency response be investigated independently of catchment scale. The paper reviews the authors' initial results and hopefully will motivate others to also investigate the issues of hydrologic scale and similarity.

1. INTRODUCTION

The way in which storm rainfall reaching the ground surface causes a response in the flow of a river is a fascinating but most difficult area of study. Scientists, as well as artists and writers, have long been inspired to examine and speculate upon the flow of water both at the surface in streams and rivers and underground. Early measurements in the 17th century by the French physicists Edme Mariotte and Pierre Perrault and by the English astronomer Edmund Halley confirmed the basic concepts of the hydrological cycle, and in particular that rainfalls over a catchment area are sufficient to maintain continuous streamflows even during dry periods. Over the next two centuries, significant advances were made in the understanding of hydrological processes, notably Dalton's work on evaporation [*Dalton*, 1802], Darcy's law of porous media flow [*Darcy*, 1856], Manning's work in open channel flow [*Manning*, 1891], Richards' development of the unsaturated flow equation [*Richards*, 1931], and Horton's work in infiltration and runoff production [*Horton*, 1933] and river basin geomorphology [*Horton*, 1945].

These, and other major figures in hydrology, have contributed much toward our understanding of catchment storm responses, yet recent work suggests that there are still many problems left to explore. The problem is, in some ways, deceptively simple. We know that in any particular storm only part of the incident rainfall reaches the stream to become discharge during the (often rapid) rise and fall of the river known as the storm hydrograph. The remainder is absorbed into the soil (referred to as infiltration) and may be returned back to the atmosphere as evapotranspiration or contribute to the stream as a subsurface flow over an extended period of time. It is therefore important to be able to estimate the proportion of the rainfall equivalent to the volume of the stream hydrograph. This proportion is commonly called the "effective rainfall." We also know that the flow processes within the catchment have both retardation and diffusive or filtering effects, so that it is also important to know the time transformation between effective rainfall and the discharge hydrograph (see Figure 1).

Quite apart from the pure scientific interest of understanding the flow processes, being able to predict catchment storm responses is of considerable practical interest in the proper management of water resources and estimation of risk to life and property during major flood events. Hydrologists have not shirked from the requirement for quantitative prediction of catchment responses. Today there is a plethora of operational computer models available, few of which reflect more than a cursory understanding of the flow processes involved. Perhaps the most widely used model in engineering hydrology remains

8755-1209/90/89RG-01615 $05.00

Reviews of Geophysics, 28, 1 / February 1990
pages 1–18
Paper number 89RG01615

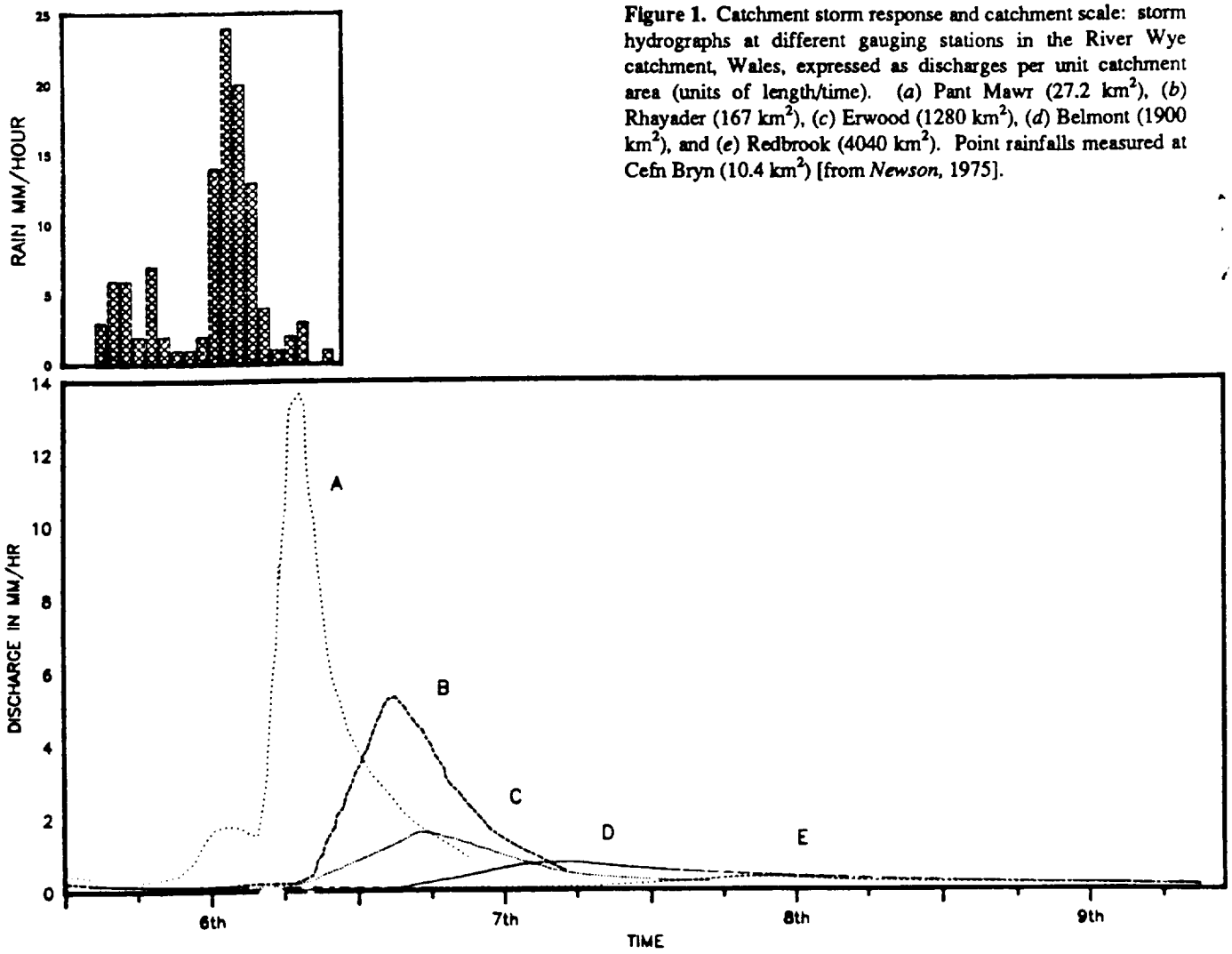

Figure 1. Catchment storm response and catchment scale: storm hydrographs at different gauging stations in the River Wye catchment, Wales, expressed as discharges per unit catchment area (units of length/time). (*a*) Pant Mawr (27.2 km^2), (*b*) Rhayader (167 km^2), (*c*) Erwood (1280 km^2), (*d*) Belmont (1900 km^2), and (*e*) Redbrook (4040 km^2). Point rainfalls measured at Cefn Bryn (10.4 km^2) [from *Newson*, 1975].

the unit hydrograph concept, developed by *Sherman* [1932] and often combined with Horton's concept that storm response is due primarily to surface runoff generated when rainfall rates exceed the infiltration capacity of the soil. The unit hydrograph represents a simple linear transfer function, assumed constant for a particular catchment, that provides the time transformation between the estimated effective rainfall and the resulting storm hydrograph in the stream channel. Thus these concepts have the two elements, a loss function for estimating effective rainfall and a time transformation, that are required to predict catchment storm response.

The difficulty in using the unit hydrograph approach lies primarily in the prediction of the effective rainfall. The proportion of storm rainfall that is equivalent to the volume of the storm hydrograph depends on many factors, notably the antecedent moisture status of the catchment, the nature of the soils in the catchment, and the storm rainfall intensities. As *Freeze* [1974, p. 627] has pointed out,

> . . . the complexity of this response tended to promote the development of generalized regional analyses that used entire drainage basins as black box response units. This type of hydrologic prediction model treats the rainfall-runoff relationship in an empirical statistical manner without considering the causal mechanisms. This approach has great power in satisfying the needs of engineering design but does not provide any insight into the internal mechanisms of the hydrologic cycle.

Ideally, a prediction of the effective rainfall should be based on a proper understanding of the processes involved, but study of these processes has revealed patterns of real complexity. During the International Hydrological Decade (1964–1974) there was a burst of activity aimed at a better understanding of hydrological processes through field experimentation. The focus of much of this research was concerned with the generation of streamflow in headwater tributaries during both storm and interstorm periods. This research is reviewed by *Freeze* [1974] and is more fully described by *Kirkby* [1978]. The most significant

development resulting from this work was a reevaluation of the Hortonian concept of storm runoff as rainfall in excess of infiltration capacity of the soil (this type of runoff is often referred to as infiltration excess runoff generation).

Runoff generation is now known to result from a complexity of mechanisms, as shown in Figure 2. During any particular storm, different mechanisms may generate runoff from different parts of a catchment. Surface runoff from these (partial) contributing areas may be generated by either the infiltration excess mechanism on low-permeability soils, or from rainfall on areas of soil saturated by a rising water table even in high-permeability soils (referred to as saturation excess runoff generation). These saturated contributing areas expand and contract during and between storm events. It is also now known, as a result of using natural tracers to determine the source of storm discharges in streams, that in many catchments a significant proportion of the storm hydrograph is derived from subsurface water that is displaced from soil and groundwater by the incoming rainfall as subsurface stormflow.

Runoff generation has thus been revealed to be a highly nonlinear and spatially variable process, involving both surface and subsurface flow pathways. It is clear that predictions of runoff generation need to deal with the spatial patterns of antecedent moisture conditions, soil hydraulic characteristics, and rainfall intensities, with the expectation that under some conditions these patterns will be highly variable in space and time. And yet, many hydrological models continue to be based on a point scale model of catchment response, with the only recognition of areal variability being a multiplication by the catchment area. In fact, if the rainfall and discharge variables are expressed in units of volume or depth per unit area then even this last step is not necessary.

Overall, very little progress has been made in relating the small-scale complexity that is apparent from observations and experimental studies of flow processes to the relative simplicity (loss function and time transformation)

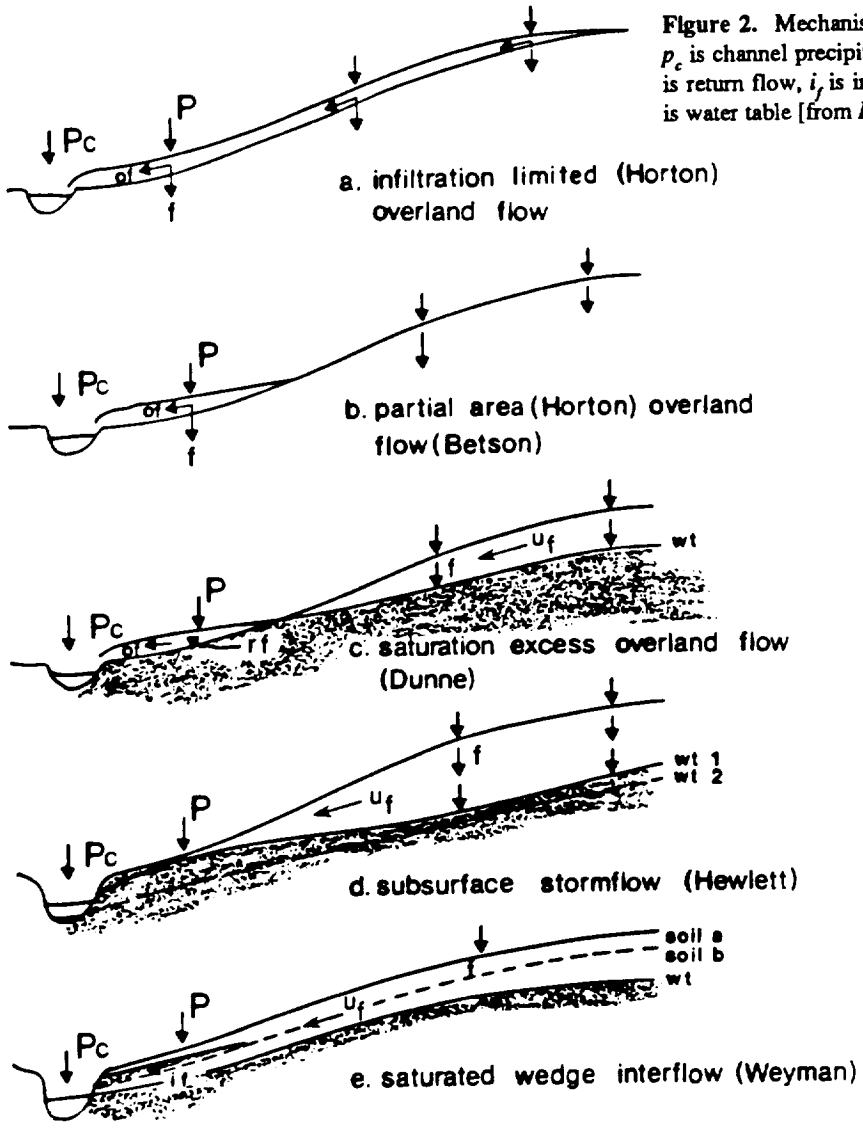

Figure 2. Mechanisms of runoff production: p is precipitation, p_c is channel precipitation, f is infiltration, of is overland flow, r_f is return flow, i_f is interflow, u_f is unsaturated zone flow, and wt is water table [from *Beven*, 1986*b*].

required for practical predictions at the catchment scale (see, for example, *Pilgrim* [1982]). It is this relationship that is the subject of this review. *Dooge* [1982] posed what we feel is a central issue facing hydrology today: What is the effect of spatial variability on the parameterization of hydrologic processes at a range of scales? As pointed out by *Gupta et al.* [1986, p. vii],

> The scale problems in hydrology stem from the recognition that the mathematical relationships describing the physical relationships are manifest at different space-time scales. The broad scientific problem then is to identify and formulate suitable relationships at the scales of practical interest, test them experimentally and seek consistent analytical connections between these relationships and those known at other scales.

The research reviewed in this paper represents the very first attempts to investigate the effects of spatial variability and scale on the quantification and parameterization of catchment storm response. As will be seen, the research to date has concentrated on the dynamic nature of surface runoff generation during storm events, perhaps the most intriguing and central problem in hydrology for both theorist and field hydrologist alike. Section 2 of this paper presents a semidistributed catchment model that incorporates the major mechanisms of runoff generation. The model takes into account the variability of topography, soils, and rainfall inputs in a physically realistic but computationally efficient way that has allowed a wide range of numerical experiments to be performed. As a result of these experiments, in section 3 the influence of spatial variability and scale are addressed in terms of a representative elementary area (REA) concept along with a macroscale model that is valid at scales larger than the REA. The first attempt at a theory of catchment hydrological similarity over a range of scales is presented for these models in section 4. Section 5 looks at similarity and scale within the context of flood frequency analysis with some results for idealized catchments. The results are drawn primarily from the papers of *Wood and Hebson* [1986], *Sivapalan et al.* [1987], *Beven et al.* [1988], *Wood et al.* [1988*a*], and *Sivapalan et al.* [1989]. Related papers included those of *Beven* [1986*a*, *b*], *Hebson and Wood* [1986], and *Sivapalan and Wood* [1986].

We feel that the first steps have now been taken toward a theoretical understanding of the role of small-scale variability and complexity in contributing to the responses at different catchment scales. The results have implications for a wide range of hydrological problems, including flood frequency analysis and understanding differences in the response of catchments within the same geographical region. In addition, the research has particular importance for the formulation of an appropriate hydrological land surface parameterization in climate modeling where it is necessary to have models at the global circulation model (GCM) grid scale that are consistent with the variability of hydrological processes at the subgrid scale. The sensitivity of GCM results to this lower boundary condition provided by the land surface hydrology may be especially important in studies of the hydrological impacts of climate change [*Environmental Protection Agency*, 1989]. We expect that the results presented will be refined and improved but hope that the work is a pointer to a productive direction for research that will be central to the progress of hydrology.

2. A MODEL OF RUNOFF PRODUCTION BASED ON CATCHMENT TOPOGRAPHY

A number of seminal field studies during the International Hydrological Decade (for example, those by *Betson* [1964], *Hewlett and Hibbert* [1963, 1967], *Hewlett and Nutter* [1970], *Dunne and Black* [1970], and *Weyman* [1970]) had a significant impact in the rethinking of runoff generation as perceived in the Horton infiltration excess overland flow–unit hydrograph approach. This work led to an increasing recognition that subsurface flows play a very important part in the redistribution of soil moisture between storm events in setting up the initial wetness conditions that govern streamflow generation for the subsequent rain event. It was also realized that for areas of relatively shallow soil, a dominant control on these subsurface flows is the local topography. In particular, areas of higher antecedent wetness, and therefore greater likelihood of generating runoff, should be expected in areas of convergent flow in plan and concave slopes in profile such as are commonly found in hillslope hollows and above the heads of the smallest ("first order") stream channels.

However, there are few hydrological models that take explicit account of the variability of catchment topography and soil characteristics. One approach that does was initiated by *Freeze and Harlan* [1969] and is based on partial differential equations describing surface and subsurface flow processes. These models are now being implemented, with some simplifications, at the catchment scale [e.g., *Bathurst*, 1986; *Beven et al.*, 1987]. The flow equations must be solved numerically, using finite element or finite difference approximations, which at the catchment scale involves a very large number of calculation nodes and large matrices to be solved for many time steps. A recent study of a small headwater catchment involving a 12,000-node simulation over a period of 150 days required a run time of 50 hours on a Cyber 205 supercomputer [see *Binley and Beven*, 1989]. Such a computational burden has generally limited the application of these detailed models to single storm simulations and together with the number of parameter values incorporated into distributed models, makes calibration to real catchments (which may involve multiple runs) very difficult.

There are other problems with this approach. While these models have a firm theoretical foundation, the

physical theory on which they are based is theory for laboratory systems with well-defined boundary conditions. For real catchment systems with heterogeneous small-scale features like variable inputs at ground level due to the effects of a vegetation cover, preferential flow pathways through the soil due to the effects of soil structure and rills and microtopography affecting surface flow, there is no assurance that the same equations should be good descriptors of flow processes in the field, or that the parameters measured in the field will have values that are appropriate at the model grid or element scale within a particular model structure (see discussion by *Beven* [1989]).

However, since soil and topography are thought to be primary controls on water flows, and the topographic form of a catchment is usually readily available for a particular catchment from maps or remote sensing techniques, it should be possible to formulate a model, computationally simpler than those described above, but complex enough to retain the essence of the controls of soil, vegetation, and topography on runoff production. With this aim, a decade ago *Beven and Kirkby* [1979] developed a model (TOPMODEL) for transforming rainfall into runoff that utilizes a spatially variable topographic index to predict the occurrence and extent of saturated areas which generate surface runoff and subsequently streamflow. They provided a theory for local hydrological similarity in which all locations within the catchment having the same value of the topographic index were assumed to respond in a similar manner to similar inputs. The calculation of the topography index using maps was very time consuming and only recently, with the advances in interactive graphics and increasing availability of digital elevation models (DEMs), can it be calculated routinely [*Band*, 1986; *Band and Wood*, 1988]. The availability of DEMs and remotely sensed data (from Système Probatoire d'Observation de la Terre (SPOT), Thematic Mapper (TM), and Synthetic Aperture Radar (SAR)) at the 20–50-m scale, allows for a distributed version of TOPMODEL where the spatial variability in topography, soils and vegetation can be properly represented.

In what follows we describe a version of the model that predicts patterns of soil saturation and their relationship to both saturation excess and infiltration excess surface runoff generation making use of information on the variability of topography and soil characteristics. For simplicity in this initial study of scale and similarity effects, we concentrate on the prediction of surface runoff generation rates and volumes only during individual storm periods. The routing of the generated runoff over hillslopes and along stream channels is not included here but has been treated elsewhere in related work [see *Beven*, 1986*a*, *b*; *Wood et al.*, 1988*a*; *Sivapalan et al.*, 1989]. Reinfiltration of surface runoff on downslope unsaturated areas is also not treated explicitly. A final simplification is that subsurface storm runoff production and subsurface flows during interstorm periods are not explicitly treated, although the importance of subsurface stormflow is recognized and its prediction is possible within the TOPMODEL framework [*Beven*, 1986*a*, *b*].

2.1. Model of Saturation Excess Runoff Production

The model starts from the premise that prior to a storm the antecedent water table within the soil can be represented as the result of a steady average vertical recharge rate r so that at any location i, downslope flow q_i will be given by

$$q_i = ar \tag{1}$$

We also assume there is relatively shallow soil so that the water table will be nearly parallel to the soil surface resulting in the local hydraulic gradient being close to the local slope angle, tan β, and that the transmissivity of the soil is an exponential function of depth, so that the downslope flow rate is also given by

$$q_i = T_i \exp(-fz_i) \tan \beta \tag{2}$$

Here f is a parameter, assumed constant in the catchment, that describes the rate of decline of soil transmissivity with depth. Combining (1) and (2) and integrating over the catchment area to obtain a catchment average depth to the water table, it can be shown that the relationship between this average depth $\bar{z}$ and a local depth z_i is given by

$$z_i - \bar{z} = \frac{1}{f}\left[\lambda - \ln\left(\frac{aT_e}{T_i \tan \beta}\right)\right] \tag{3}$$

where ln (T_e) is the areal average value of ln (T_i) across the catchment and λ is the expected value of the topographic variable ln $(a/\tan \beta)$ which is a constant for a particular catchment. *Beven* [1982] has shown that the assumption that soil permeabilities show an exponential decline with depth is reasonable for a wide range of soil types. A very similar approach to predicting areas of saturated soil has been derived independently by *O'Loughlin* [1981, 1986] for more general profiles of saturated hydraulic conductivity, but without some of the analytical advantages of the exponential assumption. Equation (3) implies that all locations in the catchment with the same value of the combined topographic-soil index $aT_e/(T_i \tan \beta)$ will have the same relationship between local depth to water table and the mean depth, i.e., it is an index of local hydrological similarity. Inspection of this equation shows that locations with high values of the topographic-soil index relative to the catchment constant λ will have smaller water table depths and will consequently have a greater propensity to saturate to the surface. In fact, for any particular value of $\bar{z}$, knowledge of the pattern of soil and topography and therefore of the topographic-soil index, allows prediction of those areas where $z_i \leq 0$ and therefore the saturated contributing area. In fact, we should strictly define the area of saturation where $z_i \leq \psi_c$, where ψ_c is the depth of the capillary fringe which is the depth of soil above the

water table that is saturated but within which water is held at a negative capillary potential. Prediction of the changes through time of $\bar{z}$ then allows the dynamic expansion and contraction of this contributing area to be modeled.

We may separate the topographic and soil contributions to the combined index by rewriting (3) as

$$f(z_i - \bar{z}) = -[\ln(a/\tan\beta) - \lambda] + [\ln(T_i) - \ln(T_e)] \quad (4)$$

The variations in the catchment of the topographic variable $(a/\tan\beta)$ and the soil transmissivity T_i may both be represented as distribution functions. Figure 3 shows the cumulative distribution functions for the Kings Creek catchment in Kansas. The right-hand side of (4) is then clearly the sum of two deviations of the local values of ln $(a/\tan\beta)$ and T_i from their catchment mean values, whereas the left-hand side represents the local deviation in water table depth from the catchment mean value scaled by the parameter f. Reference to Figure 3 shows that the expected deviations in the topographic variable are far greater than for the local values of transmissivity. Thus variability in the transmissivity will have a relatively small effect on the distribution of the combined index and consequently on the predicted patterns of water table depths and saturated contributing area for a given value of z.

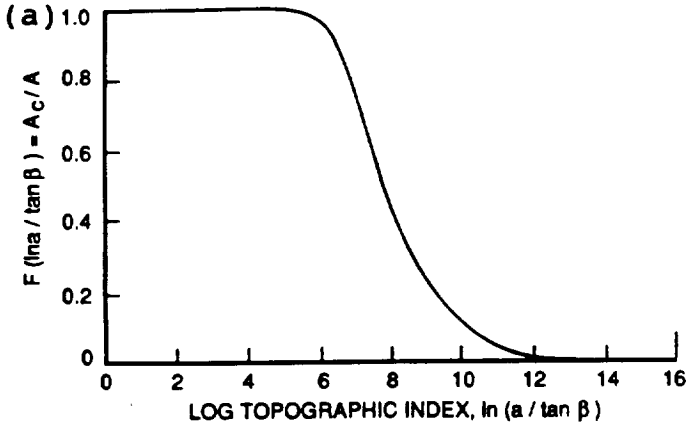

Figure 3. (*a*) Cumulative distribution of topographic index for Kings Creek, Kansas (USGS station 06879650), and (*b*) cumulative distribution of -log transmissivity for Kings Creek, Kansas (USGS station 06879650).

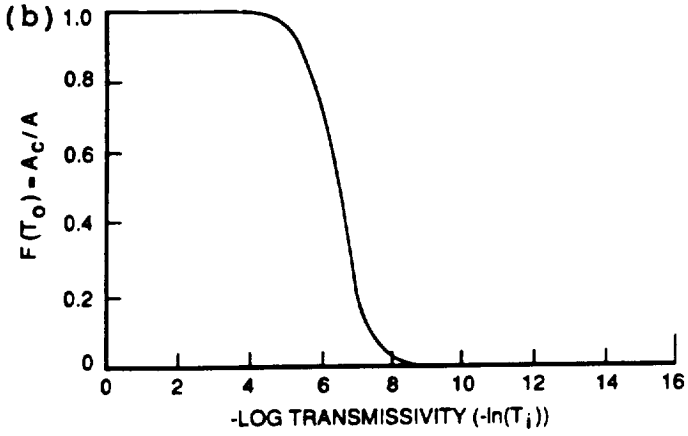

The mean transmissivity will, however, have a major control on drainage during interstorm periods and consequently on the value of $\bar{z}$ prior to any storm. Within this theoretical framework it can be shown that subsurface outflows Q_s during interstorm periods can be described by

$$Q_s = Q_o \exp(-f\bar{z}) \quad (5)$$

where $Q_o = AT_e \exp(-\lambda)$ and A is the catchment area [*Beven*, 1986*a*]. Given an initial discharge prior to a storm, (5) can be inverted to estimate a value of $\bar{z}$ and hence using (3) to give the initial saturated area and pattern of local water table depths. Rainfall onto the saturated area will become surface runoff, while during the storm, infiltration takes place at locations where $z_i > \psi_c$. Where the rainfall is great enough to fill any storage deficit above the initial water table position, additional surface runoff will be generated and the contributing area expands out from its initial position.

2.2. Model of Infiltration Excess Runoff Production

Away from the initial contributing area, rainfall rates may be such as to exceed the infiltration capacity of the soil and produce infiltration excess runoff, even though the soil profile remains in part unsaturated. This will occur most readily on areas of low-permeability soil but will also depend on the initial moisture content at the soil surface which controls the local moisture deficit and vertical hydraulic gradient. The infiltration excess component of the model presented here is based on the Philip equation [*Philip*, 1969], which is an approximate analytical solution to the nonlinear Richards' equation, modified to take into account the time taken for the rainfall to bring the soil surface just to saturation (called the time to ponding). The unsaturated soil moisture characteristics are described by the *Brooks and Corey* [1964] equations which provide the functional relationship between suction pressure ψ and soil moisture θ and between ψ and hydraulic conductivity K. The Philip equation is not strictly compatible with the TOPMODEL framework in that it does not allow for the type of exponential decline in soil permeability with depth assumed within TOPMODEL. *Beven* [1984] has derived an infiltration model which is consistent with TOPMODEL, but for the current purpose it is not analytically tractable. We do not feel that this will have a significant effect on conclusions drawn from the study.

With these assumptions the infiltration rate $g(t)$ for any particular value of the surface saturated hydraulic conductivity of the soil, K_o, is given by

$$g(t) = p \qquad t < t_p \quad (6a)$$

$$g(t) = CK_o + \frac{1}{2}S_r K_o^{1/2}(t_p - t_c)^{-1/2} \qquad t > t_p \quad (6b)$$

where t_p is the time to ponding (the time when the infiltration rate falls below the rainfall rate p). Relationships for the variables t_p, t_c, C, and S_r are functions of soil

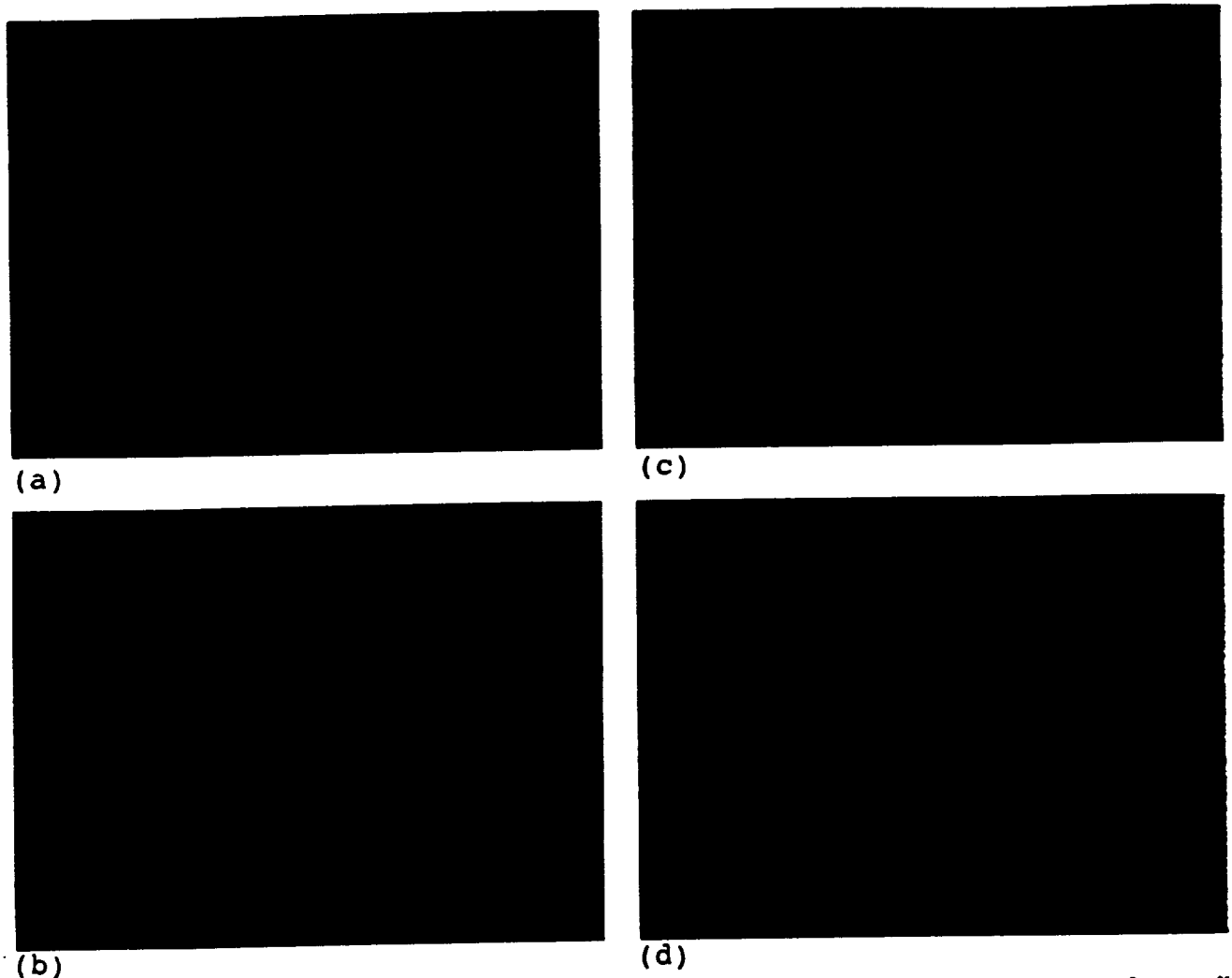

Figure 4. Results of simulations of infiltration excess and saturation excess runoff production on the Kings Creek catchment, Konza Prairie Nature Reserve, Kansas. All patterns have been superimposed on the digital elevation map of the catchment. (*a*) Pattern of soil characteristics, (*b*) rainfall pattern for the storm of August 4, 1987, (*c*) predicted runoff production assuming wet initial conditions (blue represents surface runoff production areas, and green represents no surface runoff), (*d*) predicted runoff production assuming dry initial conditions (blue represents surface runoff production areas, and green represents no surface runoff).

characteristics, the rainfall rate, and the depth to the water table (which influences the moisture content of the column). The relationships are given by *Sivapalan et al.* [1987]. At each location characterized by the topographic-soil index ln (aT_e/T_i tan β) and the saturated hydraulic conductivity at the surface, K_o, infiltration will take place at the rate $g(t)$, with runoff at the rate $(p - g)$ until the time at which the cumulative infiltrated volume $G(t)$ exceeds the initial storage deficit. Beyond this time, infiltration is assumed to be zero, and runoff occurs by the saturation excess mechanism at the rate p.

Results from the application of this model show that the predicted surface runoff production by the saturation excess mechanism follows the pattern of catchment topography, with the greatest likelihood of runoff in valley bottoms and convergent headwater areas. Infiltration excess runoff production may also be affected by topographically controlled initial moisture profiles. Predictions show that both infiltration excess and saturation excess runoff can be produced within a catchment depending on position on the hillslope, soil, and rainfall characteristics (see Figure 4).

3. RUNOFF VARIABILITY AND SCALE

For hydrologists interested in land-surface processes, the variability in runoff (and how this variability changes with catchment scale) is the raison d'être for much current research. Field observations have shown that the major sources of heterogeneity leading to spatial differences in runoff are topography, soils, and rainfall (reviews of such field work can be found in the work by *Kirkby* [1978]). Figure 3 suggests that the variability in our topographic index, and thereby variability in topography, hillslope forms, and subcatchment shapes, will play a significant role in defining the patterns of runoff at small scales as predicted by our model. This model behavior is consistent with reported field observations; for example, see the

contributions by Dunne (chapter 7) and Kirkby (chapter 9) in the work by *Kirkby* [1978]. Until recently it was very cumbersome to model the influence of topographic variability on small-scale runoff processes because maps had to be used for the calculation of any topographic index. Now the wide availability of digital elevation models (DEMs) of terrain and the graphics workstations needed to process this data removes any computational barriers that may have existed.

Several studies have looked at the influence of soil heterogeneity on storm runoff, including the modeling work of *Smith and Hebbert* [1979] and *Freeze* [1980]. In many cases we feel that topographic variability will have a greater influence on the spatial variability of runoff at the subcatchment scale than will variability in soil properties. One reason is shown in Figure 3 where variability in our topographic index dominates over soil transmissivity variability at the small subcatchment scale. If our model of a catchment's response to rainfall is reasonably correct, then this implies that soil variability will have a smaller influence on the spatial pattern of water depths and subsequent storm responses than will the local topography. *Wolock* [1988] calculated the distribution of our topographic and topographic-soil indices for 145 catchments in the northeastern part of the United States; his results support Figure 3 in that variability in topography dominates the variability in the topographic-soil index and subsequently the predicted spatial patterns of storm runoff. One can certainly imagine catchments where soil variability will dominate topographic variability but Wolock rejected only four catchments as having little or no relief in the DEM data base.

Figure 4 presents some patterns for soil transmissivity, rainfall and storm responses for Kings Creek catchment, a catchment of 11.7 km^2 that is part of the Konza Prairie Natural Reserve near Manhattan, Kansas. The patterns are overlaid on the topographic DEM for the catchment. Figure 4*b* gives the precipitation pattern for a storm which occurred on August 4, 1987, while Figures 4*c* and 4*d* give the model-predicted catchment response showing areas of storm runoff due to infiltration excess and saturation excess processes as a function of initial catchment dryness. The purpose of Figure 4 is to illustrate how the predicted patterns vary within the catchment and with initial dryness. Looking at Figure 4, one can appreciate the variability in the catchment response at the hillslope scale. In fact, if one divides up the catchment into smaller subcatchments, as is shown in Figure 5 for Kings Creek, one can investigate this variability over different scale. With increased scale, the increased sampling of hillslopes should lead to a decrease in the difference between subcatchment response. At some scale, the variance between storm responses for catchments of the same area should reach a minimum.

Wood et al. [1988*a*] suggest that this threshold scale represents a "Representative Elementary Area" which is proposed to be the fundamental building block for catchment modeling. The REA is a critical scale at which implicit continuum assumptions can be used without knowledge of the actual patterns of topographic, soil, or rainfall fields, although it would be necessary to account

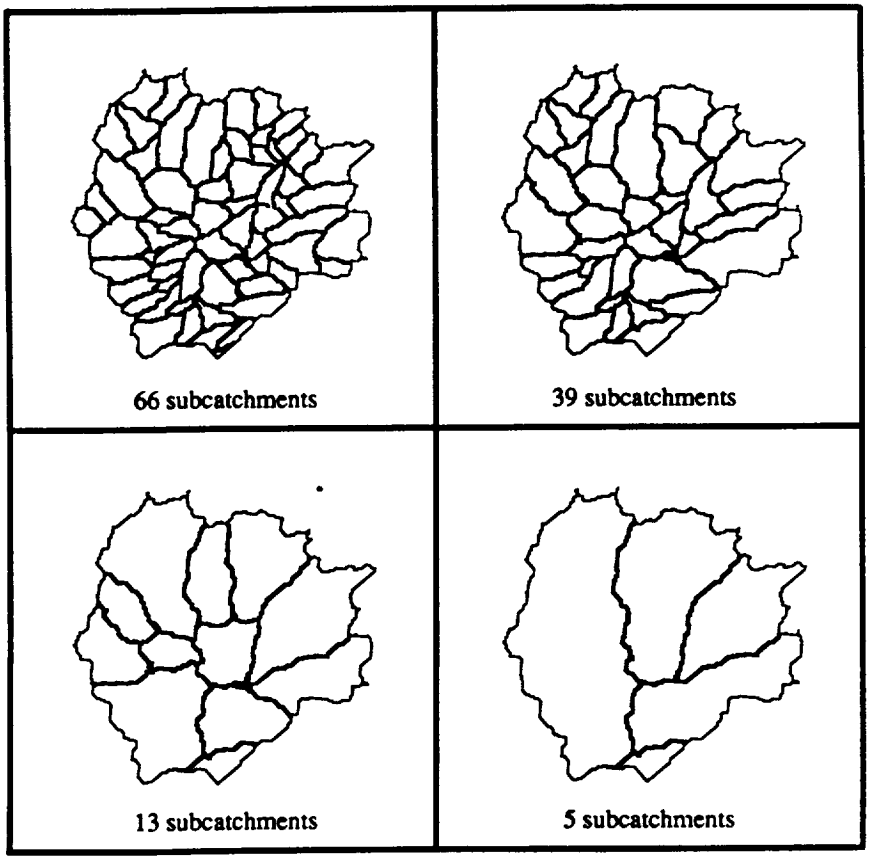

Figure 5. Natural division of Kings Creek. Division was carried out by the techniques of *Band and Wood* [1988].

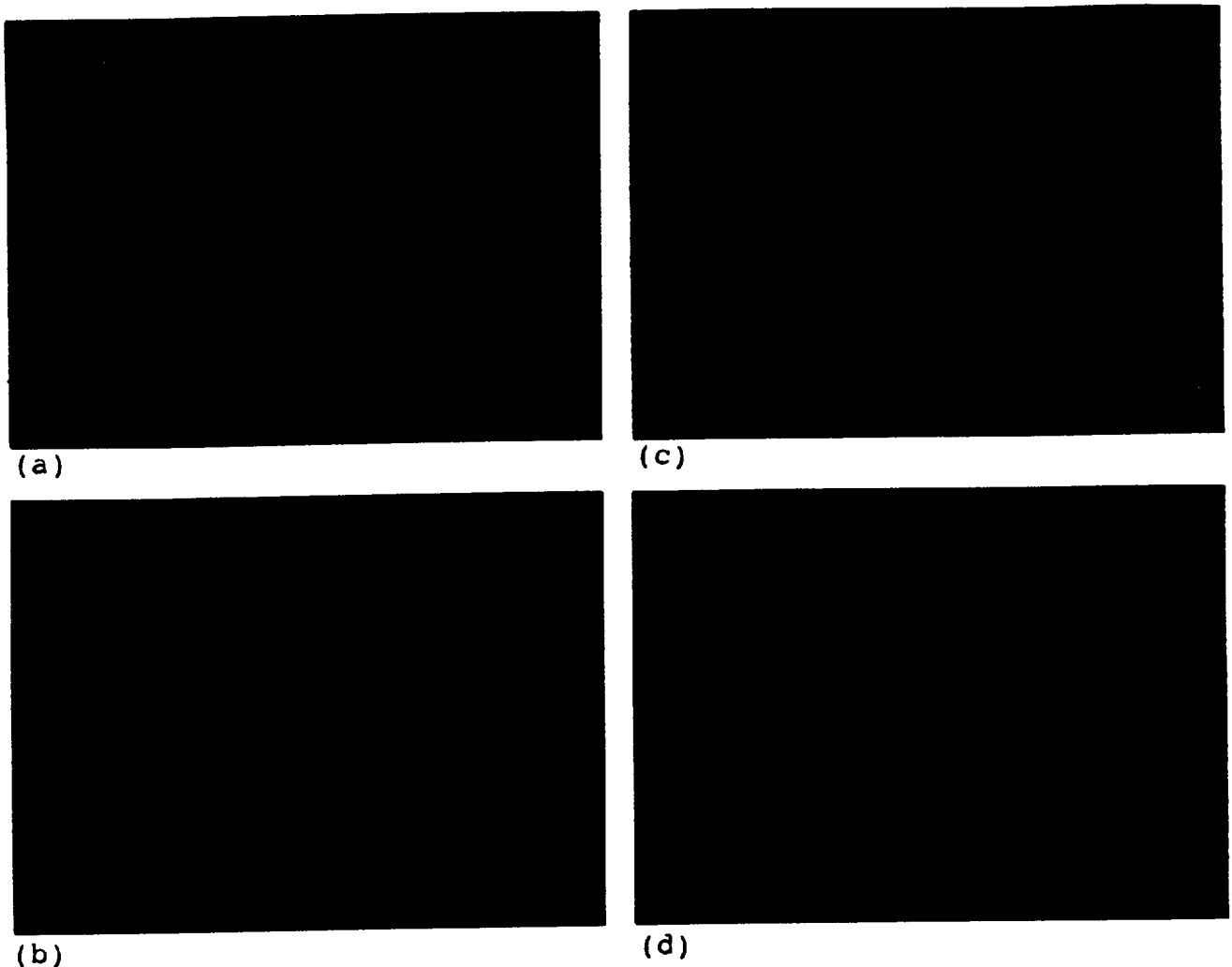

Figure 6. Rainfall intensity pattern for August 4, 1987, at four different times: (*a*) 0815, (*b*) 0845, (*c*) 0900, and (*d*) 0930.

for the underlying variability of these parameters through distributional functions.

To investigate this concept, the storm responses were modeled for the four rainstorms shown in Figure 6. Using the natural subcatchments of Figure 5, the storm runoff was calculated for each subcatchment. Since the four storms resulted in different rainfall depths, the storm runoff was rescaled by the average rainfall depth over the catchment. This ratio of storm runoff to rainfall depth is plotted in Figure 7 against the subcatchment area as represented in pixels. Here one pixel is 900 m^2, and 1100 pixels is approximately 1 km^2. By visual inspection we suggest that the size of the representative elementary area is approximately 1 km^2. It is interesting to note that in modeling a different catchment with steeper topography and using simulated rainfall patterns, *Wood et al.* [1988*a*] also found an REA of the order of 1 km^2.

The results of Figure 7 suggest that at scales larger than the REA it should be possible to simplify the representation of catchment responses, while still retaining the important effects of heterogeneity in the hydrological processes. For catchment areas much larger than the correlation lengths of soil and rainfall variability (assumptions consistent with our REA theory) one needs not consider the actual patterns in rainfall, topography, and soil but can consider them statistically through their means and variances.

Using the statistical distribution of the topographic-soil index, one can determine the fraction of the catchment that will be saturated due to the local soil storage being full. These areas will generate saturation excess runoff at the rate $\bar{p}$, the mean rainfall rate. For that portion of the catchment where infiltration occurs, the local expected runoff rate, m_q, can be calculated as the difference between the mean rainfall rate, $\bar{p}$, and the local expected infiltration rate, m_g. This difference can be expressed as

$$m_q\,[t|\ln(aT_e/T_i\tan\beta)] = \bar{p} - m_g\,[t|\ln(aT_e/T_i\tan\beta)] \quad (7)$$

where both the local expected runoff rate and the local expected infiltration rate are (probabilistically) conditioned on the topographic-soil index, $\ln(aT_e/T_i\tan\beta)$. The runoff production from the catchment is found by integrating, usually numerically, the conditional rate over the statistical

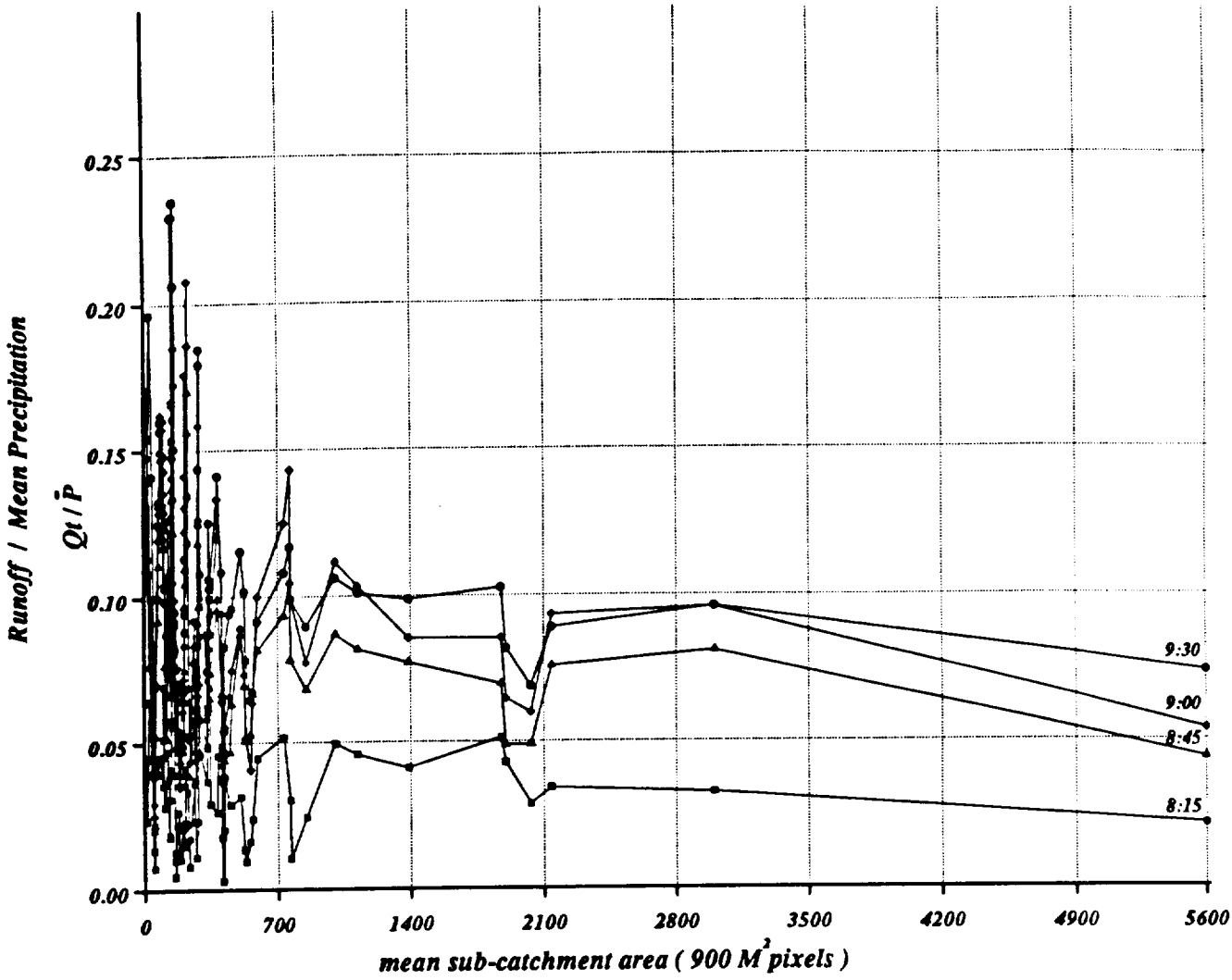

Figure 7. Rescaled modeled storm runoff as a function of mean subcatchment area for four different intervals of the August 4, 1987, storm.

distribution of the topographic-soil index. Figure 8 gives results for the storm patterns presented in Figure 6. The increase observed over the time intervals is indicative of an increase in the runoff ratio during the storm.

For the simplified case where only infiltration excess is considered, it is possible to derive analytically the macroscale model [*Sivapalan*, 1986; *Wood et al.*, 1988*a*]. Figure 9 gives results for one set of simulations in which the macroscale model is compared to the averaged microscale model.

4. CATCHMENT VARIABILITY AND HYDROLOGIC SIMILARITY

The results from the REA analysis suggest that progress has been made in understanding the transition from microscale to macroscale parameterization as we increase scale in the presence of spatial variability. This does not address the question as to how catchments may be hydrologically similar. Definitions of similarity used in the past have been based on physioclimatic characterizations without explicit recognition of the environmental controls on runoff generation. The work of *Wood and Hebson* [1986] and *Sivapalan et al.* [1987, 1989] redefine this to consider similarity relationships for catchment runoff responses that are independent of basin scale.

The development of a scaled model of storm response requires the specification of the appropriate scaling parameters. This requires scaling the topographic-soil index function, the soil characteristic relationships, and the rainfall intensity and duration. The scaling must be consistent in that the underlying equations are not altered.

Earlier in the paper it was argued that variability in topographic-soil index played a major role in determining both the patterns and magnitudes of generated runoff. It is quite reasonable that this index be described in a probability distributional form, and in doing so it allows one to define a convenient and appropriate scaling parameter. Let $x \equiv \ln (a/\tan \beta)$ and let the areal distribution of x be

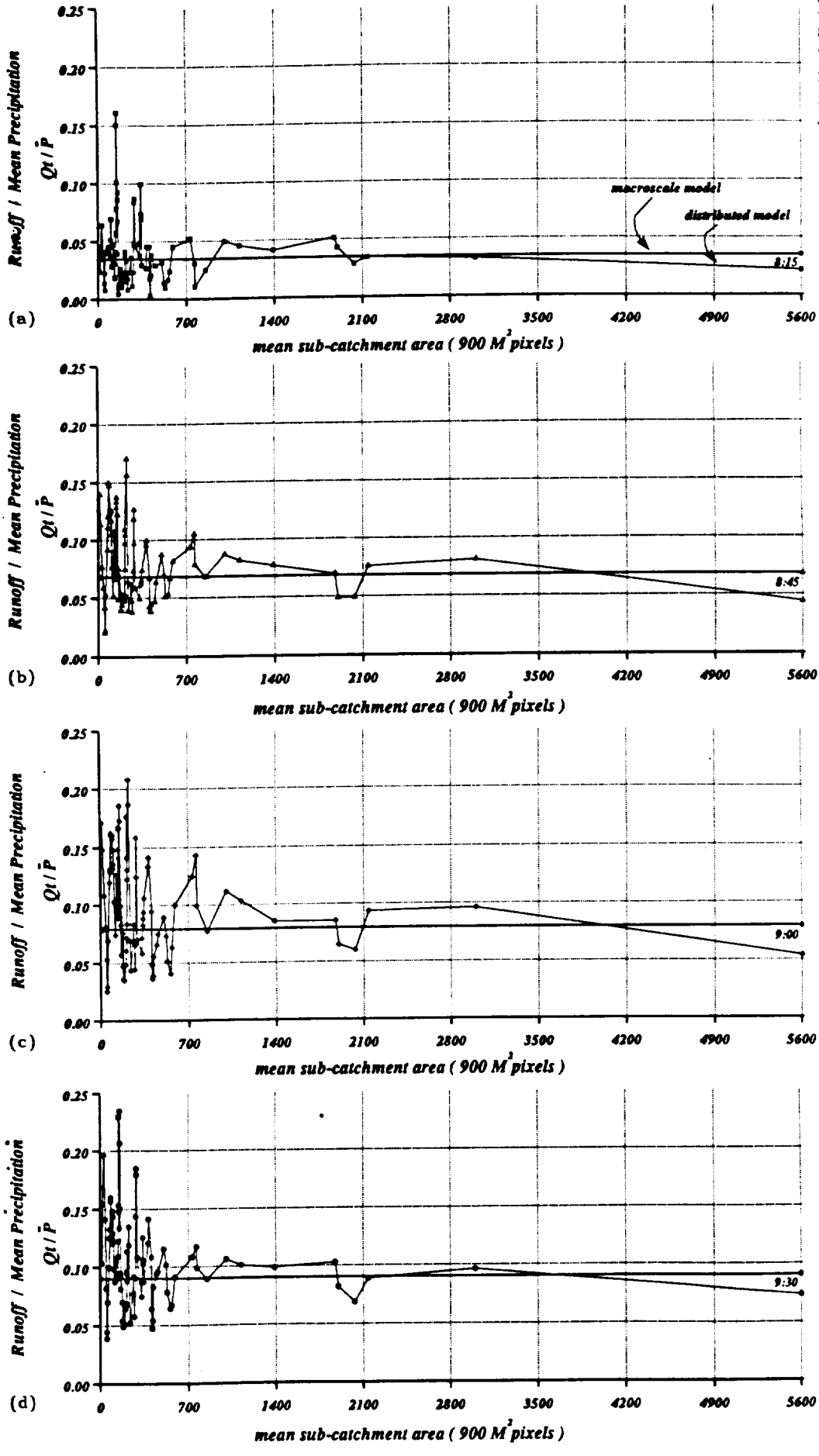

Figure 8. Comparison of storm runoff generated from the distributed model and from the macroscale model at four time intervals on August 4, 1987; (*a*) 0815, (*b*) 0845, (*c*) 0900, and (*d*) 0930.

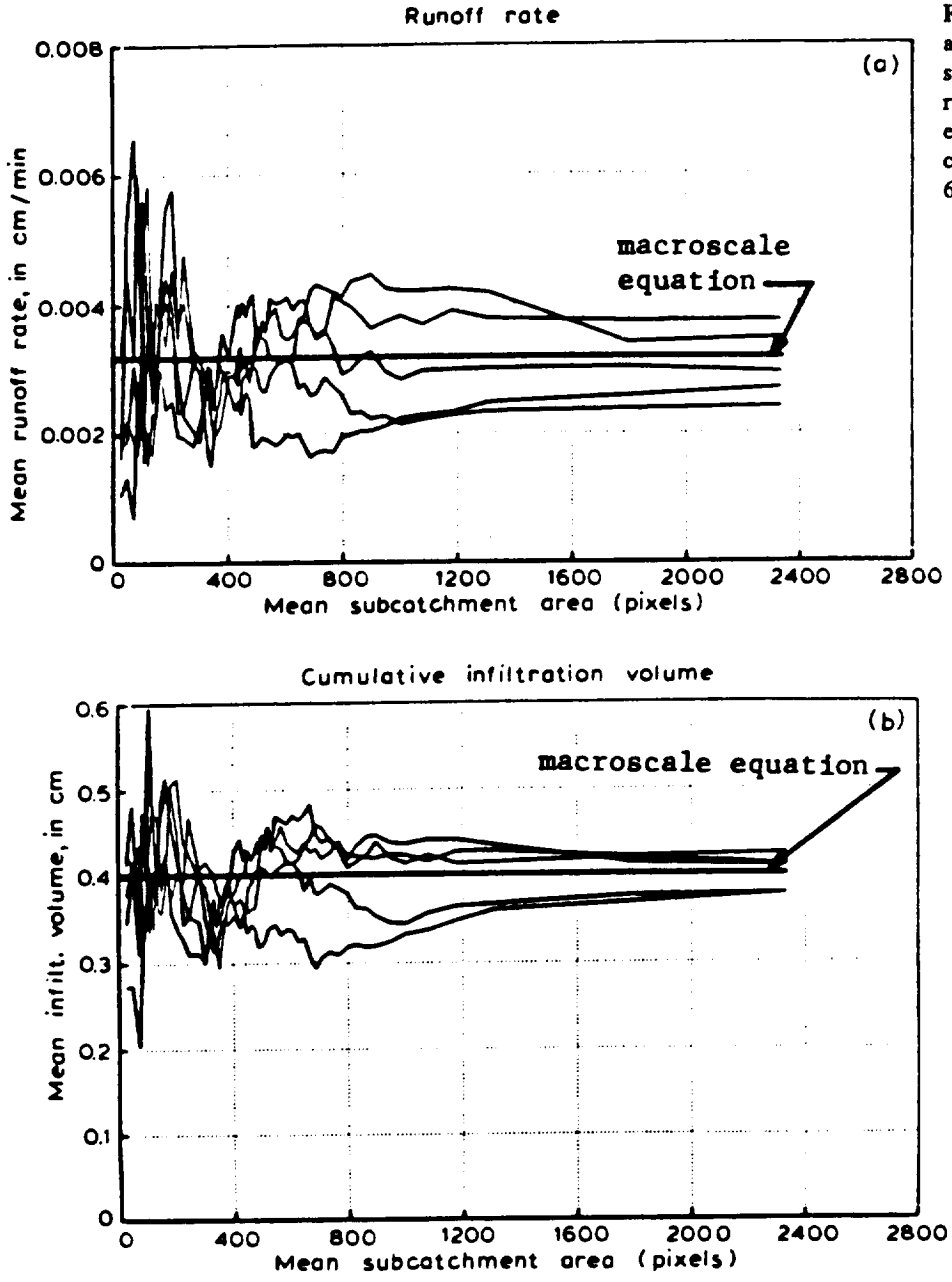

Figure 9. Comparisons of simulation and analytical results for the case of spatially variable soils and rainfall and runoff production by infiltration excess: (*a*) runoff rate and (*b*) cumulative infiltration volume, λ_p = 625 m [from *Wood et al.*, 1988*a*].

described by a three-parameter gamma probability distribution with mean $\lambda = \chi\phi + \mu$, variance $\chi^2\phi$, and coefficient of variation $C_{vT} = \chi\sqrt{\phi}/\lambda$. Figures 10*a* and 10*b* show, as an illustration, the topographic index fitted for two catchments, where A_c/A represents that fraction of the catchment having an index value greater than the abscissa value. *Wolock*'s [1988] analysis of 145 catchments found that the three-parameter gamma probability distribution fitted the calculated topographic index quite well.

Field evidence presented by *Nielsen et al.* [1973], *Russo and Bresler* [1981], *Beven* [1983*a*] and others show that saturated hydraulic conductivity of soil tends to follow a lognormal probability distribution. In developing our scaled model, we assume that variability in hydraulic conductivity represents the major influence in soil variability. This is justified with the argument that variability in runoff production will be less sensitive to other soil parameters. We assume that saturated hydraulic conductivity is lognormally distributed, which we further assume will also hold for hydraulic transmissivity. In general, we will have little or no information about the actual pattern of conductivity or transmissivity with respect to topography. If we are concerned at modeling scales larger than the REA scale, such patterns may not be important. This is supported by the results of *Beven* [1983*b*] who found through Monte Carlo simulation that the effect of soil patterns is small when its spatial correlation length scale is small relative to the catchment scale.

To a first approximation, we assume that the soil transmissivity, T_i, is independent of the topographic index and that the probability distribution for $\ln (T/T_i)$ is normal with zero mean and variance σ_T^2. By assuming for the topographic index, $\ln (a/\tan \beta)$, a three-parameter gamma probability distribution with parameters μ, ϕ, and χ, and by

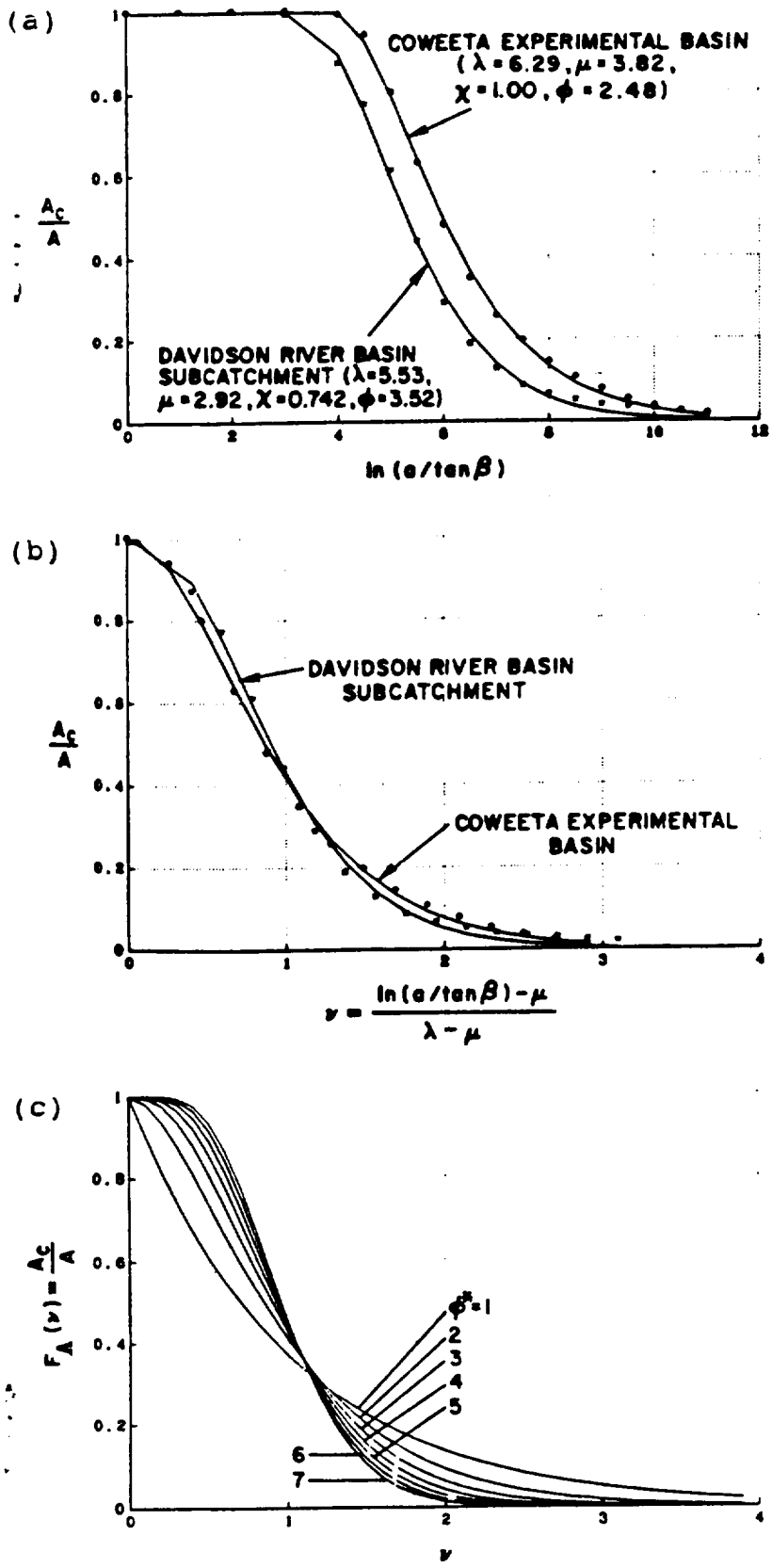

Figure 10. (*a*) Cumulative ln (a/tan β) distributions of the Coweeta Experimental Basin and a subcatchment of the Davidson River catchment (unconnected points) and their gamma approximations (solid curves), (*b*) cumulative distributions of the scaled topographic index ν for the two basins, and (*c*) cumulative distribution of ν for different values of φ* [from *Sivapalan et al.*, 1989].

defining $x^* = \ln (aT_e/T_i \tan \beta)$, the topographic-soil index, then x^* is approximately distributed as a gamma (μ^*, ϕ^*, χ^*), where

$$\mu^* = \mu \tag{8a}$$

$$\frac{1}{\phi^*} = \frac{1}{\phi} + \frac{\sigma_T^2}{\chi^2 \phi^2} \tag{8b}$$

$$\chi^* = \chi + \frac{\sigma_T^2}{\chi \phi} \tag{8c}$$

It can be shown that the scaled parameter $\nu = x^* - \mu/\lambda - \mu$ follows a one-parameter gamma distribution,

$$f_\nu(\nu) = \frac{\phi^*}{\Gamma(\phi^*)} (\nu\phi^*)\phi^{*-1} \exp(-\phi^*\nu) \tag{9}$$

with shape parameter φ*, scale parameter $1/\phi^*$, mean 1, and variance $1/\phi^*$. The variable ν is scale independent, and φ* reflects the variability in soil and topography and is independent of the scale of the catchment. Thus φ* captures in a scaled manner the net hydrological effects of the convergence, divergence, concavity, convexity, and soil transmissivity characteristics of the hillslopes constituting the catchment. Within our theory of hydrologic similarity, the topographic-soil effects of two catchments having the same φ* would be the same. Figure 10*b* shows the cumulative distributions of the scaled topographic-soil index for two catchments. Notice that their scaled topographic indices are almost identical, implying that the effect of topography on "scaled" storm surface runoff production would be similar for both catchments. Figure 10*c* shows the cumulative distribution function $f_\nu(\nu|\phi^*)$ for different values of the parameter φ*.

Based on the scaling which defined ν, a consistent scaling for the water table depth would be $f/(\lambda - \mu)$. For the saturation excess runoff generation, using (5), (3) can be written as

$$z_i^* = Q^* + (1 - \nu) \tag{10}$$

where $Q^* = -\ln [Q(0)/Q_o]/(\lambda - \mu)$, the scaled average water table depth which represents the catchment scaled wetness at the start of the rain event.

To scale the infiltration excess portion of the storm response, different scaling relationships are needed. Intuitively, we will require scaling parameters that consider soil characteristics and storm duration, since the amount of the rainfall which infiltrates depends on these two factors. We propose for the time dimension the scaling parameter t_d, the storm duration, and for the length dimension $\psi_f/(\theta_s - \theta_r)$, parameters of the Brooks-Corey soil moisture characteristic relationship [*Brooks and Corey*, 1964]. The Brooks-Corey

soil moisture relationship is a functional relationship that relates suction pressure, ψ, to the soil moisture, θ.

$$\theta(\psi) = \theta_r + (\theta_s - \theta_r)\left[\frac{\psi_c}{\psi}\right]^B \tag{11}$$

Here ψ_c is the depth of the capillary fringe, θ_s is the saturation soil moisture content (which is equal to the soil porosity), and θ_r is the residual soil moisture content, the value of θ when the soil dries and $-\psi$ becomes very large. The above scaling leads to the following scaled parameters:

$$t^* = t/t_d \tag{12a}$$

$$p^* = pt_d/\psi_c(\theta_s - \theta_r) \tag{12b}$$

$$g^*(t^*) = g(t)t_d/\psi_c(\theta_s - \theta_r) \tag{12c}$$

Equation (6) still holds but in the scaled parameter space. *Sivapalan et al.* [1987] provide the details for the scaled parameters. Similarly, (7) would also hold in the scaled parameter domain. Through scaling the runoff production process equations, the explicit consideration of spatial and temporal scales has been removed without sacrificing the modeling of the hydrological processes. Scaling of the model equations has identified five dimensionless catchment similarity parameters and three dimensionless auxiliary conditions which govern the scaled storm response. The similarity parameters include two scaled soil hydraulic conductivity parameters, the mean scaled hydraulic conductivity, $\bar{K}_o$, and the coefficient of variation for $\bar{K}_o$; two soil moisture characteristics, the scaled size of the capillary fringe, ψ_c^*, and a Brooks-Corey parameter B; and a scaled topographic-soil index parameter ϕ^*. Two catchments can be said to be hydrologically similar in terms of surface runoff production within the assumptions of our model if they are identical in these five parameters, regardless of scale. The two auxiliary conditions include a scaled initial flow Q^* and two rainfall distribution parameters, the ratio of the mean rainfall rate to the mean soil hydraulic conductivity and the coefficient of variation of the rainfall rate.

One purpose of such scaling is to investigate the relationship between environmental controls (topography, soils, and climate) and runoff production without the compounding effects of scale. *Sivapalan et al.* [1987] carried out sensitivity analysis for a number of parameters, and the reader is referred there for details. Some conclusions of those runs are worth discussing here.

As expected, topography plays a major role in defining the dominate runoff mechanism. In fact, varying the soil heterogeneity, keeping the mean hydraulic conductivity constant, had very little effect on the saturated excess runoff production. Finer grained soils tended to increase runoff by producing saturated areas more quickly and increasing their extent. Increasing (spatially) mean rainfall rates relative to mean soil conductivity has a profound effect on runoff, as one would expect: strongly increasing both saturated areas and infiltration excess runoff. On the other hand, increasing rainfall variability (e.g., convective storms or a large catchment when compared to the storm size) had little impact on saturation excess production.

It is doubtful that there would be any two catchments that satisfy jointly all the dimensionless parameters. On the other hand, there could be a range of values for each of the parameters for which similarity could be established between catchments. In addition, sensitivity analysis may indicate the most probable hydrologic regimes that would occur under given topographic, soil, and climatic combinations. Finally, it is hoped that these results would help in guiding field experiments and in interpreting data from such studies.

5. FLOOD FREQUENCY, SIMILARITY, AND SCALE

The determination of the peak runoff from a rain event requires that the generated runoff be routed down the channel network to the basin outlet or gaging point. The analysis of this process, which includes the hillslope response and the channel response, by channel routing using simplified equations of fluid flow has been investigated by *Kirkby* [1986] and *Wood et al.*, [1988*b*]. The review of this work is beyond the scope of this paper. A more simplified approach that captures the aggregated response of the basin is to model the channel response as a simple linear response function, i.e., an instantaneous unit hydrograph (IUH). The IUH is the response to a unit input occurring over a time τ, as $\tau \rightarrow 0$.

Henderson [1963] showed that if the response function was simplified to be triangular in shape, then this "triangular unit hydrograph" was sufficient for the prediction of the channel response. This simplification required that the peak and time to peak be preserved between the actual response function and the simplified response function. *Wood and Hebson* [1986] derived the peak discharge Q_p from a catchment due to storm runoff generated at a constant rate q with duration t_d by utilizing the simplified triangular IUH having a peak h_p and time to peak t_p. The resulting expression for Q_p is as follows:

$$Q_p = q\,h_p\,t_d\left(1 - \frac{h_p\,t_d}{4}\right) \qquad h_p\,t_d \le 2 \tag{13a}$$

$$Q_p = q \qquad h_p\,t_d > 2 \tag{13b}$$

The parameterization of (13) could be based on any number of expressions for the IUH peak and time to peak. A particularly interesting one is to use the results from *Rodriguez-Iturbe and Valdes* [1979] where equations for the peak and time to peak are developed in terms of Horton's geomorphological laws [*Horton*, 1945]. Channel networks were first studied quantitatively by *Horton* [1945] who defined an ordering system for individual links of the network based on the network structure. Horton

showed that the expected values for the number of streams, the length of streams, and the stream slope were significantly different for each order and suggested that the structure of individual networks could be represented by a small number of descriptive parameters.

By using these relationships of Horton to describe the structure of the channel network within a catchment and subsequently the response function of the catchment (which they call the geomorphologic unit hydrograph), *Rodriguez-Iturbe and Valdes* [1979] represent similarity in basin responses for basins having the same Horton ratios and scale. They found that the unit hydrograph peak could be expressed as

$$h_p = 0.364 R_L^{0.43} \frac{v}{L_\Omega} \tag{14}$$

where R_L is Horton's length ratio, v is the peak velocity, and L_Ω is the length of the highest-order stream. The peak h_p is the discharge per unit area per unit depth of runoff (effective rainfall), resulting in units T^{-1}.

Wood and Hebson [1986] defined a scaling time $\tau = L_\Omega/v$ which they define as the characteristic basin response time that they used to define a dimensionless geomorphic unit hydrograph (DGUH). This led to a scaled DGUH peak discharge of $h_p^* = 0.364 R_L^{0.43}$ and a scaled excess storm duration, $t_d^* = t_d/\tau$. The scaled peak runoff function, due to scaled generated runoff q^*, is found by substituting these scaled variables into (13).

The results from *Wood and Hebson* [1986] only considered temporally constant excess rainfall which allowed an analytic solution for the scaled flood frequency curve. Further, they had prespecified the probability distribution of the excess rainfall and did not consider more complex mechanisms for runoff generation. *Sivapalan et al.* [1989] relaxed these considerations and found the flood frequency curves by numerical simulation. Their runoff generation model is that described earlier in this paper which considers both infiltration excess and saturation excess (but not subsurface storm flow) mechanisms. Flood frequency curves usually plot the largest observed peak discharge during any year (annual peak discharge) against the probability that it will be equalled or exceeded in any year. The exceedance probability is usually expressed as its inverse and denoted as the "return period" for that annual peak discharge.

Only one set of results from *Sivapalan et al.* [1989] will be discussed here. The shape of the flood frequency curve appears to result from a complex interaction of topography, soil, and climate. Figure 11 shows three scaled flood frequency curves for a catchment with fixed topography; they differ in the mean rainfall when compared to the mean soil conductivity. The curves are the average curves from 25 repetitions of 4000 storms; i.e., 4000(25) storm simulations. The top two curves represent an environment where the flood peaks are dominated by infiltration excess runoff; thus the distributional characteristics of the rainfall are passed through to the flood frequency curve. The

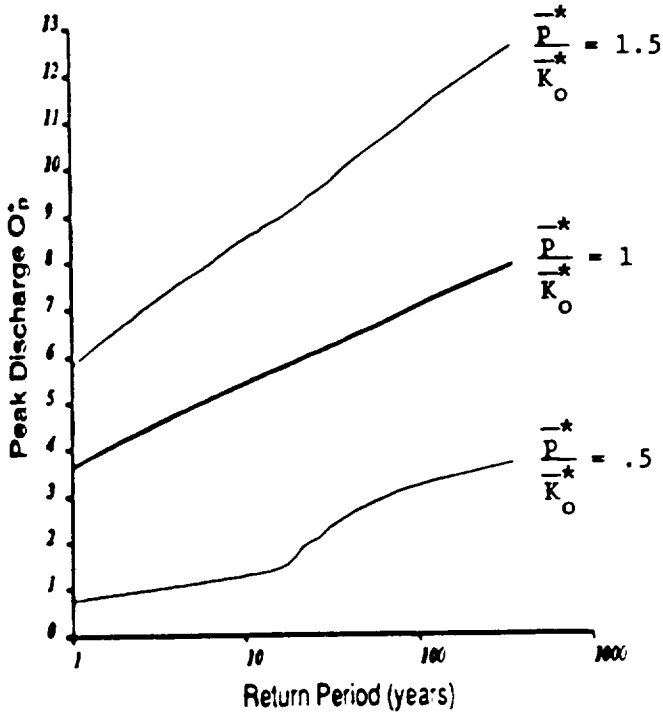

Figure 11. The sensitivity of the flood frequency distribution to the ratio of scaled storm intensity, $\bar{p}^*$, to scaled soil conductivity, $\bar{K}_o^*$ [from *Sivapalan et al.*, 1989].

bottom curve, which represents a low-rainfall climate, is dominated at low return periods by saturation excess runoff and at high return periods by infiltration excess runoff. Sensitivity analysis shows that the saturation excess flood curve is extremely stable while the infiltration excess curve is more variable (see Figure 12). At this time we believe that the above modeling has produced an important result, that for some catchments the flood frequency curve at low return periods is defined by catchment characteristics (through saturated excess storm runoff) while at high return periods it is defined by rainfall characteristics (through infiltration excess storm runoff). This finding appears to be supported by data. Figure 13 presents annual flood peak data for three catchments, and their shapes resemble the shapes of Figure 12. More work is needed to verify this hypothesis, but the modeling results provide some guidance for this work.

The purpose of this example is to demonstrate how similarity-based analyses can be used to study basic hydrological processes over a range of scales and to reveal characteristics and interactions among processes previously overlooked. Research is ongoing to gather data over a range of catchments representing different climates and scales with which this theory can be further tested and applied.

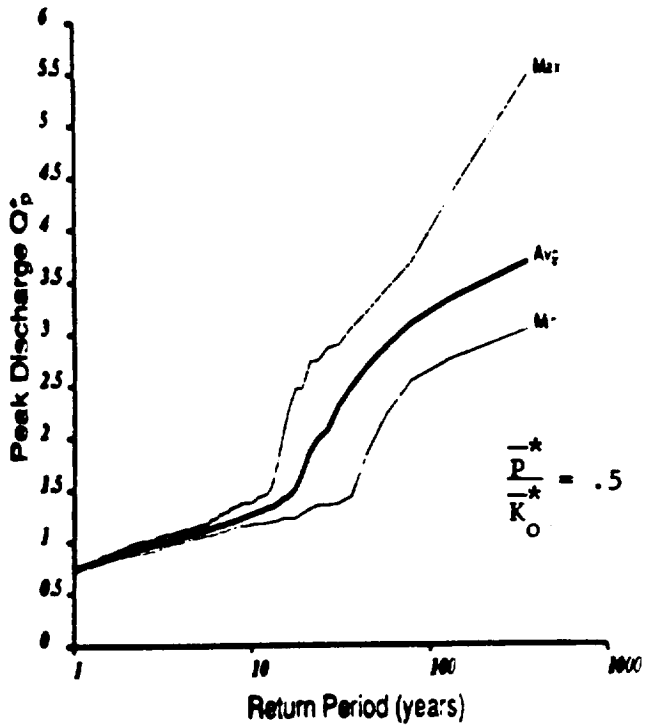

Figure 12. The envelope, over 25 repetitions, of the flood frequency distribution for the sensitivity run, $\bar{p}^*/\bar{K}_o^* = 0.5$ [from *Sivapalan et al.*, 1989].

6. CONCLUSIONS

This review has summarized research by the authors in two important interrelated areas of catchment hydrology: the effects of scale on hydrologic parameterization and the concept of hydrologic similarity. Our research into scale problems in hydrology attempts to understand the effect of spatial variability on the parameterization of hydrological processes and to seek consistent models across a range of scales. Field studies over the last 30 years have shown that two main mechanisms generate surface runoff and that these may both occur within a catchment during a rain event. These mechanisms are the infiltration excess runoff of Horton and the saturation excess runoff of Dunne. Their spatially variable controls (topography, soil, rainfall, and vegetation) lead to patterns of runoff generation across the catchment.

In the work by *Wood et al.* [1988*a*] the concept of a representative elementary area was proposed as the fundamental scale for catchment modeling. It is argued that for accurate surface runoff modeling at scales smaller than the REA, these patterns of the spatially variable controls must be modeled exactly. (Such an argument is supported by the lack of success in the literature toward accurately modeling small-scale experimental catchment areas.) For areas larger than the REA, only the statistical representations of these controls need to be considered. Further, at these larger scales, simplified models, based on these statistics, should suffice as models of the catchment

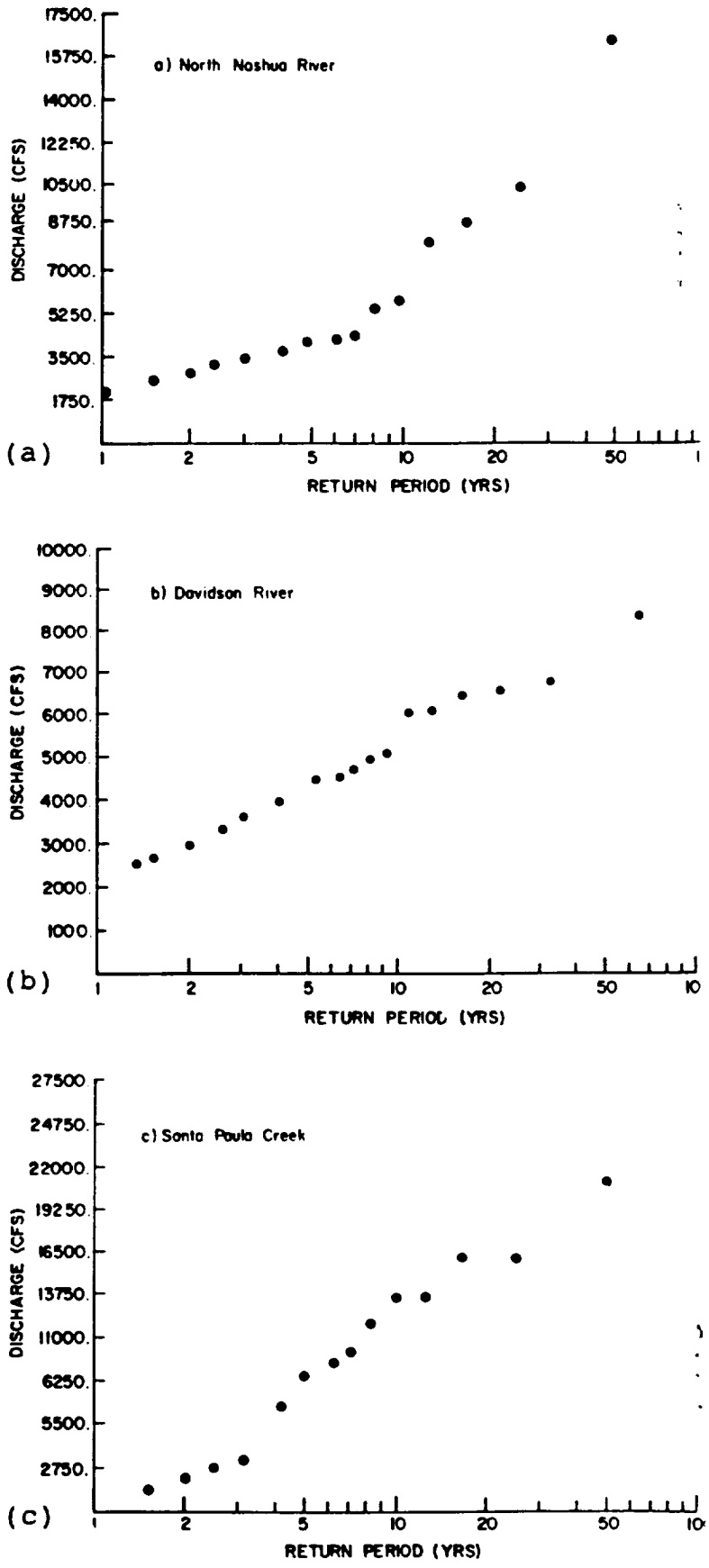

Figure 13. Flood frequency distributions for three watersheds: (*a*) North Nashua River, (*b*) Davidson River, and (*c*) Santa Paula Creek [after *Moughamian et al.*, 1987].

response. For one set of simulations, *Wood et al.* [1988*a*] found an REA of the order of 1 km^2. Simplified models consistent with the REA theory were successful in simulating the large-scale behavior.

The research in similarity was motivated by the desire to understand the influence of environmental controls on catchment storm responses independent of basin scale. Unlike previous research that related similarity to physioclimatic regimes our definition of similarity is based on similarity in runoff generation and catchment response. It was shown that consistent scaling parameters could be defined and a scaled storm response model developed. Such a scaled model was used by *Sivapalan et al.* [1987] to investigate catchment responses and by *Wood and Hebson* [1986] and *Sivapalan et al.* [1989] to study flood frequency characteristics.

The research reported here is a first step in clarifying the issues involved in understanding the parameterization of hydrological processes across a range of scales. There remains a vast amount of research to which the ideas presented here can contribute. Let us suggest only two. In the United States the recommended approach to flood frequency studies uses regionalized values for the coefficient of skewness statistic [*Interagency Advisory Committee on Water Data*, 1982]. The regionalization is based on geographical regions without thought or consideration to differing catchment response characteristics. The concept of similarity as presented here can help in understanding the relationship between the controls within the catchment and its flood frequency characteristics and can help to form the basis for grouping catchments for statistical flood analyses.

The second area where the research presented here can be extended to is the parameterization of the land portion of global climate models. The REA results give confidence that simpler macroscale models will perform well at large grid scales which have significant subgrid variability, thus questioning the wisdom of detailed land parameterization which ignores process heterogeneity. Continuing research is comparing the macroscale models developed here with current GCM parameterizations of land surface hydrology. In addition, the concepts of similarity can help in parameterizing the macroscale models by utilizing data from a number of sites and transferring data to other areas around the Earth. This effectively expands the available data base into regions where data may be sparse or lacking.

ACKNOWLEDGMENTS. The work on which this paper is based was supported in part by U.S. NASA grants NAG-5-491 and NAG-1392, U.S. Department of the Interior (USGS) grant 14-08-0001-G1138, and U.K. NERC grant GR3/6264. This support is gratefully acknowledged.

Garrison Sposito was the editor in charge of this paper. He thanks William E. Dietrich and Vijai K. Gupta for their assistance in evaluating the technical content of the paper and an anonymous associate editor for serving as cross-disciplinary referee.

REFERENCES

Band, L., Topographic partitioning of watersheds with digital elevation models, *Water Resour. Res.*, *22*, 15–24, 1986.

Band, L., and E. F. Wood, Strategies for large-scale, distributed hydrologic simulation, *Appl. Math. Comp.*, *27*(1), 23–37, 1988.

Bathurst, J. C., Physically-based distributed modeling of an upland catchment using the Systeme Hydrologique Européen, *J. Hydrol.*, *87*, 79–102, 1986.

Betson, R. P., What is watershed runoff?, *J. Geophys. Res.*, *69*(8), 1541–1551, 1964.

Beven, K. J., On subsurface stormflow, an analysis of response times, *Hydrol. Sci. J.*, *27*, 505–521, 1982.

Beven, K. J., Surface water hydrology—Runoff generation and basin structure, *Contributions in Hydrology*, U.S. National Report, 1979–1982, 18th Gen. Assem., Int. Union of Geod. and Geophys., Hamburg, Germany, August 1983*a*.

Beven, K. J., Introducing spatial variability into TOPMODEL: Theory and preliminary results, technical report, Dept. of Environ. Sci., Univ. of Va., Charlottesville, 1983*b*.

Beven, K. J., Infiltration into a class of vertically nonuniform soils, *Hydrol. Sci. J.*, *29*(4), 425–434, 1984.

Beven, K. J., Hillslope runoff processes and flood frequency characteristics, in *Hillslope Processes*, edited by A. D. Abrahams, pp. 187–202, Allen and Unwin, Winchester, Mass., 1986*a*.

Beven, K. J., Runoff production and flood frequency in catchments of order *n*: An alternative approach, in *Scale Problems in Hydrology*, edited by V. K. Gupta, I. Rodriguez-Iturbe, and E. F. Wood, pp. 107–131, D. Reidel, Hingham, Mass., 1986*b*.

Beven, K. J., Changing ideas in hydrology: The case of physically-based models, *J. Hydrol.*, *105*, 157–172, 1989.

Beven, K. J., and M. J. Kirkby, A physically-based variable contributing area model of basin hydrology, *Hydrol. Sci. J.*, *24*(1), 43–69, 1979.

Beven, K. J., A. Calver, and E. M. Morris, The Institute of Hydrology distributed model, *Rep. 98*, Inst. of Hydrol., Wallingford, United Kingdom, 1987.

Beven, K. J., E. F. Wood, and M. Sivapalan, On hydrological heterogeneity—Catchment morphology and catchment response, *J. Hydrol.*, *100*, 353–375, 1988.

Binley, A. M., and K. J. Beven, Modelling heterogeneous Darcian headwaters, paper presented at National Symposium, Brit. Hydrol. Soc., Sheffield, 1989.

Brooks, R. H., and A. T. Corey, Hydraulic properties of porous media, *Hydrol. Pap. 3*, Colo. State Univ., Fort Collins, 1964.

Dalton, J., Experimental essays on the constitution of mixed gases; on the force of steam or vapor from waters and other liquids, both in a Torricellian vacuum and in air: On evaporation; and on the expansion of gases by heat, *Mem. Proc. Manchester Lit. Philos. Soc.*, *5*, 535–602, 1802.

Darcy, H., *Les Fontaines Publiques de la Ville de Dijon*, V. Dalmont, Paris, 1856.

Dooge, J. C. I., Parameterization of hydrologic processes, in *Proceedings of the Greenbelt Study Conference*, edited by P. S. Eagleson, pp. 243–288, Cambridge University Press, New York, 1982.

Dunne, T., and R. Black, An experimental investigation of runoff production in permeable soils, *Water Resour. Res.*, *6*, 478–490, 1970.

Environmental Protection Agency, Hydrologic impacts of climate change, report to Congress, Washington, D. C., 1989.

Freeze, R. A., Streamflow generation, *Rev. Geophys.*, *12*(4), 627–647, 1974.

Freeze, R. A., A stochastic-conceptual analysis of rainfall-runoff processes on a hillslope, *Water Resour. Res.*, *16*, 391–408, 1980.

Freeze, R. A., and R. L. Harlan, Blueprints for a physically-based digitally simulated hydrologic response model, *J. Hydrol., 9*, 237–258, 1969.

Gupta, V. K., I. Rodriguez-Iturbe, and E. F. Wood, *Scale Problems in Hydrology*, D. Reidel, Hingham, Mass., 1986.

Hebson, C., and E. F. Wood, A study of scale effects in flood frequency response, in *Scale Problems in Hydrology*, edited by V. K. Gupta, I. Rodriguez-Iturbe, and E. F. Wood, D. Reidel, pp. 133–158, Hingham, Mass., 1986.

Henderson, F. M., Some properties of the unit hydrograph, *J. Geophys. Res., 68*(16), 4785–4793, 1963.

Hewlett, J. D., and A. R. Hibbert, Moisture and energy conditions within a sloping soil mass during drainage, *J. Geophys. Res., 68*(4), 1081–1087, 1963.

Hewlett, J. D., and A. R. Hibbert, Factors affecting the response of small watersheds to precipitation in humid areas, in *Forest Hydrology*, edited by W. E. Sopper and H. W. Lull, pp. 275–290, Pergamon, New York, 1967.

Hewlett, J. D., and W. L. Nutter, The varying source area of streamflow from upland basins, in *Proceedings of the Symposium on Interdisciplinary Aspects of Watershed Management*, pp. 65–83, American Society of Civil Engineers, New York, 1970.

Horton, R. E., The role of infiltration in the hydrologic cycle, *Eos Trans. AGU, 14*, 446–460, 1933.

Horton, R. E., Erosional development of streams and their drainage basins; hydrophysical approach to quantitative morphology, *Geol. Soc. Am. Bull., 56*, 275–370, 1945.

Interagency Advisory Committee on Water Data, Guidelines for determining flood flow frequency, *U.S. Geol. Surv. Bull. 17B*, 165 pp., 1982.

Kirkby, M. J. (Ed.), *Hillslope Hydrology*, pp. 325–363, John Wiley, New York, 1978.

Kirkby, M. J., A runoff simulation model based on hillslope topography, in *Scale Problems in Hydrology*, edited by V. K. Gupta, I. Rodriguez-Iturbe, and E. F. Wood, D. Reidel, Hingham, Mass., 1986.

Manning, R., On the flow of water in open channels and pipes, *Trans. Inst. Civ. Eng. Ireland, 20*, 161–207, 1891.

Moughamian, M. S., D. B. McLaughlin, and R. L. Bras, Estimation of flood frequency: An evaluation of two derived distribution procedures, *Water Resour. Res., 23*, 1309–1319, 1987.

Newson, M. D., The Plynlimon floods of August 5th/6th, 1973, *Res. Rep. 26*, Institute of Hydrology, Wallingford, United Kingdom, 1975.

Nielsen, D. R., J. W. Biggar, and K. T. Erh, Spatial variability of field-measured soil water properties, *Hilgardia, 42*(7), 215–260, 1973.

O'Loughlin, E. M., Saturation regions in catchments and their relations to soil and topographic properties, *J. Hydrol., 53*, 229–246, 1981.

O'Loughlin, E. M., Prediction of surface saturation zones in natural catchments by topographic analysis, *Water Resour. Res., 22*, 794–804, 1986.

Philip, J. R., The theory of infiltration, *Adv. Hydrosci., 5*, 215–296, 1969.

Pilgrim, D. H., I. Cordery, and B. C. Baron, Effects of catchment size on runoff relationships, *J. Hydrol., 58*, 205–221, 1982.

Richards, L. A., Capillary conduction of liquids through porous mediums, *Physics, 1*, 318–333, 1931.

Rodriguez-Iturbe, I., and J. Valdes, The geomorphologic structure of the hydrologic response, *Water Resour. Res., 15*, 1409–1420, 1979.

Russo, D., and E. Bresler, Soil hydraulic properties as stochastic processes, 1, An analysis of field spatial variability, *Soil Sci. Soc. Am. J., 45*, 682–687, 1981.

Sherman, L. K., Streamflow from rainfall by the unit-graph method, *Eng. News Rec., 108*, 501–505, 1932.

Sivapalan, M., Scale problems in rainfall, infiltration, and runoff production, Ph.D. dissertation, Dep. of Civ. Eng., Princeton Univ., Princeton, N. J., 1986.

Sivapalan, M., and E. F. Wood, Spatial heterogeneity and scale in the infiltration response of catchments, in *Scale Problems in Hydrology*, edited by V. K. Gupta, I. Rodriguez-Iturbe, and E. F. Wood, pp. 81–106, D. Reidel, Hingham, Mass., 1986.

Sivapalan, M., K. J. Beven, and E. F. Wood, On hydrological similarity, 2, A scaled model of storm runoff production, *Water Resour. Res., 23*, 2266–2278, 1987.

Sivapalan, M., E. F. Wood, and K. J. Beven, On hydrologic similarity, 3, A dimensionless flood frequency model using a generalized geomorphologic unit hydrograph and partial area runoff generation, *Water Resour. Res.*, in press, 1989.

Smith, R. E., and R. H. B. Hebbert, A Monte Carlo analysis of the hydrologic effects of spatial variability of infiltration, *Water Resour. Res., 15*, 419–429, 1979.

Weyman, D. R., Throughflow on hillslopes and its relation to the stream hydrolograph, *Bull. Int. Assoc. Sci. Hydrol., 15*(2), 25–33, 1970.

Wolock, D. M., Topographic and soil hydraulic control of flow paths and soil contact time: Effects on surface water acidification, Ph.D. dissertation, Dep. of Environ. Sci., Univ. of Va., May 1988.

Wood, E. F., and C. Hebson, On hydrologic similarity, 1, Derivation of the dimensionless flood frequency curve, *Water Resour. Res., 22*, 1549–1554, 1986.

Wood, E. F., M. Sivapalan, K. J. Beven, and L. Band, Effects of spatial variability and scale with implications to hydrologic modeling, *J. Hydrol., 102*, 29–47, 1988*a*.

Wood, E. F., M. Sivapalan, D. Thongs, K. Beven, and L. Band, A DEM based model for catchment storm response using catchment morphology (abstract), *Eos Trans. AGU, 69*, 1224, 1988*b*.

K. Beven, Centre for Research on Environmental Systems, Institute of Environmental and Biological Sciences, University of Lancaster, Lancaster LA1 4YQ, England.

M. Sivapalan, Centre for Water Research, University of Western Australia, Nedlands, Western Australia 6009.

E. F. Wood, Water Resources Program, Department of Civil Engineering and Operations Research, Princeton University, Princeton, NJ 08544.

9. EVAPOTRANSPIRATION AND RUNOFF FROM LARGE LAND AREAS: LAND SURFACE HYDROLOGY FOR ATMOSPHERIC GENERAL CIRCULATION MODELS

J. S. FAMIGLIETTI and E. F. WOOD

Department of Civil Engineering and Operations Research, Princeton University, Princeton, NJ 08544, U.S.A.

Abstract. A land surface hydrology parameterization for use in atmospheric GCMs is presented. The parameterization incorporates subgrid scale variability in topography, soils, soil moisture and precipitation. The framework of the model is the statistical distribution of a topography-soils index, which controls the local water balance fluxes, and is therefore taken to represent the large land area. Spatially variable water balance fluxes are integrated with respect to the topography-soils index to yield our large scale parameterizations: water balance calculations are performed for a number of intervals of the topography-soils distribution, and interval responses are weighted by the probability of occurrence of the interval. Grid square averaged land surface fluxes result. The model functions independently as a macroscale water balance model. Runoff ratio and evapotranspiration efficiency parameterizations are derived and are shown to depend on the spatial variability of the above mentioned properties and processes, as well at the dynamics of land surface-atmosphere interactions.

1. Introduction

One problem that climate modelers and hydrologists have in common is modeling the hydrologic cycle at large scales. Hydrologists have traditionally been interested in short and long term predictions of the water balance fluxes at the catchment scale (e.g. for flood forecasting and water supply predictions). However, there is no consensus on how to extrapolate well known point relationships to the catchment scale and beyond. Recently, hydrologists have also realized that processes operating on scales greater than the size of a watershed can be responsible for observed watershed response. For example, precipitation systems typically operate on scales larger than the catchment, and determining the origin of that water falling as precipitation may be a global scale problem (Koster, 1988). In short, hydrologists need to improve their understanding of hydrologic response at the large scale.

Climate modelers are particularly interested in large scale parameterizations of land surface hydrology for their numerical simulations of climate using atmospheric general circulation models (GCMs). But climate modelers face a scale problem of their own. Recognizing the sensitivity of GCM climate to land surface boundary conditions (e.g. Shukla and Mintz, 1982), climate modelers are seeking a more detailed grid scale parameterization than the simplified one-dimensional approach first introduced into GCMs by Manabe (1969). Although the parameterization of land surface hydrological processes at the large scale is an area of active research (e.g. Dickinson, 1984; Sellers *et al.*, 1986; Abramopolous *et al.*, 1988; Entekhabi and Eagleson, 1989), the problem is still largely unresolved.

Surveys in Geophysics **12**: 179–204, 1991.

a. LAND SURFACE HYDROLOGY AND SPATIAL VARIABILITY

The hydrologic fluxes produced by large land areas are a result of the complex interaction of climate, soils, topography, geology, and vegetation. Each of these components exhibits a high degree of spatial variability at the large scale, and individual correlation lengths are not necessarily the same. For example, soil properties may vary widely on the hillslope scale, while vegetation and climate vary on more regional scales. Remote sensing can certainly help to quantify some of this variability, but the problem that remains is how to parameterize the dynamic hydrologic response of large land areas which exhibit considerable subgrid scale spatial variability in the major process controls.

The modeling problem is compounded when one considers that hydrologic phenomena at the land surface (i.e. infiltration, runoff, subsurface flow, and evapotranspiration) operate on different space-time scales. Infiltration and runoff, for example, are storm phenomena, which operate on the same time scales as precipitation events and on localized spatial scales. Subsurface flow, however, is active during storms and interstorm periods (as subsurface storm flow and base flow, respectively), and may act over the entire area of interest.

The scientific problem at hand is then to formulate mathematical descriptions for hydrologic response at the large scale, reconciling the various space-time scales of hydrologic phenomena with the tremendous spatial variability in land surface characteristics. Unfortunately, however, much of our knowledge of these processes is derived from laboratory experiments or field work at the point scale. Consequently, we must develop mathematical expressions for the large scale response rooted in the physics known at smaller scales, while incorporating important spatial variability in land surface hydrologic processes and properties.

A major control on the land surface hydrologic fluxes at the GCM grid square scale is subgrid scale variation in surface soil moisture. The dependence of local infiltration and evapotranspiration capacities on local surface soil moisture is well known. Consequently, as the framework of our parameterization, we have chosen to model the subgrid scale space-time dynamics of surface soil moisture. Given a local value of surface soil moisture, local infiltration, evapotranspiration, and surface runoff fluxes can be computed. Given the space-time distribution of surface soil moisture, local fluxes can then be aggregated to yield the areal averaged water balanced fluxes.

It is our belief that subgrid scale variations in topography and soil dominate the process of spatial redistribution of soil moisture over large land areas. In this paper we propose the use of hydrogeomorphic relationships, which incorporate these variations by means of a local topography-soils index (Beven, 1986), to model the space-time dynamics of soil moisture redistribution. Local land surface hydrologic fluxes can be related to surface soil moisture, and through the control of topography and soils on the local water balance, to local topography-soils indices.

Therefore, knowledge of the distribution of the topography-soils index provides a consistent framework for averaging local land surfaces fluxes up to the macroscale.

Based on these concepts, we present a land surface hydrology parameterization for the areal average water balance fluxes, which includes a subgrid scale variability in precipitation, topography, soils, soil moisture, infiltration, evapotranspiration, and surface runoff. We have attempted to keep the model as simple as possible, while remaining true to the process physics, for two reasons: (i) to minimize computer run times, so that when combined with a more complicated GCM, no significant additional computational burdens arise, and (2) due to the lack of large scale data (e.g. soils, vegetation, evaporation) and enough variability to develop and verify more complex models. The model can be used by hydrologists to study the water balance over large land areas, and by climate modelers, to compute boundary conditions at the land surface for simulations of the general circulation of the atmosphere. Please note that throughout this paper, the term land area is used interchangeably with GCM land surface grid square, as the model is meant to meet the needs of both hydrologists and climatologists.

In the sections that follow, the dynamic soil moisture model is presented after a review of runoff generation mechanisms. Next, the equations for the land surface fluxes of infiltration, evaporation and transpiration are presented, with a description of how these flux rates are coupled to both surface soil moisture and atmospheric forcing. A discussion of runoff computations within the model is followed by a description of the spatial variability in rainfall. Finally, the macroscale equations for the land surface hydrologic fluxes are described.

2. Runoff Generation Mechanisms

Horton (1933) first proposed that overland flow is generated over an entire catchment, whenever the infiltration capacity of its soil is exceeded by the precipitation rate. Today we realize that the concept of an entire watershed producing Hortonian overland flow cannot fully explain the generation of storm runoff. Numerous field studies have shown that at any time during a storm, only partial areas of the catchment are contributing runoff. Additionally, the spatial variability in soil properties, antecedent surface soil moisture, topography, and rainfall will result in a range of runoff generation mechanisms operating to produce the storm hydrograph. The common feature of these mechanisms is that the partial areas which contribute runoff are dynamic; they can expand and contract during storm and interstorm periods, and they can vary seasonally as well. The difference between these partial area mechanisms is the manner in which runoff is generated, and the pathway the runoff takes to the stream.

Hortonian overland flow, or infiltration excess runoff, occurs over those areas of a catchment where the local infiltration capacity is exceeded by the local precipitation rate. This is not a common occurrence in most humid, temperate climates.

However, it may occur more frequently in arid and semi-arid climates, or where land use practices have severely altered the structure of the soil.

Rain falling directly on saturated soil areas or stream channels produces saturation excess runoff (Dunne and Black, 1970). These saturated areas are commonly located adjacent to streams, where the water table is high and soil moisture storage capacity is low. Saturation excess contributing areas grow during storms as infiltrating rainfall raises the shallow water table to the surface. The downslope redistribution of infiltrated rainfall toward the stream network also contributes to the growth of saturated areas along channels. The saturation excess runoff mechanism is most active in humid regions, with thin soils, gentle terrain, concave lower slopes, and wide valley bottoms (Dunne, 1978).

Subsurface storm flow occurs when infiltrated rainfall travels rapidly downslope, either through a network of interconnected large pores (macropores), or by flow in the saturated zone, as the water table rises during storms. Subsurface storm flow is most common in humid regions with steep, straight or convex slopes, narrow valley bottoms, and where permeable soils overlie relatively impermeable soils or bedrock (Dunne, 1978). Even when subsurface flow velocities are too small to contribute significantly to the storm by hydrograph, it may still dominate the overall response in terms of volume, as the delayed subsurface response provides the hydrograph tail (Knisel, 1973).

These runoff generation mechanisms are commonly in operation in many areas of the world. The dominant mechanism will be a function of climate and local land surface properties. However, any model for the generation of runoff from large land areas should incorporate these concepts.

3. A Physically Based Model for Space-Time Soil Moisture Dynamics

To properly model the land surface hydrologic fluxes, the spatial distribution of surface soil moistue becomes crucial. Near surface soil moisture influences infiltration and exfiltration capacities and thus the quantity of infiltration excess runoff and evapotranspiration. The amount of soil moisture storage available at any location determines the amount of saturation excess runoff produced. Subsurface flow is also dependent upon the moisture status of the area, contributing more as average soil moisture levels increase and less as they decrease.

Beven and Kirkby (1979) present a simple, physically based model for the spatial distribution of soil moisture, based on topographic controls. The model was first proposed for small to medium sized catchments in humid temperature areas, but subsequent revisions (e.g. Sivapalan *et al.*, 1987) allow for a much broader range of usage. The treatment of evapotranspiration in these papers, if present, has been weak, ignoring any spatial variations (Beven and Kirkby, 1979; Beven *et al.*, 1984). In this paper we extend the concepts of Beven (1986) and Sivapalan *et al.* (1987) to large land areas, and we have included space-time variations in precipitation and evapotranspiration.

a. THE SPATIAL DISTRIBUTION OF SOIL MOISTURE DEFICITS AND SURFACE SOIL MOISTURE

To simplify the modeling process the following assumptions regarding land surface hydrologic processes are made: (*a*) that the hydrologic response of large land areas proceeds as a series of quasi-steady states; (*b*) that the subsurface flow rate, q_i, at location i can be related to a local storage deficit, s_i, by

$$q_i = T_i \exp(-s_i/m)\tan\beta, \tag{1}$$

where $T_i \exp(-s_i/m)$ is conceptually equivalent to the local transmissivity, $\tan\beta$ is the local slope, and m is a parameter related to the decline of saturated hydraulic conductivity with depth (storage deficit in this paper refers to available porosity beyond the field capacity of the soil – positive deficits imply unsaturated areas while negative deficits imply saturated areas); (*c*) that the saturated hydraulic conductivity declines exponentially with depth, so that

$$K_s(z) = K_0 \exp(-fz), \tag{2}$$

where K_s is the saturated hydraulic conductivity, z is the depth into the soil profile, K_0 is the saturated hydraulic conductivity at the soil surface, and f is a scaling parameter; and (*d*) that at any location i, at steady state, the downslope saturated flow is given by

$$q_i = aR, \tag{3}$$

where a is the unslope contributing area which drains through the unit contour width at i, and R is defined as the steady rate of recharge to the water table.

Integrating Equation (2) from a depth Z to the water table at depth z_i, the transmissivity of the saturated soil profile, $T(z_i)$, is obtained. For large f or Z

$$T(z_i) = T_0 \exp(-fz_i), \tag{4}$$

where $T_0 = K_0/f$. Assuming a simple relationship between storage deficit and water table depth, e.g.

$$s_i = \delta\Delta\theta z_i, \tag{5}$$

where $\Delta\theta$ is the difference between saturation and residual moisture contents, and δ is a constant, then (1) is equivalent to the downslope saturated flow beneath the water table when $T_i = T_0$, and $m = \delta\Delta\theta/f$, i.e.

$$q_i = T_0 \exp(-fz_i)\tan\beta.$$

Note that these assumptions are not overly restrictive. Assumption (a) is a pragmatic decision given the large areas under consideration and the simplicity desired for compatibility with GCMs. Assumption (b) is nothing more than the kinematic wave assumption if we assume that the soil surface is roughly parallel to the bedrock and if the assumptions of the last paragraph are considered. The applicability of assumption (c) has been demonstrated by Beven (1982) for a wide

variety of soils. Assuming a steady R in (d) is not unreasonable given no way to measure spatial variations in recharge rates on upslope contributing areas.

Equating (1) and (3), and solving for s_i yields

$$s_i = -m \ln\left(\frac{aR}{T_0 \tan \beta}\right). \tag{6}$$

The average moisture status of the area can be characterized by $\bar{s}$, where

$$\bar{s} = \frac{1}{A} \int_A s_i \, \mathrm{d}A. \tag{7}$$

Substituting (6) into (7), while solving (6) for R and using in (7), after some manipulation, an expression for storage deficit at any loction i is given as:

$$(\bar{s} - s_i) = m\left\{\ln\left(\frac{a}{\tan \beta}\right) - \lambda\right\} - \{\ln T_0 - \ln T_e\} \tag{8a}$$

or

$$s_i = \bar{s} - m\left\{\ln\left(\frac{aT_e}{T_0 \tan \beta}\right) - \lambda\right\} \tag{8b}$$

where

$$\ln T_e = \frac{1}{A} \int_A \ln T_0 \, \mathrm{d}A, \tag{9}$$

$$\lambda = \frac{1}{A} \int_A \ln\left(\frac{a}{\tan \beta}\right) \mathrm{d}A, \tag{10}$$

and $\ln(aT_e/T_0 \tan \beta)$ is the local value of the topography-soils index.

Equation (8a) states that the deviation of the local storage deficit from its areal average results from the deviation of the local value of $\ln(a/\tan \beta)$ from its areal average and the deviation of the local transmissivity coefficient from its areal average. Restated, given any average moisture level $\bar{s}$, the local storage deficit at steady state is determined by a topographic effect and a soils effect. Equation (8b) states that at any point on the land surface, for a given $\bar{s}$, one need only the local value of the topography-soils index to determine the storage deficit.

To infer surface soil moisture from storage deficit the following assumptions are made. When the storage deficit is zero or negative, the soil is saturated and the surface soil moisture is equivalent to the saturation moisture content of the soil. When the storage deficit is positive, the location is unsaturated, and the soil profile is assumed to have reached gravity drainage. Local surface soil moisture content can then be determined from the Brooks and Corey (1964) soil moisture characteristic relations for the unsaturated zone, where

$$\theta(\psi) = \theta_r + (\theta_s - \theta_r)\left(\frac{\psi_c}{\psi}\right)^B \psi > \psi_c \tag{11}$$

and θ is the moisture content, ψ is the matric head equal to $z_i - z$, θ_r is the residual moisture content, θ_s is the saturation moisture content, ψ_c is the height of the capillary fringe, and B is the pore size distribution index. At the soil surface, where $z = 0$ and $\psi = z_i$, the surface soil moisture, θ_i, is

$$\theta_i = \theta_r + (\theta_s - \theta_r)\left(\frac{\psi_c}{z_i}\right)^B. \tag{12}$$

The relationship between z_i and s_i, i.e. $z_i = s_i/\delta\Delta\theta$, is obtained by integrating the soil moisture characteristic from the top of the capillary fringe to the soil surface (Sivapalan *et al.*, 1987). Therefore, for any unsaturated location, the water table depth and the surface soil moisture can be computed.

The spatial distribution of storage deficits and surface soil moisture can now be computed given $\bar{s}$, the topography-soils index, and some soil parameters. The topography index can be calculated using digital elevation models (DEMs) or topographic maps. A number of algorithms are currently available to extract information such as upslope contributing area and slope from DEMs. Where available, data on hydraulic conductivity may be used to determine the topography-soils index. When these data are not available, the mean and standard deviation of hydraulic conductivity will suffice (discussed later). Also discussed in a later section is the estimation of $\bar{s}$ and f or m. For simplicity, the soil parameters θ_r, θ_s, ψ_c, and B are taken as constants for the land surface area. Although they are dependent on soil type, we believe that other land surface parameters will have a more pronounced effect on the hydrologic fluxes.

Continuous updating of $\bar{s}$ after each time step yields an updated spatial distribution of surface soil moisture. Note also that Equation (8b) can be used to determine the location of saturated areas. Saturated areas are those for which $s_i \leqslant 0$, or

$$\ln\left(\frac{aT_e}{T_0 \tan\beta}\right) \geqslant \frac{\bar{s}}{m} + \lambda. \tag{13}$$

The growth and decay of saturated areas along stream channels can then be predicted by continuous soil moisture accounting, i.e. continuous updating of $\bar{s}$. Continuous accounting of $\bar{s}$ is analogous to the accounting done in current GCM land surface parameterizations of grid average soil moisture.

a. The spatial distribution of the topography-soils index as a model framework

The spatial distribution of the topography-soils index forms the foundation of our parameterization, through its control on soil moisture storage, water table depths, and its influence on near surface soil moisture. Infiltration and evapotranspiration capacities will be shown to depend on surface soil moisture, and thus the topography-soils index, in a later section. In this section, we discuss methods for quantifying the spatial variation in the topography-soils index. Once the variation in surface

soil moisture has been quantified, the spatial variability in the water balance fluxes can be determined, and areal averaged fluxes can be computed.

Dealing with the large quantities of topographic and soils data associated with large land areas can quickly become an overwhelming task, particularly when the global scale is considered. When the data is available, it is often in the form of a digital elevation model or a geographic information system (GIS). A common approach to utilize this data has been through the use of distributed models, where the land surface is treated as a collection of pixels whose size depends on the resolution of the data. The DEM represents the catchment digitally, and GIS data such as soil type and land use are layered over the DEM to represent land surface properties. The topography-soils index can then be calculated for each pixel. This approach works well at the catchment scale, but as larger scales are approached, computational and storage burdens can become excessive.

A simpler way to characterize the variability in the topography-soils index is by the use of probability density functions. In this paper we represent the large land area by its statistical distribution of the topography-soils index. The implicit assumption in this procedure is that knowledge of the exact pattern of the topography-soils index is not necessary to compute the land surface water balance fluxes. Research into a threshold scale, above which such exact patterns can be represented statistically, is in progress. This scale, called the representative elementary area (REA) by Wood *et al.* (1988), has been identified in the context of storm response modeling. Its existence in other branches of the water balance is currently being explored.

To perform water balance computations, the distribution is divided into a number of intervals. Each interval of the distribution represents the fraction of land surface area having that particular $\ln(aT_e/T_0 \tan \beta)$ value. A representative value of $\ln(aT_e/T_0 \tan \beta)$ for the interval provides the necessary information for land surface hydrology calculations: for each interval value of $\ln(aT_e/T_0 \tan \beta)$, the water table depth, soil moisture, and storage in the unsaturated zone are known. The corresponding land surface fluxes for each interval can be computed and weighted by the probability of occurrence of the interval. The areal averaged land surface hydrologic fluxes result. This averaging procedure is presented analytically in a later section as our land surface hydrology parameterization.

To draw an analogy to current land surface hydrologic 'bucket' models, this model will treat the grid square land surface as a distribution of buckets, whose capacity and surface soil moisture vary with topography, soil properties, and $\bar{s}$. The resulting large scale hydrologic response is simply a weighted average of the responses of the individual buckets.

Sivapalan *et al.* (1987) have fit a three-parameter gamma distribution to the $\ln(a/\tan \beta)$ values of two catchments in North Carolina. (Wolock *et al.* (1989) also fit gamma distributions to 145 catchments in the northeastern United States, and Wolock (personal communication), in other studies, has found that even the largest catchments fit a gamma distribution.) Assuming independence between transmissiv-

ity and $\ln(a/\tan\beta)$ values, Sivapalan *et al.* (1987) combine the gamma (μ, ϕ, χ) for $\ln(a/\tan\beta)$ with a normal $(0, \sigma_K^2)$ for $\ln(T_e/T_0)$ and arrive at a gamma (μ^*, ϕ^*, χ^*) for $\ln(aT_e/T_0 \tan\beta)$. They show that the parameters μ^*, ϕ^*, and χ^*, can be obtained from the parameters μ, ϕ, and χ and an estimate of the variance of the saturated hydraulic conductivity. Therefore, only a topographic map or a DEM (to determine μ, ϕ, and χ), and an estimate of the variance of the conductivity are required to characterize the distribution of $\ln(aT_e/T_0 \tan\beta)$.

In the following sections we describe the appropriate equations for the water balance processes to be applied to each interval of the $\ln(aT_e/T_0 \tan\beta)$ distribution. In a later section we present the analytical formulations of the averaging procedure which constitute the mathematical statement of our large scale parameterizations for grid square averaged land surface hydrologic fluxes.

4. Local Computation of Land Surface Water Balance Fluxes

a. Infiltration at the soil surface

The governing equation for soil water flow in the unsaturated zone is given by Richards (1931) as

$$\frac{\partial\theta}{\partial t} = \frac{\partial}{\partial z}\left[K(\psi)\frac{\partial\psi}{\partial z} + K(\psi)\right], \tag{14}$$

where θ is the moisture content, ψ is the matric head, and K is the hydraulic conductivity. As is well known, the solution of (14) is not easy, due to the highly nonlinear nature of $K(\psi)$, hysteresis, and the boundary conditions encountered in nature.

Philip (1957) solved (14) with the simplified boundary conditions of an initially uniform moisture profile in the unsaturated zone, and a step change in soil moisture at the soil surface:

$$\theta = \theta_i \qquad t = 0 \quad z \geqslant 0$$

$$\theta = \theta_0 \qquad t > 0 \quad z = 0.$$

His simplified infiltration equation is given by

$$f_i^* = \frac{1}{2} S t^{-1/2} + cK_S, \tag{15}$$

where f_i^* is the infiltration capacity, S is the sorptivity (given by Sivapalan *et al.*, 1987), K_S is the saturated hydraulic conductivity, and cK_S includes the effect of graviy.

In this study, the spatial variation in infiltration rates arises because the sorptivity expression varies with $\ln(aT_e/T_0 \tan\beta)$ through its dependence on surface soil moisture. Consequently, f_i^* will vary with each interval of the distribution. A mean areal value for K_s is used in calculating f_i^* for two reasons. First, the effect of

spatially variable conductivity is already incorporated by the control of $\ln(aT_e/T_0 \tan\beta)$ on the local water balance. Second, we have assumed independence between hydraulic conductivity and the value of $\ln(a/\tan\beta)$. For a given interval of the $\ln(aT_e/T_0 \tan\beta)$ distribution, specifying a local value of K_s would imply knowledge of the covariation of hydraulic conductivity with $\ln(a/\tan\beta)$. However, we have assumed that this covariance is zero. Figure 1a displays the variation of the depth of infiltrated water at capacity (Equation (15) integrated with $\Delta t = 15$ min) with soil moisture. Soil moisture is expressed as percent by volume, and the range of values shown extends roughly from the driest to the wettest conditions likely to be encountered on the land surface.

To couple the infiltration flux rate at the land surface to the atmosphere one must consider the rate at which rainfall is supplied to the soil. If the rainfall rate is very high, the infiltration capacity will be exceeded, and the actual infiltration rate will be equal to the capacity. However, if the precipitation rate is low, then all the rainfall can infiltrate. Therefore, the actual infiltration rate is given by

$$F_i = min[f_i^*, P], \tag{16}$$

where f_i is the actual infiltration rate, and P is the precipitation rate.

b. EVAPORATION FROM SOIL

Two stages have been recognized in the unsteady drying of a soil profile (see Brutsaert, 1982, and Hillel, 1980). In the first stage, the moist soil profile has no problem supplying all the water that the atmosphere demands. Thus, this stage is known as the atmosphere controlled stage. Evaporation proceeds at the potential rate, which is dictated by external climatic conditions. The duration of this stage depends on the rate of the atmospheric demand and the ability of the soil to supply moisture at this rate. Hillel (1980) notes that this stage is frequently brief, and usually ceases within a few days.

As the soil near the surface dries out, moisture can no longer be delivered at the rate demanded by the atmosphere. Instead, the moisture delivery rate is limited by the properties of the soil profile. Thus, this stage of soil drying is known as the soil controlled, or falling rate stage. Brutsaert (1982) notes that at any one point, the transition from soil to atmosphere control is rapid, but over the entire catchment, the changeover will be gradual.

The governing equation for the soil controlled stage of evaporation is obtained by combining soil water continuity with Darcy's law, which yields

$$\frac{\partial\theta}{\partial t} = \frac{\partial}{\partial z}\left[K(\psi)\frac{\partial\psi}{\partial z} - K(\psi)\right]. \tag{17}$$

A simplified formulation considers the soil controlled stage as a desorption problem only. Neglecting gravity, (17) becomes

$$\frac{\partial\theta}{\partial t} = \frac{\partial}{\partial z}\left[K(\psi\,\frac{\partial\psi}{\partial z}\right]. \tag{18}$$

For the simplified boundary conditions

$$\theta = \theta_i \qquad t = 0 \quad z \geqslant 0$$

$$\theta = \theta_d \qquad t > 0 \quad z = 0$$

where θ_d is the moisture at the dry soil surface, (18) can be solved using the Boltzman transform ($\phi = zt^{-1/2}$). Equation (18) reduces to an ordinary differential equation, and the evaporation capacity, f_e^*, is given by

$$f_e^* = \frac{1}{2} D t^{-1/2} \tag{19}$$

where D is the desorptivity (Sivapalan, unpublished), which is dependent on soil type, θ_d, and the surface soil moisture, θ_i. In Equation (19), the desorptivity varies with soil moisture content and thus $\ln(aT_e/T_0 \tan \beta)$. As in the infiltration case, f_i^* will vary with each interval of the $\ln(aT_e/T_0 \tan \beta)$ distribution. Figure 1b displays the variation of the depth of evaporated water at capacity (Equation (19) integrated with $\Delta t = 15$ min) with soil moisture. As in Figure 1a, the range of soil moisture values shown extends roughly from the driest to the wettest conditions likely to be encountered on the land surface.

Coupling this evaporation expression to the atmosphere requires a knowledge of the atmospheric demand for water vapor. When the atmospheric demand, or potential evaporation, can be met by the local land surface area, then the actual evaporation rate is equal to the potential evaporation, and that fraction of the land surface area is subject to atmosphere controlled evaporation. When the local land surface area can no longer meet the atmospheric demand for water vapor, the actual evaporation rate is equal to the evaporation capacity, and that fraction of land surface experiences soil controlled evaporation. At any time, the actual evaporation rate can be expressed locally as

$$f_e = \min[f_e^*, e_{pe}] \tag{20}$$

where f_e is the actual rate of evaporation, and e_{pe} is the potential rate. The potential evaporation is assumed known from atmospheric data or GCM variables.

c. Transpiration by vegetation

The importance of vegetation in the hydrologic cycle cannot be underestimated. Molz (1981) points out that well over half of the water returned to the atmosphere as evapotranspiration flows through the soil-plant system. It has also been recognized that plants are not simply passive wicks conducting moisture from soil water reservoirs to the atmosphere. Rather vegetation is a dynamic component of the soil-plant-atmosphere system, which actively regulates its internal mechanisms (e.g. stomatal closure) in response to changing soil and atmosphere conditions.

The current state of knowledge of transpiration processes should be reflected in any model of the vegetative component of the hydrologic system. As with the storm

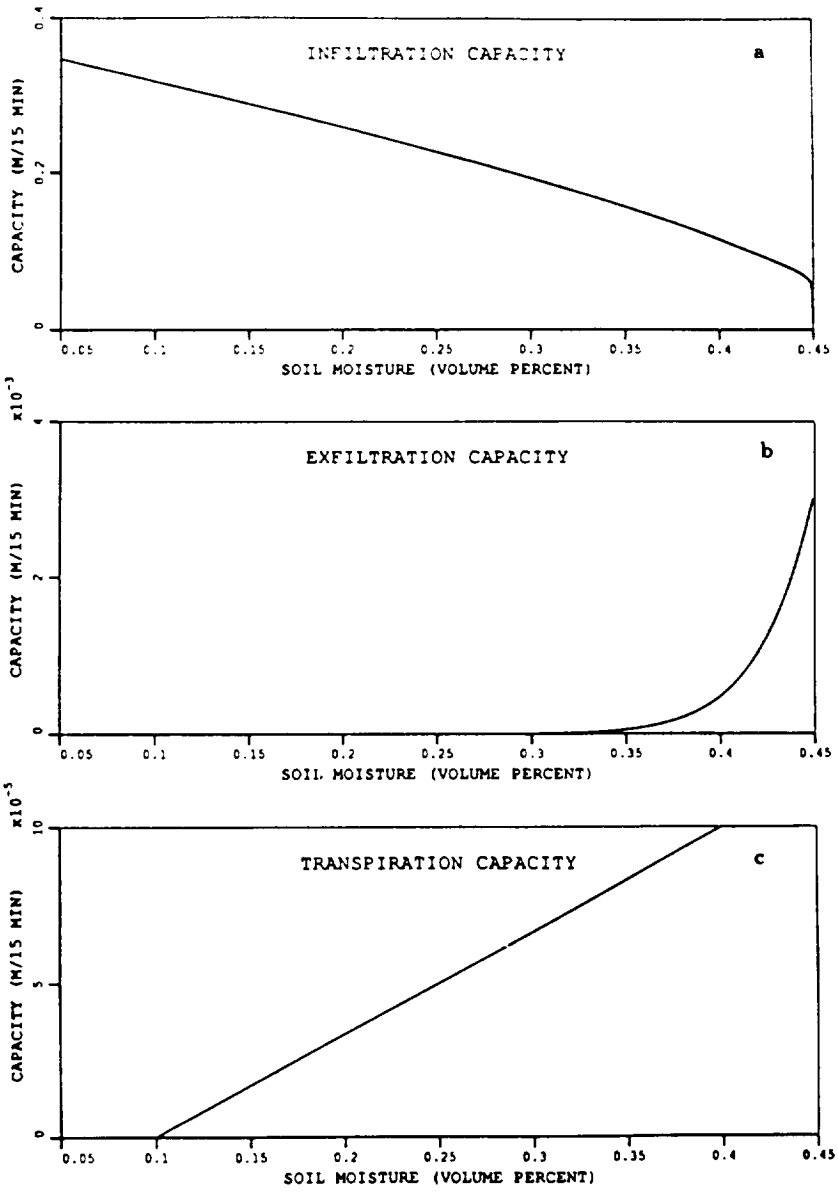

Fig. 1. (a) Infiltration capacity (f_i^*) vs soil moisture; (b) Exfiltration capacity (f_e^*) vs soil moisture; (c) Transpiration capacity (S) vs soil moisture; $\Delta t = 0.25$ hr.

response model, our approach is to keep the transpiration component simple, while maintaining the appropriate level of the process physics, which are briefly described below.

Denmead and Shaw (1962) are credited with first confirming the effects of dynamic soil and atmosphere conditions on transpiration rates. They showed that the ratio of actual to potential transpiration depended on both the potential rate of

transpiration and soil moisture content. In dry soils, vegetation can transpire at the potential rate if that potential is low; in wet soils, actual transpiration can fall below the potential rate if that demand is too high.

We have chosen to model the uptake of soil moisture by roots using the extraction function of Feddes *et al.* (1976). A macroscopic approach is assumed, where the entire root system is viewed as a diffuse moisture sink, rather than considering flow to individual roots in a geometrically complex root system (microscopic approach). This extraction function is shown below.

$$S = S_{\max} \quad \theta_i \geq \theta_1 \tag{21a}$$

$$S = S_{\max} \frac{(\theta_i - \theta_2)}{\theta_1 - \theta_2)} \quad \theta_2 \leq \theta_i < \theta_1 \tag{21b}$$

$$S = 0 \quad \theta_1 < \theta_2 \tag{21c}$$

S is the actual rate of transpiration, and $S_{\max}$ is the maximum rate at which the vegetation can deliver moisture to the atmosphere. $S_{\max}$ is taken as the potential rate of transpiration, e_{pt}, and is assumed known from atmospheric data or GCM variables. The value of surface soil moisture at which transpiration can no longer be sustained at the potential rate is expressed as θ_1, and θ_2 is the wilting point for vegetation. When $\theta_i \geq \theta_1$, transpiration occurs at the potential rate. When $\theta_2 \leq \theta_i < \theta_1$, vegetation transpires at a maximum sustainable rate, or capacity, which depends on the availability of soil moisture. When θ_i remains below θ_2 for extended periods, wilting follows.

The supply and demand dynamics described by Denmead and Shaw are incorporated by allowing the value of θ_1 to vary with atmospheric demand and surface soil moisture, so that at low levels of potential transpiration, even dry areas can transpire at the potential rate, etc. For simplicity, this value of θ_1 is taken to be the same value at which the change from atmosphere controlled to soil controlled evaporation occurs. The wilting value of soil moisture, θ_2, is however taken as a constant.

For each interval of the $\ln(aT_e/T_0 \tan \beta)$ distribution, θ_1, the surface soil moisture, will vary. Consequently, during any time step, a proportion of the vegetated land surface will transpire at the potential rate, and a proportion will transpire at the transpiration capacity, i.e., a fraction of the vegetated land surface will be subject to atmosphere controlled transpiration, and another fraction will be under 'vegetation controlled' transpiration. In areas where soil moisture conditions are exceedingly dry, an additional fraction of vegetated land surface will experience wilting conditions. Figure 1c displays the variation of the depth of transpired water (Equation (19) multiplied by a Δt of 15 min) with soil moisture.

d. SURFACE RUNOFF

Three types of surface runoff are computed within the model; saturation excess runoff, infiltration excess runoff, and subsurface flow.

1. Saturation Excess Runoff

Given a value of $\ln(aT_e/T_0 \tan \beta)$ for a particular interval of the distribution, the available soil moisture storage can be calculated using (8). Rain falling on saturated areas ($s_i \leqslant 0$) is transformed immediately into runoff. Additionally, over parts of the land surface where the available soil moisture storage is small, for example, close to streams where the water table is high, the local storage deficit may be satisfied during a storm. To determine when saturation excess runoff occurs on these areas, one need only keep track of the volume of infiltration and compare it to s_i. When the infiltrated volume of moisture exceeds available soil moisture storage, saturation excess runoff occurs on that interval of the distribution.

2. Infiltration Excess Runoff

Infiltration excess runoff occurs when the local infiltration capacity is exceeded by the precipitation intensity, or $P > f_i^*$. That rainfall that is not infiltrated runs off downslope to the stream channel.

3. Subsurface Flow

The contribution of the land surface to runoff by subsurface flow, Q_s is given by integrating the downslope saturated flow, q_i along both sides of the stream network:

$$Q_s = \int_L q_i \, dL \tag{22}$$

or

$$Q_s = Q_0 \exp\left(-\frac{\bar{s}}{m}\right) \tag{23}$$

where

$$Q_0 = AT_e \exp(-\lambda) \tag{24}$$

(Sivapalan *et al.*, 1987) L is the total length of the channel network (both sides), and A is the area of the land surface. Again, this is the subsurface flow exiting the hillslope at the stream channel. Note that the quasi-steady state approach implicitly incorporates the dynamics of subsurface flow on hillslopes during storms; as $\bar{s}$ is updated, the water table profile shifts in response.

The parameters m and Q_0 are physically based, and can be obtained from field and map information (Beven and Kirkby, 1979; Beven *et al.*, 1984) Alternatively, they can be determined by calibration to a number of recession curves (Beven and Wood, 1983). The average storage deficit at the start of a simulation can then be obtained by inverting (17).

For large land areas and particularly for GCM grid squares, appropriate streamflow data is most likely not available. Research is in progress in which we attempt to extract these parameters from remotely sensed soil moisture.

5. The Spatial Distribution of Precipitation Intensity

Given the large areas under consideration, subgrid scale rainfall intensities will vary considerably. When using spatially distributed models, this poses no problem: rainfall inputs can vary with each node or pixel in the model. Space-time varying inputs can be determined from radar estimates of rainfall, stochastic rainfall models, or from weighted point measurements from raingauges. However, in a lumped modeling approach such as this, only one value of rainfall can be used as input. Hydrologists realize that such an average estimate of rainfall cannot possibly capture the natural spatial variability of the rainfall process. The experience of climatologists suggests that the one value of precipitation computed for a GCM grid square is unrealistically low.

One way to reconcile this disparity is to assume that the rainfall intensity predicted by the GCM, or averaged from ground data, is the mean of a distribution of possible intensities falling on any one location. We assume that the point rainfall intensity, P, is exponentially distributed (Eagleson *et al.*, 1987), with mean $E[P]$, as

$$f_p(P) = \frac{1}{E[P]} \exp(-P/E[P]) \qquad P \geqslant O \tag{25}$$

In this manner, each interval of the $\ln(aT_e/T_0 \tan \beta)$ distribution, i.e. each fraction of the land surface, can be subjected to a range of possible rainfall intensities, each with an associated probability of occurrence. For each interval of the $\ln(aT_e/T_0 \tan \beta)$ distribution, an expected response to the distribution of rainfall intensities will be calculated. These interval responses will themselves be aggregated to yield the expected or areal averaged storm response for the land surface.

6. Macroscale Parameterizations for Land Surface Water Balance Fluxes

In this section we domonstrate how to aggregate the water balance fluxes of the individual intervals of the $\ln(aT_e/T_0 \tan \beta)$ distribution. This procedure is equivalent to calculating the areal averaged fluxes for the land surface. Computationally, fluxes for each interval are weighted by the corresponding probability of the interval, and large scale average fluxes result. The analytical formulations are presented here. These constitute our land surface parameterizations for storm runoff and evaportranspiration processes. The equations are proposed for use in GCMs or for use in a large scale water balance model. Calculations require minimal computer time, and only a knowledge of the topography and some soils and vegetation properties is needed in addition to routine land surface information. In the equations presented, the distributions of precipitation and the topography soils-index are assumed to be independent. Also, flux rates for precipitation, infiltration, evapotranspiration, and potential evapotranspiration, are assumed to now represent a depth over some specific time interval.

Equation (13) gives the relationship between the topography-soils index and saturated areas: those points with a topography-soils index greater than or equal to the right side of (13) are saturated. For convenience, let us define a 'saturation' value of the topography-soils index, $\ln^*(aT_E/T_0 \tan \beta)$. This is the value at which the storage deficit, s_i, is just equal to zero. Topography-soils indices greater than or equal to $\ln^*(aT_E/T_0 \tan \beta)$ are associated with saturated areas. The saturation value of the topography-soils index is given as

$$\ln^*\left(\frac{aT_E}{T_0 \tan \beta}\right) = \frac{\bar{s}}{m} + \lambda. \tag{26}$$

Now we can proceed with the land surface hydrological parameterizations.

a. Storm Runoff

1. The Expected Value of Infiltration Excess Runoff

The expected value of the depth of infiltration excess runoff for the large land area, $E[Q_{inf}]$, is

$$E[Q_{inf}] = \int_0^{x = \ln^*(aT_E/T_0 \tan \beta)} \int_{P = f_i^*}^{\infty} (P - f_i^*) f_p(P) f_x(x)\, dp\, dx, \tag{27}$$

where $x = \ln(aT_E/T_0 \tan \beta)$. Equation (27) states that on unsaturated areas of the land surface ($0 \leqslant x < \ln^*(AT_E/T_0 \tan \beta)$), infiltration excess runoff occurs when the local infiltration capacity has been exceeded. As previously mentioned, infiltration capacity is parameterized here as a function of surface soil moisture which depends only on the local value of the topography-soils index.

2. The Expected Value of Saturation Excess Runoff

All rain falling on saturated areas of the land surface is transformed immediately into saturation excess runoff. Additionally, over some fractions of the land surface, storage deficits will be satisfied during a time step. Rain falling on these newly saturated areas will also be transformed into saturation excess runoff. The expected value of the depth of saturation excess runoff, $E[Q_{sat}]$, is then

$$E[Q_{sat}] = \int_{x = \ln^*(aT_E/T_0 \tan \beta)}^{x = \infty} \int_{P = 0}^{P = \infty} P f_p(P) f_x(x)\, dp\, dx + \int_{x = 0}^{x = \ln^*(aT_E/T_0 \tan \beta)} \int_{P = S_i}^{P = \infty} (P - S_i) f_p(P) f_x(x)\, dp\, dx. \tag{28}$$

The first term on the right hand side represents runoff generated on those areas that are saturated at the start of a time step, while the second term represents the runoff generated on those areas that become saturated during a time step.

3. *The Expected Value of Total Storm Runoff*

The expected value of the depth of total storm runoff, $E[Q_t]$ is given by summing (27), (28), and (23), where

$$E[Q_t] = E[Q_{\text{inf}}] + E[Q_{\text{sat}}] + Q_s \tag{29}$$

for any time step.

b. EVAPOTRANSPIRATION

The long term distribution of vegetation type and density depends on the interaction of climate, topography, and soils. We can observe, for example, that vegetation density increases along stream networks where the water table is high (high values of $\ln(aT_e/T_0 \tan \beta)$). We can hypothesize that vegetation type, and thus wilting point, θ_2, will vary locally with $\ln(aT_e/T_0 \tan \beta)$, and regionally with the large scale average soil moisture deficit, $\bar{s}$. At present, the spatial variation in these parameters can be quantified somewhat by remote sensing. Nevertheless, their relationship to the distribution of the topography-soils index has received little attention.

Extracting this information from remotely sensed data and investigating these relationships is an area worthy of future research: however, for the purposes of this paper, some simplifying assumptions will be made. First, we assume that each interval of the $\ln(aT_e/T_0 \tan \beta)$ distribution is covered by a constant vegetated fraction, F_v. Second, as previously mentioned, we assume that one value of θ_2 applies to the entire vegetated canopy. Now we can proceed with our land surface evapotranspiration parameterizations.

1. *Areal Averaged Bare Soil Evaporation*

Saturated areas will evaporate at the potential rate. The areal averaged depth of bare soil evaporation by saturated areas is given by

$$E_{s_{ac}} = \int_{x = \ln^*(aT_e/T_0 \tan \beta)}^{x = \infty} e_{pc} f_x(x)\, dx \tag{30}$$

where the subscript s implies saturation and the subscript ac implies atmosphere control.

In addition to saturated areas, at each time step there will be areas on the land surface that are unsaturated, but can still supply moisture at the rate demanded by the atmosphere. The contribution of these areas is given by

$$E_{u_{ac}} = \int_{x = \ln^{rs}(aT_e/T_0 \tan \beta)}^{x = \ln^*(aT_e/T_0 \tan \beta)} e_{pc} f_x(x)\, dx \tag{31}$$

where the subscript u implies unsaturated areas, and $\ln^{rs}(aT_e/T_0 \tan \beta)$ is obtained by setting

$$e_{pc} = f_t^*$$

solving for θ_t, the surface soil moisture (which is a parameter of D) and inverting

(12), (5), and (8). Because the parameterization of D employed is unpublished, we cannot present an expression for $\ln^{ts}(aT_c/T_0 \tan \beta)$. Still, we point out that this value of the topography-soils index is effectively a threshold between atmosphere and soil controlled areas of bare soil evaporation (the superscript *ts* indicates a threshold for soil control.). The threshold value depends on both soil moisture conditions and the atmospheric demand, so that for any time step, the total average depth of evaporation contributed by atmosphere controlled areas is given by

$$E_{ac} = \int_{\lambda = \ln^{ts}(aT_c/T_0 \tan \beta)}^{\lambda = \lambda} e_{pc} f_\lambda(\lambda)\, d\lambda. \tag{32}$$

The areal average depth of evaporation contributed by soil controlled areas is given by

$$E_{sc} = \int_{\lambda = 0}^{\lambda = \ln^{ts}(aT_c/T_0 \tan \beta)} f_c^* f_\lambda(\lambda)\, d\lambda, \tag{33}$$

where the subscript *sc* implies soil controlled evaporation. The total bare soil evaporation depth, E_{bs}, is given by summation of (30), (31), and (33) to yield

$$E_{bs} = E_{sat} + E_{uac} + E_{usc}. \tag{34}$$

2. Areal Averaged Transpiration by Vegetation

All saturated areas will transpire at the rate demanded by the atmosphere. The areal average depth of transpiration by these areas is given by

$$T_{sac} = \int_{\lambda = \ln^{*}(aT_c/T_0 \tan \beta)}^{\lambda = \lambda} e_{pc} f_\lambda(\lambda)\, d\lambda, \tag{35}$$

where again the subscript *s* implies saturation and the subscript *ac* implies atmosphere control.

Analogous to the bare soil case, there will be land surface areas which are not saturated, but can still maintain transpiration at the potential rate. The threshold topography-soils index distinguishing 'vegetation' controlled transpiration from atmosphere controlled transpiration $\ln^{tr}(aT_c/T_0 \tan \beta)$ is for simplicity assumed equal to the threshold index for the bare soil case, $\ln^{ts}(aT_c/T_0 \tan \beta)$. Those areas that are unsaturated and transpiring at the potential rate yield an average depth of

$$T_{uac} = \int_{\lambda = \ln^{tr}(aT_c/T_0 \tan \beta)}^{\lambda = \ln^{*}(aT_c/T_0 \tan \beta)} e_{pc} f_\lambda(\lambda)\, d\lambda \tag{36}$$

where again the subscript *u* implies unsaturated areas.

Unsaturated areas that are unable to meet the atmospheric transpirational demands, i.e. those land surface areas under plant controlled transpiration, produce an average depth given by

$$T_{usc} = \int_{\lambda = \ln^{tr}(aT_c/T_0 \tan \beta)}^{\lambda = \ln^{tr}(aT_c/T_0 \tan \beta)} S f_\lambda(\lambda)\, d\lambda \tag{37}$$

where the subscript vc implies vegetal control, and $\ln^*(aT_c/T_0 \tan \beta)$ is the value of the topography-soils index where θ_r is equal to the wilting value, θ_2, and is obtained from Equations (12), (5) and (8).

Total transpiration for the vegetated land surface area, T_t, is given by

$$T_t = T_{s_{ac}} + T_{u_{ac}} + T_{u_{vc}}. \tag{38}$$

This expression is obtained by summing (35), (36), and (37).

3. Areal Averaged Evapotranspiration

Finally, areal average evapotranspiration, ET is given by

$$ET = (1 - F_v)E_{bs_t} + F_v T_t. \tag{39}$$

4. Model Operation

The first step in model operation is to estimate the areal averaged initial soil moisture deficit, $\bar{s}$. This can be accomplished by inverting (23), or with the help of remotely sensed soil moisture, or from measurements (since $\bar{s}$ is a function of average water table depth by (5), regional estimates of average water table depth would suffice). Since $\bar{s}$ implies a distribution of surface soil moisture through Equations (8), (5), and (12), then the areal averaged fluxes of runoff and evapotranspiration can be computed, given the atmospheric forcing and Equations (29) and (39). These fluxes can then be used to update $\bar{s}$, and the procedure is repeated for the next time step.

c. Runoff Ratio and Evaporation and Transpiration Efficiency

Manipulations of the equations presented above yield the dimensionless runoff ratio and evaporation and transpiration efficiencies.

The ratio of surface runoff to precipitation, or the runoff ratio, $R = E[Q_t]/E[P]$ is given as

$$R = \frac{A_s}{A} + \frac{E[Q_{\inf}]}{E[P]}, \tag{40}$$

where A_s/A represents the fraction of saturated land surface. In this expression, we ignore the contribution of subsurface flow to total runoff, and consider only the ratio of surface runoff to precipitation.

The bare soil evaporation efficiency, $\beta_s = E_{bs_t}/e_{pe}$, given by dividing Equation (34) by e_{pe}, as

$$\beta_s = \frac{A_s}{A} + \frac{A_{\text{trans}_s}}{A} + \frac{E_{u_{sc}}}{e_{pe}} \tag{41}$$

where A_{trans_s}/A represents that fraction of land surface not saturated but still able to evaporate at the potential rate. The subscript 'trans' implies a 'transitional' region where soil moisture decreases from saturation values to a threshold value

below which evaporation proceeds at the soil controlled rate. The subscript s represents bare soil.

The transpiration efficiency, $\beta_t = T_t/e_{pt}$, is obtained by dividing Equation (38) by e_{pt}, to yield

$$\beta_t = \frac{A_s}{A} + \frac{A_{\text{trans}_t}}{A} + \frac{T_{u_{ts}}}{e_{pt}}. \tag{42}$$

Analogous to the bare soil case, A_{trans_t}/A represents that fraction of land surface area not saturated but still able to transpire at the potential rate, the subscript 'trans' implies 'transitional' between atmosphere controlled and vegetation controlled transpiration, and the subscript v represents vegetation.

8. Discussion

The runoff ratio and evaporation and transpiration efficiencies effectively characterize the large scale hydrologic response. The various modes of land surface behavior in response to atmospheric forcing are represented by the individual terms in each of the ratios. The evaporation efficiency consists of a term representing the fraction of saturated land surface, where β_s is 1, a term representing a transitional region where the soil is unsaturated, but the evaporation efficiency is still 1, and a soil controlled area term. The transpiration efficiency is composed of analogous terms to β_s: a saturated area term where transpiration is at the potential rate, a transitional area term where transpiration is still at the potential rate but the soil moisture is decreasing, and a vegetation controlled term. The runoff ratio consists of a saturated area term, where runoff is a maximum, and although a transitional area term does not fall out neatly from the parameterization, it is in fact contained within the infiltration excess runoff term in (40). It is easy to conceptualize that as surface soil moisture decreases from saturation values to drier values, a threshold value of soil moisture will be encountered, beyond which infiltration capacities are too high to produce runoff. Over the range of soil moisture between saturation and this threshold value, runoff will decrease from a maximum rate to zero. The fraction of land surface with surface soil moisture lower than this threshold value will produce no runoff. Because $E[Q_{\text{inf}}]$ in (28) is an integral over all unsaturated areas, both the transitional region term and the drier region term are contained in the infiltration excess runoff term in (40).

In Figure 2a–c the runoff ratio, R, is plotted versus $\bar{s}$, the average storage deficit, for increasing levels of rainfall intensity. The range in magnitude of $\bar{s}$ can be considered due to seasonal variation, with higher numbers representing drier conditions. The solid line in each plot represents the runoff ratio. For one value of the average storage deficit, R increases as the rainfall intensity increases from Figure 2a to 2c. There are two explanations for this. First, infiltration excess runoff is occurring over a large fraction of the land surface as the rainfall intensity increases. This is shown by the difference between the solid line (R) and the dashed line (A_s/A)

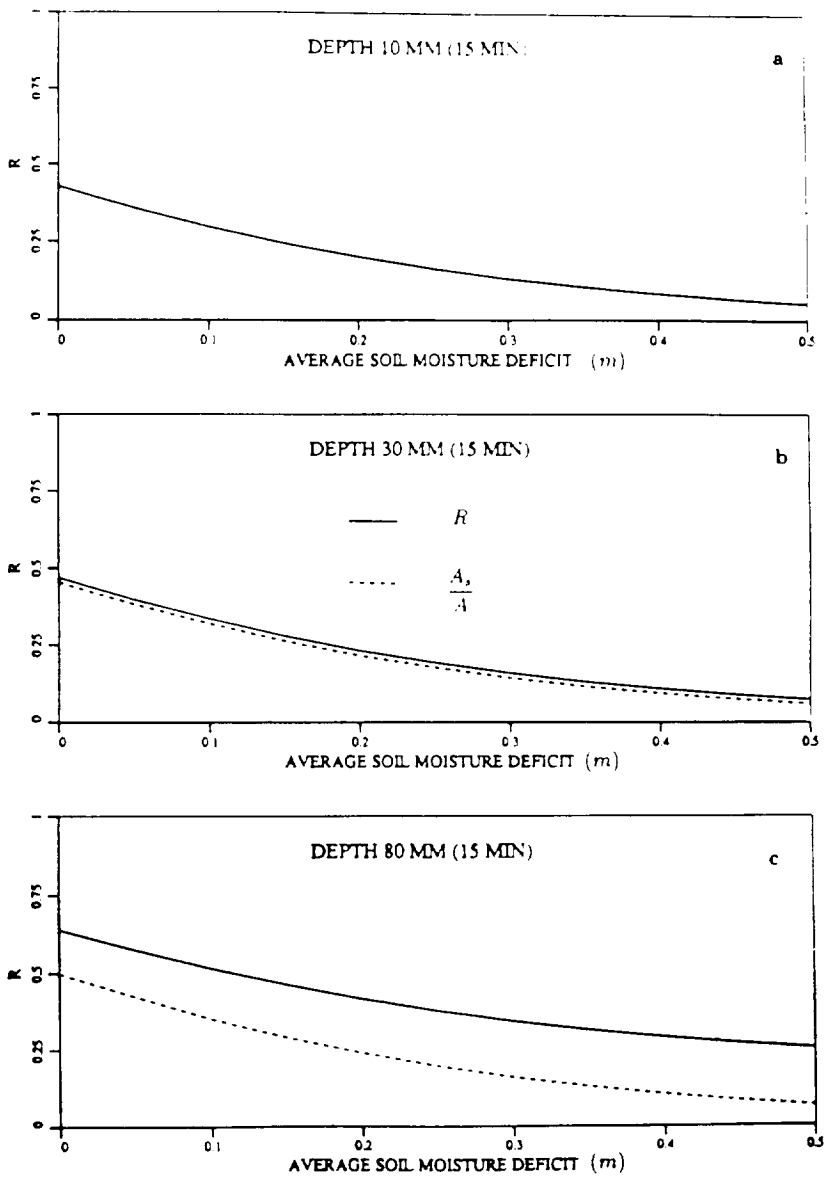

Fig. 2. Runoff ratio (R) vs average store deficit ($\bar{s}$): (a) 10 mm rainfall in 15 min; (b) 30 mm; (c) 80 mm.

in Figures 2a–c. (In Figure 2a these two lines coincide.) This difference represents the contribution to surface runoff by the infiltration excess mechanism. The second reason is that as rainfall intensity increases from Figure 2a to 2c, there is more saturation excess runoff occurring, as the smaller storage deficits on the land surface are satisfied by the rainfall. Notice how the fraction of saturated area, as shown by the dashed line, increases with increasing rainfall intensity from Figure 2b to 2c.

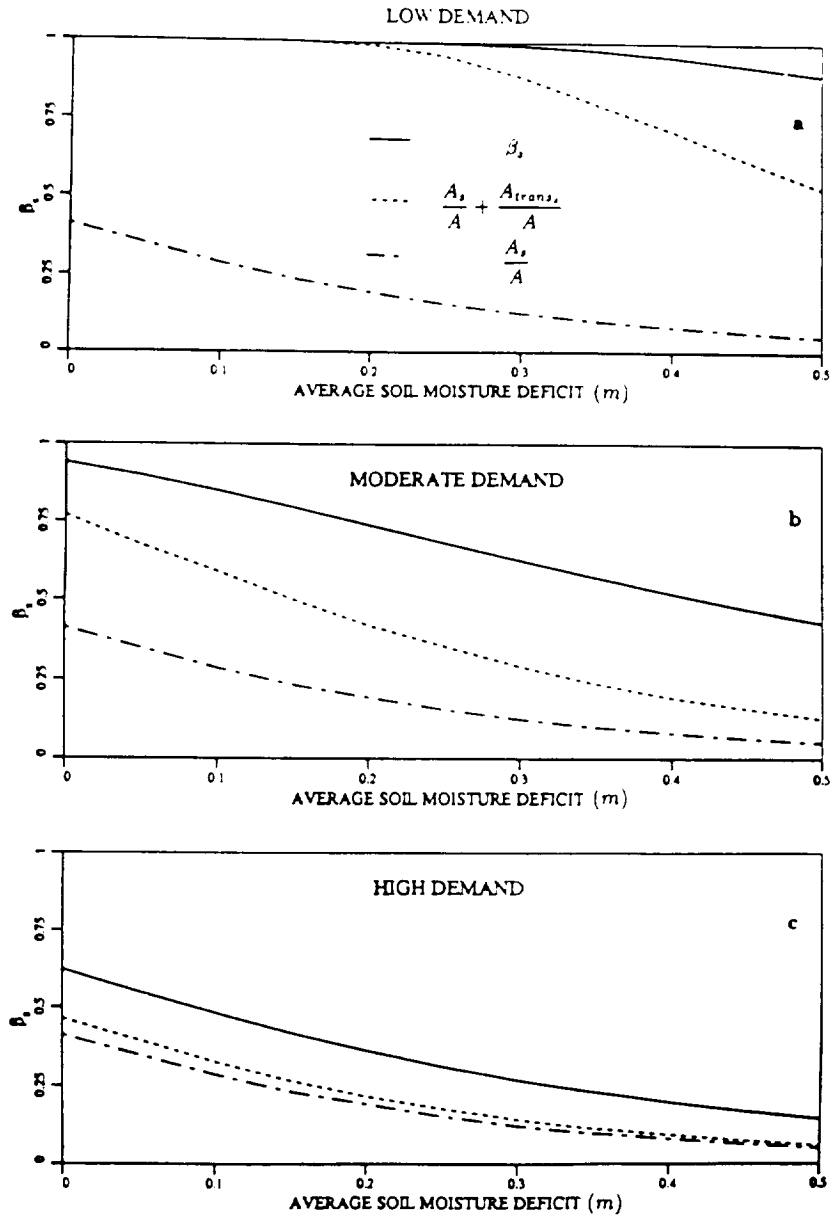

Fig. 3. Evaporation efficiency (β_s) vs average storage deficit ($\bar{s}$) with potential evaporation equal to (a) 9.0×10^{-6} m h^{-1}; (b) 3.0×10^{-5} m h^{-1}; (c) 1.5×10^{-4} m h^{-1}; $\Delta t = 0.25$ hr.

Note that to generate significant amounts of infiltration excess runoff, extremely high intensities of rainfall are required.

Studying any one of Figures 2a–c shows that as $\bar{s}$ increases (i.e. with increasing dryness) the runoff ratio decreases. This can be explained by the decrease in saturation excess runoff producing areas as the average soil moisture deficit

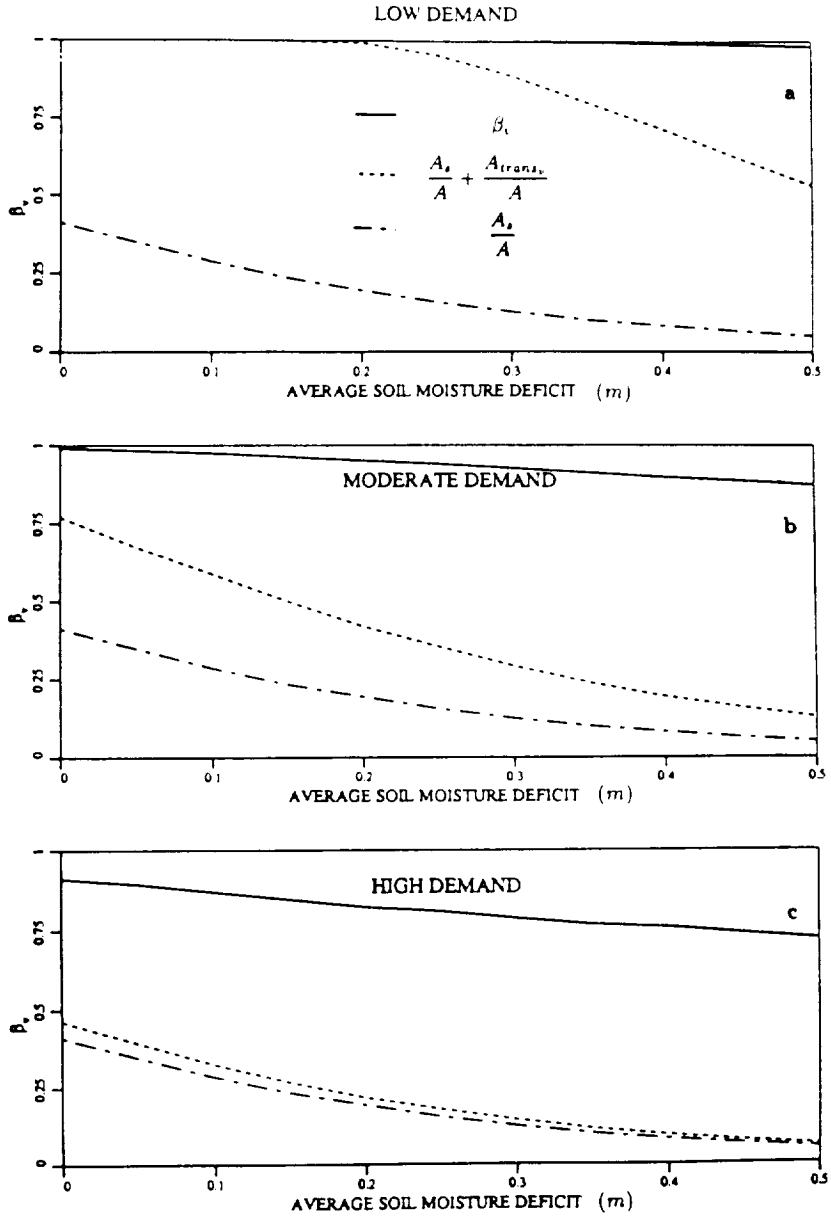

Fig. 4. Transpiration efficiency (β_e) vs average storage deficit ($\bar{s}$) with potential transpiration equal to (a) 9.0×10^{-6} m h^{-1}; (b) 3.0×10^{-5} m h^{-1}; (c) 3.0×10^{-4} m h^{-1}; $\Delta t = 0.25$ hr.

increases. This is shown by the dashed line in each of Figures 2a–c, which again represents the fraction of saturated land surface, A_s/A.

Figures 3a–c are plots of the evaporation efficiency versus $\bar{s}$ for increasing levels of atmospheric demand. In general, for one value of $\bar{s}$, the evaporation efficiency decreases with increasing atmospheric demand, i.e. from Figure 3a to 3c. This is

TABLE I
Parameters used in the calculation of R, β_s, β_t

Q_0	0.00025 m h^{-1}
m	0.179 m
ψ_s	0.1
B	0.2
θ_s	0.45
θ_r	0.05
$\Delta\theta$	0.4
K_s	0.192 m h^{-1}
λ	6.24
χ^*	0.05
μ^*	3.94
ϕ^*	2.43
θ_2	0.1

explained by the fact that less of the land surface can supply moisture to the atmosphere at the potential rate as that potential increases. This fact is demonstrated by studying the middle line in Figures 3a through 3c for one value of $\bar{s}$. This line is the sum of the first two terms on the right hand side of (41), i.e. this line represents the total fraction of land surface under atmosphere controlled evaporation. As the atmospheric demand increases, less of the land surface can supply moisture at the potential rate, and at the highest levels of demand, only saturated areas and another very small fraction of land surface area can contribute moisture at the rate demanded by the atmosphere (Figure 3c). Similar results are shown in Figures 4a–c for the transpiration efficiency, although for the same level of atmospheric forcing β_t is greater than β_s.

In any of Figures 3a–c, as $\bar{s}$ increases, β_s generally decreases. As soil moisture conditions dry out, less of the land surface is able to supply moisture to the atmosphere at the potential rate. Again this is shown by the middle line in any of Figures 3a–c. As $\bar{s}$ increases, the proportion of land surface area under atmosphere control decreases. The same trend is evident in Figures 4a–c for the transpiration efficiency.

The parameters used to generate Figures 2–4 are given in Table I.

9. Summary

A macroscale model for the land surface hydrologic fluxes is presented. The model is proposed for use in atmospheric GCMs to improve upon the current simplified land surface hydrology parameterizations. Additionally, the model functions independently of a GCM as a large scale water balance model.

The model incorporates subgrid scale spatial variability in topography, soils, vegetation, and rainfall to predict the space-time distribution of surface soil moisture over a large catchment or GCM grid square. Given the distribution of

surface soil moisture and the associated probabilities, the distribution of surface runoff, evaporation, and transpiration rates can be computed, and the areal averaged hydrologic fluxes can be determined by integration over the distribution of soil moisture.

The parameterization presented here suggests that the interactions between the land and the atmosphere that produce the macroscale water balance fluxes are dominated by three broad divisions of the surface soil moisture distribution: saturated, transitional, and relatively dry. The relative magnitude of the saturated area varies seasonally, and on the shorter time scale of storms. The magnitudes of the transitional and relatively dry areas is a function of both climatic forcing and the state of the soil surface, and the threshold values of soil moisture between regions will vary with flux type. Saturated areas contribute runoff and evapotranspiration at the maximum rate. Transitional areas contribute runoff at a decreasing rate (spatially) as the soil moisture decreases (and infiltration capacities increase) within the boundaries of this region. Transitional areas contribute evapotranspiration at the maximal rate. Relatively dry areas contribute no runoff and contribute evapotranspiration at a decreasing rate (spatially) as the soil moisture decreases within these regions.

Embedded in this parameterization is the subgrid scale variability in hydrologic processes and land surface properties which we believe are crucial to the dynamics of land surface/atmosphere interactions. In response to these water balance dynamics, the saturated and threshold areas will expand or contract diurnally and seasonally. It is precisely this subgrid scale heterogeneity in surface properties and dynamics that we believe are important in determining the large scale averaged response. The temporal variation in the terms of the above ratios, their sensitivity to various climates, vegetation, and topography-soils characteristics, and validation of the model on large watersheds, are the subjects of future research.

Acknowledgements

The work presented in this paper was supported in part by NASA grant NAG-1392, "Research into the influence of spatial variability and scale on the parameterization of hydrologic processes", NASA Graduate Student Research Program grant NGT-60153, "Effects of spatial variability and scale on interstorm evaporation processes", and USGS grant 14-08-001-G1753, "Development of a macroscale land surface hydrological model for GCMs". This research support is gratefully acknowledged. The advice and support of M. Sivapalan, as well as his generous contribution of unpublished material, is greatly appreciated.

References

Abramopoulos, F., Rosenzweig, C., and Choudhury, B.: 1988, 'Improved Ground Hydrology Calculations for Global Climate Models (GCMs): Soil Water Movement and Evapotranspiration', *J. Climate* **1(9)**, 921–941.

Beven, K. J.: 1982, 'On Subsurface Stormflow, an Analysis of Response Times,', *Hydrol. Sci. J.* **27**, 505–521

Beven, K.: 1986, 'Runoff Production and Flood Frequency in Catchments of Order *n*: An Alternative Approach', in V. K. Gupta *et al.* (eds.), *Scale Problems in Hydrology*, Kluwer Acad. Publ., Dordrecht, Holland, pp. 107–131.

Beven, K. J. and Kirkby, M. J.: 1979, 'A Physically Based Variable Contributing Area Model of Basin Hydrology', *Hydrol. Sci. Bull.* **24**(1), 43–69.

Beven, K. J., Kirkby, M. J., Schofield, N., and Tagg, A. F.: 1984, 'Testing a Physically-Based Flood Forecasting Model (TOPMODEL) for Three U.K. Catchments', *J. Hydrol.* **69**, 119–143.

Beven, K. and Wood, E. F.: 1983, 'Catchment Geomorphology and the Dynamics of Runoff Contributing Areas', *J. Hydrol.* **65**, 139–158.

Brutsaert, W.: 1988, *Evaporation into the Atmosphere. Theory, History, and Applications*, Kluwer Acad. Publ. Dordrecht, Holland.

Denmead, O. T. and Shaw, R. H.: 1962, 'Availability of Soil Water to Plants as Effected by Soil Moisture Content and Meteorological Conditions', *Agron. J.* **54**, 385–390.

Dickenson, R. E.: 1984, *Modelling Evapotranspiration for Three-Dimensional Global Climate Models*, Climate Processes and Climate Sensitivity, Geophysical Monograph 29, Maurice Ewing Volume 5, American Geophysical Union, Washington, DC, pp. 58–72.

Dunne, T.: 1978, 'Field Studies of Hillslope Flow Processes', in M. J. Kirkby, (ed.), *Hillslope Hydrology*, John Wiley and Sons, pp. 227–293.

Dunne, T. and Black, R. D.: 1970, 'Partial Area Contributions to Storm Runoff in a Small New England Watershed', *Wat. Resour. Res.* **6**(5), 1296–1311.

Eagleson, P. S., Fennessey, N. M., Wang, Q., and Rodriguez-Iturbe, I.: 1987, 'Application of Spatial Poisson Models to Air Mass Thunderstorm Rainfall', *J. Geophys. Res.* **92**(D8), 9661–9678.

Entekhabi, D. and Eagleson, P. S.: 1989, 'Land Surface Hydrology Parameterization for Atmospheric General Circulation Models Including Subgrid Scale Spatial Variability', *J. Climate* **2**(8), 816–831.

Feddes, R. A., Kowalik, P. J., Malinka, K. K., and Zaradny, H.: 1976, 'Simulation of Field Water Uptake by Plants Using a Soil Water Dependent Root Extraction Function', *J. Hydrol.* **31**, 13–26.

Hillel, D.: 1980, *Applications of Soil Physics*, Academic Press, New York.

Horton, R. E.: 1933, 'The Role of Infiltration in the Hydrologic Cycle', *Trans. Am. Geophys. Union* **14**, 446–460.

Knisel, W. G.: 1973, Comments on 'Role of Subsurface Flow in Generating Storm Runoff', by R. A. Freeze. *Wate. Resour. Res.* **9**(4), 1107.

Koster, R. D., Eagleson, P. S., and Broecker, W. S.: 1988, *Tracer Water Transport and Subgrid Precipitation Variation within Atmospheric General Circulation Models*, Ralph M. Pearsons Lab. Rep. No. 317, Department of Civil Engineering, Massachusetts Institute of Technology, 364 pp.

Manabe, S.: 1969, 'Climate and Ocean Circulation: I. The Atmospheric Circulation and the Hydrology of the Earth's Surface', *Mon. Wea. Rev.* **97**, 739–774.

Molz, F. J.: 1981, 'Models of Water Transport in the Soil-Plant System: A Review', *Wat. Resour. Res.* **17**(5), 1245–1260.

Philip, J. R.: 1957, 'Evaporation, and Moisture and Heat Fields in the Soil', *J. Meteorol.* **14**, 354–366.

Philip, J. R.: 1957, 'The Theory of Infiltration', *Soil Science* **83**, **84**, and **85**.

Sellers, P. J., Mintz, Y., Sud, Y. C., and Dalcher, A.: 1986, 'A Simple Biosphere Model (SiB) for Use within General Circulation Models', *J. Atmos. Sci.* **43**(6), 505–531.

Shukla, J. and Mintz, Y.: 1982, 'Influence of Land-Surface Evapotranspiration on the Earth's Climate', *Science* **215**, 1498–1501.

Sivapalan, M., Beven, K., and Wood, E. F.: 1987, 'On Hydrologic Similarity, 2, A Scaled Model of Storm Runoff Production', *Wat. Resour. Res.* **23**(12), 2266–2278.

Wolock, D. M., Hornberger, G. M., Beven, K. J., and Campbell, W. G.: 1989, 'The Relationship of Catchment Topography and Soil Hydraulic Characteristics to Lake Alkalinity in the Northeastern United States', *Wat. Resour. Res.* **23**(5), 829–837.

Wood, E. F., Sivapalan, M., Beven, K., and Band, L.: 1988, 'Effects of Spatial Variability and Scale with Implications to Hydrologic Modeling', *J. Hydrol.* **102**, 29–47.

HETEROGENEITY AND SCALING LAND-ATMOSPHERIC WATER AND ENERGY FLUXES IN CLIMATE SYSTEMS

Eric F. Wood

Water Resources Program
Princeton University
Princeton, NJ
08544

Presented at the IHP/IAHS George Kovacs Colloquium
on
Space and Time Variability and Interdependencies
in Various Hydrological Processes.

July 3 - 4, 1992

UNESCO, Paris

Abstract.

The effects of small-scale heterogeneity in land surface characteristics on the large-scale fluxes of water and energy in the land-atmosphere system has become a central focus of many of the climatology research experiments. The acquisition of high resolution land surface data through remote sensing and intensive land-climatology field experiments (like HAPEX and FIFE) has provided data to investigate the interactions between microscale land-atmosphere interactions and macroscale models. One essential research question is how to account for the small scale heterogeneities and whether 'effective' parameters can be used in the macroscale models. To address this question of scaling, three modeling experiments were performed and are reviewed in the paper. The first is concerned with the aggregation of parameters and inputs for a terrestrial water and energy balance model. The second experiment analyzed the scaling behaviour of hydrologic responses during rain events and between rain events. The third experiment compared the hydrologic responses from distributed models with a lumped model that uses spatially constant inputs and parameters. The results show that the patterns of small scale variations can be represented statistically if the scale is larger that a representative elementary area scale, which appears to be about 2 - 3 times the correlation length of the process. For natural catchments this appears to be about 1 - 2 sq km. The results concerning distributed versus lumped representations are more complicated. For conditions when the processes are non-linear, then lumping results in biases; otherwise a one-dimensional model based on 'equivalent' parameters provides quite good results. Further research is needed to fully understand these conditions.

Introduction.

The complex heterogeneity of the land surface through soils, vegetation and topography, all of which have different length scales, and their interaction with meteorological inputs that vary with space and time, result in energy and water fluxes whose scaling properties are unknown. Research into land-atmospheric interactions suggest a strong coupling between land surface hydrologic processes and climate (Charney et al., 1977; Walker and Rowntree, 1977; Shukla and Mintz, 1982; and Sud et al.,1990.) Due to this coupling, the issue of 'scale interaction' for land surface-atmospheric processes has emerged as one of the critical unresolved problems for the parameterization of climate models.

Understanding the interaction between scales has increased in importance when the apparent effects of surface heterogeneities on the transfer and water and energy fluxes are observed through remote sensing and intensive field campaigns like HAPEX and FIFE (Sellers et al., 1988). The ability to parameterize macro-scale models based on field experiments or remotely sensed data has emerged as an important research question for programs such as the Global Energy and Water Experiment (GEWEX) or the Earth Observing System (Eos). It is also important for the parameterization of the macroscale land-surface hydrology necessary in climate models, and crucial in our understanding in how to represent sub-grid variability in such macroscale models.

From a modeling perspective, it's important to establish the relationship between spatial variability in the inputs and model parameters, the scale being modeled and the proper representation of the hydrologic

processes at that scale. Figure 1 presents a schematic for modeling over a range of scales. Let us consider this figure in light of the terrestrial water balance, which for a control volume may be written as:

$$\left\langle \frac{\partial S}{\partial t} \right\rangle = \langle P \rangle - \langle E \rangle - \langle Q \rangle \qquad (1)$$

where S represents the moisture in the soil column, E evaporation from the land surface into the atmosphere, P the precipitation from the atmosphere to the land surface, and Q the net runoff from the control volume. The spatial average for the control volume is noted by $\langle \cdot \rangle$.

Equation (1) is valid over all scales and only through the parameterization of individual terms does the water balance equation become a 'distributed' or 'lumped' model. By 'distributed' model, we mean a model which accounts for spatial variability in inputs, processes or parameters. This accounting can be either deterministic, in which the actual pattern of variability is represented -- examples include the European Hydrological System model (SHE) (Abbott et. al., 1986a,b) and the 3-D finite element models of Binley et al. (1989) or Paniconi and Wood (1992); or statistical, in which the patterns of variability are represented statistically -- examples being models like TOPMODEL (Beven and Kirkby, 1979) and its variants (see Wood et al, 1990; Famiglietti et. al., 1992a; Moore et al, 1988; and Wood et al. 1992) in which topography and soil plays an important role in the distribution of water within the catchment.

By a 'lumped' model we mean a model that represents the catchment (or control volume) as being spatially homogeneous with regard to inputs and parameters. There are a wide number of hydrolgic water balance models of varying complexity that don't consider spatial variability. These range from

the well-known unit hydrograph and its variants, the water balance models of Eagleson (1978), to complex atmospheric-biospheric models being proposed for GCMs (examples being, the Biosphere Atmosphere Transfer Scheme (BATS) of Dickinson (1984) and the Simple Biosphere Model (SiB) of Sellers et al. (1986).

The terrestrial water balance, including infiltration, evaporation and runoff, has been revealed to be a highly nonlinear and spatially variable process. Yet, little progress has been made in relating the observed small-scale complexity that is apparent from recent field and remote sensing experiments to models and predictions at large scales. It is this relationship that is the subject of this paper. The research being presented represents recent work in investigating the effects of spatial variability and scale on the quantification and parameterization of the terrestrial water balance. The results draw primarily from the papers of Wood et al., (1988); Wood et al., (1990); Wood and Lakshmi (1992); and Famiglietti and Wood (1992c). Important related papers are those of Wood et al., (1986); Sivapalan et al., (1987); Beven et al., (1988); Beven (1988).

Changing Scale and Water Balance Fluxes.

Large scale field experiments such as FIFE and HAPEX, and remote sensing experiments like MAC-HYDRO (see Wood et al., 1992) and MAC-EUROPE (see Lin et al., 1993), have shown the significant variability across a catchment with regards to runoff production, soil moisture levels and actual evaporation rates. The heterogeneity in hillslope forms, soil properties and vegetation combine with variability in rainfall to produce different runoff processes and responses across hillslopes, different soil moisture conditions and interstorm (dry period) moisture redistribution and evapotranspiration.

For a hillslope, it may be possible to develop a distributed model which explicitly considers variability in soil and vegetation properties. In fact, the simulations of Smith and Hebbert (1979) show that the actual patterns of soil properties may be important in simulating the runoff response from a hillslope.

At the scale of a small catchment, it may be possible to consider the variability in topography, soil and vegetation as if they came from a stationary statistical distribution (Beven, 1988, Wood et al., 1990.) Thus the distributed model would consider patterns of variability statistically. Within a physioclimatic region, we can consider that there may be a population of small catchments that is statistically similar but whose actual patterns of topography, soil and vegetation properties and therefore responses vary quite differently (Beven, 1988).

As scale increases, so does the sample of the small catchments and therefore the sample of the properties that control the water balance fluxes. This increased sampling of small catchments leads to a decrease in the difference between small catchment responses, eventhough the patterns of the properties are quite different across these small catchments (Beven, 1988; Wood et al., 1990). At some scale, the variance between the hydrologic responses for catchments (or areas) should reach a minimum. Wood et al. (1988) suggested that this theshold scale be referred to as the 'Elementary Representative Area' (REA) which they define as:

> the critical scale at which implicit continuum assumptions can be used without explicit knowledge of the actual patterns of topographic, soil, or rainfall fields. It is sufficient to represent these fields by their statistical characterization.

Predicting the water balance at the REA scale may very well require

considering heterogeneity at smaller scales, through its statistical characterization; it should not imply the use of equivalent and average parameters. In terms of Figure 1, changing scale helps us understand the aggregation of the output from the distributed response. The concept of the REA scale helps us in clarifying the relationship between a distributed model and the lumped model, and how this relationship may vary with scale.

In this paper we report on a series of numerical experiments that investigate aggregation and scaling of land-surface hydrological processes. Famiglietti (1992) and Famiglietti et al. (1992a,b) have developed a water and energy balance model within a TOPMODEL-like structure that predicts water and energy balance fluxes for areas of hetrogeneous soil, hillslopes, rainfall and net radiation characteristics. The models are summarized in Appendix A, and were developed to predict water and energy fluxes for the Intensive Field Campaigns (IFCs) of FIFE (Famiglietti and Wood, 1992a,b) and subsequent remote sensing experiments (Wood et al., 1992; Lin et al., 1992). The models have also been used to analyze the water balance fluxes for catchments of different scales, in which the small catchments were sampled from a particular topography -- in this case the topography of the FIFE area (Famiglietti and Wood, 1992b).

The experiments that will be reported here are as follows. The first is the aggregation of distributed inputs for the water balance model; specifically the representation of soil and topography, and vegetation. The second is the aggregation of the hydrologic responses in a catchment due to rainfall during a storm event and due to evaporative demands during interstorm periods. These two sets of experiments allows us to infer the nature of aggregation in parameters and processes. The third experiment will

compare the aggregated fluxes from the distributed model to the predicted fluxes from a lumped version of the model.

Changing Scale and Model Inputs.

Scaling of Topography. Appendix A provides a summary of the water and energy balance models. The models were applied to the Kings Creek catchment in the FIFE area in Kansas. The FIFE area is 15 km x 15 km, with a rolling topography with an approximate elevation range is 325 m to 460 m. Except for heavier vegetation at the bottom of stream valleys, the vegetation consists on short crops, pasture and natural grasses. The Kings Creek catchment, which is 11.7 sq km in area, is in the north-west portion of the FIFE area in the Konza Prairie preserve. Figure 3 shows the division of the catchment into subcatchments -- the number ranging from 5 to 66 depending on the scale. All subcatchments represent hydrologically consistent units in that runoff flows out of the subcatchments through one flow point, and that the surface runoff flux across the other boundaries is zero.

Equation A.2 provides the relationship between variability in topography and soil, and variability in local water table depths and soil moisture. Wood et al. (1990) have shown that the variability in topography dominates variability in soil properties for Kings Creek. The TOPMODEL theory uses the topographic-soil index to predict local water fluxes and soil moisture. Further, as discussed earlier, larger catchments can be considered to be composed of a population of smaller catchments that are statistically similar but whose actual patterns vary quite considerably. The question remains: at what catchment scale is the sample of hillslopes and small catchments sufficiently large so that their actual patterns of the soil-topographic index can be represented statistically. The average value

of the topographic index, λ, was calculated for each of the subcatchments shown in Figure 3 and plotted against subcatchment area. Each pixel is 900 sq m. The behavior of the catchment shows that at small scales there is extensive variability in hillslope forms leading to variability in λ, but at a scale of approximately 1 sq km the increased sampling of hillslopes and small catchments leads to a decrease in the difference between topographies.

Wolock (personal communication) has found similar behavior over a wider range of scales for Sleepers River, VT. Figure 4 gives his results for λ over catchments scales up to approximately 45 sq km. Again, there appears to be a significant decrease in λ at about 1 to 2 sq km.

Scaling of Vegetation. In the first experiment, scaling of the topographic index was explored due to its role in subsurface water fluxes and the redistribution of soil moisture. Vegetation type and density determine the stomatal and canopy resistances, and therefore transpiration rates in the water and energy balance models (see equations A.3 - A.5.) What can be said about the scaling behavior of satellite derived estimates for vegetation?

Wood and Lakshmi (1992) used high resolution thermatic mapper (TM) satellite data to derive the normalized difference vegetation index (NDVI), latent heat and sensible heat fluxes for the August 15, 1987 overpass and to investigate their scaling properties. The scaling for the vegetation will be reviewed here. The resolution of TM is 30 m for bands 1 through 5, and 120 m for the thermal band. The scaling question investigated here is whether averaging the TM bands prior to calculating NDVI provides the same derived quantities as would be found by calculating the quantities at the TM resolution and averaging. The equivalence of the two approaches depends on

the degree of non-linearity represented by in functions that relate NDVI to TM data.

The following procedure was followed. The normalized difference vegetation index (NDVI) was calculated at the 30 m TM resolution using:

$$NDVI = \frac{(B_4 - B_3)}{(B_4 + B_3)} \qquad (2)$$

where B_3 represents band 3 (0.63 - 0.69 μm) and B_4 represents band 4 (0.76 - 0.90 μm). The first often being referred to as the red and the latter the near infrared band. The NDVI image corresponding to a TM scene acquired over the FIFE area for August 15, 1987, is given in Figure 5. The TM scene was fully calibrated before the calculations were carried out.

For the aggregated scales, two procedures were followed. One was to spatially aggregate the TM bands and then use equation (2) while the second procedure is to spatially aggregate the NDVI based on the 30 m TM data. This procedure was used for aggregation levels of 300 x 300 m, 750 x 750 m and 1500 x 1500 m. A resolution equivalent to AVHRR would lie between the last two cases. Figure 6 shows the aggregated NDVI, using the second procedure, for the aggregation level of 300 x 300 m. Comparisons between the two aggregation procedures can be best shown by a scatter plot between the aggregated 30 m-based NDVI and the NDVI derived using aggregated TM bands; these comparisons are presented in Figure 7.

One striking observation arises from comparing Figures 5 - 7. Notice that the detailed structure observable in Figure 5 is lost in Figure 6, and yet the averaged NDVI from the two aggregation schemes are essentially the same as can be seen in scatter plot of Figure 7. Figure 7 does show that a small bias exists between the two aggregation procedures but its magnitude

is rather insignificant. These results indicate that NDVI calculated from spatially averaged TM (or lower resolution AVHRR data) will be equivalent to the NDVI scaled up from the full resolution image.

Changing Scale and Derived Hydrologic Responses.

In a manner similar to the investigation of the scaling properties in topography, the scaling in infiltration and evapotranspiration were also investigated. For this study the water balance model described in Famiglietti et al. (1992a) (see Appendix A) was applied to the Kings Creek catchment of the FIFE area in Kansas. For a rainfall storm on August 4, 1987, the average runoff for the subcatchments shown in Figure 2 was calculated for two times and plotted in Figure 8 against subcatchment area measured in pixels. Notice that the runoff, Q_t is normalized by the average precipitation, $\bar{P}$. The same type of plot was done for selected times during an interstorm period that extended from July 18 through July 31, 1987 and is presented as Figure 9. The behavior of the catchment shows that at small scales there is extensive variability in both storm response and evaporation. This variability appears to be controlled by variability in soils and topography whose length scales are on the order of 10^2-10^3 m -- the typical scale of a hillslope. With increased scale, the increased sampling of hillslopes leads to a decrease in the difference between subcatchment responses.

These results are not too surprising given the linkage within the model between topography and the water balance fluxes -- namely that variations in topography play a significant role in the spatial variation of soil moisture within a catchment, setting up spatially variable initial

conditions for both runoff from rainstorms and evaporation during interstorm periods.

The results also suggest that at larger scales it would be possible to model the responses using a simplified macroscale model (given in Appendix A as equations A.6 and A.7) based on the statistical representation of the heterogeneities in topography, soils and hydrologic forcings (rainfall and potential evaporation). Predictions based on these equations are also shown in Figures 8 and 9 as the 'macroscale model'. Since the macroscale model is scale invariant, it appears as a straight line in Figures 8 and 9.

Scaling remotely sensed soil moisture. To date only a very limited number of catchments have been analyzed in the manner described here. Furthermore, they have all had moderate relief and located in regions with humid climates. For these, the REA-scale appears to be quite consistent at about 1-2 sq km for both the runoff and evaporation processes. Clearly additional catchments representing a broader range of climates and catchment sizes need to be analyzed before definitive statements concerning the REA-scale can be made.

To investigate whether these scaling results are model determined or reflective of actual hydrologic processes, a similar analysis was done using airborne radar from the MAC-HYDRO field experiment of 1990 in Mahantango Creek, PA, a USDA experimental catchment. This experiment focused on estimating soil moisture through passive microwave (L-band) radiation using the PBMR sensor with an effective spatial resolution of approximately 90 m and through an active radar sensor (AIRSAR) at C-, L- and P-band at a 6 x 12 m pixel resolution. The AIRSAR remote sensing of soil moisture for

MAC-HYDRO is described in Wood et al. (1992) and Lin et al. (1992) but basically the return from the radar is affected by surface soil moisture conditions. Confounding effects are due to topography, roughness and vegetation -- especially large forested areas which have high reflectivity.

Much of the catchment is covered with pasture and small grains and the return in L-band provides a good estimate of the surface soil moisture. The catchment was divided into 19 subcatchments that ranged in size up to 3.5 sq km. The division was done in a manner similarly to Kings Creek which is shown in Figure 2. Figure 10 plots the average return with catchment scale. Due to the small size of Mahantango Creek and the large areas of forest, the variance hasn't settled down as fast as that shown for the modeled results in FIFE. Nonetheless, the same behavior can be observed, again in the range of 1 - 2 sq km -- our proposed REA scale. The importance of the AIRSAR remote sensing results is that it provides an independent assessment based on measurements of the scaling behavior of soil moisture.

Lumped Versus Distributed Models.

Figure 1 presented a framework for considering the relationship between distributed and lumped models. In an earlier section, the behaviour of aggregated inputs and hydrologic responses lead to the concept of the representative elementary area, a scale where a statistical representation can replace actual patterns of variability. In this section we compare the output between a macroscale, distributed model and a lumped model.

The macroscale model is based on the model described as 'model-b' in Appendix A. This model has been applied to the intensive field campaign periods (IFCs) during FIFE of 1987 and can include variability in topography,

soils, net radiation and vegetation. The first two, topography and soils, leads to variations in soil moisture under the TOPMODEL framework; the latter two lead to variations in potential and actual transpiration.

A lumped representation (or what will also be referred to as a one-dimensional representation) is obtained by using spatially constant values for all of the above variables. The effect of representing the distributed model by a lumped model, or equivalently by replacing the spatially variable parameters and inputs by average values, will depend on nonlinearities in the model. Conceptually this can be seen by considering a second order Taylor's series expansion about the mean for the function $y = g[x,\theta]$ where θ are fixed parameters and x variable with mean $\mu(x)$ and variance $\sigma(x)$. A first order approximation for y is $\mu_1(y) \simeq g[\mu(x),\theta]$, while a second order approximation would be

$$\mu_2(y) \simeq g[\mu(x),\theta] + \frac{1}{2} \frac{d^2g}{dx^2}\Big|_{\mu(x)} \sigma(x) \qquad (3)$$

Differences between $\mu_1(y)$ and $\mu_2(y)$ depend on the magnitude of the second term in equation (3) -- the sensitivity term. As an illustrative example, consider the estimation of downslope subsurface flows, q_i, within TOPMODEL with and without considering variability in the local water table z_i. TOPMODEL relates q_i to z_i by $q_i = T_i \tan\beta \exp(-f\, z_i)$. Thus a first order approximation of the mean subsurface flow would be

$$\mu_1(q_i) = T_i \tan\beta \exp(-f\, \bar{z}) \qquad (4)$$

while a second order approximation would be

$$\mu_2(q_i) = T_i \tan\beta \exp(-f\, \bar{z}) + \frac{1}{2} \{ T_i \tan\beta\, f \}^2 \exp(-f\, \bar{z})\, \sigma(z_i) \qquad (5)$$

If we scale $\mu_2(q_i)$ by $\mu_1(q_i)$ and use equation (A.2) to recognize that

$$\sigma(z_i) = f^2\, \sigma(\ln \frac{a T_e}{T_i \tan\beta}) \qquad (6)$$

we obtain

$$\frac{\mu_2(q_i)}{\mu_1(q_i)} = 1 + 0.5\,\sigma(\ln \frac{aT_e}{T_i \tan\beta}) \qquad (7)$$

Analysis of the soil-topographic index for Kings Creek yields a variance of 3.25. This results in the first order estimate for q_i of being biased low by approximately 65%. Since the subsurface flows and the local water table are related and since the local water table depth effects the surface soil moisture which subsequently determines the soil evaporation and infiltration rates, it's clear that the lumped model may very well lead to significant biases in the water balance fluxes.

For more complex models the sensitivities must be determined through simulation. For certain functions the sensitivities will change with the state of the catchment (wet or dry). For example Figure 11 gives the vegetation transpiration and soil exfiltration capacities used to model the FIFE data (Famiglietti and Wood, 1992a). Notice that at low and high soil moisture values the transpiration capacity function is essentially linear and the sensitivity would be low to soil moisture variations in these ranges. For volumetric moisture contents in the range 0.2 - 0.3, the sensitivity of the transpirtaion capacity function is high. As can be seen from Figure 11, sensitivity characteristics for soil exfiltration capacity would be high for soil moisture values greater than about 0.3.

To test the sensitivity due to dry soil condidtions and to compare the distributed water-energy balance model to a lumped representation (one-dimensional model or a first order model), comparisions were made between the models for 5 days during the October 1987 FIFE intensive field campaign, IFC-4. This period had the driest conditions observed during the 1987 experiment. Figure 12 shows the simulations for October 5 - 9, 1987.

The models were run at a 0.5 hour time step to capture the diurnal cycle in potential evapotranspiration. Three models are compared: a fully distributed model, a macroscale model in which the spatial variability is considered statistically and a lumped one-dimensional model in which parameters and inputs are spatially constant.

The one-dimensional model predicts well the evapotranspiration during the morning and late afternoon when the atmospheric demand is low, but fails to accurately predict this flux during the middle portion of the day when soil and vegetation controls limit the actual evapotranspiration. It is during this period that the sensitivity is high and by ignoring the spatial variability in soil moisture the lumped model serverely underestimates the catchment-scale evapotranspiration. During wet periods, the one-dimensional model may work quite well. This complicates the linkage between a distributed and lumped representation since the appropriateness of the simpler representation varies with the state of the system.

Results and Discussion.

The purpose of the paper is to review recent results for the scaling of water and energy fluxes from the land component of the climate system. Three sets of experiments were presented. The first was the aggregation of distributed inputs to determine their scaling properties and to determine whether a statistical respresentation for these parameters could be used. For topography, it appears that for catchment scales larger than about 1 - 2 sq km, a statistical representation is reasonable. The second part of this experiment studied scaling of the normalized vegetation index (NDVI) as derived from a thermatic mapper (TM) overpass of the FIFE area on August 15, 1987. Variations in surface conditions due to vegetation

characteristics as well as topography and soils, leads to significant variation in the TM-derived variables, as is shown in the presented images. Nonetheless, aggregated values of the TM band data gave accurate estimates of the aggrtegated NDVI derived from the 30 m TM data.

The second set of experiments analyzed the hydrologic response at the catchment scale (but could easily be at a GCM grid scale) in which spatial variability in topography, soils and hydrologic inputs (rainfall,in this case) resulted in spatially variable responses. These results support the concept of the representative elementary area (REA) (Wood et al., 1988) and its usefulness in determining the scale at which the macroscale model is a valid model for the scaled process. The results of the experiments carried out here suggest that the REA concept has wide applicability for a range of climate problems and that it appears that the REA will be on the order of a few (1.5 to 3) correlation lengths of the dominant heterogeneity. At scales larger than the REA scale, there has been enough 'sampling' of the heterogeneities that the average response is well represented by a macroscale model with average parameters.

The third experiment compared evapotranspiration derived from distributed models with that derived from a lumped model. The models simulated five dry days during IFC-4 of the FIFE 1987 experiment. The non-linear behaviour of the soil and vegetation control of evapotranspiration (with respect to soil moisture) coupled the dry conditions and high mid-day potential evapotranspiration, resulted in the lumped model underestimating the evaporative fluxes. This results wouldn't be observed for very wet or very dry conditions, showing the subtle difficulties in understanding whether models can be represented by averaged parameters and inputs.

Current research suggests two competing approaches for handling sub-grid heterogeneity: (1) The first approach is based on the belief that subgrid processes have significant effect on processes at GCM-scales and that the non-linearity in subgrid scale processes prevents simple scaling. (2) The second approach is to ignore the variability in sub-grid processes, and represent these processes at larger scales through models with effective parameters. This is essentially the approach of the constant canopy biospheric models where horizontal variability is ignored. It is also the approach of using small-scale micrometeorological field studies for calibration (Sellers and Dorman, 1987; Sellers et al., 1989).

The results from the experiments presented here show a rather more complicated picture. One in which macroscale models can be contructed that account for observed variability across catchments without having to account for the actual patterns of variability. Experiments to date suggest that these macroscale models will accurately predict water and energy fluxes over a wide range of catchment conditions. With regards to one-dimensional or lumped models, they may work or they may not work depending on whether the catchment conditions (soil moisture levels, potential evapotranspiration, etc) lead to significant nonlinearities. The results presented in this paper must be balanced with the knowledge that the presented experiments were neither exhaustive nor complete. For example, the satellite experiments represented a particular condition in which the range of temperatures was reasonably small, resulting in effectively linear models that transfer radiances to fluxes. Whether such ranges are typical of natural systems is unknown until a greater number of analyses are done.

It is hoped that the experiments presented in this paper motivate

related research through a wider range of climatic data that can help resolve the basic issue concerning scaling in natural systems. What must be determined are the scaling properties for reasonably sized domains in natural systems where the range of variability (in vegetation, rainfall, radiance, topography, soils, etc) is reflective of these natural systems.

Acknowledgements.

The research presented here was supported in part by the National Aeronautics and Space Administration (NASA) through Grants NAGW-1392 and NAG-5-899; this support is gratefully acknowledged. The author also wish to thank Jay Famiglietti who helped develop the water and energy balance model for Kings Creek, Dom Thongs for helping with running the model and with the graphics and V. Lakshmi who analyzed the TM data. Finally, thanks to Keith Beven, M. Sivapalan and Jay Famiglietti whose extensive discussions over the last five years have helped form my ideas on aggregation and scaling.

References

Abbott, M.B., J.C. Bathurst, J.A. Cunge, P.E. O'Connell, and J. Rasmussen, "An Introduction to the European Hydrological System-Systeme Hydrologique Europeen SHE, 1, History and Philosophy of a Physically-Based, Distributed Modelling System", *Journal of Hydrology*, **87**, 45-59, 1986a.

Abbott, M.B., J.C. Bathurst, J.A. Cunge, P.E. O'Connell, and J. -Rasmussen, "An Introduction to the European Hydrological System-Systeme Hydrologique European SHE, 2, Structure of a Physically-Based, Distributed Modelling System", *Journal of Hydrology*, **87**, 61-77, 1986b.

Beven, K.J., "Hillslope Runoff Processes and Flood Frequency Characteristics", in A.D. Abrahams (ed.), *Hillslope Processes*, Allen and Unwin, Boston, 1986, pp 187-202.

Beven, K.J., "Scale Considerations", in D.S. Bowles and P.E. O'Connell (eds.), *Recent Advances in the Modeling of Hydrologic Systems*, Kluwer Academic Publishers, Dordrecht, 1988, pp 357-372.

Beven, K. and M. J. Kirkby, "A Physically Based, Variable Contributing Area Model of Basin Hydrology, *Hydrol. Sci. Bull.*, **24(1)**, 43-69, 1979.

Beven, K., Eric F. Wood and M. Sivapalan "On Hydrological Heterogeneity: Catchment Morphology and Catchment Response", *Journal of Hydrology*, **100**, 353-375, 1988.

Binley, A.M., J. Elgy and K.J. Beven, "A Physically-Based Model of Heterogeneous Hillslopes", *Water Resources Research* , **25**, 1219-1226, 1989.

Brooks, R.H. and A.T. Corey, "Hydraulic Properties of Porous Media", *Hydrology Paper No. 3*, Colorado State University, Ft. Colins, Colorado, 1964.

Brutsaert, W., *Evaporation into the Atmosphere: Theory, History, and Applications*, D. Reidel Publishing Company, Dordrecht, 1982.

Charney, J., W. Quirk, S. Chow and J. Kornfield, "A Comparative Study of the Effects of Albedo Change on Drought in Semi-Arid Regions", *Journal of the Atmospheric Sciences*, **34**, 1366-1385, 1977.

Dickinson, R.E., "Modeling Evapotranspiration in Three Dimensional Global Climate Models" in *Climate Processes and Climate Sensitivity*, Geophysical Monograph 29, Maurice Ewing Volume 5, American Geophysical Union, Washington, D.C., 58-72, 1984.

Eagleson, P.S., "Climate, Soil and Vegetation", *Water Resources Research*, **14(5)**, 705-776, October, 1978.

Famiglietti, J.S., "Aggregation and Scaling of Spatially-Variable Hydrological Processes: Local, Catchment-Scale and Macroscale Models of Water and Energy Balance", Ph.D. Dissertation, Department of Civil Engineering and Operations Research, Princeton University, October, 1992, pp 203.

Famiglietti, J.S. and Eric F. Wood, "Aggregation and Scaling of Spatially-Variable Hydrological Processes, 2, A Catchment-Scale Model of Water and Energy Balance", submitted to *Water Resources Research*, October, 1992a.

Famiglietti, J.S. and Eric F. Wood, "Aggregation and Scaling of Spatially-Variable Hydrological Processes, 3, A Macroscale Model of Water and Energy Balance", submitted to *Water Resources Research*, October, 1992b.

Famiglietti, J.S. and Eric F. Wood, "Aggregation and Scaling of Spatially-Variable Hydrological Processes, 4, Effects of Spatial Variability and Scale on Areal-Average Evapotranspiration", submitted to *Water Resources Research*, October, 1992c.

Famiglietti, J.S., Eric F. Wood, M. Sivapalan and D.J. Thongs, "A Catchment Scale Water Balance Model for FIFE", *Journal of Geophysical Research*, November, 1992a.

Famiglietti, J.S., P.C.D. Milly and Eric F. Wood, "Aggregation and Scaling of Spatially-Variable Hydrological Processes, 1, A Local Model of Water and Energy Balance", submitted to *Water Resources Research*, October, 1992b.

Lin, D.-S., Eric F. Wood, M. Mancini, P. Troch and T.J. Jackson, "Comparisons of Remotely Sensed and Model Simulated Soil Moisture over a Heterogeneous Watershed", submitted to *Remote Sensing of Environment*, 1992.

Lin, D.-S., Eric F. Wood, K. Beven and M. Mancini, "Soil Moisture Estimation During Mac-Europe'91 Using AIRSAR", 25th International Symposium on Remote Sensing and Global Environmental Change, Graz, Austria, April, 1993.

Moore, I.D., E. M. O'Laughlin and G.J. Burch, "A Contour-Based Topographic Model for Hydrological and Ecological Applications", *Earth Surf. Processes Landforms*, **13**, 305-320, 1988.

Paniconi, C. and Eric F. Wood, "A Detailed Model for Simulation of Catchment Scale Subsurface Hydrologic Processes", *Water Resources Research*, in press (1992).

Sellers, P.J., and J.L.Dorman, "Testing the Simple Biosphere Model (SiB) Using Point Micrometereological and Biophysical Data", *J. of Climate and Applied Meteorology*, **26**, 622-651, 1987.

Sellers, P.J., Y. Mintz, Y.C. Sud and A. Dalcher, "A Simple Biosphere Model (SiB) for use within General Circulation Models", *Journal of the Atmospheric Sciences*, **43**, No. 6, 1986.

Sellers, P.J., F.G. Hall, G. Asrar, D.E. Strebel and R.E. Murphy, "The First ISLSCP Field Experiment (FIFE)", *Bulletin of the American Meteorological Society*, **69**, 22-27, 1988.

Sellers, P.J., W. J. Shuttleworth, J.L. Dorman, A. Dalcher and J.M. Roberts, "Calibrating the Simple Biosphere Model for Amazonian Tropical Forest using Field and Remote Sensing Data. Part I: Average Calibration with Field Data", *Journal of Applied Meteorology*, **28(8)**, 727-759, 1989.

Shukla, J. and Y. Mintz, "The Influence of Land-Surface Evapotranspiration on Earth's Climate", *Science*, **215**, 1498-1501, 1982.

Sivapalan, M., K.J. Beven and Eric F. Wood, "On Hydrological Similarity: 2. A Scaled Model of Storm Runoff Production", *Water Resources Research*, **23**, 2266-2278, 1987.

Smith, R.E. and R.H.B. Hebbert, "A Monte Carlo Analysis of the Hydrologic Effects of Spatial Variability of Infiltration", *Water Resources Research*, **15**, 419-429, 1979.

Sud, Y. C., P. Sellers, M. D. Chow, G. K. Walker and W. E. Smith "Influence of Biosphere on the Global Circulation and Hydrologic Cycle - A GCM Simulation Experiment", *Agricultural and Forestry Meteorology*, **52**, 133-188, 1990.

Troch, P.A., M. Mancini, C. Paniconi and Eric F. Wood, "Evaluation of a Distributed Catchment Scale Water Balance Model", submitted to *Water Resources Research*, June, 1992.

Walker, J.M. and P.R. Rowntree, "The Effect of Soil Moisture on Circulation and Rainfall in a Tropical Model", *Quart. J.R. Meteor. Soc.*, **103**, 29-46.

Wood, Eric F., M. Sivapalan and K. Beven "Scale Effects on Infiltration and Runoff Production", in *Conjunctive Water Use*, S.M. Gorelick (ed.), IAHS Publ. **156**, 375-390, 1986.

Wood, Eric F., K. Beven, M. Sivapalan and L. Band, "Effects of Spatial Variability and Scale with Implication to Hydrologic Modeling", *Journal of Hydrology*, **102**, 29-47, 1988.

Wood, Eric F., M. Sivapalan and K.J. Beven, "Similarity and Scale in Catchment Storm Response", *Reviews in Geophysics*, **28(1)**, 1-18, February 1990.

Wood, Eric F., D.P. Lettenmaier and V.G. Zartarian, "A Land Surface Hydrology Parameterization with Sub-Grid Variability for General Circulation Models", *Journal of Geophysical Research*, **97/D3**, 2717 - 2728, February 28, 1992.

Wood, Eric F. and V. Lakshmi, "Scaling Water and Energy Fluxes in Climate Systems: Three Land-Atmospheric Modeling Experiments", *J. of Climate*, in press (1992).

Wood, Eric F., D.-S. Lin, M. Mancini, D. Thongs, P.A. Troch, T.J. Jackson and E.T. Engman, "Intercomparisons Between Passive and Active Microwave Remote Sensing, and Hydrological Modeling for Soil Moisture", Symposium A.3, Progress in Scientific Hydrology and Water Resource Management using Remote Sensing, *Proceedings of the*

29th Plannery Meeting of the Committee on World Space Research, (COSPAR), Washington, D.C.August 28-September 5, 1992.

C-2

Appendix A.: Spatially-Distributed Water and Energy Balance Models.

As shown by Beven and Kirkby (1979), variations in topography play a significant role in the spatial variation of soil moisture within a catchment, setting up spatially variable initial conditions for both runoff from rainstorms and evaporation during interstorm dry periods. Beven and Kirkby (1979) were the first to develop a saturated storm response model (TOPMODEL). This model has been further expanded to include infiltration excess runoff (see Beven, 1986; Sivapalan et al., 1987), interstorm evaporation (Famiglietti et al., 1992a) and a coupled water and energy balance model (Famiglietti et al., 1992b, Famiglietti and Wood, 1992a). These latter two models will be described below.

Grid Element Fluxes.

At the surface of each grid element, the coupled water-energy balance model (Famiglietti et al., 1992b) (which will be referrred to as model-b) recognizes bare and vegetated land cover. Vegetation is further partitioned into wet and dry canopy. The soil column between the land surface and the water table is partitioned into a near surface root zone and a deeper transmission or percolation zone. At each grid element in the catchment, a land surface energy balance is used to calculate the potential evaporation for bare soil, unstressed transpiration for the dry canopy, and evaporation from the wet canopy. A canopy water balance is used to calculate the net precipitation. These variables, in conjunction with precipitation on bare soils, constitute the atmospheric forcing in the model.

The earlier water balance model of Famiglietti et al. (1992a) (which we will refer to as model-a) consisted of a single soil zone, and used computed potential evapotranspiration, E_p, as the interstorm atmospheric forcing. Land cover consisted only of bare soil even though vegetated surfaces were considered implicitly through the computation of the E_p.

The storm response portion of the models captures the spatial distribution of local characteristics, such as topography and soil type, and their role in partitioning precipitation into runoff, infiltration into the unsaturated zone and percolation from the unsaturated zone to the saturated zone. The interstorm portion of the model determines whether atmospherically demanded evapotranspiration (potential evapotranspiration, E_p) can be met by the soil-vegetation system. At locations where it can be met, actual evapotranspiration, E, is at the potential rate, at locations where it can't be met, the actual rate is at some lower, soil or vegetaion controlled rate.

Infiltration and Runoff.

Soil Description. Soil type, texture, and properties are modeled using the description proposed by Brooks and Corey (1964). The five parameters utilized in this description include the saturated hydraulic conductivity, the saturation moisture content, the residual moisture content, the pore size distribution index, and the bubbling pressure, or the height of the capillary fringe above the water table. Using this soil parameterization, soil moisture and hydraulic conductivity in unsaturated soils can be described in terms of the matric head.

Local Computation of Vertical Soil Moisture Transport. The equations for vertical transport of soil moisture for model-b include infiltration into bare and vegetated soils, evaporation from bare soil, transpiration by vegetation, capillary rise from the water table, drainage from the root zone and transmission zone, and runoff from bare and vegetated soils. Each of these vertical moisture fluxes depends on the soil moisture status of the local root zone or the transmission zone, and the local soil properties. The infiltration, evapotranspiration and surface runoff fluxes also depend on local levels of atmospheric forcing. Canopy and soil water balance equations are applied at each grid element in the catchment to monitor the states of wetness in the local canopy, root zone and transmission zone.

For model-a, the infiltration and evaporation processes consider only bare soil. The atmospheric forcings of precipitation and potential evapotranspiration are provided as inputs to the model. As in model-b, it is determined by the model whether the soil-system can infiltrate the precipitation or provide the necessary water during evaporation to satisfy the atmospheric demand.

Infiltration is computed using the time compression approximation to Philip's equation to compute a local infiltration rate, g_i, under local time varying rainfall, p_i. The rate g_i is

$$g_i = \min [g_i^*(G), p_i] \qquad (A.1)$$

in which G is the cumulative infiltration during the storm and g_i^* the local infiltration capacity, which is a function of initial soil wetness, G and

soil parameters. Infiltration excess direct runoff occurs when p_i exceeds g_i^*.

Water Table Dynamics. Saturated subsurface flow between catchment elements is assumed to be controlled by the spatial variability in topographic and soil properties following the TOPMODEL approach of Beven and Kirkby (1979), Beven (1986a,b) and Sivapalan et al. (1987). This approach develops a relationship between the catchment average water table depth, $\bar{z}$, and the local water table depth, z_i, in terms of the local topographic-soil index. This relationship is

$$z_i = \bar{z} + \frac{1}{f}\left[\lambda - \ln\left(\frac{a\, T_e}{T_i \tan\beta}\right)\right] \qquad (A.2)$$

where T_i is the local soil transmissivity (saturated hydraulic conductivity divided by f), f is a parameter that describes the exponential rate of decline in soil transmissivity with depth and is assummed constant within a catchment, $\ln(T_e)$ is the areal average of $\ln(T_i)$, λ is the expected value of the topographic variable $\ln(a/\tan\beta)$ and is constant for a particular catchment topography, a is the area drained through the local unit contour, and β is the local slope angle.

Drainage (baseflow) between storm events is assumed to follow an exponential function of average depth to the water table (soil wetness) and has the form $Q_s = Q_o \exp(-f\,\bar{z})$ where $Q_o = AT_e \exp(-\lambda)$, A being the catchment area. Given a recession curve prior to a storm, Troch et al. (1992) have developed a procedure for estimating $\bar{z}$ and hence using (A.2) to provide the initial patterns of local water table depths, saturated areas and soil moisture values. The areal average water table depth is updated by

consideration of catchment-scale mass balance.

Evapotranspiration. For model-b, evaporation from the surface is based on solving the energy balance equation, $R_n = \lambda E + H + G$, which links the energy balance to the water balance through λE, the latent heat flux term. Here R_n refers to the net radiation at the land surface, H to the sensible heat flux and G the ground heat flux. A bulk transfer formulation for latent heat flux can be represented by (Brutsaert, 1982)

$$\lambda E = \frac{\rho C_p \, (e^*(T_l) - e_a)}{\gamma \, (r_a + r_{st})} \qquad (A.3)$$

where ρ is the density of air, C_p is the specific heat of air at constant pressure, γ is the psychrometric constant, $e^*(T_l)$ is the saturation vapour pressure at the temperature of the surface, T_l, and e_a is the vapour pressure at a reference level above the soil or canopy surface, r_a is an aerodynamic resistance and r_{st} is a bulk stomatal resistance. Equation (A.3) can be linearized about a suitable temperature, such as the air temperature T_a, leading to the Penman-Monteith formulation. In model-b the evaporation from the wet canopy is determined by the energy balance equations for the temperature of the wet vegetated surface. Setting the aerodynamic resistance consistent with the type of vegetation surface, $r_c = 0$, and letting T_l represent the temperature of the wet vegetated surface yields the partitioning of R_n into λE and H. The unstressed transpiration from a canopy, E_c^*, whose density is represented by a leaf area index (LAI), is obtained from (A.3) in which r_{st} is replaced with a canopy resistance $r_c = r_{st}/LAI$. Here, r_{st} is a minimum resistance corresponding to the wet vegetated surface.

The potential evaporation for bare soil is calculated using the nonlinear energy balance equations described above with G nonzero, r_{st} equal zero, aerodynamic resistance consistent with the particular type of soil and T_1 refering to the temperature of the wet bare soil. The actual evaporation for the soil is found by applying a desorptivity based Philip-like evaporation equation like the that given in (A.1) for infiltration..

For a dry canopy the actual rate of transpiration, E_c, is related to the soil moisture through

$$\tau = \frac{\psi_s - \psi_p}{R_s + R_p} \qquad (A.4)$$

where τ is the transpiration supply, ψ_s is the soil matric potential, ψ_p is the plant water potential, R_s is the hydraulic resistance of the soil and R_p is the hydraulic resistance of the plant. The actual transpiration rate is given as

$$E_c = \min[\tau, E_c^*] \qquad (A.5)$$

Catchment-Scale Water and Energy Fluxes. The catchment-scale water and energy balance fluxes can be computed two ways. The first is when the models are run in a 'fully distributed' mode in which the fluxes are computed grid by grid. In this mode, the grid size is usually taken to be the resolution of the digital elevation model (DEM) for the topography and therefore the resolution at which the topographic index is computed. Thus the catchment scale water balance fluxes is just the summation over all the elements whose flux values are determined from the process equations discussed above. In this mode, patterns of inputs (like vegetation, precipitation, radiation, etc) can be included in the flux calculations.

The second approach is to employ the similarity assumption inherent in TOPMODEL; namely that points in the catchment with the same value of the soil-topographic index respond similarly hydrologically. Since soil moisture in a dominant variable for the water and energy fluxes, this assumption appears quite reasonable. In this approach, fluxes will be determined conditional on values of the soil-topographic index, $\ln(\alpha T_e / T_i \tan\beta)$. For cases where significant variation occurs (like vegetation characteristics) within an area, the conditioning can be taken one step further -- i.e. calculate the fluxes condtional on $\ln(\alpha T_e / T_i \tan\beta)$ and vegetation. This conditioning approach leads to macroscale models for inflitration and evapotranspiration, which are described below.

Macroscale model for infiltration and runoff. Using the statistical distribution of the topographic-soil index, one can determine the fraction of the catchment that will be saturated due to the local soil storage being full. These areas will generate saturation excess runoff at the rate $\bar{p}$, the mean rainfall rate. For that portion of the catchment where infiltration occurs, the local expected runoff rate at time t, m_q, can be calculated as the difference between the mean rainfall rate, $\bar{p}$, and the local expected infiltration rate, m_g. This implies that m_q and m_g are conditioned upon a topographic-soil index whose statistical distribution is central to the REA macroscale model. The difference between averaged rainfall and infiltration can be expressed as

$$m_q\{t|\ln(\alpha T_e / T_i \tan\beta)\} = \bar{p} - m_g\{t|\ln(\alpha T_e / T_i \tan\beta)\}. \qquad (A.6)$$

As discussed above, m_q and m_g are time varying functions whose values at any particular time are equal for points within the catchment having the same

topographic-soil index; this dependance is indicated in equation (A.6) by the |. The full development of the topographic-soil index is provided in Beven and Kirkby (1979), Beven (1986a,b), Sivapalan et al. (1987) and Wood et al. (1990). Both the local expected runoff rate and the local expected infiltration rate are (probabilistically) conditioned on the topographic-soil index, $\ln(\alpha T_e / T_i \tan\beta)$. The runoff production from the catchment is found by integrating, usually numerically, the conditional rate over the statistical distribution of topographic-soil index.

Macroscale model for evapotranspiration. In a similar way, a macroscale evaporation model is developed for interstorm periods. As stated earlier, topography plays an important role in the interstorm redistribution of soil moisture and therefore in the initial conditions for the evaporation calculations. For those portions of the catchment for which the soil column can deliver water at rate sufficient to meet the potential evapotranspiration or atmospheric demand rate, E_p, the actual rate E equals E_p; otherwise, the rate will be at a lower soil controlled rate E_s. Within the TOPMODEL framework, locations with the same value of the topographic-soil index will respond similarly; implying a macroscale model of the following form, which is conditioned on that index.

$$m_E\{t|\ln(\alpha T_e / T_i \tan\beta)\} = \min[m_{E_s}\{t|\ln(\alpha T_e / T_i \tan\beta)\}, \bar{E}_p(t)] \quad (A.7)$$

where m_E refers to the mean evaporation rate at locations in the catchment with the same index, m_{E_s} refers to the mean soil controlled rate and $\bar{E}_p$ to the spatially average potential or atmospheric demand rate.

List of Figures.

Figure 1: Schematic of Aggregation and Scaling in Hydrologic Modeling.

Figure 2: Natural subcatchment divisions for Kings Creek, Kansas.

Figure 3: Comparisons of λ, mean of $\ln(\frac{a}{\tan \beta})$, for the subcatchments of Kings Creek, KS shown in Figure 2. Each pixel is 0.9 sq km.

Figure 4: Comparisons of λ, mean of $\ln(\frac{a}{\tan \beta})$, for the subcatchments of Sleepers River, VT. (a) for catchments up to 1 sq km, (b) for catchments up to 5 sq km, (c) for catchments up to 45 sq km. (Wolock, personal communication).

Figure 5: Normalized vegetation index (NDVI) derived for part of the FIFE area from the August 15, 1987 overpass. Resolution is 30 m.

Figure 6: 300 x 300 m aggregated normalized vegetation index (NDVI) for part of the FIFE area for August 15, 1987. The images were derived using data from Figure 5.

Figure 7: Comparisons between NDVI derived from aggregated NDVI data of Figure 9 and derived from Equation (2) using aggregated thermatic mapper (TM) data. Levels of aggregation are (a) 300 x 300 m, (b) 750 750 m, (c) 1500 x1500 m..

Figure 8: Comparison of storm runoff generated from the distributed model-a (see Appendix A) and from the macroscale water balance model (Equation A.6) for two time intervals on August 4, 1987: (a) 8:45 am, and (b) 9:30 am.

Figure 9: Comparison of interstorm evapotranspiration from the distributed model-a (see Appendix A) and from the macroscale water balance model (Equation A.7) for four times during the July 18 - 31, 1987 interstorm period.

Figure 10: Comparisons of the average radar return (L-band, HH-polarization) in digital numbers for subcatchments within Mahantango Creek, PA. Data from the July 10, 1990 AIRSAR aquisition.

Figure 11: Transpiration and soil exfiltration capacities versus volumetric soil moisture content, after Famiglietti and Wood (1992a).

Figure 12: Computed catchment-average evapotranspiration from the distributed model-b (see Appendix A), the statistically aggregated macroscale model, and a lumped, one-dimensional model with spatially constant parameters. Results are for Kings Creek, KS for October 5-9, 1987.

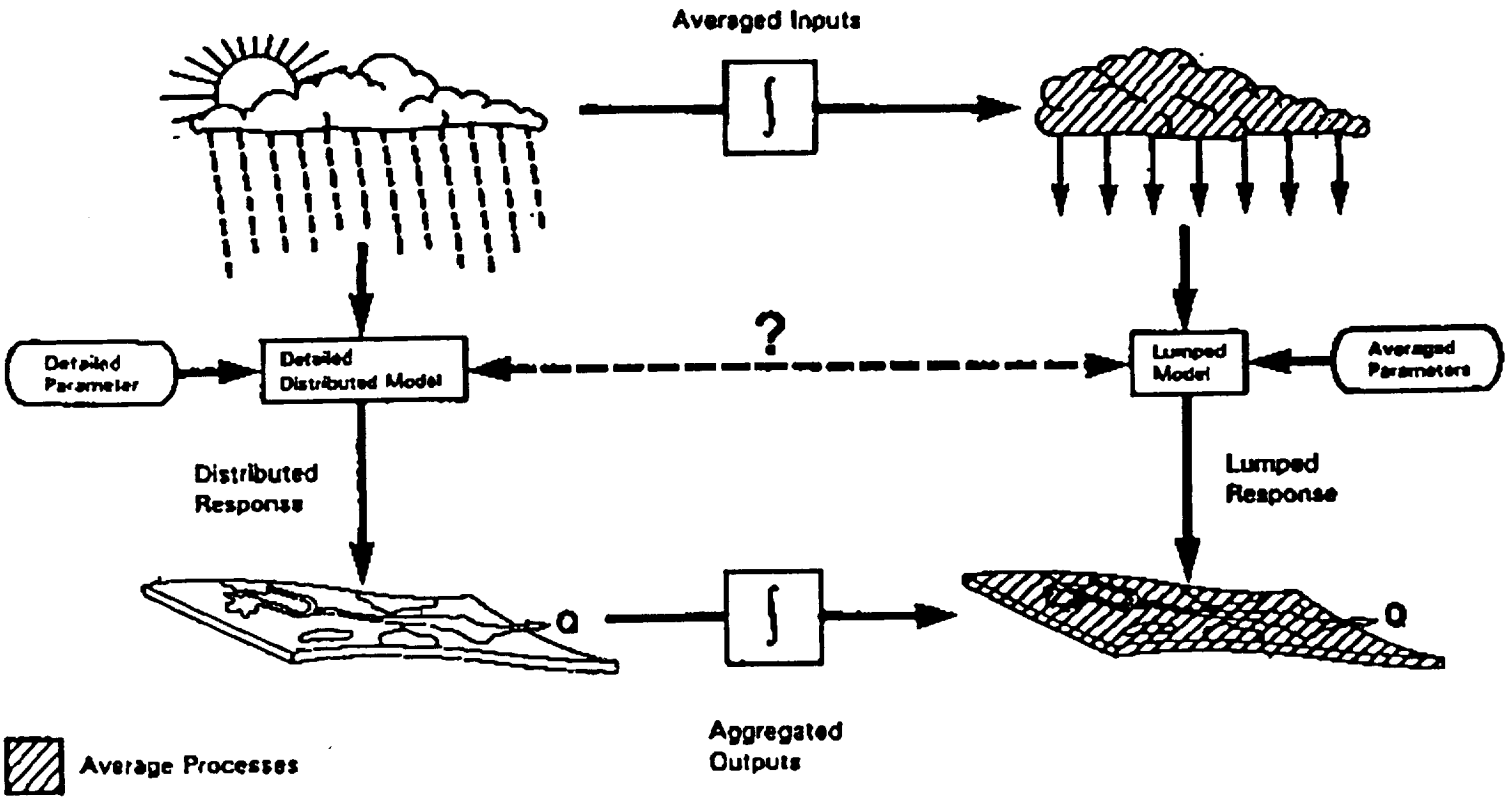

Figure 1: Schematic of Aggregation and Scaling in Hydrologic Modeling.

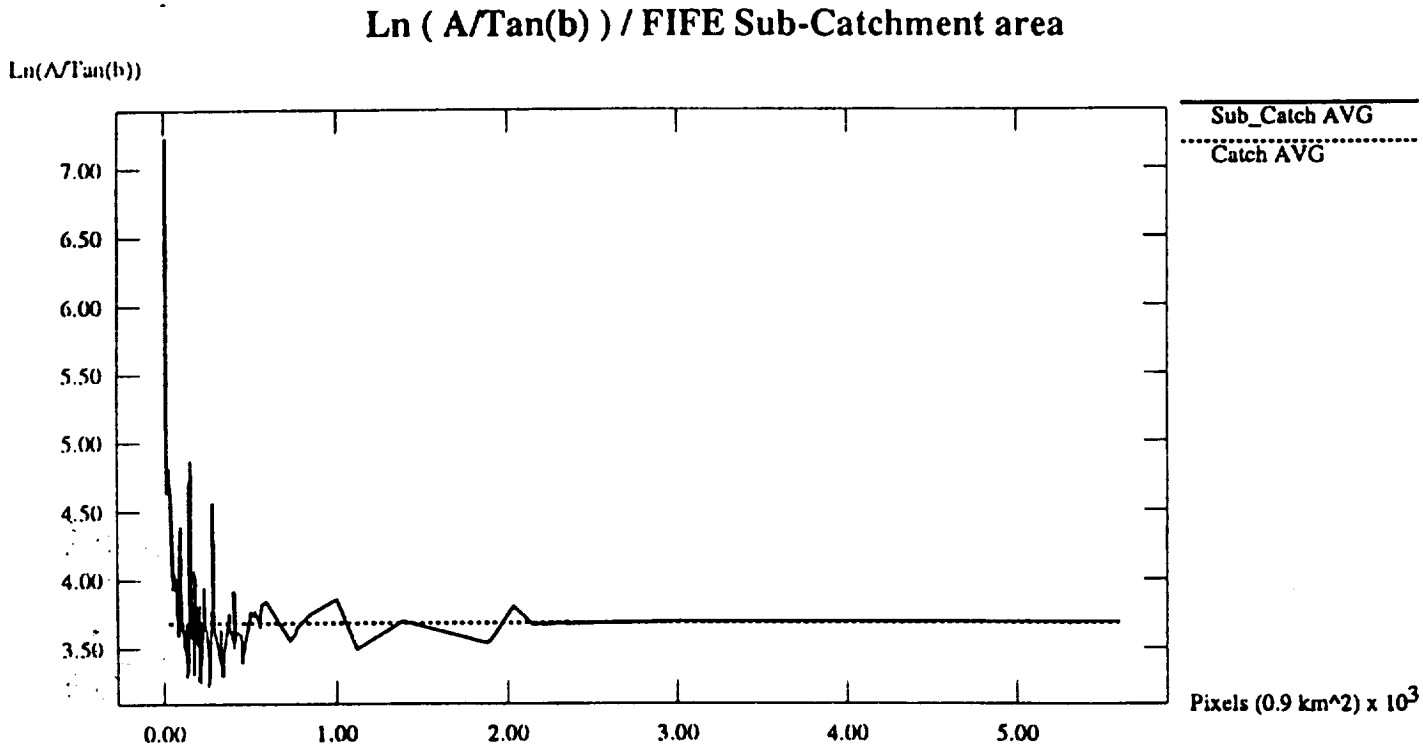

Figure 3: Comparisons of λ, mean of $\ln(\frac{a}{\tan \beta})$, for the subcatchments of Kings Creek, KS shown in Figure 2. Each pixel is 0.9 sq km.

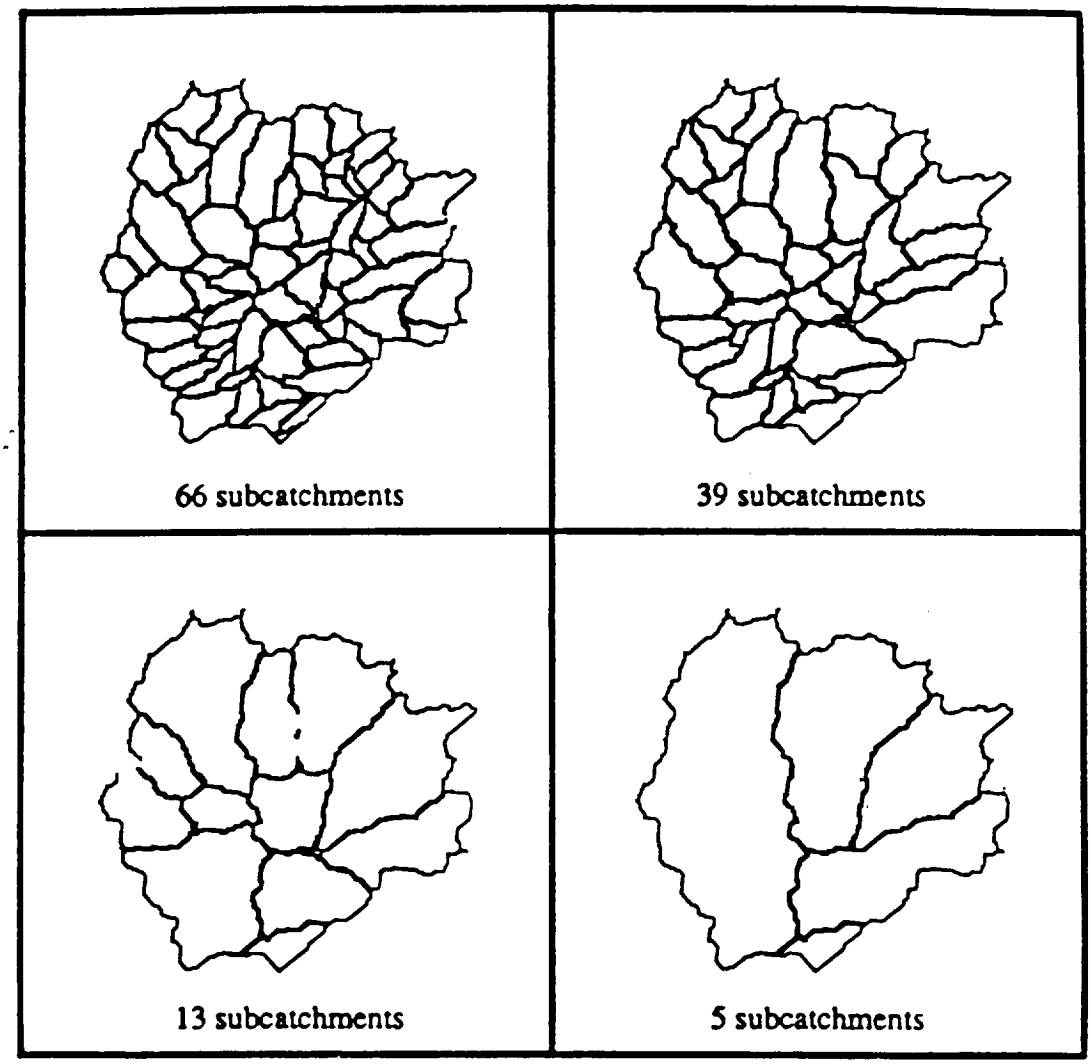

Figure 2: Natural subcatchment divisions for Kings Creek, Kansas.

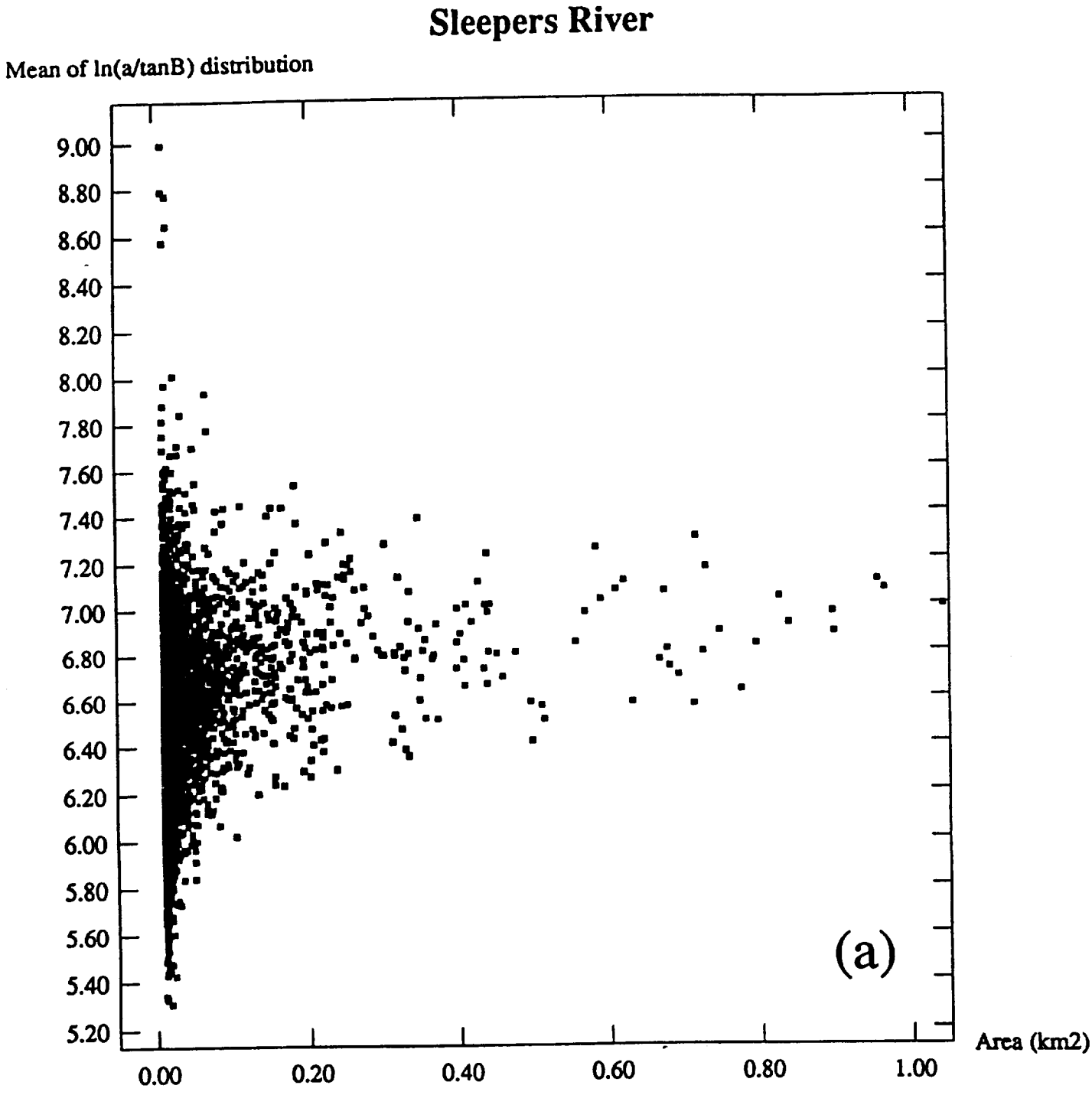

Figure 4: Comparisons of λ, mean of $\ln(\frac{a}{\tan \beta})$, for the subcatchments of Sleepers River, VT. (a) for catchments up to 1 sq km. (Wolock, personal communication).

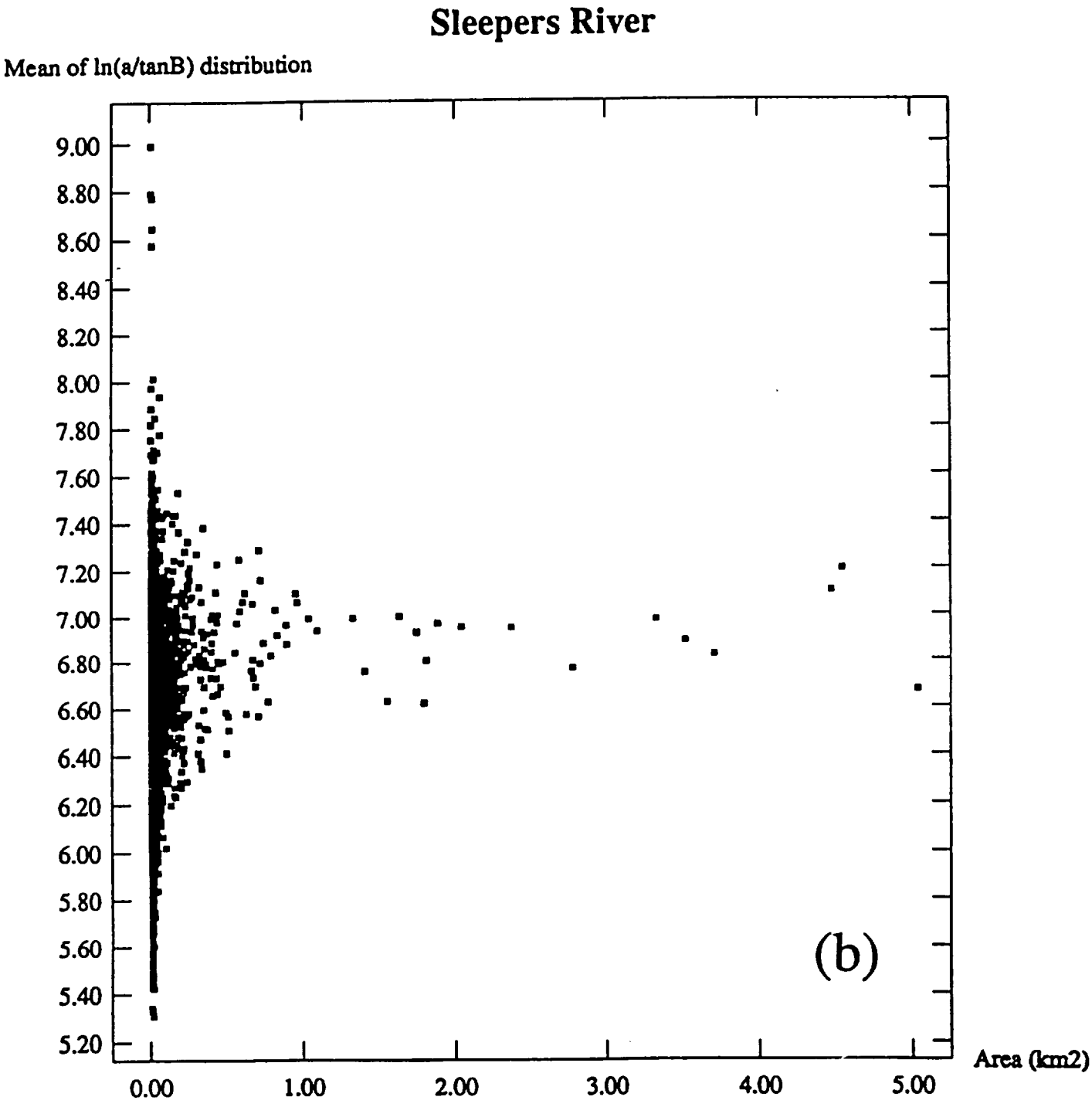

Figure 4: Comparisons of λ, mean of $\ln(\frac{a}{\tan \beta})$, for the subcatchments of Sleepers River, VT. (b) for catchments up to 5 sq km. (Wolock, personal communication).

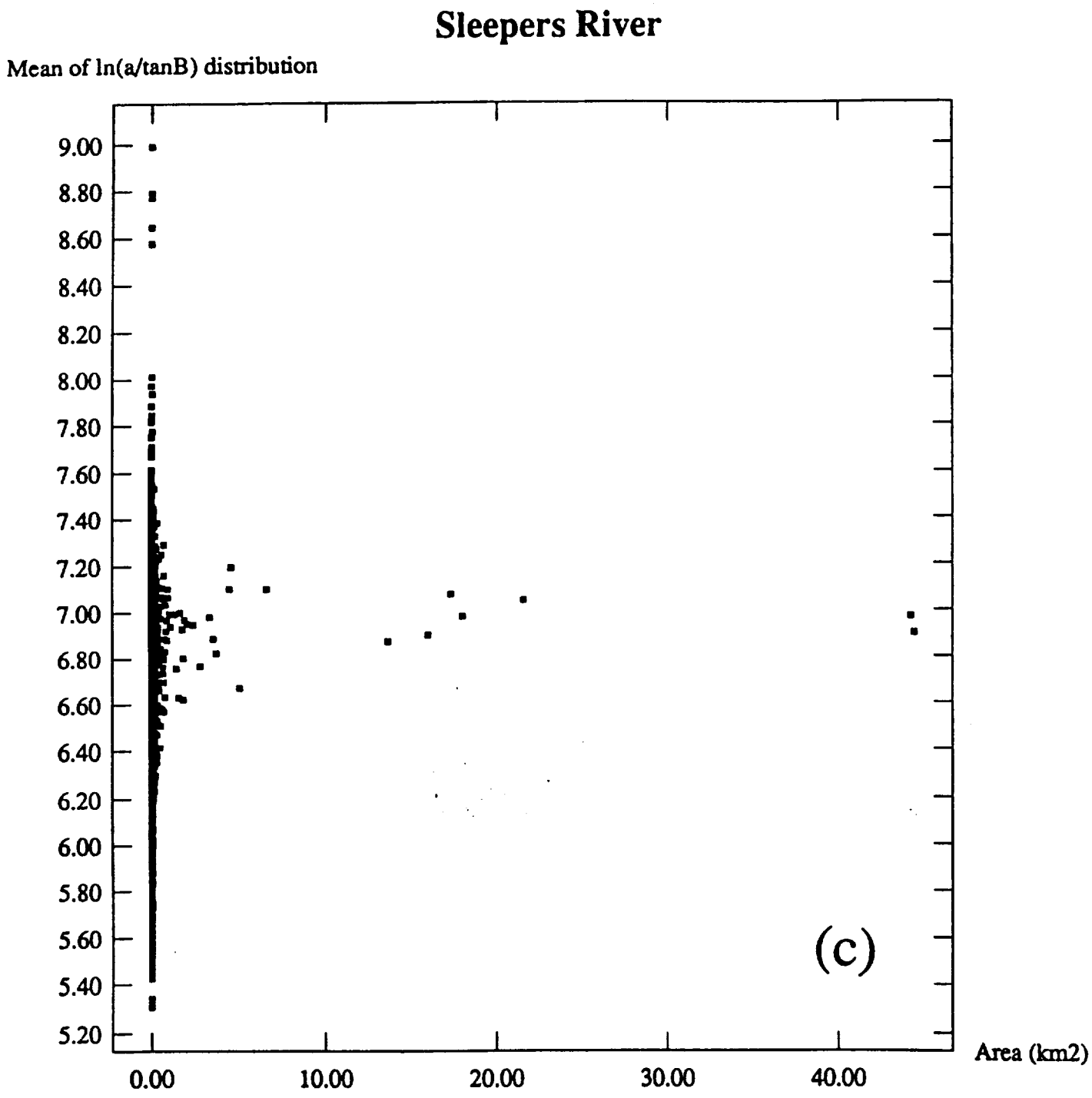

Figure 4: Comparisons of λ, mean of $\ln(\frac{a}{\tan \beta})$, for the subcatchments of Sleepers River, VT. (c) for catchments up to 45 sq km. (Wolock, personal communication).

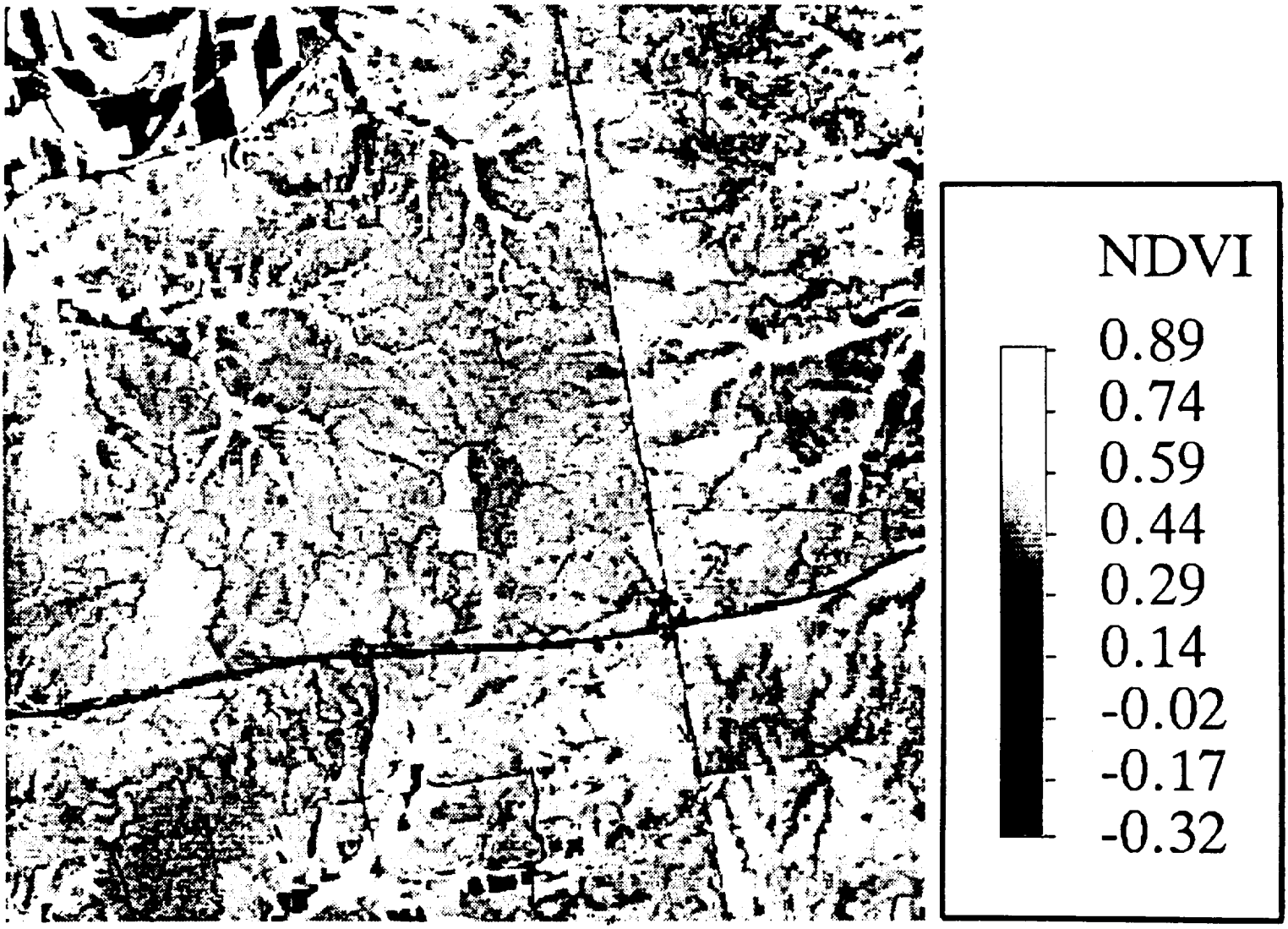

Figure 5: Normalized vegetation index (NDVI) derived for part of the FIFE area from the August 15, 1987 overpass. Resolution is 30 m.

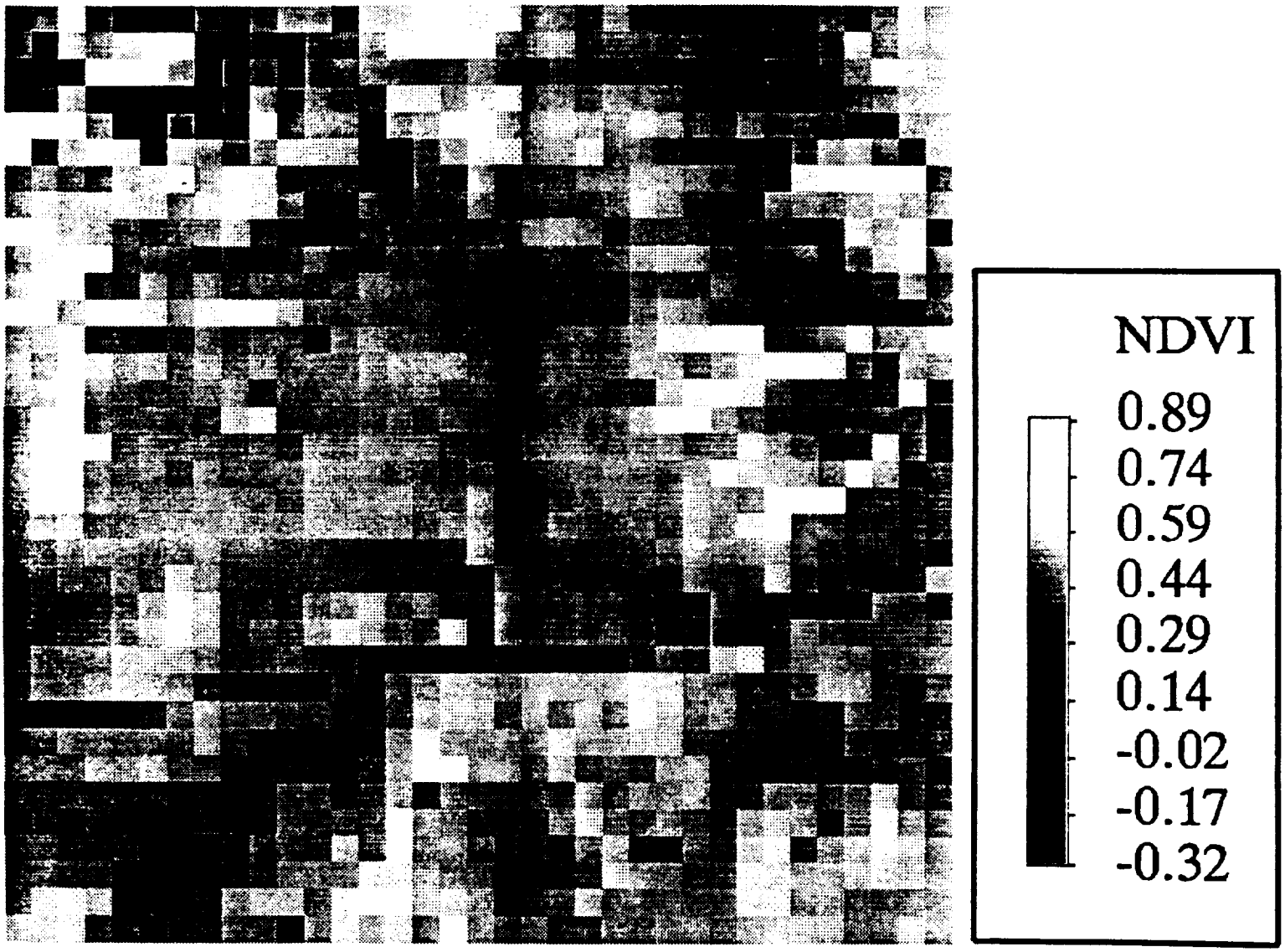

Figure 6: 300 x 300 m aggregated normalized vegetation index (NDVI) for part of the FIFE area for August 15, 1987. The images were derived using data from Figure 5.

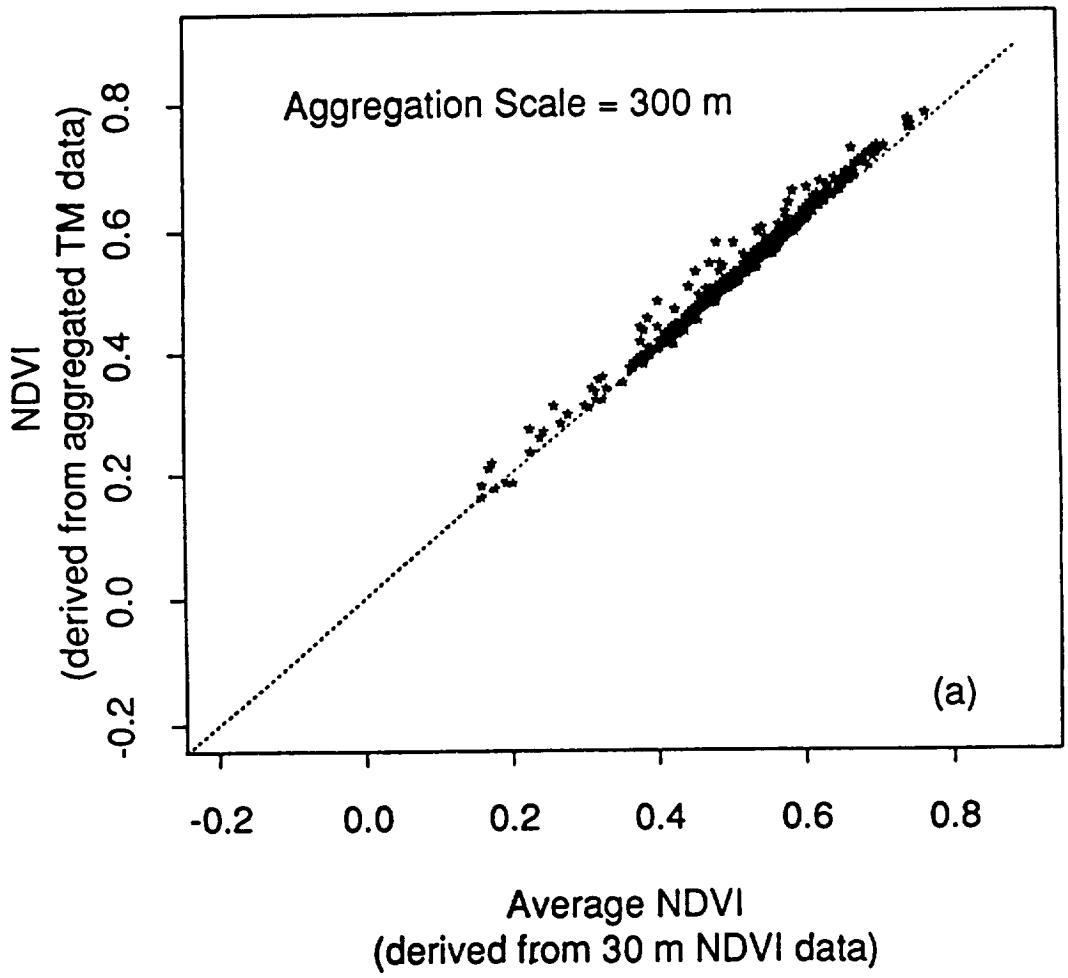

Figure 7: Comparisons between NDVI derived from aggregated NDVI data of Figure 9 and derived from Equation (2) using aggregated thermatic mapper (TM) data. Levels of aggregation are (a) 300 x 300 m.

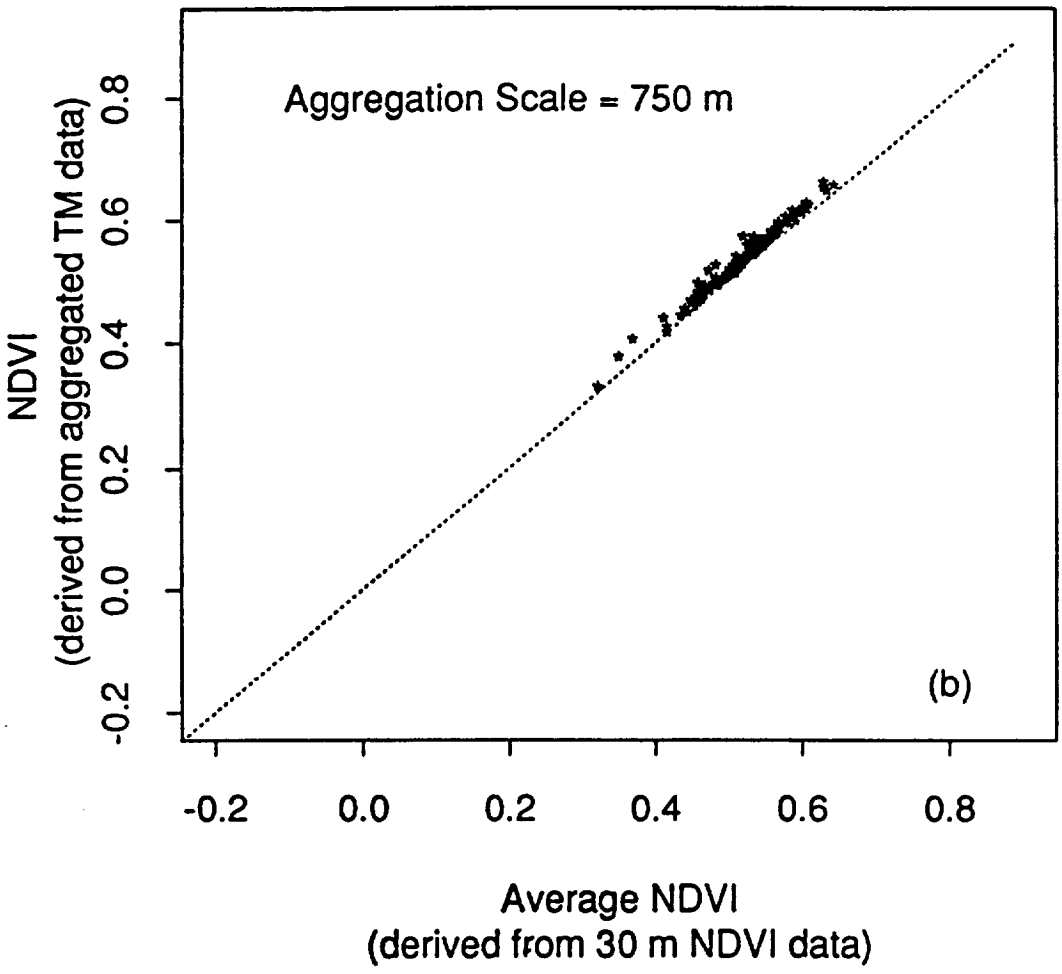

Figure 7: Comparisons between NDVI derived from aggregated NDVI data of Figure 9 and derived from Equation (2) using aggregated thermatic mapper (TM) data. Levels of aggregation (b) 750 750 m.

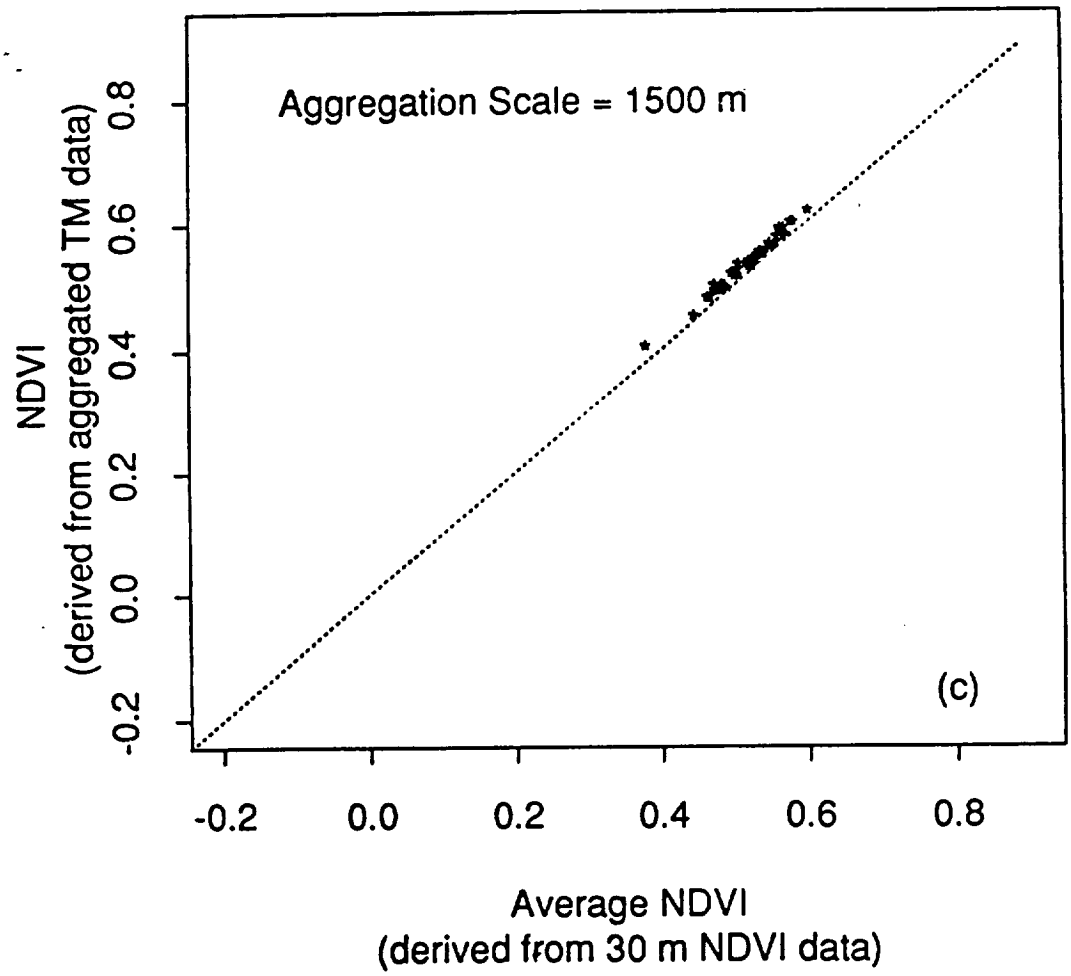

Figure 7: Comparisons between NDVI derived from aggregated NDVI data of Figure 9 and derived from Equation (2) using aggregated thermatic mapper (TM) data. Levels of aggregation (c) 1500 x1500 m.

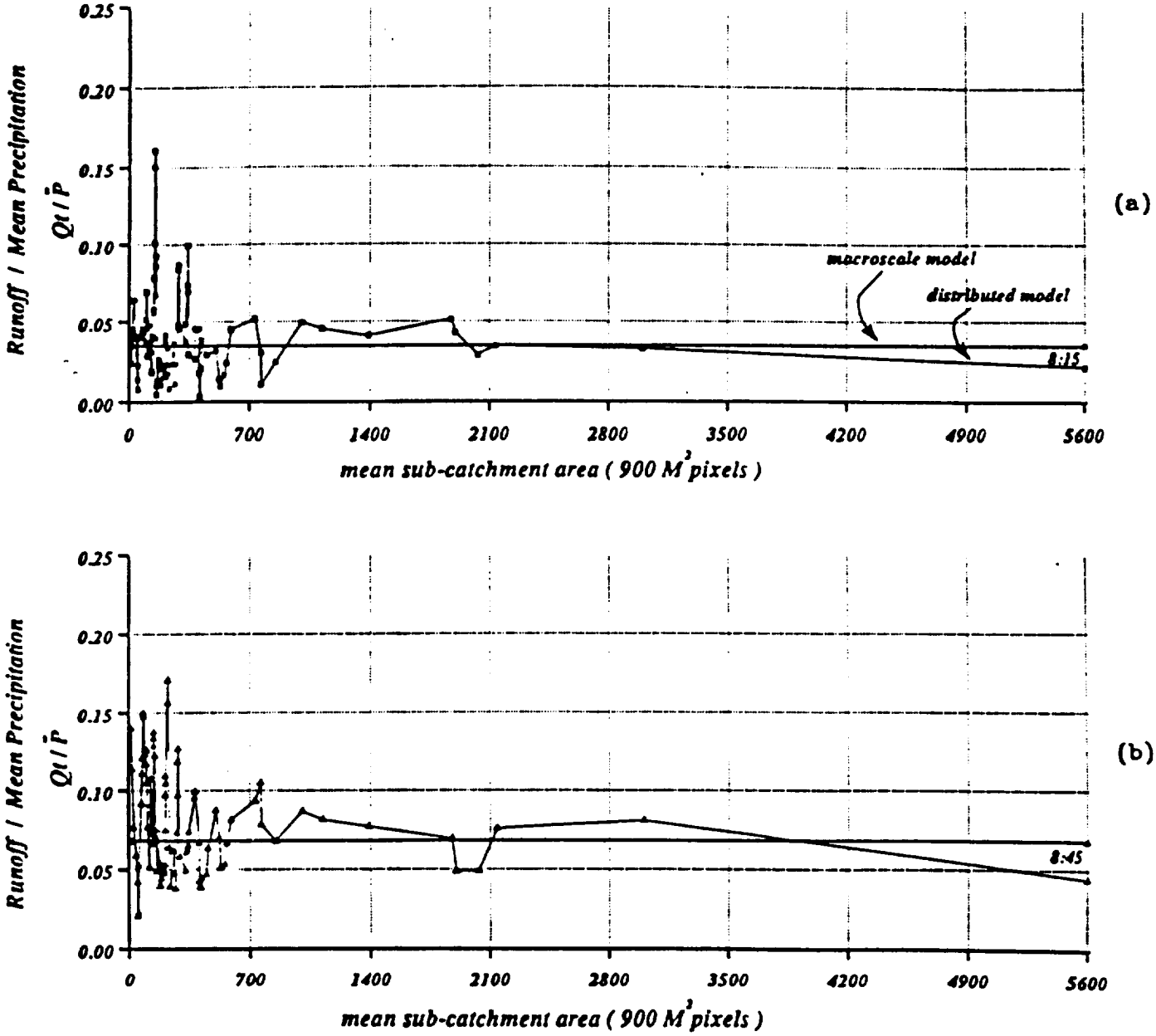

Figure 8: Comparison of storm runoff generated from the distributed model-a (see Appendix A) and from the macroscale water balance model (Equation A.6) for two time intervals on August 4, 1987; (a) 8:45 am, and (b) 9:30 am.

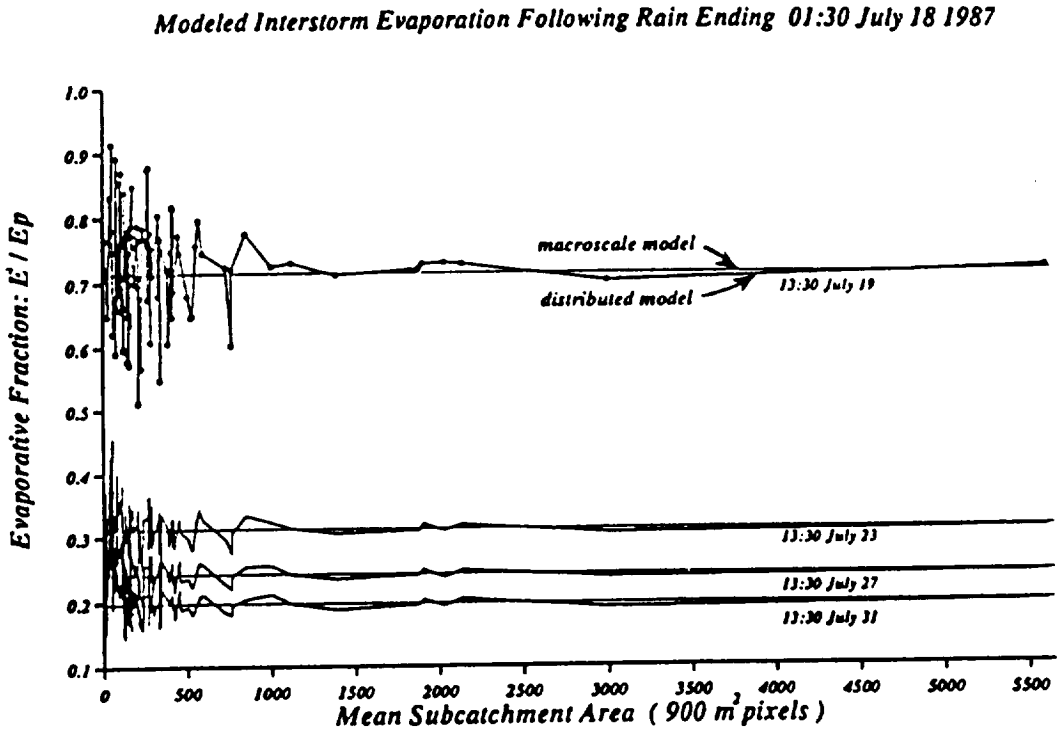

Figure 9: Comparison of interstorm evapotranspiration from the distributed model-a (see Appendix A) and from the macroscale water balance model (Equation A.7) for four times during the July 18 - 31, 1987 interstorm period.

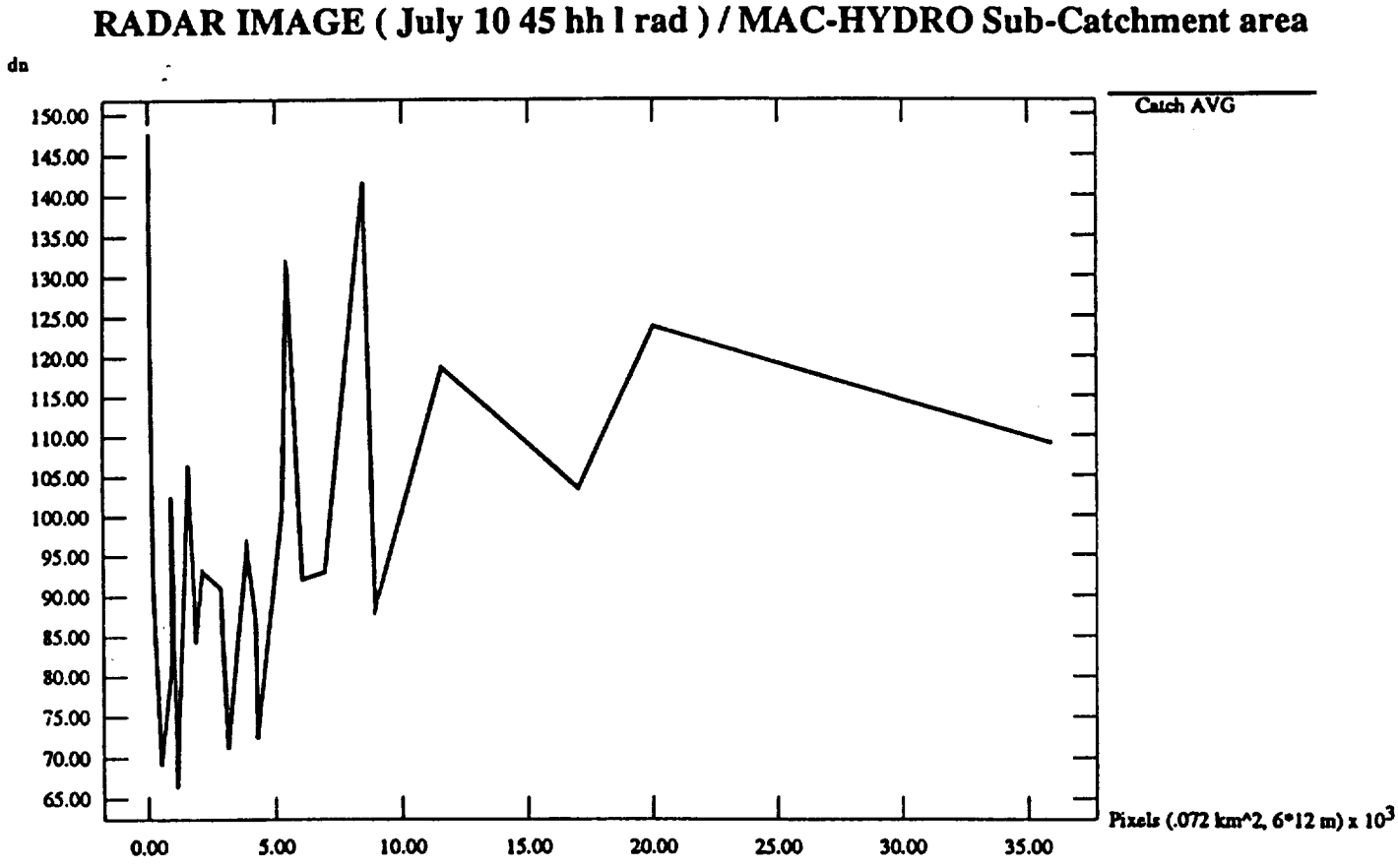

Figure 10: Comparisons of the average radar return (L-band, HH-polarization) in digital numbers for subcatchments within Mahantango Creek, PA. Data from the July 10, 1990 AIRSAR aquisition.

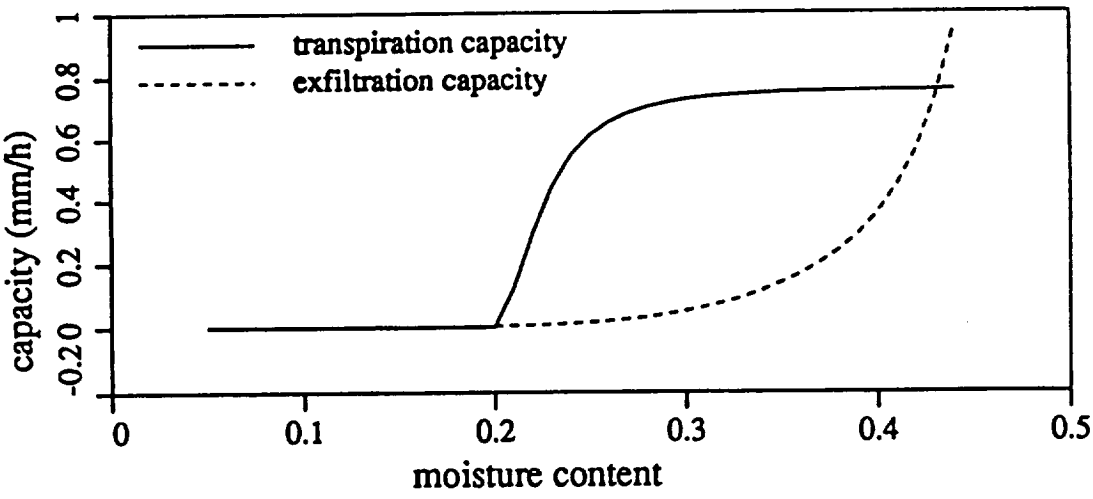

Figure 11: Transpiration and soil exfiltration capacities versus volumetric soil moisture content, after Famiglietti and Wood (1992a).

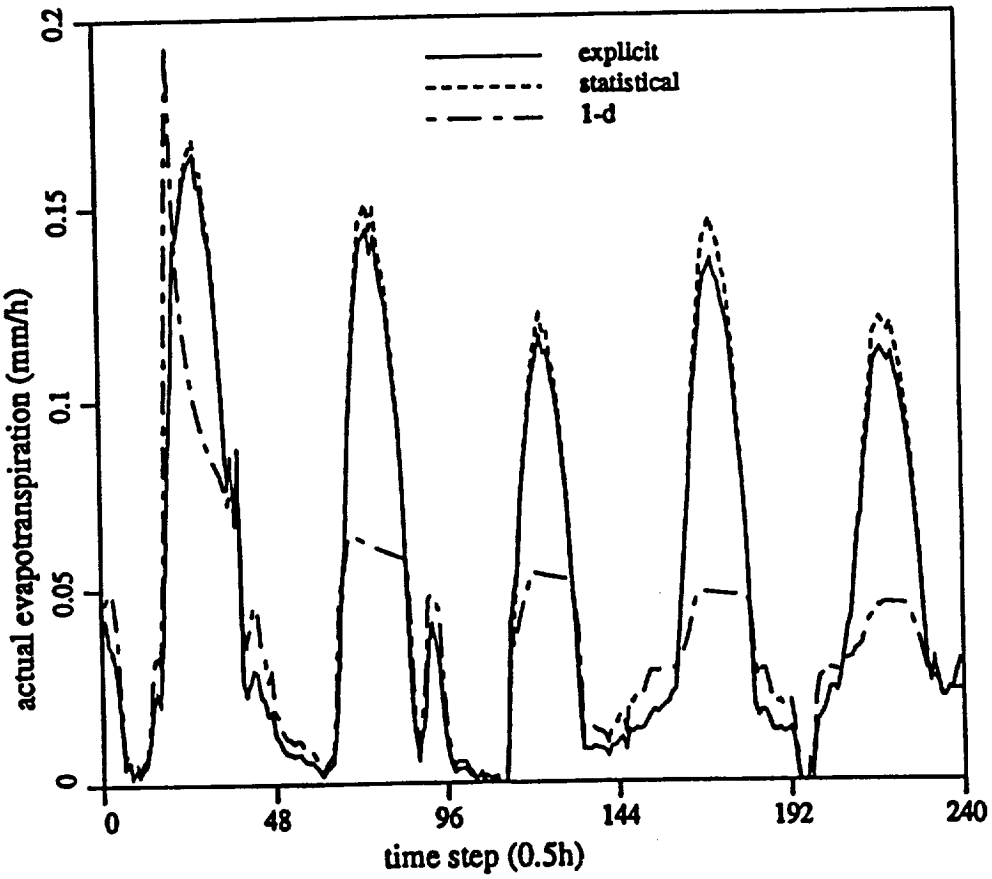

Figure 12: Computed catchment-average evapotranspiration from the distributed model-b (see Appendix A), the statistically aggregated macroscale model, and a lumped, one-dimensional model with spatially constant parameters. Results are for Kings Creek, KS for October 5-9, 1987.

Reprinted from JOURNAL OF CLIMATE, Vol. 6, No. 5, May 1993
American Meteorological Society

Scaling Water and Energy Fluxes in Climate Systems: Three Land–Atmospheric Modeling Experiments

ERIC F. WOOD AND VENKATARAMAN LAKSHMI

Water Resources Program, Princeton University, Princeton, New Jersey

(Manuscript received on 25 October 1991, in final form 15 June 1992)

ABSTRACT

The effects of small-scale heterogeneity in land-surface characteristics on the large-scale fluxes of water and energy in the land–atmosphere system have become a central focus of many of the climatology research experiments. The acquisition of high-resolution land-surface data through remote sensing and intensive land-climatology field experiments (like HAPEX and FIFE) has provided data to investigate the interactions between microscale land–atmosphere interactions and macroscale models. One essential research question is how to account for the small-scale heterogeneities and whether "effective" parameters can be used in the macroscale models. To address this question of scaling, three modeling experiments were performed and are reviewed in the paper. The first is concerned with the land-surface hydrology during rain events and between rain events. The second experiment applies the Simple Biosphere Model (SiB) to a heterogeneous domain and the spatial and temporal latent heat flux is analyzed. The third experiment uses thermatic mapper (TM) data to look at the scaling of the normalized vegetation index (NDVI), latent heat flux, and sensible heat flux through either scaling of the TM-derived fields using the TM data or the fields derived from aggregated TM data.

In all three experiments it was found that the surface fluxes and land characteristics can be scaled, and that macroscale models based on effective parameters are sufficient to account for the small-scale heterogeneities investigated. The paper also suggests that the scale at which a macroscale model becomes valid, the representative elementary scale (REA), is on the order 1.5–3 correlation lengths, which for land processes investigated appears to be about 1000–1500 m. At scales less than the REA scale, exact patterns of subgrid heterogeneities are needed for accurate small-scale modeling.

1. Introduction

The complex heterogeneity of the land surface through soils, vegetation, and topography, all of which have different length scales, and their interaction with meteorological inputs that vary with space and time result in fluxes of energy and water whose scaling properties are unknown. Research into land–atmospheric interactions suggests a strong coupling between land-surface hydrologic processes and climate (Charney et al. 1977; Walker and Rowntree 1977; Shukla and Mintz 1982; Rowntree and Bolton 1983; Shukla et al. 1990; Sud et al. 1990). The issue of "scale interaction" for land-surface–atmospheric processes has emerged as one of the critical unresolved problems for the parameterization of climate models.

Understanding the interaction between scales has increased in importance when the apparent effects of surface heterogeneities on the transfer and water and energy fluxes are observed through remote sensing and intensive field campaigns like HAPEX and FIFE (Sellers et al. 1988). The ability to parameterize macroscale models based on field experiments or remotely sensed data has emerged as an important research question for programs such as the Global Energy and Water Experiment (GEWEX) or the Earth Observing System (EOS). It is also important for the parameterization of the macroscale land-surface hydrology necessary in climate models, and crucial to our understanding of how to represent subgrid variability in such macroscale models.

Current land-surface parameterization schemes can be put into three groups. The first is best represented by the bucket hydrology based on the work of Budyko (1956), which forms the basis for current long-term climate simulation. The second group would be the aggregated models with biospheric processes. This group of models is represented by the Biosphere Atmosphere Transfer Scheme (BATS) (Dickinson 1984) and the Simple Biosphere Model (SiB) (Sellers et al. 1986) in which the vertical structure of the canopy is well represented and the spatial characteristics are assumed constant. Wood (1991) has referred to these as "constant canopy" models. The final group incorporates subgrid heterogeneity at varying levels of detail, from fractional areas (Abramopolous et al. 1988) to statistical distribution for the subgrid processes (Entekhabi and Eagleson 1989; Famiglietti and Wood 1991a).

Corresponding author address: Eric F. Wood, Water Resources Program, Department of Civil Engineering and Operations Research, Princeton University, Princeton, NJ 08544.

Current research suggests two competing approaches for handling subgrid heterogeneity. (i) The first approach is based on the belief that subgrid processes have significant effect on processes at GCM scales and that the nonlinearity in subgrid-scale processes prevents simple scaling. This approach is supported by the observations of sea breezes arising from the significantly different characteristics between land and water. Avissar and Pielke (1989) also found that heterogeneity in land characteristics resulted in sea-breeze-like circulations and significant differences in surface temperatures and energy fluxes across the patches. It is important to note that in their hypothetical domain the patches are large with respect to the size of the domain. In natural domains the scale of such patches is often much smaller, which may lead to lower variability across the domain. (ii) The second approach is to ignore the variability in subgrid processes and to represent these processes at larger scales through models with effective parameters. Similarly, one may use aggregated inputs to drive these "macroscale" processes models at the large scale. This is essentially the approach of the constant-canopy biospheric models, where horizontal variability is ignored. It is also the approach of using small-scale micrometeorological field studies for calibration (Sellers and Dorman 1987; Sellers et al. 1989).

In this paper a series of numerical experiments are reported on that investigate the scaling of land-surface processes—either of the inputs or parameters—and compare the aggregated processes to the spatially variable case. Three experiments will be reported. These are as follows. The first is the aggregation of the hydrologic response in a catchment due to rainfall during a storm event and due to evaporative demands during interstorm periods. The second set of experiments is the spatial and temporal aggregation of latent heat fluxes, as calculated from SiB. The third set of experiments is the aggregation of remotely sensed land vegetation and latent and sensible heat fluxes using thermatic mapper (TM) data from the FIFE experiment of 1987 in Kansas.

2. Aggregation of hydrologic responses

Runoff generation is now known to result from a complexity of mechanisms; during a particular storm different mechanisms may generate runoff from different parts of a catchment. As reviewed in Wood et al. (1990), these mechanisms include runoff due to rainfall on areas of low-permeability soils (referred to as the infiltration excess mechanism) and from rainfall on areas of soil saturated by a rising water table even in high-permeability soil (referred to as saturation excess runoff generation). These saturated contributing areas expand and contract during and between storm events.

As first shown by Beven and Kirkby (1979), variations in topography play a significant role in the spatial variation of soil moisture within a catchment, setting up spatially variable initial conditions for both runoff from rainstorms and evaporation during interstorm periods. Beven and Kirkby (1979) were the first to develop a saturated storm-response model (TOPMODEL). This model has been further expanded to include the above mechanisms (see Beven 1986a,b; Sivapalan et al. 1987). A complete description of the models, incorporating spatial variability in topography and soils, is provided in Wood et al. (1990) and will not be repeated here.

During interstorm periods, topography plays an important role in the downslope redistribution of soil moisture and, with soil properties, sets up the initial conditions for evaporation. The maximum evaporation rate is that rate demanded by atmospheric conditions, referred to as the potential rate, and this rate is met if the soil column can deliver the moisture to the surface. Rates lower than the potential rate will be at a "soil controlled" rate to be determined by soil properties and soil-moisture levels. The model with both storm and interstorm processes is fully described in Famiglietti et al. (1992).

The water-balance model described in Famiglietti et al. (1992) was applied to the Kings Creek catchment of the FIFE area in Kansas. Figure 1 shows the division of the 11.7 km^2 catchment into subcatchments—the number ranging from 5 to 66 depending on the scale. All subcatchments represent hydrologically consistent units, in that runoff flows out of the subcatchment through one flow point and that the surface-runoff flux across the other boundaries is zero.

For a rainfall storm on 4 August 1987, the average runoff for the subcatchments was calculated for two times and plotted in Fig. 2 against a subcatchment area measured in pixels. Each pixel is 900 m^2. Notice that the runoff Q_i is normalized by the average precipitation, $\bar{P}$. The same type of plot was done for selected times during an interstorm period that extended from 18 July through 31 July 1987 and is presented as Fig. 3. The behavior of the catchment shows that at small scales there is extensive variability in both storm response and evaporation. This variability appears to be controlled by variability in soils and topography whose length scales are on the order of 10^2–10^3 m—the typical scale of a hill slope. With increased scale, the increased sampling of hill slopes leads to a decrease in the difference between subcatchment responses. At some scale, the variance between hydrologic responses for catchments of the same scale should reach a minimum (Wood et al. 1990). Wood et al. (1988) suggest that this threshold scale represents a representative elementary area (REA), which is proposed to be the fundamental building block for hydrologic modeling, as defined in Wood et al. (1988) and Wood et al. (1990).

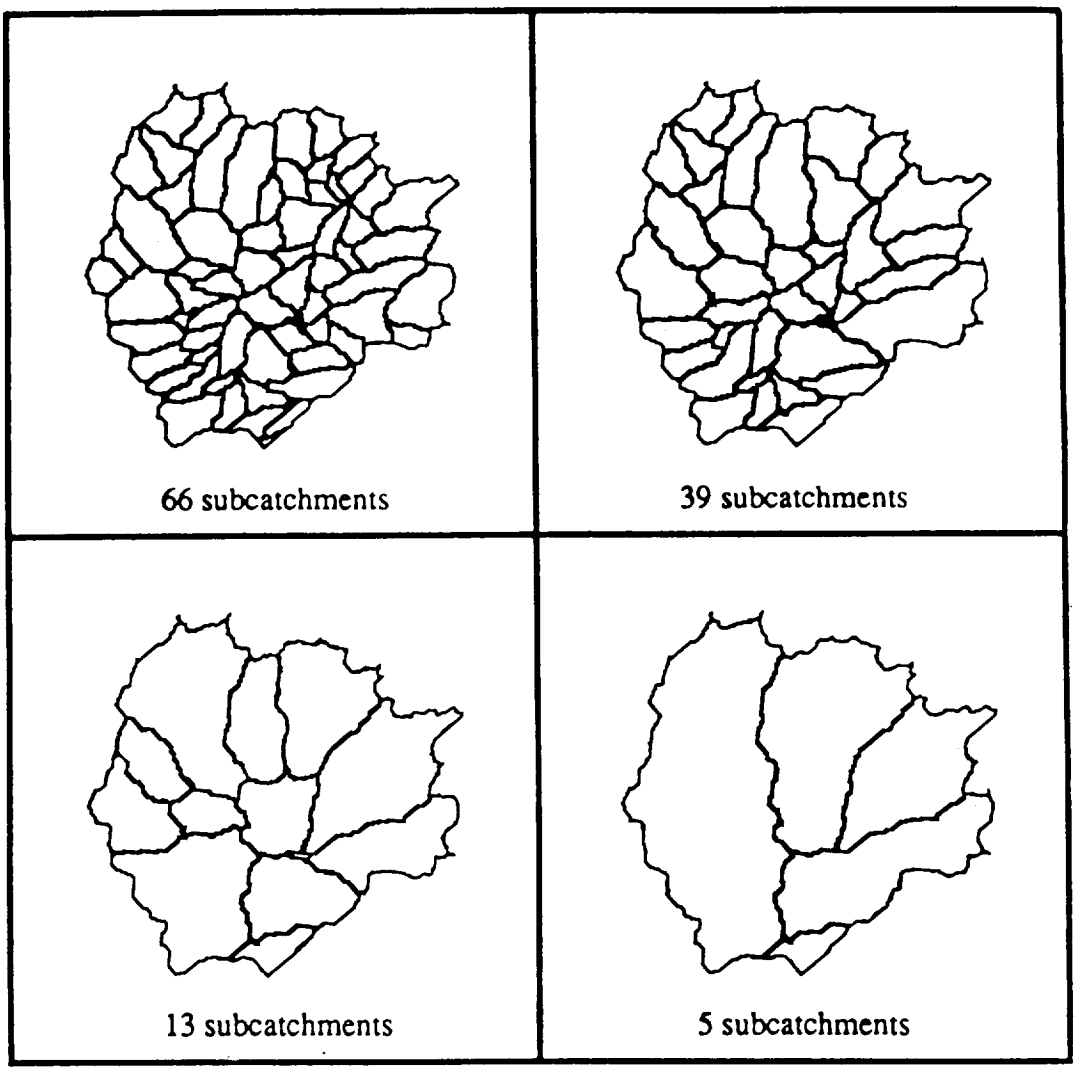

FIG. 1. Natural subcatchment divisions for Kings Creek, Kansas.

The REA is the critical scale at which implicit continuum assumptions can be used without explicit knowledge of the actual patterns of topographic, soil, or rainfall fields. It is sufficient to represent these fields by their statistical characterization.

By inspecting Figs. 2 and 3, it appears that the size of the REA is on the order of 1 km^2 (about 1000–1200 pixels, each of which are 900 m^2). The results also suggest that at larger scales it would be possible to model the responses using a simplified macroscale model based on the statistical representation of the heterogeneities in topography, soils, and hydrologic forcings (rainfall and potential evaporation). To date, only a limited range of catchments has been analyzed, all having moderate topography and located in regions with humid climates. The REA scale appears to be quite consistent at about 1–2 km^2 and to be the same scale for both runoff and evaporation processes. Clearly, additional catchments representing a broader range of climates and catchment sizes need to be analyzed before definitive statements concerning the REA scale can be made.

Using the statistical distribution of the topographic-soil index, one can determine the fraction of the catchment that will be saturated due to the local soil storage being full. These areas will generate saturation excess runoff at the rate $\bar{p}$, the mean rainfall rate. For that portion of the catchment where infiltration occurs, the local expected runoff rate at time t, m_q, can be calculated as the difference between the mean rainfall rate, $\bar{p}$, and the local expected infiltration rate, m_g. This implies that m_q and m_g are *conditioned* upon a topographic-soil index whose statistical distribution is central to the REA macroscale model. The difference be-

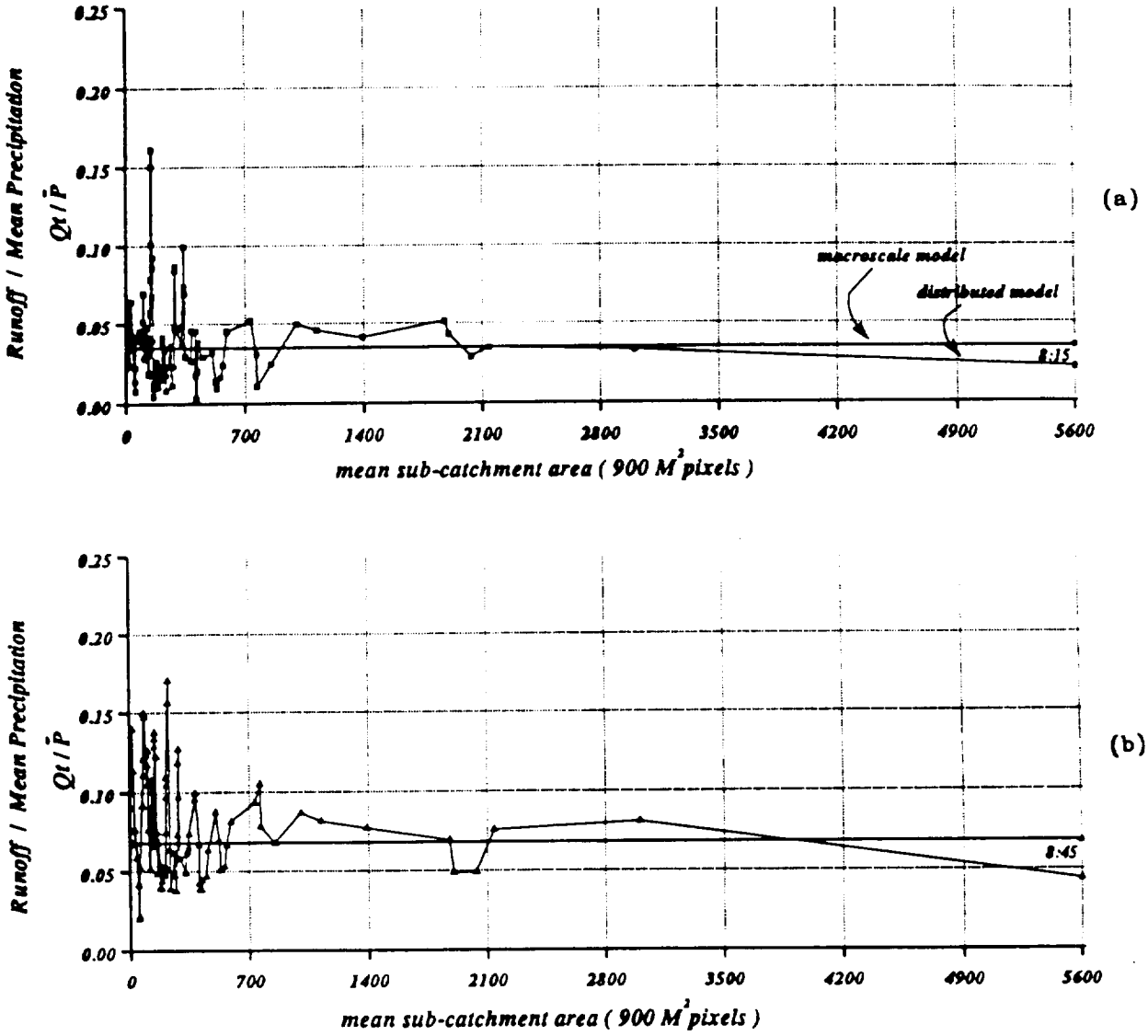

FIG. 2. Comparison of storm runoff generated from the distributed model and from the macroscale water-balance model for two time intervals on 4 August 1987: (a) 0845 LDT and (b) 0930 LDT.

tween averaged rainfall and infiltration can be expressed as

$$m_q[t|\ln(aT_e/T_i \tan\beta)] = \bar{p} - m_g[t|\ln(aT_e/T_i \tan\beta)], \quad (1)$$

where $\ln(aT_e/T_i \tan\beta)$ is the topographic-soil index for a location i in the catchment and is a function of α, the contributing area upslope to i; $\tan\beta$, the local slope angle; T_i, the soil transmissivity at i; and T_e, the catchment average of T_i. As discussed above, m_q and m_g are time-varying functions whose values at any particular time are equal for points within the catchment having the same topographic-soil index; this dependance is indicated in Eq. (1) by the |. The full development of the topographic-soil index is provided in Beven and Kirkby (1979), Beven (1986a,b), Sivapalan et al. (1987), and Wood et al. (1990). Both the local expected runoff rate and the local expected infiltration rate are (probabilistically) conditioned on the topographic-soil index, $\ln(aT_e/T_i \tan\beta)$. The runoff production from the catchment is found by integrating, usually numerically, the conditional rate over the statistical distribution of topographic-soil index. Figure 2 also gives results for the macroscale model along with the distributed model. Since the macroscale model is scale invariant, it appears as a straight line in Fig. 2.

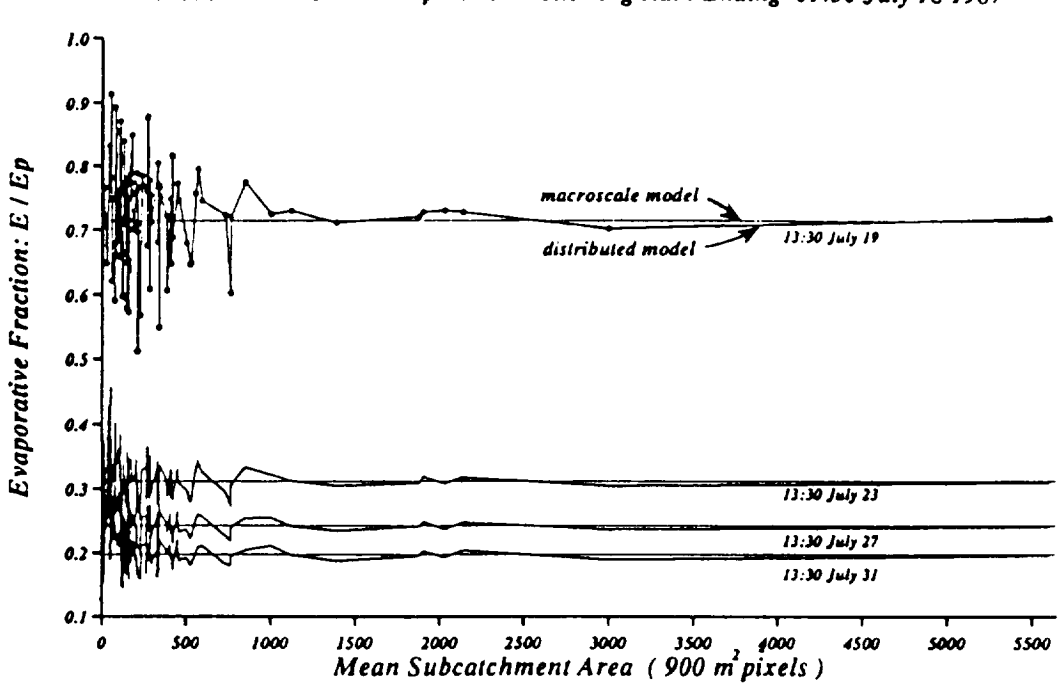

FIG. 3. Comparison of interstorm evapotranspiration from the distributed model and from the macroscale water-balance model for four times during the 18–31 July 1987 interstorm period.

In a similar way, a macroscale evaporation model is developed for interstorm periods. As stated earlier, topography plays an important role in the interstorm redistribution of soil moisture. Variations in soil properties and topography lead to variations in soil moisture and the initial conditions for the evaporation calculations. For those portions of the catchment for which the soil column can deliver water at a rate sufficient to meet the potential evapotranspiration or atmospheric demand rate E_p, the actual rate E equals E_p; otherwise, the rate will be at a lower soil-controlled rate E_s. Within the TOPMODEL framework, locations with the same value of the topographic-soil index will respond similarly, implying a macroscale model conditioned on that index. The macroscale model can be written as:

$$m_E[t|\ln(aT_e/T_i \tan\beta)] = \min\{m_{E_s}[t|\ln(aT_e/T_i \tan\beta)], \bar{E}_p(t)\}, \quad (2)$$

where m_E refers to the mean evaporation rate at locations in the catchment with the same index, m_{E_s} refers to the mean soil-controlled rate, and $\bar{E}_p$ to the spatially average potential or atmospheric demand rate. Figure 3, which compares the evaporation rates from the distributed model across the range of scales for Kings Creek, also includes the derived rates from the macroscale evaporation model. As in Figure 2, the macroscale model is scale invariant and appears as a straight line.

a. Summary on hydrological scaling

The results from the REA analysis suggest that progress has been made in understanding the transition in hydrologic responses during storm and interstorm periods as scale is increased in the presence of spatial variability. In particular, the results indicate that the macroscale models that preserve the statistical characterization of the small-scale variability in the hydrologic controls (topography and soils) can accurately represent both storm and interstorm water fluxes. The results presented here are based on a specific model applied to the FIFE study site. Good agreement between model predictions and observations have been obtained (see Famiglietti and Wood 1991b; Famiglietti et al. 1992). The model representation of soil water movement (infiltration and evapotranspiration) is highly nonlinear, so we are confident that the scaling of these processes across a range of heterogeneous hill slopes and soils, which leads to the macroscale model, is reasonable. Nonetheless, the results presented here need to be expanded over a wider range of catchment and climatic scales to further verify the concepts of the representative elementary area.

3. Spatial and temporal scaling using a biospheric transfer model

The development of models that have biospheric–atmospheric interactions is motivated by recent ad-

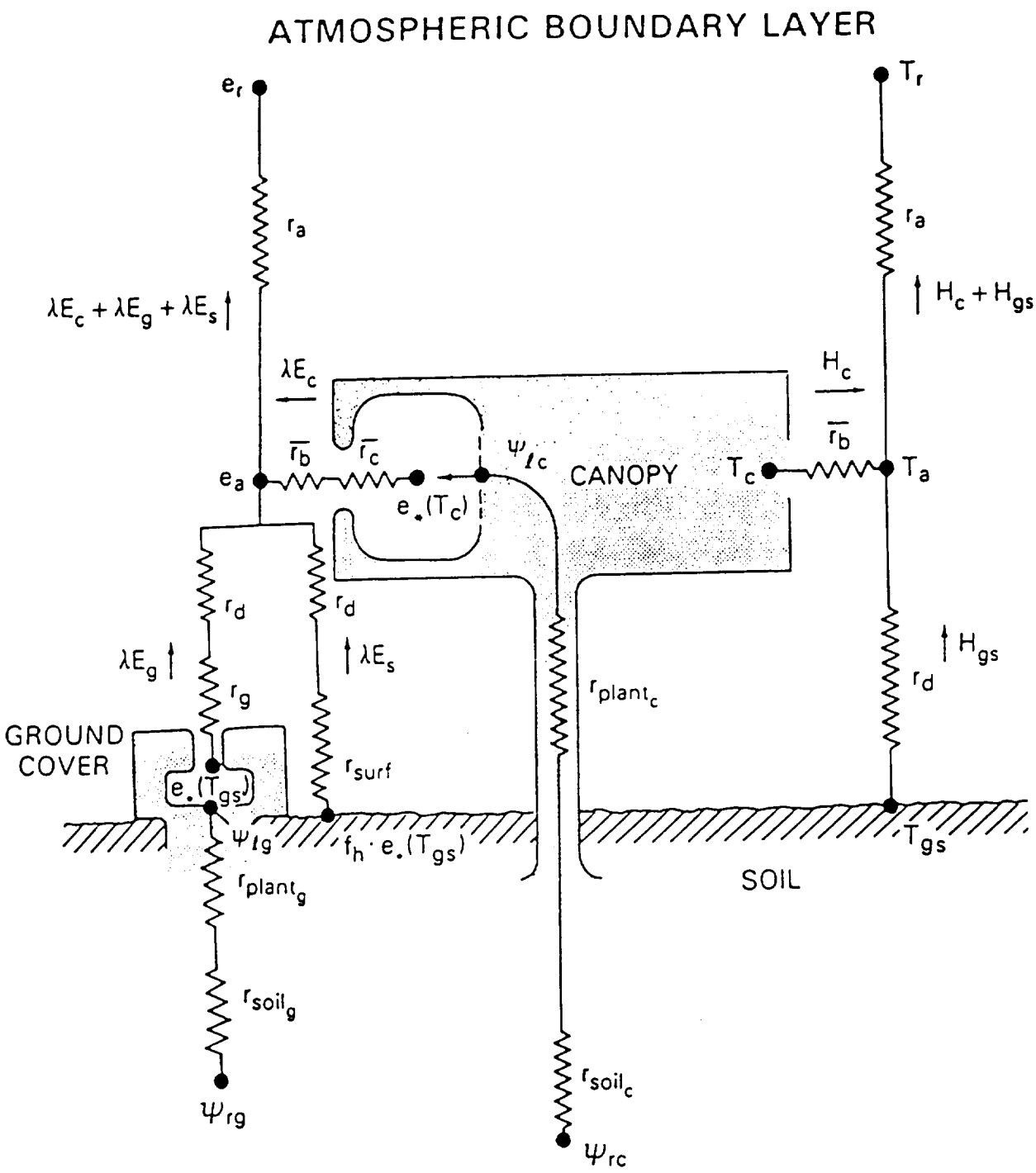

FIG. 4. Framework of the Simple Biosphere Model (SiB). The transfer pathways for the latent and sensible heat fluxes are shown on the left- and right-hand sides of the diagram, respectively. The treatment of radiation and intercepted water has been omitted for clarity. Symbols are as defined in Sellers et al. (1986) [from Sellers et al. (1986)].

vances in plant physiology, micrometerology, and hydrology and our ability to integrate all of these small-scale physical processes that control biosphere–atmosphere interactions. Two of the most widely used models are the Simple Biosphere Model (SiB) (Sellers et al. 1986) and the Biosphere–Atmosphere Transfer

Scheme (BATS) Model (Dickinson et al. 1986). The models attempt to separate the vegetation canopy from the soil surface and to represent the energy and water fluxes from the canopy in detail. Thus, the resulting models have a complex representation of the soil–vegetation–atmosphere system, which gives them the appearance of having tremendous vertical resolution and structure. On the horizontal scale, these models usually assume homogeneous conditions; that is, the parameters for the soil and vegetation properties are assumed constant within a GCM grid, thus ignoring spatial heterogeneity. This has lead to describing these models as "big-leaf" or "constant-canopy" models.

Figure 4 gives a schematic for the parameterization of SiB. As described by Sellers et al. (1986), the parameterization consists of a two-layer vegetation canopy whose elements and roots are assumed to extend uniformly throughout the GCM grid. From the prescribed physical and physiological properties of the vegetation and soil, the model calculates (i) the reflection, transmission, absorption, and emission of direct and diffuse radiation in the visible, near-infrared, and thermal wavelength intervals; (ii) the interception of rainfall and its evaporation from leaf surfaces; (iii) the infiltration, drainage, and storage of residual rainfall in the soil; (iv) the control of photosynthetically active radiation and the soil-moisture potential, inter alia, over the stomatal functioning and, thereby, over the return transfer of the soil moisture to the atmosphere through the root–stem–leaf system of the vegetation; and (v) the aerodynamic transfer of water vapor, sensible heat, and momentum from the vegetation and the soil to a reference level within the atmospheric boundary layer. The model originally had seven prog-

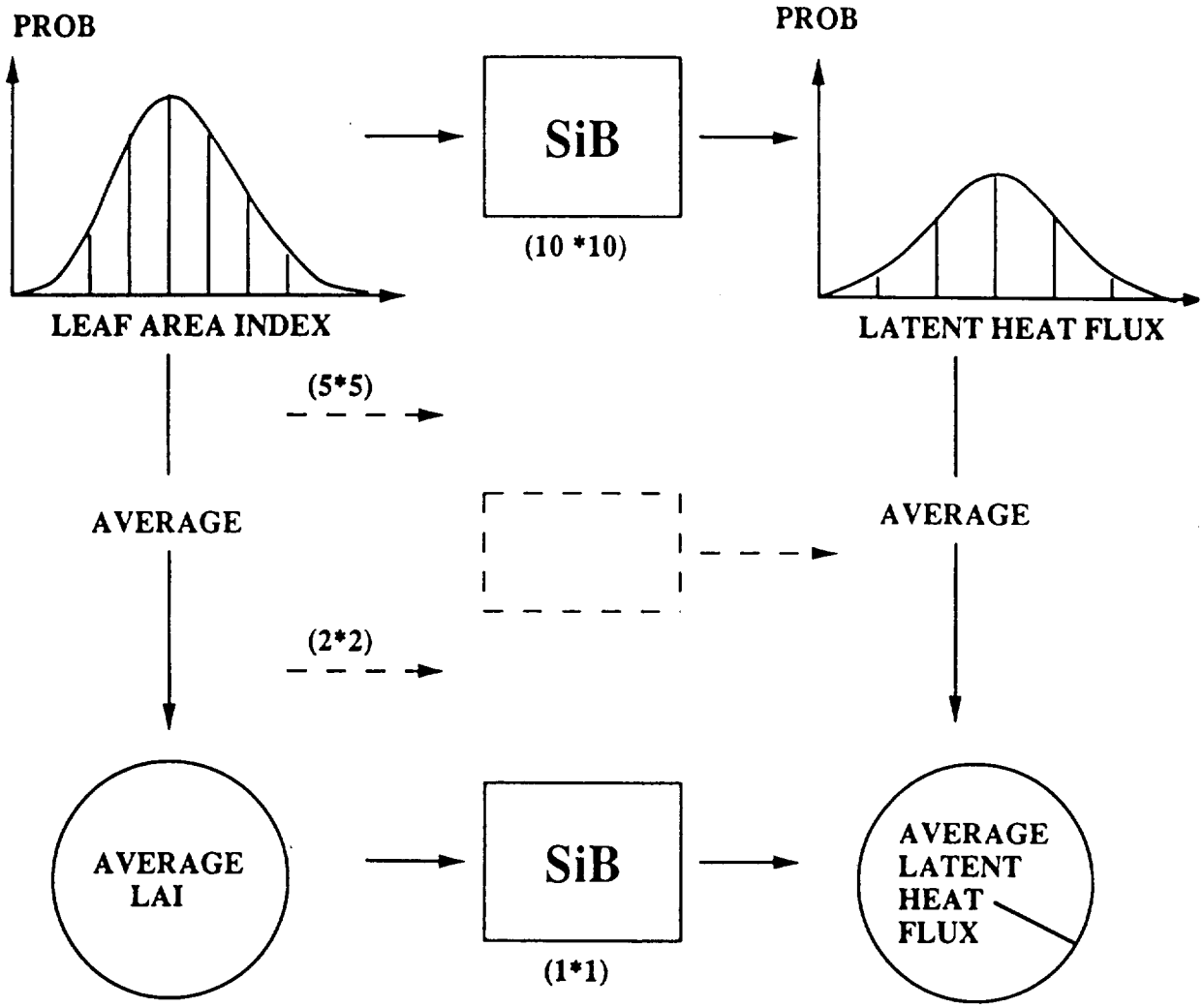

FIG. 5. Schematic diagram for the biosphere–atmosphere scaling experiment. The spatially variable inputs and derived outputs are shown on the left- and right-hand sides of the diagram, respectively. Low aggregation to high aggregation of inputs are shown from top to bottom, respectively.

nostic physical-state variables: two temperatures (a canopy temperature and ground temperature), two interception water storages (one for the canopy and one for the ground cover), and three soil-moisture storages of which two are for the two classes of vegetation and one for the soil recharge layer (Sellers et al. 1986). Recently an eighth prognostic variable was added for following the deep-soil temperature. SiB has been tested in a climate model by Sato et al. (1989) in which SiB is compared to the bucket model land-surface parameterization.

To investigate the effect of subgrid variability on the scaling of latent heat fluxes as derived from SiB, the following numerical experiment was carried out. A gridded domain was defined in which the vegetation density (as described by its leaf-area index), precipitation, and initial soil wetness were allowed to be spatially variable. At the finest scale, a 10 × 10 grid, the scale of the grid (L_G) divided by the scale of the domain (L_D) is 0.1. The average parameters for the domain were based on a calibration of SiB for data collected in Amazonia and reported in Sellers et al. (1989). The data consisted of 43 days of meteorological observations at a 1-h time interval.

The scaling analysis is presented schematically in Fig. 5. While all three variables were allowed to vary, Fig. 5 is simplified to show only the leaf-area index. Within the 10 × 10 domain, the random field for the spatially variable parameter is generated from a normal distribution with coefficient of variation of 0.25. For the results presented here, spatial correlation was not included. SiB can then be run for each grid. This structure ignores any horizontal interaction among grids. From the 10 × 10 SiB runs, the probability distribution for the latent heat flux can be constructed.

Spatial scaling is investigated by averaging the inputs (leaf-area index, initial soil wetness, and rainfall) from adjacent grids. The levels considered were aggregated domains having L_G/L_D ratios of 0.2 (a 5 × 5 gridded domain), L_G/L_D = 0.5, and L_G/L_D = 1.0; the latter case being the spatially average, homogeneous case. Comparisons can be made between the derived latent heat fluxes from the aggregated inputs (the left-hand side of Fig. 5) and the averaging of the 10 × 10 (detailed) domain. If the inputs operate within SiB in a highly nonlinear manner, then the two averaging schemes would lead to a significant difference. The spatially averaged inputs would be biased compared to the spatially distributed parameter case.

Figure 6 shows the 43-day mean latent heat flux across the range of aggregations. In Fig. 6a, only the leaf-area index is varied, while all three inputs are varied in 6b. Figure 7 presents a scatterplot comparison between the hourly latent heat fluxes averaged over the 10 × 10 grid domain and the fluxes derived from the averaged inputs.

Three observations are in order. At the finest scale,

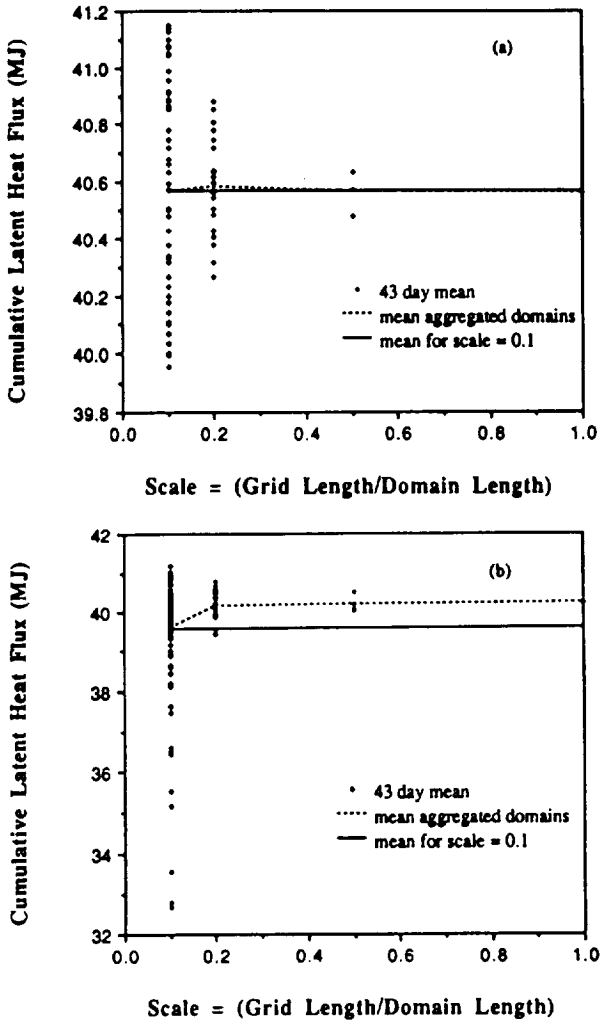

FIG. 6. Comparisons of latent heat fluxes, derived using SiB, over a range of domain scales: (a) leaf-area index (LAI) spatially variable and (b) LAI, rainfall, and initial soil moisture variable. The fluxes were modeled using data from Sellers et al. (1989) and are shown as cumulative fluxes over 43 days.

L_G/L_D = 0.1, there is substantial variability across the grids compared to the higher levels of aggregation. Nonetheless, the absolute range of variability is very small, given what we feel is a realistic range for the input variability. For the hourly data presented in Fig. 7, the range of variability due to lumping is extremely small when compared to the range of calculated latent heat fluxes over the observation period. Second, a small bias is observed for the case where all three parameters are varying. This bias is due to the variability in initial soil wetness, the input parameter that appears to have the greatest influence on the average latent heat flux. Finally, we believe that the REA concept appears to hold for these experiments and is about L_G/L_D = 0.2. In fact, subsequent analysis shows that the REA is re-

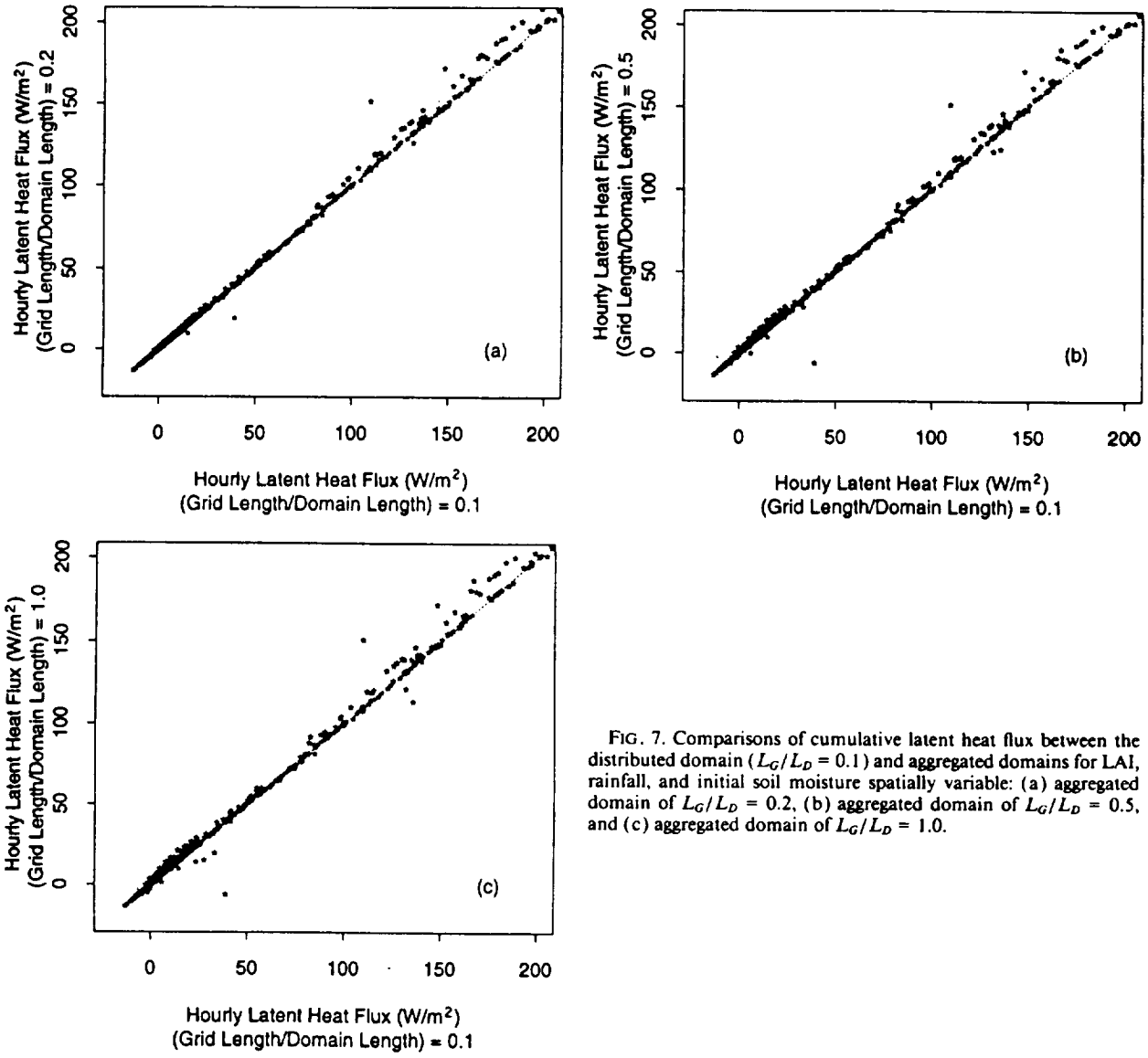

FIG. 7. Comparisons of cumulative latent heat flux between the distributed domain ($L_G/L_D = 0.1$) and aggregated domains for LAI, rainfall, and initial soil moisture spatially variable: (a) aggregated domain of $L_G/L_D = 0.2$, (b) aggregated domain of $L_G/L_D = 0.5$, and (c) aggregated domain of $L_G/L_D = 1.0$.

lated to the correlation length of the subgrid heterogeneities. Increased spatial correlation in the parameters leads to larger REAs. Further field studies are needed to establish realistic correlation lengths for these parameters.

The results presented in Figs. 6 and 7 used rainfall data at a temporal resolution of 1 h. The effect of temporal averaging is shown in Fig. 8 with a scatterplot of the latent heat fluxes, as computed using hourly rainfall, and temporally averaged at either 2 h or 24 h. The effect is a strong bias and variability between the two aggregation schemes. This demonstrates that temporal averaging of the rainfall input (which results in a reduction of rainfall intensity) has a significant impact on the surface water balance (runoff, soil moisture) and subsequent latent heat fluxes.

4. Scaling TM-derived surface variables

The earlier two numerical experiments were concerned with scaling hydrologic and energy fluxes using a water-balance and land-surface biospheric model. In this third experiment, high-resolution thermatic mapper (TM) satellite data were used to derive the normalized difference vegetation index (NDVI), latent heat, and sensible heat fluxes for the 15 August 1987 overpass. The resolution of TM is 30 m for bands 1 through 5, and 120 m for the thermal band that was used for the sensible and latent heat flux calculations.

The scaling question investigated here is whether averaging the TM bands prior to calculating NDVI or the fluxes provides the same derived quantities as would be found by calculating the quantities at the TM res-

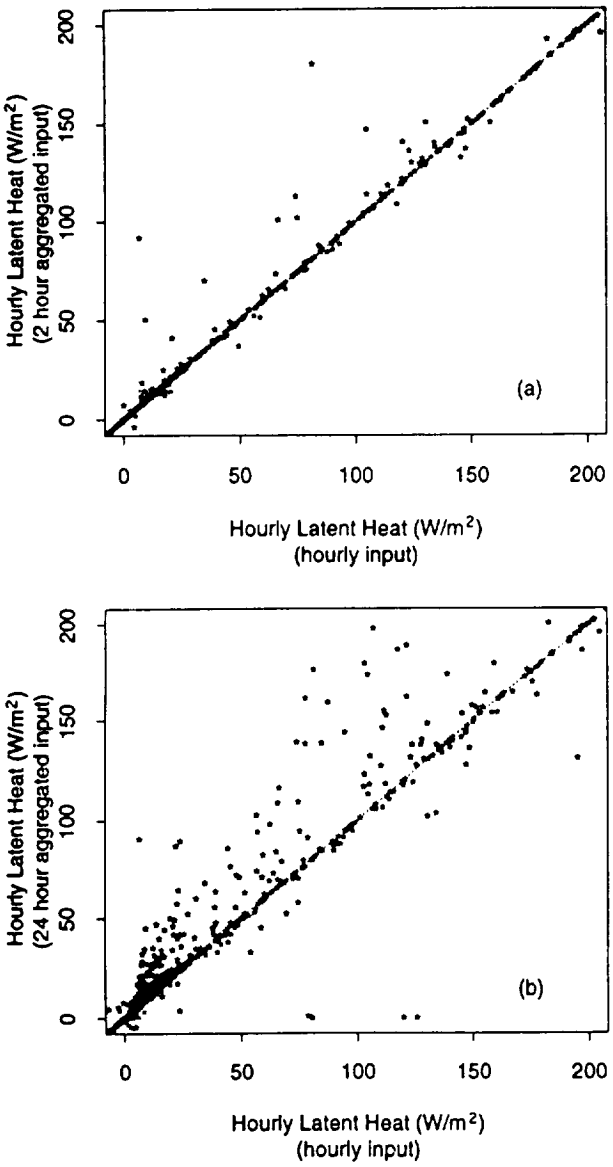

FIG. 8. Comparisons of cumulative latent heat flux between hourly rainfall and temporally averaged rainfall: (a) rainfall aggregated over 2 h, (b) rainfall aggregated over 24 h. The variables LAI, rainfall, and initial soil moisture are spatially constant.

olution and averaging. The equivalence of the two approaches depends on the degree of nonlinearity represented by functions that relate NDVI and fluxes to TM data.

a. *Scaling NDVI*

The following procedure was followed: the normalized difference vegetation index (NDVI) was calculated at the 30-m TM resolution using

$$\text{NDVI} = \frac{(B_4 - B_3)}{(B_4 + B_3),} \tag{3}$$

where B_3 represents band 3 (0.63–0.69 μm), and B_4 represents band 4 (0.76–0.90 μm). The first is often referred to as the red and the latter the near-infrared band. The NDVI image corresponding to a TM scene acquired over the FIFE area for 15 August 1987 is given in Fig. 9. The TM scene was fully calibrated before the calculations were carried out.

At aggregated scales, two procedures were followed. One was to spatially aggregate the TM bands and then use Eq. (3), while the second procedure is to spatially aggregate the NDVI based on the 30-m TM data. Figure 10 shows the aggregated NDVI, using the second procedure, for aggregation levels of 300 × 300 m, 750 × 750 m, and 1500 × 1500 m. A resolution equivalent to AVHRR would lie between the last two cases. Comparisons between the two aggregation procedures can best be shown by a scatterplot between the aggregated 30-m-based NDVI and the NDVI derived using aggregated TM bands; these comparisons are presented in Fig. 11.

One striking observation arises from comparing Figs. 9 through 11. Notice that the detailed structure observable in Fig. 9 is lost in Fig. 10, and yet the averaged NDVI from the two aggregation schemes are essentially the same as can be seen in scatterplot of Fig. 11. Figure 11 does show that a small bias exists between the two aggregation procedures but its magnitude is rather insignificant. These results indicate that NDVI calculated from spatially averaged TM (or lower-resolution AVHRR data) will be equivalent to the NDVI scaled up from the full-resolution image.

b. *Scaling up TM-derived latent and sensible heat fluxes*

Latent and sensible heat fluxes over the FIFE area during 15 August 1987 were estimated using the thermatic mapper (TM) thermal band (10.45–12.5 μm, with a resolution of 120 m) aboard Landsat 5 and a procedure presented by Holwill and Stewart (1992). The Landsat overflight was at 1632:50 UTC and the fluxes estimated for 1600–1700 UTC. The relationship between surface radiometric temperature and emittance is given for the Landsat thermal channel by Markham and Barker (1986) as

$$T_s = K_2/\ln(K_1/R_s + 1), \tag{4}$$

where R_s is surface emittance in (W m^{-2} Sr^{-1} μm^{-1}), K_1 and K_2 are coefficients that, after atmospheric calibration for 15 August 1987, have values of K_1 = 607.76 W m^{-2} Sr^{-1} μm^{-1} and K_2 = 1260.56 K (Goetz 1991, personal communication).

The procedure developed by Stewart and Holwill (1992) combines the spatial TM thermal data with data

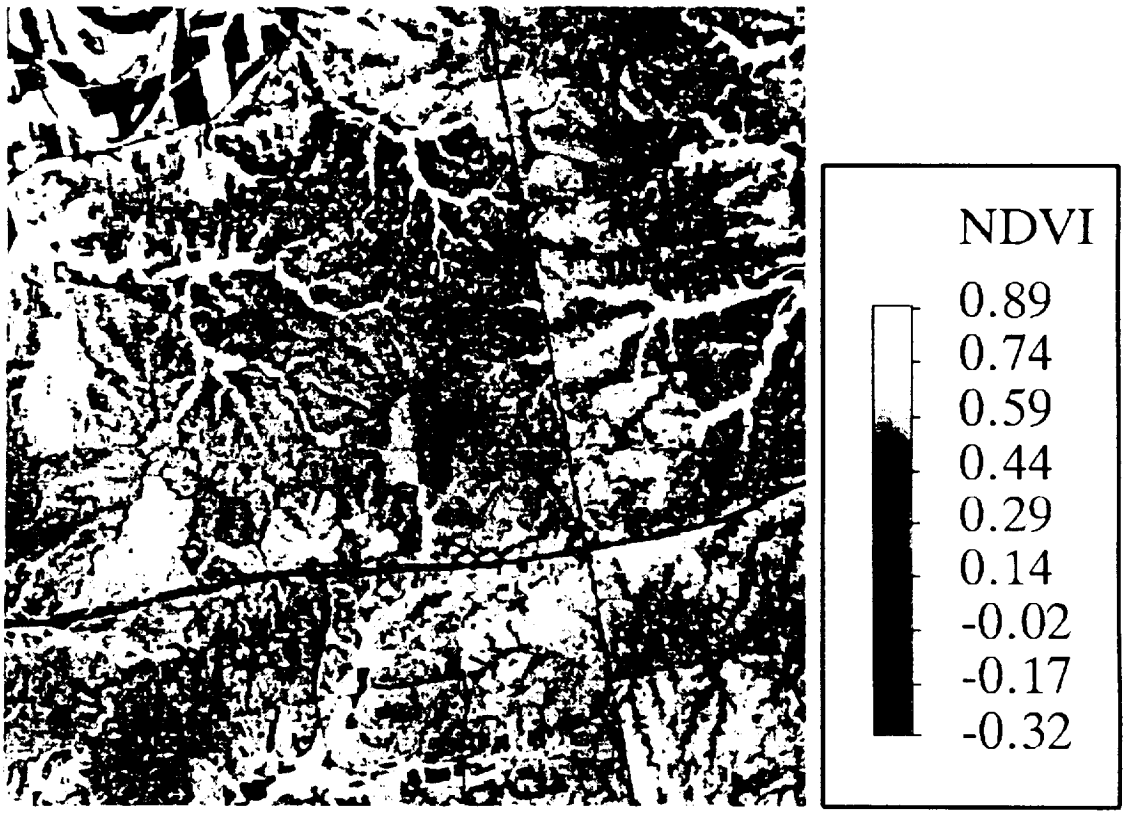

FIG. 9. Normalized vegetation index (NDVI) derived for part of the FIFE area from the 15 August 1987 overpass. Resolution is 30 m.

at the surface flux measurement stations. A principal aim of the procedure is to extend the observations of sensible and latent heat fluxes spatially from the surface flux stations by combining the TM satellite thermal data with the station data. A TM-derived estimate of surface temperature was estimated for the locations within the FIFE area, corresponding to the different surface flux stations. In the 15 km × 15 km FIFE area, there were 19 flux stations that were used in this analysis (see Sellers et al. 1989; Hall et al. 1992). The TM surface temperature estimates and the station sensible heat measurements can be combined to provide a transfer coefficient of the following form for the TM data:

$$g_{st} = \frac{H_{st}}{\rho C_p (T_s - T_a)}, \tag{5}$$

where ρ is air density (1.19 kg m^{-3}), C_p is specific heat for air at constant pressure (at 25°C, 1005 J kg K^{-1}), H_{st} is the observed station sensible heat, T_a is the observed station air temperature, and T_s the TM-derived surface temperature. Equation (5) is constructed so that g_{st} is equivalent to the inverse of the aerodynamic resistance term, assuming that all the variables on the right-hand side of (5) are measured accurately. The variable g_{st} can be interpreted as an "effective" coefficient that represents not only the aerodynamic resistance but also the effect of errors in T_s and measurement errors in H_{st}. The latter two may be quite large (Smith et al. 1992; Hall et al. 1992). In the analysis by Hall et al. (1992), they found that the TM-derived surface temperatures are high by about 3°C, which is sufficient to result in large errors in computed sensible heat fluxes.

The 19 g_{st} factors were interpolated across the 15 km × 15 km FIFE area through geostatistical kriging. Similarly, T_a was also interpolated across the site. Using this field and the TM-derived surface temperature (both at a 120-m resolution), the sensible heat flux can be estimated over the domain by inverting (5). This allowed the estimation of the sensible heat across the FIFE area in a manner that is consistent with surface flux station observations. This field is referred to herein as H_d.

The TM-derived latent heat flux was estimated assuming that the sum of the averaged latent and sensible heat fluxes for the station data and the TM-derived fluxes would be equal.

While the above procedure could be refined, the resulting spatial patterns of sensible and latent heat fluxes appear to reflect quite accurately the underlying features within the FIFE area. Figures 12 and 13 give the

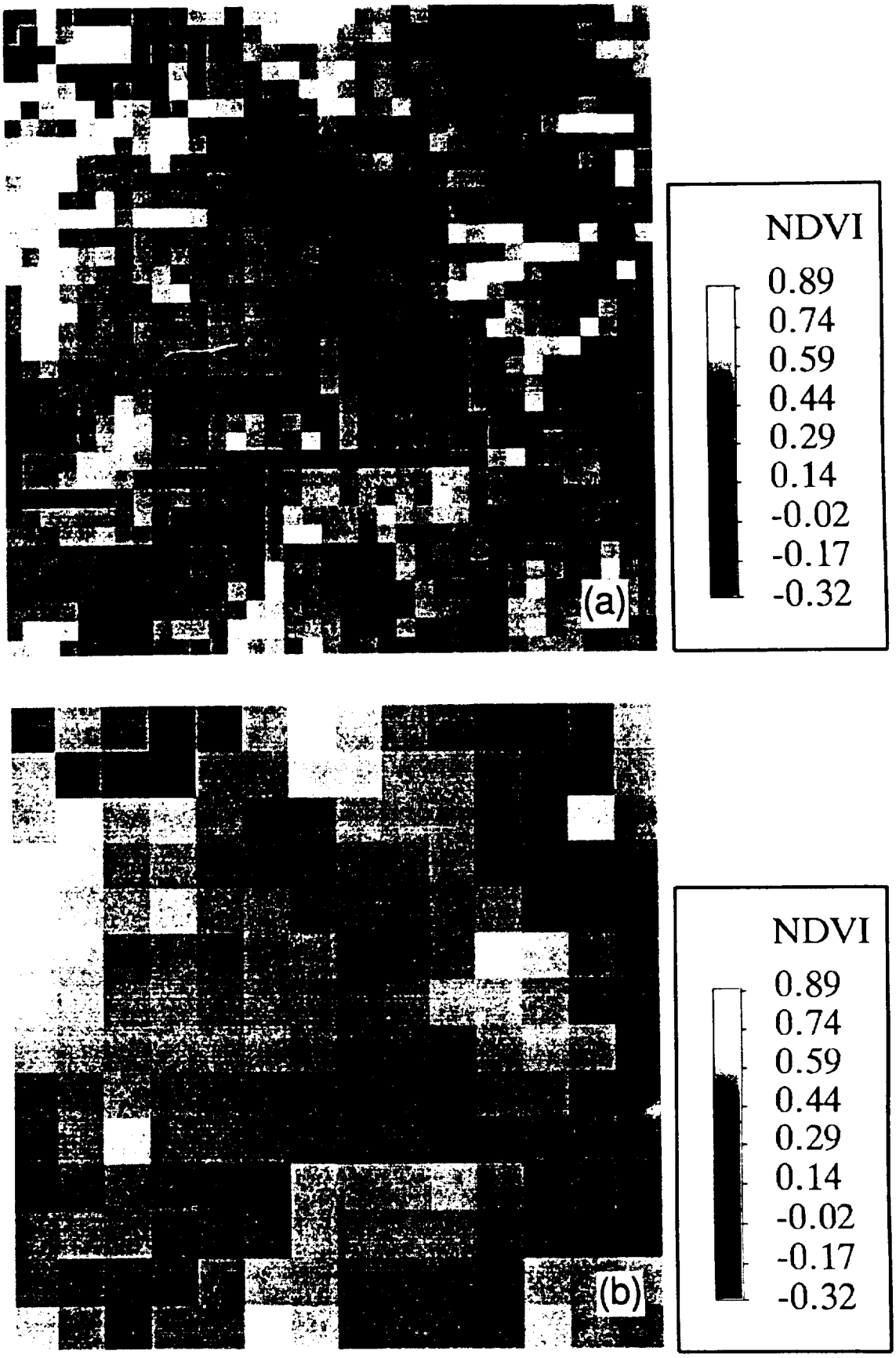

FIG. 10. Aggregated normalized vegetation index (NDVI) for part of the FIFE area for 15 August 1987. The images were derived using data from Fig. 9. Levels of aggregation into each are (a) 300 m × 300 m, (b) 750 m × 750 m, and (c) 1500 m × 1500 m.

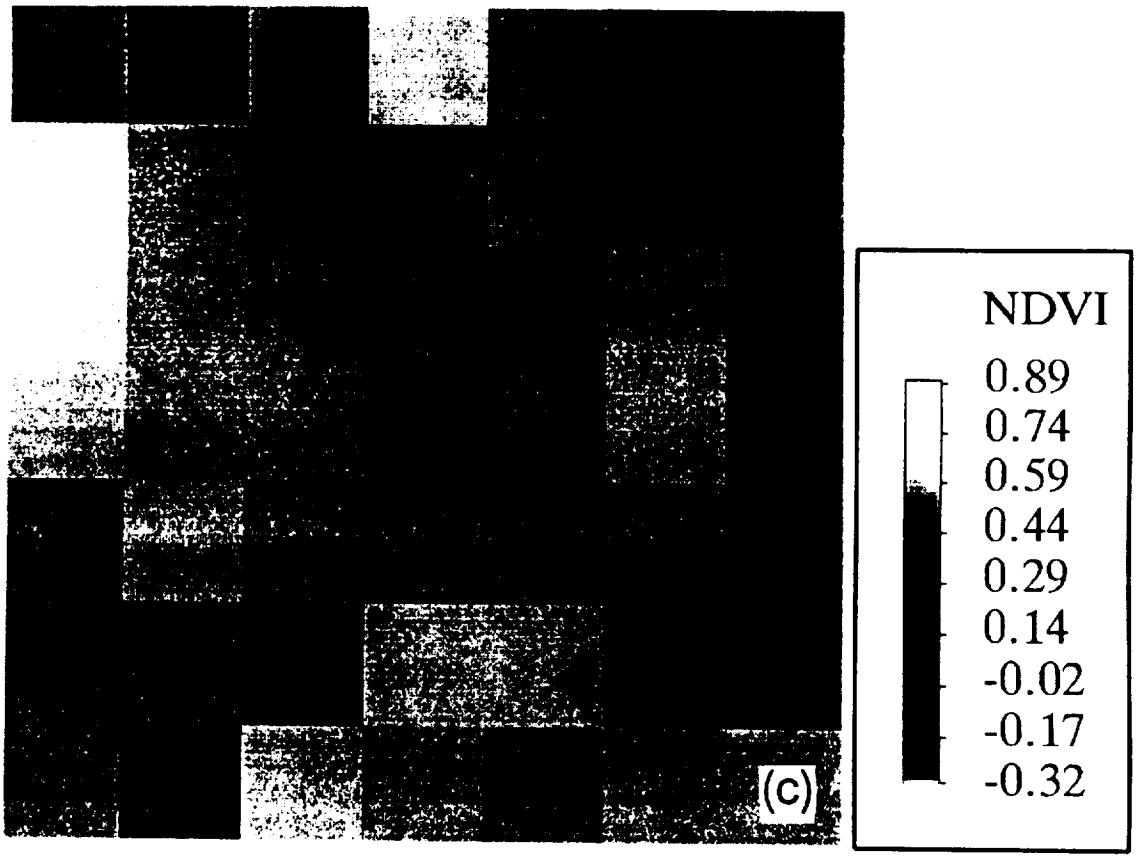

FIG. 10. (*Continued*)

derived images. Notice that the heavy vegetation in the southwest portion of the area (lower left) show up as having low sensible heat and high latent heat fluxes, as one would expect. Also, the interstate highway that crosses the area (east–west) can also be seen quite clearly. Some effect of the kriging can be seen as striping within the image.

The estimates in Figs. 12 and 13 are based on the TM surface radiances at a 120-m resolution. The images were also calculated using radiances that were first aggregated five times (into 600 m × 600 m pixels) and aggregated 25 times (into 3000 m × 3000 m pixels). Using these aggregated resolutions, the sensible and latent heat fluxes were calculated over the FIFE area in the same manner as for the 120-m data. Figures 14 and 15 present the aggregated images for sensible and latent heat fluxes.

Scatter plots comparing the aggregated fluxes (using the 120-m thermal data) and the derived fluxes, based on aggregated radiances, are presented in Figs. 16 and 17 for the case when the level of aggregation was 25 times. These figures show that the scaling of thermal radiances prior to estimating scaled sensible and latent heat fluxes results in the same derived fluxes as obtained from scaling up small-scale derived fluxes; that is, the scaling of sensible and latent heat fluxes is linear, at least for the 15 August 1987 FIFE TM data. Figures 18 and 19 show the variability across FIFE, with different levels of aggregation for sensible and latent heat fluxes. Also shown are the means derived from the detailed image (solid line) but based on the aggregated image (dashed line). For both images (and especially the latent heat fluxes shown in Fig. 19), it is essentially impossible to differentiate these two means, indicating that the scaling is linear.

5. Results and discussion

The purpose of this paper is to review recent results for the scaling of water and energy fluxes from the land component of the climate system. Three sets of experiments were presented. The first was the hydrologic response at the scale of a catchment (but could easily be at a GCM grid scale), in which spatial variability in topography, soils, and hydrologic inputs (rainfall, in this case) resulted in spatially variable responses.

The second experiment was the application of SiB to a spatially heterogeneous domain based on data from Amazonia. Here, the experiments studied the impacts of variability in vegetation density (through the leaf-area index), initial soil wetness, and rainfall (both spa-

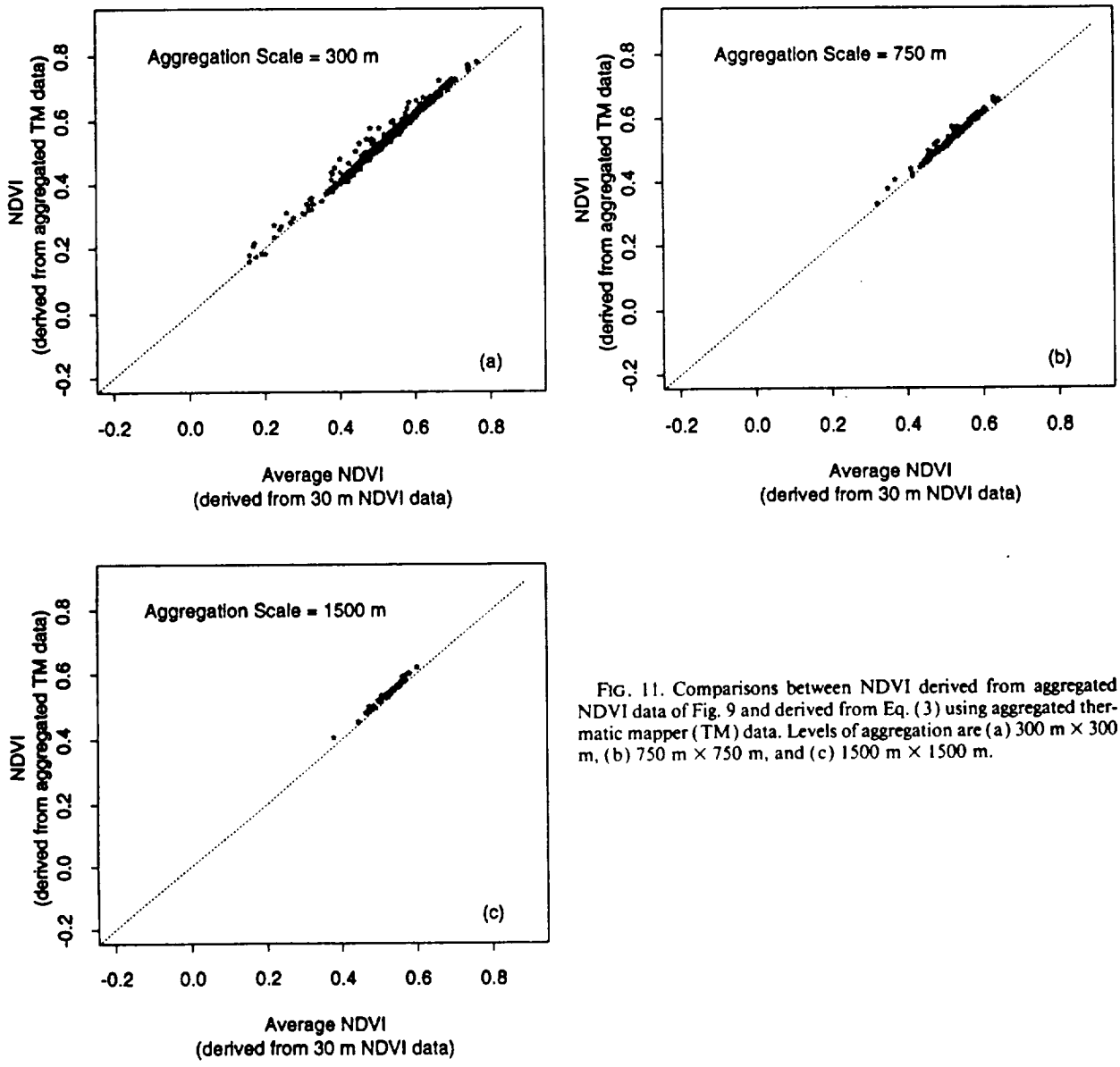

FIG. 11. Comparisons between NDVI derived from aggregated NDVI data of Fig. 9 and derived from Eq. (3) using aggregated thermatic mapper (TM) data. Levels of aggregation are (a) 300 m × 300 m, (b) 750 m × 750 m, and (c) 1500 m × 1500 m.

tially and temporally) on the derived latent heat flux over a 43-day observation period.

The third set of experiments studied the scaling in the normalized vegetation index (NDVI) and sensible and latent heat fluxes as derived from a thermatic mapper (TM) overpass of the FIFE area on 15 August 1987. Variations in surface conditions due to vegetation characteristics, as well as topography and soils, lead to significant variations in the TM-derived variables, as is shown in the presented images.

The major result from the three sets of experiments is that the scaled fields are equivalent to the fields derived from scaled inputs and parameters. The implication of this result is that the fluxes and land characteristics essentially scale linearly. More importantly, these results appear to suggest that "equivalent" parameters can be used in scaled models (or macroscale models) for the calculation of spatially averaged quantities as long as the equivalent parameters reflect the statistical characteristics of the subscale variability. The one exception to this result was the temporal averaging of rainfall in the SiB experiment. In this case, the temporally averaged latent heat fluxes were significantly different from the latent heat fluxes derived from the temporally averaged rainfall. This implies that the latent heat scales nonlinearly with respect the rainfall rates.

These results must be balanced with the knowledge that the experiments presented were neither exhaustive nor complete. The modeling results with SiB did not

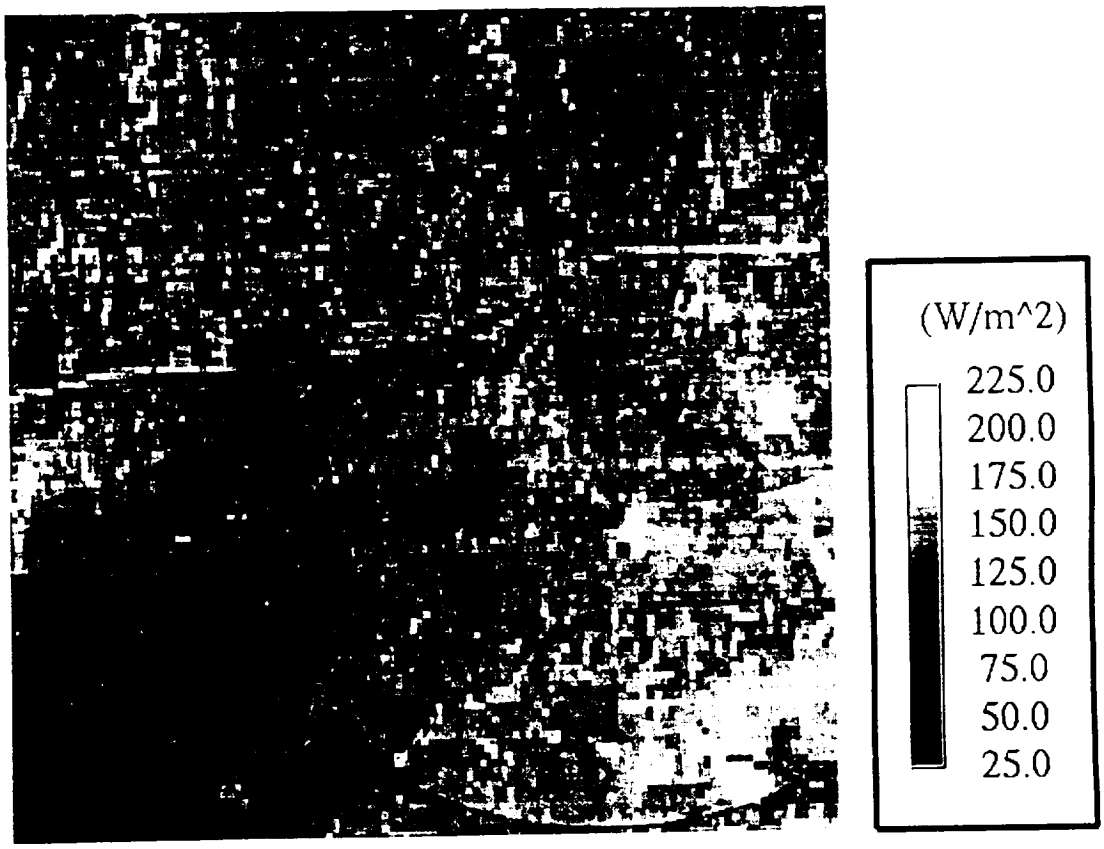

FIG. 12. Sensible heat flux for the FIFE area. The data are averaged over 15 August 1987 and are derived from the thermatic mapper (TM) overpass. Resolution is 120 m.

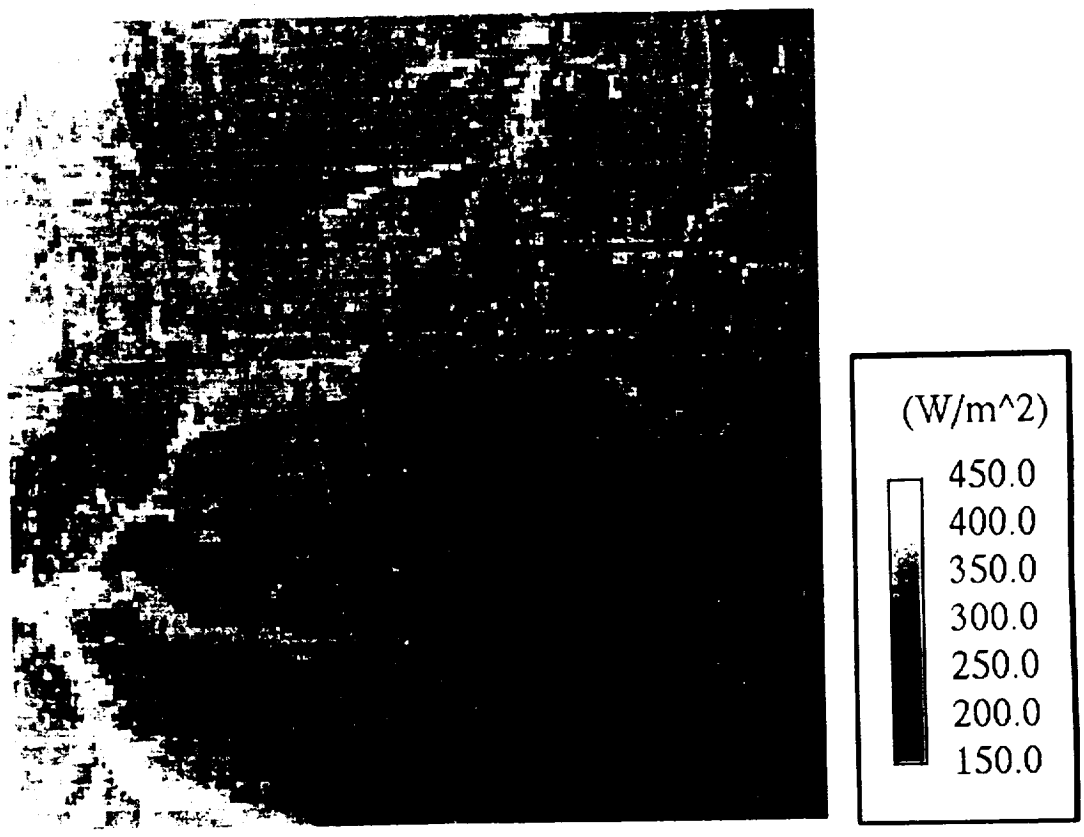

FIG. 13. Latent heat flux for the FIFE area. The data are averaged over 15 August 1987 and are derived from the thermatic mapper (TM) overpass. Resolution is 120 m.

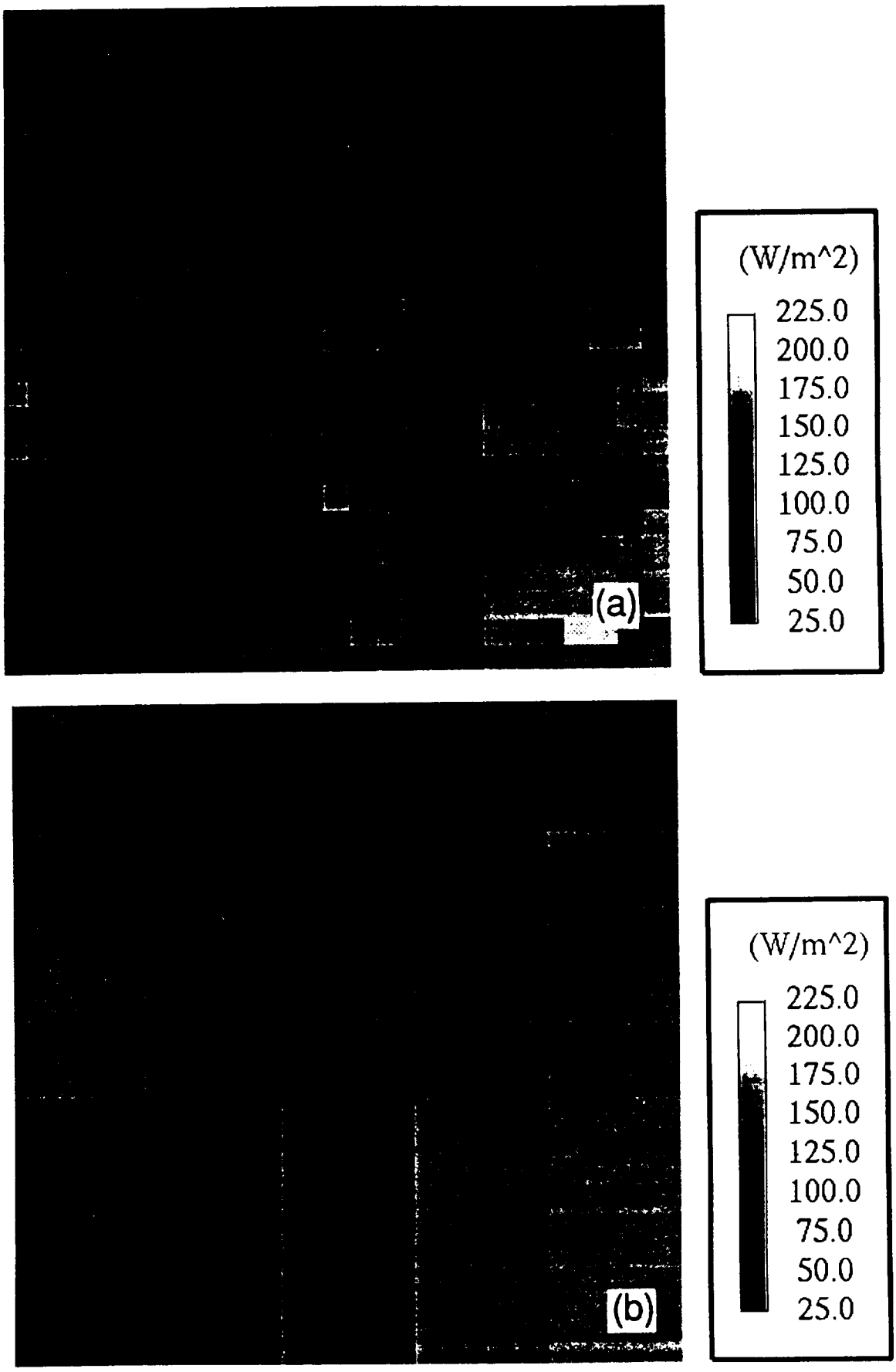

FIG. 14. Aggregated sensible heat flux for the FIFE area using data from Fig. 12. Levels of aggregation are (a) 600 m × 600 m and (b) 3000 m × 3000 m.

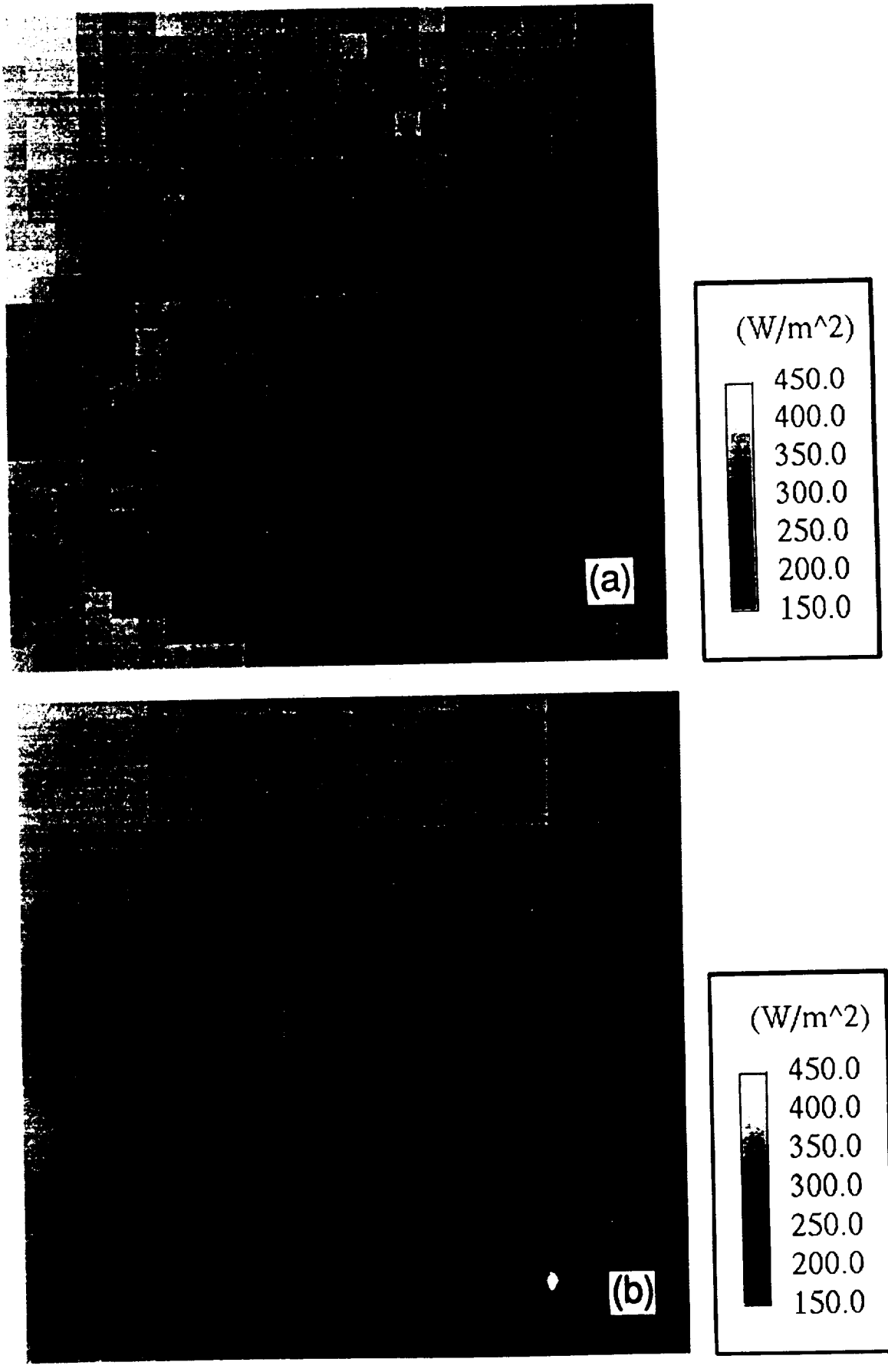

FIG. 15. Aggregated latent heat flux for the FIFE area using the data from Fig. 13. Levels of aggregation are (a) 600 m × 600 m and (b) 3000 m × 3000 m.

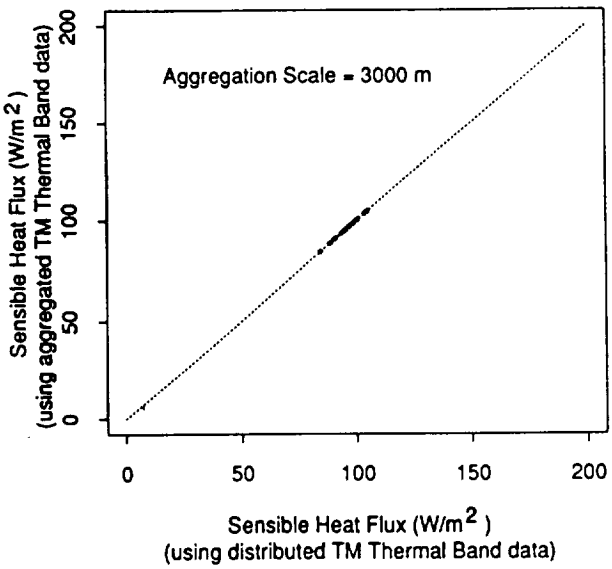

FIG. 16. Comparisons between sensible heat flux derived from aggregated sensible heat flux data of Fig. 12 and derived from aggregated thermatic mapper (TM) thermal-band radiances at an aggregation level of 3000 m × 3000 m.

include an interactive boundary layer whose effects can lead to nonlinearities under specific heterogeneities (Avissar and Pielke 1989). The satellite experiments represented a particular condition in which the range of temperatures was reasonably small, resulting in effectively linear models that transfer radiances to fluxes. Whether such ranges are typical of natural systems is

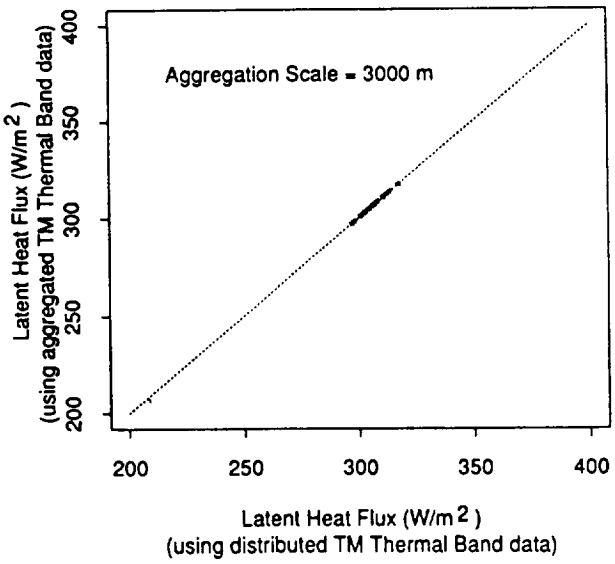

FIG. 17. Comparisons between latent heat flux derived from aggregated latent heat flux data of Fig. 13 and derived from aggregated thermatic mapper (TM) thermal-band radiances at an aggregation level of 3000 m × 3000 m.

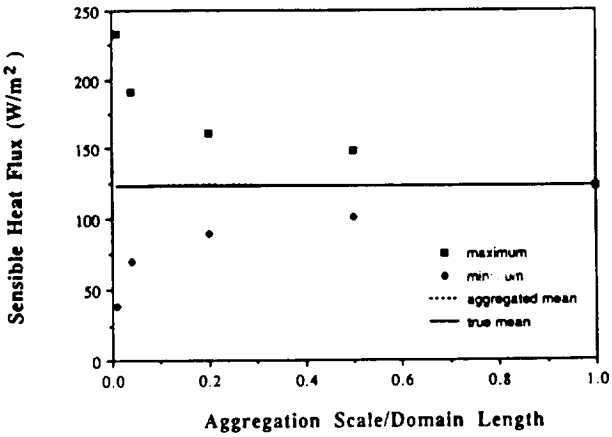

FIG. 18. Effect of aggregation on the variability of sensible heat across the FIFE domain for the 15 August 1987 TM overpass.

unknown until a greater number of analyses are done.

In the Introduction it was suggested that there were two current thoughts concerning subgrid variability: (i) that subgrid processes have a significant, nonlinear effect on large-scale processes that prevents simple scaling, and (ii) effective parameters within an appropriate macroscale model can represent large climatic fluxes. This basic scaling question is still unresolved, but hopefully the work presented here has provided some insight into these issues.

In the hydrologic-response experiment, the concept of the representative elementary area (REA) (Wood et al. 1988) was used to find the scale in which the macroscale model is a valid model for the scaled process. The results of the experiments carried out here suggest that the REA concept has wide applicability for a range of climate problems, and that it appears that the REA will be on the order of a few (1.5 to 3)

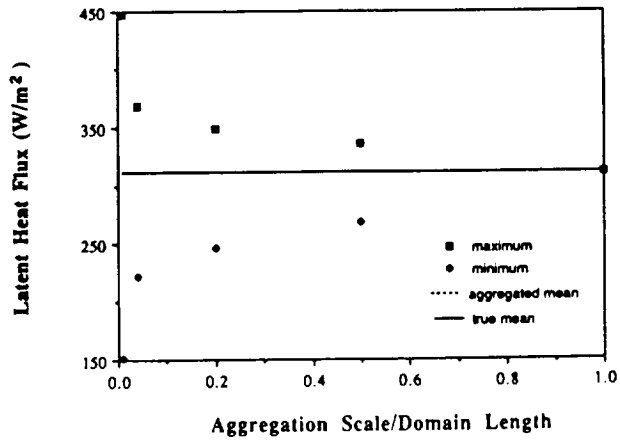

FIG. 19. Effect of aggregation on the variability of latent heat across the FIFE domain for the 15 August 1987 TM overpass.

correlation lengths of the dominant heterogeneity. At scales larger than the REA scale, there has been enough "sampling" of the heterogeneities that the average response is well represented by a macroscale model with average parameters.

It is hoped that the experiments presented in this paper motivate related research, possibly with more complex land–atmospheric models or through a wider range of satellite data, that can help resolve the basic issue concerning scaling in natural systems. What must be determined are the scaling properties for reasonably sized domains in natural systems, where the range of variability (in vegetation, rainfall, radiance, topography, soils, etc.) is reflective of these natural systems. The results in this paper provide one perspective.

Acknowledgments. The research presented here was supported in part by the National Aeronautics and Space Administration (NASA) through Grants NAGW-1392 and NAG-899; this support is gratefully acknowledged. The authors also wish to thank Jay Famiglietti who helped develop the water-balance model for Kings Creek and Dom Thongs for helping with running the model and with the graphics.

REFERENCES

Abramopoulos, F., C. Rosenzweig, and B. Choudhury, 1988: Improved ground hydrology calculations for global climate models (GCMs): Soil water movement and evapotranspiration. *J Climate*, **1**, 921–941.

Avissar, R., and R. A. Pielke, 1989: A parameterization of heterogeneous land surface for atmospheric numerical models and its impact on regional meteorology. *Mon. Wea. Rev.*, **117**, 2113–2136.

Beven, K. J., 1986a: Runoff production and flood frequency in catchments of order *n*: An alternative approach. *Scale Problems in Hydrology*, V. K. Gupta, I. Rodriguez-Iturbe, and E. F. Wood, Eds., D. Reidel, 107–131.

——, 1986b: Hillslope runoff processes and flood frequency characteristics. *Hillslope Processes*, A. D. Abrahams, Ed., George Allen and Unwin, 187–202.

——, and M. J. Kirkby, 1979: A physically based variable-contributing area model of basin hydrology. *Hydrol. Sci. Bull.*, **24**, 43–69.

Budyko, M. I., 1956: *Heat balance of the earth's surface*. U.S. Weather Bureau, Washington, DC.

Charney, J., W. Quirk, S. Chow, and J. Kornfield, 1977: A comparative study of the effects of albedo change on drought in semiarid regions. *J. Atmos. Sci.*, **34**, 1366–1385.

Dickinson, R. E., 1984: Modeling evapotranspiration for three dimensional global climate models; climate processes and climate sensitivity. *Geophys. Monogr.*, **29**, *Maurice Ewing Volume 5*, Amer. Geophys. Union, Washington, DC, 58–72.

——, A. Henderson-Sellers, P. J. Kennedy, and M. F. Wilson, 1986: Biosphere-atmosphere transfer scheme (BATS) for the NCAR community climate model. NCAR Technical Note, 69 pp.

Entekhabi, D., and P. S. Eagleson, 1989: Land surface hydrology parameterization for atmospheric general circulation models including subgrid scale spatial variability. *J. Climate*, **2**, 816–831.

Famiglietti, J., and E. F. Wood, 1991a: Evapotranspiration and runoff from large land areas: Land surface hydrology for atmospheric general circulation models. *Land Surface–Atmospheric Interactions for Climate Models: Observations, Models, and Analyses*, Eric F. Wood, Ed., Kluwer, 179–204.

——, and ——, 1991b: Comparison of passive microwave and model-derived estimates for soil moisture fields. *Proc. Fifth International Colloquim—Physical Measurements and Signatures in Remote Sensing*, Courchevel, France, European Space Agency, 321–326.

——, E. F. Wood, M. Sivapalan, and D. J. Thongs, 1992: A catchment scale water balance model for FIFE. *J. Geophys. Res.*, **97**(D17), 18 997–19 007.

Hall, F. G., K. F. Huemmrich, S. J. Goetz, P. J. Sellers, J. E. Nickeson, 1992: Satellite Remote Sensing of Surface Energy Balance: Success, Failures and Unresolved Issues in FIFE. *J. Geophys. Res.*, in press.

Holwill, C. J., and J. B. Stewart, 1992: Spatial variability of evaporation derived from aircraft and groundbased data. *J. Geophys. Res.*, **97**(D17), 18 673–18 680.

Markham, B. L., and J. L. Barker, 1986: Landsat MSS & TM post-calibration dynamic ranges, exoatmospheric reflectones and at satellite temperatures. *EOSAT Landsat Tech. Note*, **1**, 3–8.

Rowntree, P. R., and J. R. Bolton, 1983: Simulation of the atmospheric response to soil moisture anomalies over Europe. *Quart. J. Roy. Meteor. Soc.*, **109**, 501–526.

Sato, N., P. J. Sellers, D. A. Randall, E. K. Schneider, J. Shukla, J. L. Kinter III, Y-T Hou, and E. Albertazzi, 1989: Effects of implementing the simple biosphere model in a general circulation model. *J. Atmos. Sci.*, **46**, 2757–2782.

Sellers, P. J., and J. L. Dorman, 1987: Testing the simple biosphere model (SiB) using point micrometereological and biophysical data. *J. Climate Appl. Meteor.*, **26**, 622–651.

——, Y. Mintz, Y. C. Sud, and A. Dalcher, 1986: A simple biosphere model (SiB) for use within general circulation models. *J. Atmos. Sci.*, **43**, 1986.

——, F. G. Hall, G. Asrar, D. E. Strebel, and R. E. Murphy, 1988: The First ISLSCP Field Experiment (FIFE). *Bull. Amer. Meteor. Soc.*, **69**, 22–27.

——, W. J. Shuttleworth, J. L. Dorman, A. Dalcher, and J. M. Roberts, 1989: Calibrating the simple biosphere model for amazonian tropical forest using field and remote sensing data. Part I: Average calibration with field data. *J. Appl. Meteor.*, **28**, 727–759.

Shukla, J., and Y. Mintz, 1982: The influence of land-surface evapotranspiration on earth's climate. *Science*, **215**, 1498–1501.

——, C. Nobre, and P. J. Sellers, 1990: Amazon deforestation and climate change. *Science*, **247**, 1322–1325.

Sivapalan, M., K. J. Beven, and E. F. Wood, 1987: On hydrological similarity. II: A scaled model of storm runoff production. *Water Resour. Res.*, **23**, 2266–2278.

Smith, E. A., A. Y. Hsu, W. L. Crosson, R. T. Field, L. J. Fritschen, R. J. Gurney, E. T. Kanemasu, W. Kustas, D. Nie, W. J. Shuttleworth, J. B. Stewart, S. B. Verma, H. Weaver, and M. Wesley, 1992: Area averaged fluxes and their time–space variability over the FIFE Experimental Domain. *J. Geophys. Res.*, **97**(D17), 18 599–18 622.

Sud, Y. C., P. Sellers, M. D. Chow, G. W. Walker, and W. E. Smith, 1990: Influence of biosphere on the global circulation and hydrologic cycle—A GCM simulation experiment. *Agric. For. Meteor.*, **52**, 133–188.

Walker, J. M., and P. R. Rowntree, 1977: The effect of soil moisture on circulation and rainfall in a tropical model. *Quart. J. Roy. Meteor. Soc.*, **103**, 29–46.

Wood, E. F., 1991: Global scale hydrology: Advances in land surface modeling. *Rev. Geophys., Suppl.*, **29**, 193–201.

——, M. Sivapalan, K. J. Beven, and L. Band, 1988: Effects of spatial variability and scale with implications to hydrologic modeling. *J. Hydrol.*, **102**, 29–47.

——, ——, ——, 1990: Similarity and scale in catchment storm response. *Rev. Geophys.*, **28**, 1–18.

WATER RESOURCES RESEARCH, VOL. 29, NO. 6, PAGES 1805–1817, JUNE 1993

Evaluation of a Distributed Catchment Scale Water Balance Model

PETER A. TROCH,[1] MARCO MANCINI,[2] CLAUDIO PANICONI,[3,4] AND ERIC F. WOOD[5]

The validity of some of the simplifying assumptions in a conceptual water balance model is investigated by comparing simulation results from the conceptual model with simulation results from a three-dimensional physically based numerical model and with field observations. We examine, in particular, assumptions and simplifications related to water table dynamics, vertical soil moisture and pressure head distributions, and subsurface flow contributions to stream discharge. The conceptual model relies on a topographic index to predict saturation excess runoff and on Philip's infiltration equation to predict infiltration excess runoff. The numerical model solves the three-dimensional Richards equation describing flow in variably saturated porous media, and handles seepage face boundaries, infiltration excess and saturation excess runoff production, and soil driven and atmosphere driven surface fluxes. The study catchments (a 7.2-km^2 catchment and a 0.64-km^2 subcatchment) are located in the North Appalachian ridge and valley region of eastern Pennsylvania. Hydrologic data collected during the MACHYDRO 90 field experiment are used to calibrate the models and to evaluate simulation results. It is found that water table dynamics as predicted by the conceptual model are close to the observations in a shallow water well and therefore, that a linear relationship between a topographic index and the local water table depth is found to be a reasonable assumption for catchment scale modeling. However, the hydraulic equilibrium assumption is not valid for the upper 100 cm layer of the unsaturated zone and a conceptual model that incorporates a root zone is suggested. Furthermore, theoretical subsurface flow characteristics from the conceptual model are found to be different from field observations, numerical simulation results, and theoretical baseflow recession characteristics based on Boussinesq's groundwater equation.

1. INTRODUCTION

Scale effects on hydrologic response have received much attention during the past decade. One of the central issues concerns the extent to which small scale details of the relevant physical processes should be represented in hydrologic models applicable over a wide range of scales. Past research efforts have resulted in the formulation of scale-related concepts that summarize basin characteristics. Examples can be found in the works by *Gupta and Waymire* [1983] and *Mesa and Mifflin* [1986], who used the network width function to describe channel flow routing; *Gupta and Waymire* [1989] and *Tarboton et al.* [1989], who developed a stochastic theory to describe spatial variability in link heights in river networks; *Beven and Kirkby* [1979] and *Sivapalan et al.* [1987], who used the topographic index distribution of a drainage basin to model saturation excess runoff; and *Wood et al.* [1988] and *Wood et al.* [1990], who introduced the concept of the representative elementary area (REA) as the scale at which continuum assumptions concerning small scale heterogeneity hold.

Based on these ideas, conceptual models have been developed to describe and explain hydrologic response at the basin scale. What these models have in common is their representation of physical process dynamics using analytically tractable solutions to governing equations. To obtain such closed form solutions, it is in general necessary to consider simplifications in the mathematical formulation of the processes, such as linearizing the governing equations or assuming a restricted set of initial and boundary conditions. Moreover, different and often contrasting analytical solutions are used to represent the various hydrologic processes of interest. It is then hoped that the hydrologic model will be capable of simulating some average response of the basin. In this spirit, calibration and validation of conceptual models is often based on lumped hydrologic fluxes such as total discharge at the catchment outlet. However, current usage of conceptual models is not restricted to prediction of average hydrologic behavior. In environmental studies, for instance, accurate prediction of the temporal and spatial structure of each component of the hydrologic cycle has become increasingly important.

It is the purpose of this paper to evaluate some of the simplifying assumptions in a distributed basin scale water balance model. The conceptual model under study is described in detail by *Famiglietti et al.* [1992]. The model relies on a topography-soil index to predict saturation excess runoff [*Beven and Kirkby*, 1979; *Sivapalan et al.*, 1987] and on Philip's equation [*Brutsaert*, 1976; *Philip*, 1957*a*, *b*] to predict infiltration excess runoff. In this paper, we examine conceptualizations concerning the spatial distribution and temporal evolution of the water table depth, the distribution of soil moisture and pressure head in the unsaturated zone, and the characteristics of base flow recession. The topography-soil index, an index of hydrologic similarity [*Wood et al.*, 1990], is used to compute the local depth to the water table. In the model this water table depth will determine the storage capacity and hydraulic properties in the unsaturated zone, and it therefore plays a central role in the generation of surface runoff. The local storage deficit is calculated based

[1]Laboratory of Hydrology and Water Management, Ghent University, Gent, Belgium.
[2]Dipartimento di Ingegneria Idraulica, Ambientale e del Rilevamento, Politecnico di Milano, Milan, Italy.
[3]Dipartimento di Metodi e Modelli Matematici, Università di Padova, Padua, Italy.
[4]Now at CRS4, Cagliari, Italy.
[5]Water Resources Program, Department of Civil Engineering and Operations Research, Princeton University, Princeton, New Jersey.

Paper number 93WR00398.
0043-1397/93/93WR-00398$05.00

on a hydraulic equilibrium assumption for pressure head, from which the vertical distribution of soil moisture is obtained. This hydraulic equilibrium assumption also yields the surface soil moisture value which in turn is used to calculate the parameters in Philip's infiltration equation. It is further assumed that during a rainfall event the average water table depth remains constant. Immediately after cessation of rainfall the change in groundwater storage is proportional to the infiltrated and drained volume, and this information is used to update the water table depth. During an interstorm period the water table depth is a function of evaporation and subsurface flow, and is updated at every time step. In the model subsurface contributions to total streamflow depend on an exponential relationship between base flow and groundwater storage.

To investigate the assumptions described above we compare simulation output from different components of the conceptual model with results obtained from a three-dimensional numerical model and with field observations. The numerical model used in this study is described by *Paniconi and Wood* [1993] and is based on the three-dimensional transient Richards equation. This model handles evaporation and precipitation inputs at the catchment surface and predicts saturation excess and infiltration excess runoff generation. The evaluation of the conceptual model is carried out at two basin scales: for a 7.2-km^2 catchment and for a 0.64-km^2 subcatchment. These study catchments (WE-38 and WD-38 Mahantango Creek) are located in the North Appalachian ridge and valley region of eastern Pennsylvania. Detailed hydrologic information for both catchments was collected during the 12-day Multisensor Airborne Campaign 1990 (MACHYDRO 90). One of the objectives of this campaign is to apply the multisensor data in detailed water balance studies of the regulating effect of soil moisture on hydrologic processes.

Numerical models based on the Richards equation have been used in the past to simulate hillslope and catchment scale hydrologic processes [e.g., *Freeze*, 1971; *Smith and Hebbert*, 1983; *Binley et al.*, 1989]. These physically based models have proved useful in evaluating the underlying assumptions in conceptual models. Examples can be found in the works by *Gan and Burges* [1990*a*, *b*] (rainfall-runoff models on small hypothetical catchments), *Sloan and Moore* [1984] (one- and two-dimensional subsurface storm flow models), and *Ibrahim and Brutsaert* [1968] and *Reeves and Miller* [1975] (one-dimensional infiltration models to test the time compression approximation). The numerical model used in this study is based on the following assumptions and limitations: flow is laminar and isothermal, inertial forces and chemical gradients are neglected, and the air phase is continuous and at atmospheric pressure. In addition, the model does not account for hysteresis and it is assumed that the porous medium is isotropic. Finally, we consider only flow within the soil matrix, neglecting flow through macropores.

In the following section we present the main features of the conceptual model and the numerical model. Both models can handle spatially and temporally variable inputs and are designed to take advantage of digital elevation data bases and of information extracted from these data bases by topographic analysis. Mechanisms of streamflow generation are discussed. Geophysical characteristics of the study catchments are given in section 3.1. The Mahantango Creek watershed is characterized by long even-crested ridges, which alternate with broad, rolling valleys. The catchment experiences a humid climate with approximately 1000 mm of annual precipitation, distributed uniformly throughout the year. The data and parameters used in the two models are described in sections 3.2 and 3.3, with additional discussion in section 3.4 of initial conditions and the estimation of an effective depth to the water table. The calibration of both models is discussed in section 3.5 and is based on a comparison between observed and simulated runoff volume.

In the conceptual model the local water table depth is assumed to be a linear function of the topography-soil index. This hypothesis is tested in section 4.1 by comparing the distribution of the topography-soil index with the distributions of the water table depth generated by the numerical model for subcatchment WD-38 at the end of a 12-day simulation period. To minimize the effect of initial conditions, longer test runs with the numerical model are also performed. In section 4.2 assumptions in the conceptual model about the temporal evolution of the local and average water table depth are studied. Piezometric observations from a shallow and a deep well are compared with simulation results from both the conceptual and numerical models. In the following section the hydraulic equilibrium assumption for the vertical distribution of soil moisture is tested by generating moisture profiles at fixed points along a hillslope situated in subcatchment WD-38 using the numerical model. In section 4.4 the characteristics of base flow recession for the conceptual and numerical models are compared with observations and with analytical solutions to Boussinesq's hydraulic groundwater equation.

2. Description of the Models

2.1. *Conceptual Water Balance Model*

The conceptual water balance model used in this study is developed by *Sivapalan et al.* [1987] and *Famiglietti et al.* [1992]. We present here a brief description of the basic equations of the model. The water balance for a catchment with drainage area A is given by

$$Ae = Ap - Q - \frac{dS_u}{dt} - \frac{dS_g}{dt} \tag{1}$$

where t is time, e is the catchment average evaporation rate, p is the lumped rainfall intensity, Q is the streamflow at the basin outlet, S_u is the volume of water stored in the unsaturated zone, and S_g is the groundwater storage. Other contributions to the water balance, such as deep percolation and the storage in surface water bodies, are assumed to be of minor importance and are neglected.

2.1.1. *Streamflow generation.* The conceptual model predicts soil saturation and its relationship to both saturation excess and infiltration excess surface runoff generation using spatially variable soil and topographic data. The initial storage capacity in the unsaturated zone is a function of the depth to the water table. The local depth to the water table z_i can be computed as [*Sivapalan et al.*, 1987]

$$z_i = \bar{z} - \frac{1}{f}\left\{\ln\left(\frac{aT_e}{T_i \tan\beta}\right) - \lambda\right\} \tag{2}$$

where

$\bar{z}$ areal average of z_i;
T_i local value of the transmissivity coefficient $T = K_{s_0}/f$;
K_{s_0} saturated hydraulic conductivity at the surface;
f describes the exponential decay of hydraulic conductivity with depth;
$\ln(T_e)$ expected value of $\ln(T_i)$;
λ expected value of the topographic index $\ln(a/\tan\beta)$;
a local draining area per unit contour length;
β land surface slope angle.

The derivation of (2) is based on the assumption that the water table is nearly parallel to the soil surface and that the saturated hydraulic conductivity K_s declines exponentially with depth z_d according to

$$K_s(z) = K_{s_0} \exp(-f z_d) \tag{3}$$

Assuming hydraulic equilibrium for the vertical pressure distribution, the local storage capacity S_i can be expressed in terms of z_i and given soil parameters as

$$S_i = (\theta_s - \theta_r)\left\{ z_i - \psi_c - \frac{1}{1-B}\left[\left(\frac{\psi_c}{z_i}\right)^B z_i - \psi_c\right]\right\} \tag{4}$$

where θ_s is the saturation moisture content and θ_r is the residual moisture content. The air entry pressure head value ψ_c and the pore size distribution index B are the parameters in the soil moisture characteristic relationship formulated by *Brooks and Corey* [1964]:

$$\theta(\psi) = \theta_r + (\theta_s - \theta_r)\left(\frac{\psi_c}{\psi}\right)^B \qquad \psi \le \psi_c$$
$$\theta(\psi) = \theta_s \qquad \psi \ge \psi_c \tag{5}$$

$$K(\psi) = K_s\left(\frac{\psi_c}{\psi}\right)^{2+3B} \qquad \psi \le \psi_c$$
$$K(\psi) = K_s \qquad \psi \ge \psi_c \tag{6}$$

where θ is volumetric moisture content, ψ is pressure head, and K is hydraulic conductivity. Whenever the cumulative infiltration volume exceeds the local soil moisture storage capacity, saturation excess runoff is generated.

The infiltration excess component of the model applies the time compression approximation to Philip's equation to compute the local infiltration rate g_i under local erratic rainfall p_i [*Famiglietti et al.*, 1992]:

$$g_i = \min[g_i^*(G), p_i] \tag{7}$$

in which G is cumulative infiltration and the local infiltration capacity g_i^* is calculated as

$$g_i^*(G) = cK_{s_0}\left\{1 + \left[\left(1 + \frac{4cK_{s_0}G}{S_r^2}\right)^{1/2} - 1\right]^{-1}\right\} \tag{8}$$

where S_r is sorptivity and cK_{s_0} accounts for the effect of gravity on the infiltration rate. The parameter c ranges from 0.5 to 1.0 and depends on the saturation of the soil profile. Analytical expressions for c and S_r are given in the work by *Sivapalan and Wood* [1986]. Infiltration excess runoff is generated on those parts of the catchment where $p_i > g_i^*$.

The model assumes an exponential relationship between base flow and groundwater storage such that the base flow contribution Q_b to total streamflow is given by

$$Q_b = Q_0 \exp(-f\bar{z}) \tag{9}$$

where Q_0 represents subsurface flow when $\bar{z} = 0$. During a rainstorm the average depth to the water table $\bar{z}$ is kept fixed and redistribution of soil moisture is neglected. After cessation of rainfall a new value for $\bar{z}$ is calculated taking into account the total amount of water infiltrated and drained.

The total streamflow for the catchment is obtained by summing the contributions to surface runoff from saturation excess, infiltration excess, and subsurface flow. In this version of the model overland flow and channel flow routing are not considered.

2.1.2. *Evaporation.* Saturated areas are allowed to evaporate at the potential rate e_p (atmosphere controlled stage). As the soil near the surface dries out the moisture delivery rate is limited by the properties of the soil profile (soil controlled stage). The model uses an analytical solution to the one-dimensional desorption problem and again applies the time compression approximation which results in the following expression:

$$e_a = \min[e_a^*(E_a), e_p] \tag{10}$$

in which e_a is the actual evaporation rate and e_a^* represents the evaporation capacity as a function of cumulative evaporation E_a:

$$e_a^*(E_a) = S_e^2/2E_a \tag{11}$$

where S_e is the desorptivity, which varies with soil moisture content. Transpiration is not considered in this version of the model.

During interstorm periods the water table is updated at each time step, taking into account evaporative and drainage losses.

2.2. *Numerical Model*

The numerical catchment simulation model is presented in the works by *Paniconi* [1992] and *Paniconi and Wood* [1993]. We will highlight the main features of the model. The three-dimensional Richards equation with pressure head ψ as the dependent variable can be written as

$$S(\psi)\frac{\partial\psi}{\partial t} = \nabla\cdot(K_s K_r(\psi)\nabla(\psi + z)) \tag{12}$$

where z is the vertical coordinate, positive upward, and the hydraulic conductivity K is expressed as a product of the conductivity at saturation and the relative conductivity K_r. An extension of the van Genuchten characteristic equations [*van Genuchten and Nielsen*, 1985] is used to describe the nonlinear dependencies of θ, K_r, and specific moisture capacity S on the pressure head [*Paniconi*, 1992]:

$$\theta(\psi) = \theta_r + (\theta_s - \theta_r)[1 + \beta]^{-m} \qquad \psi \le \psi_0$$
$$\theta(\psi) = \theta_r + (\theta_s - \theta_r)[1 + \beta_0]^{-m} + S_s(\psi - \psi_0) \qquad \psi \ge \psi_0 \tag{13}$$

TABLE 1. Soil Parameters for WE-38 Mahantango Creek

Soil Number	Soil Name	Soil Texture	K_{s_0}, m/hour	θ_s	θ_r	Water Retention Parameters: Brooks-Corey ψ_s, m	Brooks-Corey B	van Genuchten ψ_s, m	van Genuchten n
71	Albrights	silt loam	0.036	0.501	0.015	0.21	0.211	0.43	1.29
57	Alvira	silt loam	0.036	0.501	0.015	0.21	0.211	0.43	1.29
8	Basher	silt loam	0.036	0.501	0.015	0.21	0.211	0.43	1.29
145	Berks	silt loam	0.073	0.501	0.015	0.21	0.211	0.43	1.29
45	Calvin	silt loam	0.057	0.501	0.015	0.21	0.211	0.43	1.29
73	Conyngham	silt loam	0.036	0.501	0.015	0.21	0.211	0.43	1.29
32	Dekalb	sandy loam	0.090	0.450	0.041	0.15	0.322	0.24	1.38
54	Hartleton	silt loam	0.057	0.501	0.015	0.21	0.211	0.43	1.29
149	Klinesvil	silt loam	0.090	0.501	0.015	0.21	0.211	0.43	1.29
75	Laidig	gravel loam	0.090	0.460	0.027	0.11	0.220	0.17	1.25
66	Leck Kill	silt loam	0.057	0.501	0.015	0.21	0.211	0.43	1.29
69	Meckesville	loam	0.036	0.501	0.015	0.21	0.211	0.43	1.29
70	Meckesville	stony loam	0.090	0.501	0.015	0.21	0.211	0.43	1.29
38	Shelmadine	silt loam	0.036	0.501	0.015	0.21	0.211	0.43	1.29
47	Weickert	silt loam	0.073	0.501	0.015	0.21	0.211	0.43	1.29

$$S(\psi) = \frac{d\theta}{d\psi} = \frac{(n-1)(\theta_s - \theta_r)|\psi|^{n-1}}{|\psi_s|^n(1+\beta)^{m+1}} \qquad \psi \le \psi_0$$

$$S(\psi) = \frac{d\theta}{d\psi} = S_s \qquad \psi \ge \psi_0 \tag{14}$$

$$K_r(\psi) = (1+\beta)^{-5m/2}[(1+\beta)^m - \beta^m]^2 \qquad \psi \le 0$$

$$K_r(\psi) = 1 \qquad \psi \ge 0 \tag{15}$$

where S_s is the specific storage, $m = 1 - 1/n$, $\beta \equiv (\psi/\psi_s)^n$, $\beta_0 \equiv \beta(\psi_0)$, ψ_s is a fitting parameter, and n can be interpreted as a pore size distribution index; ψ_0 is a continuity parameter which is calculated from (14) given S_s. The exponential relationship (3) is used to model vertical heterogeneity of saturated hydraulic conductivity. Hysteresis effects on moisture redistribution in the soil profile are not taken into account. We remark here that different soil moisture characteristic relationships are used in the conceptual model (equations (5) and (6)) and the numerical model (equations (13) and (15)). Any discrepancy this may cause is minimized by fitting both sets of equations to the same field observations (see Table 1). Since the soils in Mahantango Creek show a wide pore size distribution, the van Genuchten water retention equation fitted the observed data better than the Brooks-Corey equation. *Troch et al.* [1993] and P. A. Troch et al. (Hydrologic controls of large floods in a small basin: North Appalachian case study, submitted to the *Journal of Hydrology*, 1993) have developed a more general formulation of the conceptual model based on the van Genuchten characteristic equations. The effect of the use of different soil characteristic curves in catchment modeling is under investigation.

A finite element Galerkin discretization in space and a finite difference discretization of the time derivative term is used to solve (12) numerically. The resulting system of nonlinear equations is linearized using either Picard or Newton iteration [*Paniconi et al.*, 1991].

The catchment simulation model comprises two programs: a grid generator which constructs the finite element mesh and initializes various parameters, and the actual simulation program which numerically solves the three-dimensional Richards equation over a specified time period for a given set of boundary and initial conditions.

2.2.1. *Streamflow generation.* The potential inflows to the model consist of precipitation (positive) and evaporation (negative) flux inputs at the catchment surface. The actual (simulated) inflows are determined according to the type of boundary condition imposed, and during a simulation the model automatically adjusts this boundary condition according to changes in pressure head and flux values at the surface. When the potential flux is positive, the difference between potential and actual soil inflow is the total runoff. Surface runoff is produced when the surface becomes saturated, either due to a rising water table (saturation excess mechanism) or to the infiltration capacity of the soil falling below the rainfall rate (infiltration excess mechanism). In both cases the boundary condition at the point on the surface where saturation occurs switches from a Neumann type (atmosphere controlled inflow) to a Dirichlet type (soil controlled inflow). Subsurface runoff in the model is produced at seepage faces or when subsurface water exits the soil matrix from a saturated region on the surface (return flow). Overland flow (surface runoff and return flow) generated at a point on the catchment is routed to the stream using a time delay determined from the overland flow velocity (assumed constant for the catchment) and the shortest distance from the point to the stream. In this version of the model channel flow is not considered.

2.2.2. *Evaporation.* When evaporation is atmosphere controlled and the pressure head at a point on the surface becomes smaller than the "air dry" pressure head value ψ_{min} [*Hillel*, 1980, p. 121], the boundary condition at that point is switched from specified flux (Neumann) to constant head (Dirichlet) and thus the evaporation process becomes soil controlled. The boundary condition switches back to a Neumann type when the magnitude of the computed flux across the soil surface exceeds the magnitude of the potential evaporation rate, or when a rainfall event begins. Root

extraction is not included in the numerical model and therefore the model cannot simulate evaporation from vegetated surfaces when the actual rate falls below the potential rate.

3. Description of the Catchments and Model Inputs

3.1. *Mahantango Creek Experimental Catchment*

The Mahantango Creek watershed (approximately 420 km^2) is characterized by long, even-crested ridges 300–400 m in elevation, which alternate with broad, rolling valleys, 150–300 m in elevation. The mountain ridges run in the NE-SW direction. The ridges are underlain by erosion-resistant sandstones, orthoquartzite, and conglomerate. The valleys are underlain by less erosion-resistant shales, siltstones, and sandstones [*Urban*, 1977]. The catchments used in this study are part of the Mahantango Creek watershed. WE-38 Mahantango Creek is one of the experimental catchments of the Agricultural Research Service (ARS) of the U.S. Department of Agriculture (USDA). The total drainage area is 7.2 km^2 and it includes a 0.64-km^2 subcatchment, WD-38, which has been the subject of intensive hydrologic research [e.g., *Engman*, 1974; *Engman and Rogowski*, 1974].

The catchments experience a humid climate, typical for the northeastern United States, with approximately 1000 mm of annual precipitation, distributed uniformly throughout the year. The average rainfall during the month of July (the month of the MACHYDRO 90 experiment) is 104 mm [*Gburek*, 1977]. The frequent rains keep the soils at or near field capacity, except near the surface. Even the fragipan soils near the stream, which have only limited moisture holding capacity and root penetration as a result of the confining layer, remain relatively moist because of this frequent rainfall and their proximity to the high water table. Soil moisture is generally variable only to about the 100 cm depth [*Gburek*, 1977]. Below this depth soil moisture content remains nearly constant at near field capacity throughout the year. Based on measurements from more than 30 groundwater wells, *Urban* [1977] constructed a water table map for WE-38. The groundwater profile is highly correlated with topography. Because of the relatively high moisture content of the soils the actual evapotranspiration (ET) is at or near its potential rate much of the time. There are short periods, however, during which soil moisture deficit limits evapotranspiration. *Gburek* [1977] estimated that baseflow at WE-38 is about 70% of yearly streamflow.

3.2. *Hydrologic Data*

The hydrologic data used in this study were gathered during the 12-day Multisensor Airborne Campaign 1990 (MACHYDRO 90). The objective of this campaign is to study the role of soil moisture and its regulating effect on hydrologic processes. The experiment was held from July 9 to July 20, 1990. During this period the spatial and temporal distribution of precipitation was measured by 14 rain gages with 0.2 mm accuracy at a sampling interval of 15 min. Figure 1 shows the catchment average rainfall recorded during the 12-day period. The observed accumulated rainfall is 66 mm. This rainfall fell during the first half of the experiment. The maximum observed rainfall intensity is about 20 mm/hour, a value lower than the minimum saturated hydraulic conductivity reported for the soils in Mahantango Creek. Infiltration excess runoff is thus impossible during this period.

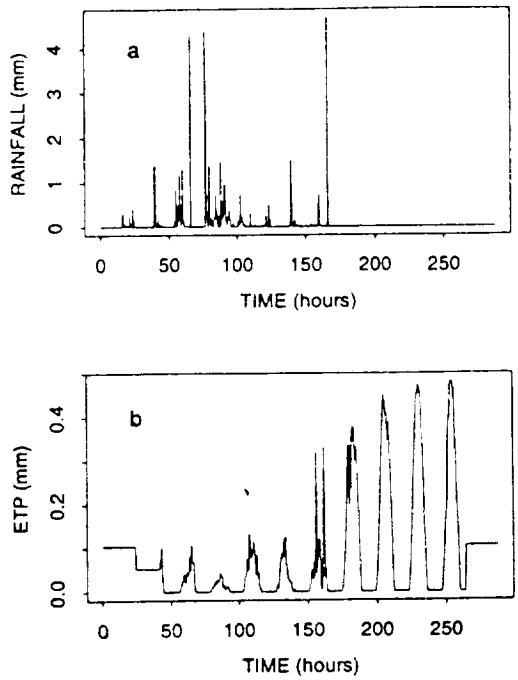

Fig. 1. (*a*) Areal average precipitation data for the 12-day period July 9–20, 1990 calculated from 15-min observations at 14 rain gages. (*b*) Estimated potential evaporation based on 30-min measured net radiation and estimates based on weather reports (flat lines at the beginning and end of the graph).

Potential evaporation from July 11 to July 19 is calculated based on the Priestley-Taylor method using measured net radiation from a micrometeorological station. Radiation was measured at a sampling interval of 30 min. For July 9, 10, and 20, when the meteorological station was not operating, daily potential evaporation values of 5, 2.5, and 5 mm, respectively, are estimated based on weather reports. The total potential evaporation for the 12-day period is 45 mm. The temporal evolution of potential evaporation is shown in Figure 1. Based on these meteorological observations a strong drydown can be expected during the second half of the experiment.

The temporal evolution of the phreatic surface was observed at four piezometers. The measured depth to the water table ranged from 1 to 4 m. Soil samples were taken along fixed transects, from which the gravimetric and volumetric moisture content in the top soil layer could be estimated. These data are not used in this study but will be analyzed and compared with the models' output in future studies. Streamflow is observed at the outlet of catchment WE-38 and subcatchment WD-38 (Figure 2). The level response at 180 hours in catchment WE-38 is an artifact. No attempts were made to correct for this anomalous observation since no detailed information about the data collection was available to the authors. During the 12-day experiment, it is estimated that only 1 or 2% of the total rainfall became direct runoff. Base flow tends to be low during summer months. During the experiment the volume of base flow was about equal to the direct runoff volume. The remaining rainfall observed during the experiment is either stored in the unsaturated and groundwater zones or is evaporated into the atmosphere.

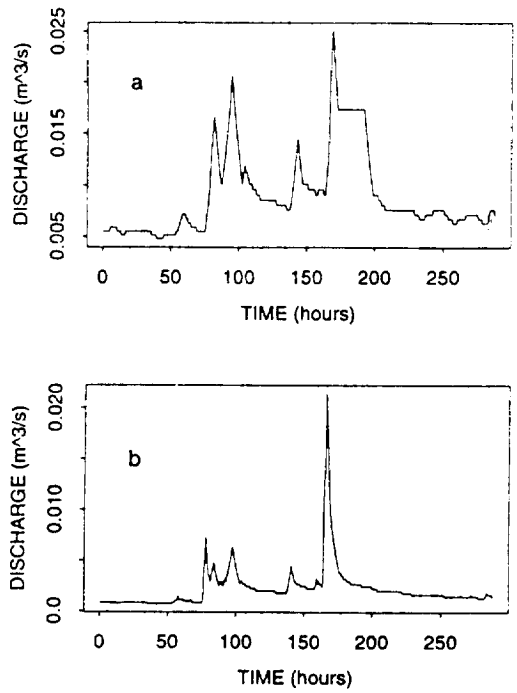

Fig. 2. Observed streamflow data for the 12-day period July 9–20, 1990 for (*a*) catchment WE-38 and (*b*) catchment WD-38.

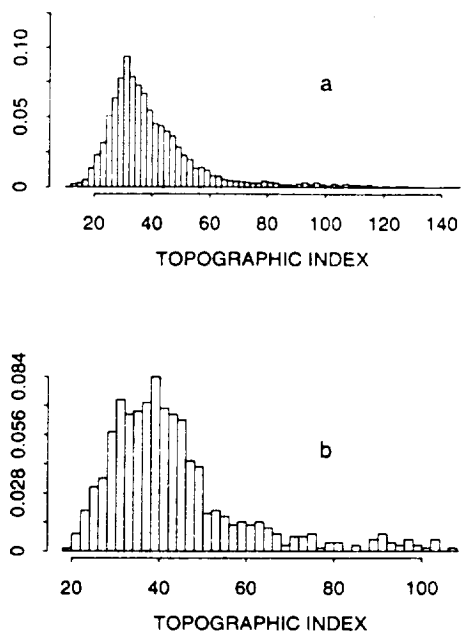

Fig. 3. Distribution of the local topographic index 10 ln (a/tan β) for (*a*) catchment WE-38 and (*b*) catchment WD-38.

Figure 2 demonstrates the nonlinear response to rainfall of the two basins during the experiment. The initial storm response is almost negligible. The runoff production of the two basins during the last rainfall event is more pronounced and is dominated by the saturation excess mechanism.

3.3. *Model Parameters*

3.3.1. *Soils.* In WE-38 Mahantango Creek, 15 different soil types can be identified (Table 1). From Table 1 it can be seen that the spatial distribution of θ_s, θ_r, ψ_c (ψ_s), and $B(n)$ can be neglected for catchment WE-38, and therefore for subcatchment WD-38 as well. The following parameter values are used to characterize the soil water retention properties in WE-38 and WD-38: $\theta_s = 0.501$, $\theta_r = 0.015$, $\psi_c = 0.21$ m, $\psi_s = 0.43$ m, $B = 0.211$, and $n = 1.29$. The areal average value of saturated hydraulic conductivity at the surface $\bar{K}_{s_0}$ is 0.062 m/hour. However, this parameter varies considerably from 0.036 to 0.090 m/hour and therefore is explicitly taken into account in both models. We refer to *Rogowski et al.* [1974] and *Loague and Freeze* [1985] for a detailed soil map of both WE-38 and WD-38. The value of specific storage S_s used in (13) and (14) is 0.005/m. For the numerical model the parameter ψ_{min}, which controls the switching of evaporation boundary conditions, was set at a value low enough to ensure that actual evaporation remained at its potential rate throughout the simulation, in accordance with field observations.

3.3.2. *Topography.* Catchment topography is represented by a 30 × 30 m U.S. Geological Survey digital elevation model (DEM). From this DEM the topographic index ln (a/tan β) can be determined for each grid square. Figure 3 shows the distribution of the topographic index in the two catchments. *Sivapalan et al.* [1987] used a three-parameter gamma distribution to model the topographic index:

$$f_\Gamma(x) = \frac{1}{\chi\Gamma(\phi)}\left(\frac{x-\mu}{\chi}\right)^{\phi-1}\exp\left\{-\frac{x-\mu}{\chi}\right\} \qquad (16)$$

where x = ln (a/tan β), ϕ is a shape parameter, χ is a scale parameter, μ is a shift parameter, and $\Gamma(\ )$ represents the gamma function. The parameter values for (16) applied to the two catchments were estimated by the method of moments and are given in Table 2.

3.3.3. *Numerical parameters.* In the numerical model the vertical soil profile is discretized into six layers of thickness 5, 5, 12.5, 75, 127.5, and 275 cm, with the thinnest layers closest to the surface. This results in an impervious layer (the base of the catchment) at a depth of 5 m, running parallel to the land surface. The horizontal discretization is taken equal to the grid size in the digital elevation model, that is 30 m by 30 m. The spatial discretization of subcatchment WD-38 yields 3804 elements and 4935 nodes. The

TABLE 2. Topographic Characteristics for Catchments WE-38 and WD-38

	Topographic Index, ln (a/tan β)			Gamma Distribution Parameters		
Catchment	Mean	Variance	Coefficient of Variation	ϕ	χ	μ
WE-38	4.03	2.88	0.42	5.651	0.714	0.0
WD-38	4.37	2.48	0.36	7.700	0.567	0.0

sensitivity of the simulated results to the grid resolution is an important issue, especially for areas in the catchment with large vertical pressure variations. Such areas would be near the streams and other runoff producing areas. *Paniconi and Wood* [1993] investigate the accuracy of the model to grid resolution and show that for grid sizes like those used in this study, good model simulations will be obtained. An adaptive time stepping algorithm is used in the numerical model, with a minimum time step size of 5 min and a maximum of 15 min (equal to the sampling interval of the rainfall data). During each time step the numerical solution is assumed to converge when the maximum change in nodal pressure head between nonlinear iterations is less than 6 cm. An average of four nonlinear iterations per time step is required for the simulations.

3.4. *Initial Conditions*

In the conceptual model the average depth to the water table $\bar{z}$ determines the initial catchment wetness conditions. For short-term simulations the output of the conceptual model is highly sensitive to this parameter, and it should therefore be carefully determined. Recently, *Troch et al.* [1993] developed a physically meaningful technique to estimate the effective depth to the water table, as a measure of the initial storage capacity of a basin. The analysis is based on Boussinesq's hydraulic groundwater equation and uses streamflow measurements at the outlet of the basin. Boussinesq's equation describes the water table height $h(x, t)$ in the case of outflow into a stream channel from an idealized unconfined aquifer with width L placed on a horizontal impermeable layer:

$$\frac{\partial h}{\partial t} = \frac{k}{n_e}\frac{\partial}{\partial x}\left(h\frac{\partial h}{\partial x}\right) \tag{17}$$

where t represents the time since the start of the recession, x is horizontal distance, $h(x, t)$ is the transient free groundwater surface profile, k is the hydraulic conductivity of the aquifer, and n_e is the drainable or effective porosity (sometimes referred to as specific yield). For small t, as the outflow rate q at $x = 0$ starts, the effect of the impermeable wall at $x = L$ (representing the divide) is negligible and the solution to (17) can be taken to be the same as if $L = \infty$. *Polubarinova-Kochina* [1962] has presented an exact solution for this case. The response of the aquifer water table to sudden drainage at $t = 0$ is not unlike a propagating wave. As soon as the wave reaches the end of the aquifer, at $x = L$, the small t solution is no longer valid. At this point, Boussinesq's solution can be used. *Boussinesq* [1904] obtained an exact solution to the nonlinear differential equation by assuming that the initial water table has the form of an inverse incomplete beta function [see also *Polubarinova-Kochina*, 1962, pp. 515–517]. This solution is not valid for small t, when the aquifer is close to being fully saturated. Based on this large time solution, *Troch et al.* [1993] derived the following expression for the effective water table height:

$$\bar{h} = 0.773D\left[1 + 1.115\left(\frac{kD}{n_e L^2}\right)t\right]^{-1} \tag{18}$$

where D represents depth to the bedrock. The catchment base flow Q_b can now be expressed as [*Troch et al.*, 1993*a*]

$$Q_b = 5.772k(D - \bar{z})^2 D_d L_t \tag{19}$$

where k and D can be considered as catchment scale effective values of hydraulic conductivity and depth to the bedrock, respectively. D_d represents drainage density, and L_t is the total length of the perennial channels. One can determine D, once k is known, by defining a critical value of the base flow Q_c, corresponding to a situation where it is assumed that the aquifers start to behave in accordance with Boussinesq's solution:

$$Q_c = 3.450kD^2 D_d L_t \tag{20}$$

Equation (19) can then be used to estimate $\bar{z}$ from observed base flow at the start of the simulation period.

To estimate the parameters in (19) and (20), a method for base flow analysis based on the following relationship is adopted:

$$dQ/dt = \Phi(Q) \tag{21}$$

Brutsaert and Nieber [1977] have shown that, for several solutions based on the Dupuit-Boussinesq hydraulic theory, $\Phi(\ )$ can be written in the form of a power function:

$$dQ/dt = -a_1 Q^{b_1} \tag{22}$$

where a_1 and b_1 can be related to hydraulic and geomorphologic characteristics of the basin. Using Boussinesq's solution it follows immediately that [*Brutsaert and Nieber*, 1977]

$$a_1 = \frac{4.804k^{1/2}L_t}{n_e A^{3/2}} \qquad b_1 = 3/2 \tag{23}$$

For the small time solution it can be shown that

$$a_1 = \frac{1.133}{kn_e D^3 L_t^2} \qquad b_1 = 3 \tag{24}$$

In Figure 4 we have plotted historical observed daily recession flow data for WE-38 and WD-38 versus its time derivative. Only uninterrupted recession flow data starting the second day after the cessation of rainfall are considered. For WE-38 (Figure 4*a*) the data are fitted by a regression line (not shown on the figure) with slope 1.498 and a correlation coefficient of 0.88; the regression for WD-38 (Figure 4*b*) has a slope of 1.35 and a correlation coefficient of 0.89. This suggests that the Dupuit-Boussinesq hydraulic theory holds: the observed slope is close to the theoretical slope of 1.5. Figure 4 shows a lower envelope with slope 1.5 that excludes about 5% of the data points. A lower envelope is chosen to eliminate other outflow components such as overland flow, interflow, channel drainage, and evaporation losses. However, the exact position of this lower envelope is uncertain. *Troch et al.* [1993] suggest the use of a 5 or 10% lower envelope. In this study a lower envelope excluding 5% of the data points is adopted. The corresponding intercept values a_1 are 1.7861×10^{-6} $(m^3/s)^{-1/2}$ for WE-38 and 8.6792×10^{-6} $(m^3/s)^{-1/2}$ for WD-38.

The critical base flow value Q_c represents an upper limit for the applicability of the large time solution. *Troch et al.* [1993] therefore suggest that this parameter should be estimated by the abscissa value of the intersection of the lower envelope curves with slopes 1.5 and 3 on a log-log diagram. They observed that, for a river basin in Belgium, the value of Q_c is rather insensitive to the actual position of these lines.

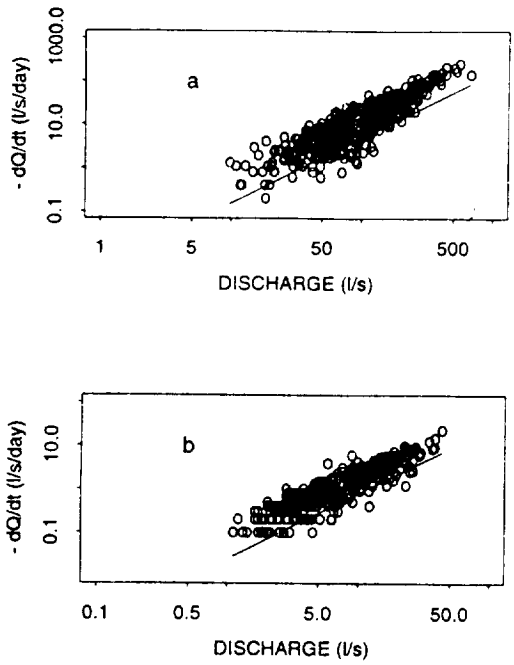

Fig. 4. Log-log plot of $-dQ/dt$ versus observed discharge Q for (*a*) catchment WE-38 and (*b*) catchment WD-38; also shown are the lower envelopes (solid lines) which exclude 5% of the data points.

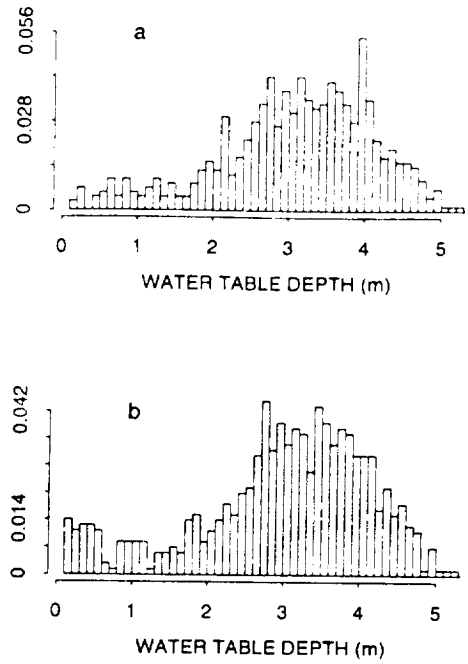

Fig. 5. (*a*) Distribution of the local water table depth at the start of the numerical simulation as calculated from (2). (*b*) Distribution of the local water table depth at the end of the numerical simulations for the 12-day period of the MACHYDRO 90 experiment.

However, for the catchments under study, the slope of 3 is not apparent in the data. Therefore the critical value is estimated to be equal to the maximal observed base flow value in Figure 4 (0.500 m^3/s and 0.050 m^3/s, respectively).

Table 3 summarizes the results of applying (23) and (20). Results are given for a range of n_e values, namely, from 0.02 to 0.07. These are reasonable values for the catchments under study [*Freeze and Cherry*, 1979, p. 61]. The geomorphologic parameters D_d and L_t are estimated from the DEM data by means of an automated extraction algorithm [*Band*, 1986]. This algorithm produces a mapping of stream channels, ridges, and drainage basins. The total length of perennial channels, as defined by the blue lines on the topographic maps for WE-38 is about 12 km, which results in a drainage density of 1.6×10^{-3} m^{-1}; corresponding values for WD-38 are 0.9 km and 1.5×10^{-3} m^{-1}.

The observed base flow at the beginning of the experiment is 0.006 m^3/s for WE-38 and 0.001 m^3/s for WD-38. By means of (17) and using an average value of drainable porosity of 0.04, the effective depth to the water table $\bar{z}$ is of the order of 3.3 m for WE-38 and 2.3 m for WD-38. These values are used as initial conditions in the conceptual water balance model.

TABLE 3. Estimated Aquifer Parameters for Catchments WE-38 and WD-38

Drainable Porosity	WE-38 (Q_c = 0.500 m^3/s)		WD-38 (Q_c = 0.050 m^3/s)	
	k, cm/h	D, m	k, cm/h	D, m
0.02	53	7.16	134	5.19
0.03	120	4.78	301	3.46
0.04	213	3.58	536	2.60
0.05	333	2.87	837	2.08
0.06	480	2.39	1205	1.73
0.07	653	2.05	1641	1.49

The initial conditions required for a transient simulation with the numerical model are nodal pressure head values. The initial heads are generated based on knowledge of the initial water table distribution given by (2) (see Figure 5*a*). The local water table depth is converted into a vertical pressure head distribution using the hydrostatic assumption. This means that if at a given location the depth to the water table is 3 m, the pressure head at the surface node is −3 m.

3.5. *Model Calibration*

Both the conceptual and the numerical model were calibrated in order to preserve total runoff volume. During the simulation period the dominating runoff production mechanism is saturation excess. This is not surprising considering the rainfall characteristics during MACHYDRO 90 and the soil characteristics of the basin. The parameter f was used in both models as a fitting parameter. For different soil types and land use, *Beven* [1982] reports fitted values for the parameter f to observed soil hydraulic characteristics. The values range from 1.0 m^{-1} to about 10.0 m^{-1}. For sandy loam to silt loam soils a typical value of 2.5 m^{-1} is suggested. For one of the soil types in the catchment (Albrights; see Table 1), *Rogowski et al.* [1974] estimated this parameter to be of order 1.2 m^{-1}. In this study a catchment-wide effective value of f = 2.5 m^{-1} was found for the conceptual model, and a value of 1.05 m^{-1} was used for the numerical model. It is noted that the optimized values of f correspond to observed values reported in the literature.

The model parameters that were estimated or inferred from data outside the 12 day simulation period are as follows: soil parameters described in section 3.3.1 (estimated

from detailed soil survey data), topographic parameters described in section 3.3.2 (from USGS DEM data) and initial water table depths described in section 3.4 (inferred from historical streamflow recession data). This leaves only f which was estimated during model calibration, as described above.

4. Evaluation of the Conceptual Water Balance Model

4.1. *Spatial Distribution of Local Water Table Depth*

In the conceptual model the difference between the local water table depth and its areal average is a linear function of the combined topography-soil index $\ln (aT_e/T_i \tan \beta)$, as expressed by (2). Based on field evidence, *Wood et al.* [1990] concluded that the deviation of the topographic variable from its expected value λ is far greater than the standard deviation of the local values of the transmissivity coefficient. Therefore variability in the transmissivity coefficient will have a relatively small effect on the predicted patterns of water table depths in the conceptual model compared to the effect of topographic variability. The observations of *Urban* [1977] support this result for Mahantango Creek. Figure 5*a* shows the initial distribution of local water table depth for the WD-38 catchment calculated based on (2). This distribution is used in the initial conditions for both the conceptual and the numerical model. During simulations with the numerical model the water table profile, as a function of space (x and y coordinates) and time, is calculated based on the three-dimensional equations governing flow in porous media. At the end of the 12-day simulation period which involved hydrologic fluxes of significant magnitude (66 mm of rainfall and 45 mm of potential evaporation), the numerical model preserves, to a certain extent, the initial distribution of the water table depth. This suggests that the estimate of the initial conditions based on (2) is consistent with groundwater hydraulics and that the use of (2) in a basin scale water balance model is reasonable.

To test the effect of initial conditions, longer numerical simulations for the WD-38 catchment were performed. During the first 100 days of a 400-day simulation, we apply zero-flux boundary conditions at the surface (no precipitation and no evaporation), in order to allow redistribution within the saturated zone. For the next 150 days a constant rainfall rate of 0.1 mm/hour is applied as the surface boundary condition. This is followed by a second zero-flux boundary condition period of 150 days. The distribution of the water table depth at the end of the first 100 days is shown in Figure 6*a*, while the distribution at the end of the simulation period for the same catchment is given in Figure 6*b*. After the first 100-day period the distribution of the local water table depth closely resembles the initial distribution. This means that, even after a longer simulation period, the model shows no tendency to drift away from the initial conditions set by (2). At the end of the 400-day simulation, however, the distribution tends to become more uniform. We also observe a shift in the areal average water table depth due to the large amount of rainfall (360 mm) during this period. We conclude from these tests that the linear relationship between water table depth and topographic index given by (2) appears to be a reasonable assumption except when the catchment is highly stressed or far removed from its steady or equilibrium state as may occur during prolonged periods of rainfall.

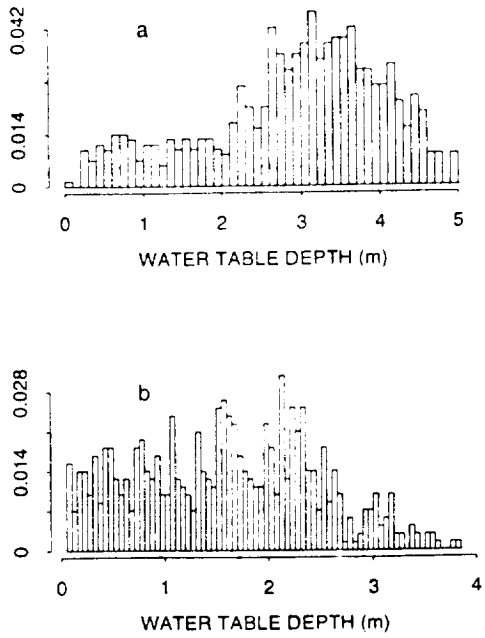

Fig. 6. (*a*) Distribution of the local water table depth after 100 days of a 400-day numerical simulation, with zero-flux boundary conditions at the surface for the first 100 days. (*b*) Distribution of the local water table depth at the end of the 400-day numerical simulation, with total rainfall of 360 mm.

4.2. *Temporal Evolution of Water Table Depth*

During a rainstorm the conceptual model does not update the depth to the water table. Immediately after cessation of rainfall a new value of mean water table depth is calculated taking into account the infiltrated and drained volume from the previous storm. This aspect of the model is apparent in Figure 7*a*. Line 1 in Figure 7*a* shows the variation of areal average water table depth about its mean value, calculated with the conceptual model for WD-38. The mean water table depth during the simulation is 2.13 m. During the dry down at the end of the experiment the evolution of mean water table depth is controlled by evaporative and drainage losses. Line 2 in Figure 7*a* shows the variation of areal average water table depth about its mean value, as computed with the numerical model for WD-38. The calculated mean value is 2.85 m. The updating of the water table is now controlled by the percolation and a much smoother curve is obtained.

The variation of local water table depth with respect to its local mean as computed by the conceptual model is similar to line 1 in Figure 7*a*. This is due to the fact that the soil characteristics which are controlling the updating of the water table are assumed to be spatially invariant and that runoff production is dominated by the saturation excess mechanism. Therefore we can compare the areal average simulation results for the conceptual model to observed variations in water table for the catchment. Line 3 in Figure 7*b* shows the simulated variation in water table depth by means of the numerical model for a site along the transect shown in Figure 8. The mean water table depth for this site during the experiment is 1.43 m. Comparing line 3 in Figure 7*b* with line 2 in Figure 7*a* we can see that the variation of areal average water table depth calculated with the numerical model reflects the variation for sites in the catchment exhibiting deeper water table depths. Therefore it is inter-

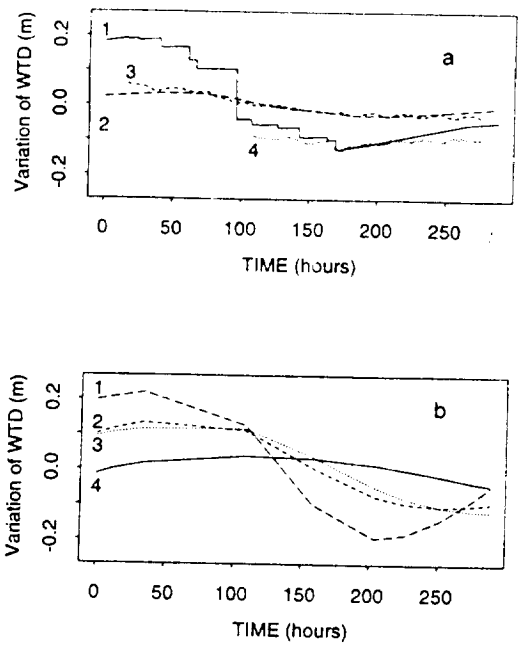

Fig. 7. (*a*) Line 1: variation about the mean value (2.13 m) of the areal average water table depth (WTD) calculated with the conceptual model for the 12-day period; line 2: variation about the mean value (2.85 m) of the areal average WTD calculated with the numerical model for the 12-day period; line 3: observed variation of WTD in a deep well (mean value 3.63 m); and line 4: observed variation of WTD in a shallow well (mean value 0.91 m). This line is shifted from the zero mean to overlap with line 1. (*b*) Numerically simulated evolution of local water table depth at four locations along a transect; line 1: mean WTD value 0.32 m (node closest to the channel); line 2: mean WTD value 1.13 m; line 3: mean WTD value 1.43 m; and line 4: mean WTD value 1.92 m (node farthest from the channel).

esting to compare the areal average simulation results for the numerical model to observed variations in deeper piezometers. Line 4 in Figure 7*a* shows the observed variation in depth to water table for a shallow piezometer (mean value during the experiment: 0.91 m) and line 3 shows the observed variation for a deeper well (mean value: 3.63 m). The irregular fluctuation of the shallow well observations is probably due to evapotranspiration losses. The groundwater hydrograph, as observed by the shallow piezometer, shows more or less the same temporal evolution as simulated by the conceptual model. During the last rainfall period the water balance model predicts a rise in water table of about 2–3 cm and the observations show a comparable evolution. After the rainfall the simulated drop in water table is in good agreement with the response in the shallow well. After a few days, however, the conceptual model overestimates the rate of decline of the water table. The evolution of mean water table depth as calculated by the numerical model and the observation for the same period in the deeper well are in remarkably good agreement. The absolute mean values are different (2.85 and 3.63 m, respectively) but the general trend in lines 2 and 3 is very close. The diurnal variation in the observation in the deep well during the last days of the experiment (which is also exhibited by other piezometers, not shown in Figure 7) is explained by diurnal variations in atmospheric pressure. Similar results were obtained using data observed in the other piezometers.

These results seem to indicate that the simplifying assumption in the conceptual model concerning the temporal evolution of the water table holds for those parts of the catchment with a shallow water table. This could be explained by the fact that the time delay between infiltration and percolation to the water table is small for these sites. To further test this hypothesis we computed, from the numerical simulation of WD-38, the temporal evolution of the water table for different locations along a hillslope transect. The four unshaded pixels in Figure 8 show the location of the surface nodes selected for detailed vertical profile output. The results for the 12-day simulation period are given in Figure 7*b*. It is clear from this graph that infiltration and percolation effects are more damped uphill (line 4), where the water table is deeper. The range of variation of depth to the water table close to the channel (line 1) compares reasonably well to the one predicted by the conceptual model. It has a mean value of 0.30 m.

It is interesting to refer to earlier research concerning groundwater level fluctuations performed in the same basin. *Urban* [1977] reports groundwater recharge events for three wells in September 1973. For the shallow well (water table at about 1 m below the land surface) a similar response to rainfall, as observed in the shallow well during MACHYDRO 90, is reported. For a comparable rainfall event the variation is a few centimeters. However, the response measured in the deep well (water level at about 18 m below the land surface) is much more pronounced than that observed during MACHYDRO 90, with a variation of the order of 1 m. The measured water table in this well is in the outcrop of a sandstone. The sandstone is covered with coarse gravelly colluvial soils. These geologic conditions are not represented in the numerical simulations reported here.

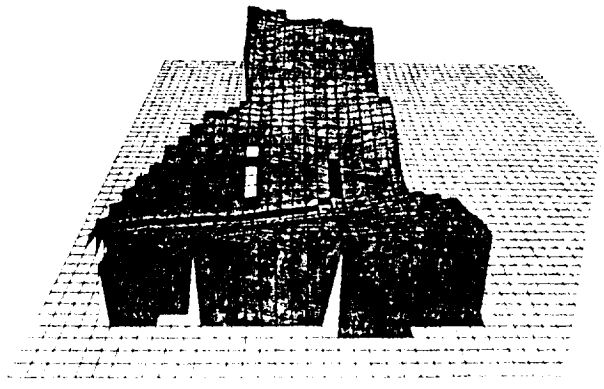

Fig. 8. Elevation image of subcatchment WD-38 (30 × 30 m grid resolution) showing stream (heavily shaded pixels) and location of the transect of four surface nodes selected for vertical profile output (unshaded pixels).

4.3. *Soil Moisture Profiles*

The conceptual model calculates unsaturated zone storage capacity based on the hydraulic equilibrium assumption. This assumption also affects the local infiltration parameters needed in Philip's equation. Figure 9 shows simulated pressure head profiles produced by the numerical model for catchment WD-38. The locations of these vertical profiles in the catchment are those shown in Figure 8. We can see that

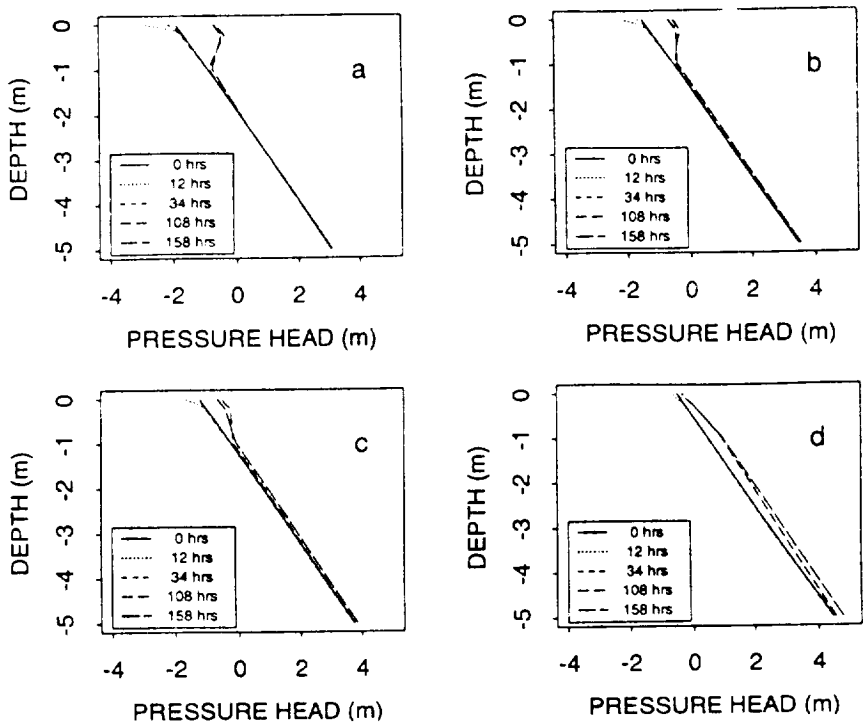

Fig. 9. Vertical pressure head profiles for five different time steps during the 12-day numerical simulation and at the four locations along the transect shown in Figure 8: (*a*) node farthest from the channel; (*d*) node closest to the channel.

in the upper 1 m of the unsaturated zone the pressure head profiles are not consistent with the hydraulic equilibrium assumption. This fact is detected for the pixels furthest from the stream where the water table is deepest. Below 1 m depth the simulated profiles do not deviate significantly from hydraulic equilibrium. Based on field evidence collected at the Mahantango Creek watershed, *Gburek* [1977] concluded that variation in soil moisture is limited to the upper 1 m layer, and that below this depth soil moisture content remains nearly constant and near field capacity throughout the year.

These results suggest that we can improve the conceptual model by using two layers instead of one to model the unsaturated zone. The upper layer in such a two-layer model can also incorporate root zone processes. This extension has been made to the conceptual model and is being tested on the First ISLSCP Field experiment (FIFE) data set from Kansas [*Famiglietti*, 1992; J. S. Famiglietti and E. F. Wood, Aggregation and scaling of spatially variable hydrological processes, 2, A catchment scale model of water an energy balance, submitted to *Water Resources Research*, 1993].

4.4. *Base Flow Recession Characteristics*

The parameters a_1 and b_1 of (22) in the case of an exponential subsurface saturated soil water store are given by

$$a_1 = f/A \qquad b_1 = 2 \tag{25}$$

In contrast to observations for catchment WE-38 and subcatchment WD-38 (Figure 4) and to Boussinesq's hydraulic groundwater theory (equations (23)), the predicted subsurface flow contributions from the conceptual model will yield a slope of 2 on a log (dQ/dt) versus log Q diagram (see line 2 in Figure 10). We believe that this is not an unreasonable slope value for characterizing base flow recession in steeper catchments, where the influence of the hillslopes on groundwater flow is significant, at least during the initial stage of a recession period, and thus where Boussinesq's theory is not valid [*Zecharias and Brutsaert*, 1988]. For the catchments used in this study, however, topographic effects on base flow recession characteristics are negligible and base flow observations correspond to Boussinesq's groundwater equation and therefore give a slope close to 1.5 on the log (dQ/dt) versus log Q diagram. For catchments with mild slopes the

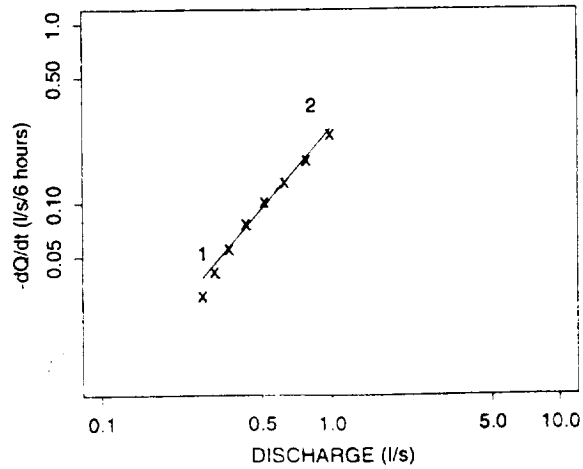

Fig. 10. Theoretical versus simulated base flow recession characteristics. X: log-log plot of $-dQ/dt$ versus discharge Q for numerically simulated base flow contribution; line 1: least squares fit to the data points (slope 1.57); and line 2: theoretical base flow characteristic from the conceptual model (slope 2).

base flow equation in the conceptual model should be modified in order to fully represent the recession dynamics.

Since the numerical model solves the three-dimensional Richards equation in an isotropic soil matrix it is not surprising that the calculated subsurface flow contributions (plotted points in Figure 10) during the drydown period in the simulation run for subcatchment WD-38 behave as predicted by Boussinesq's theory. In fact, the results from the numerical model yield a slope of 1.57 in Figure 10 (line 1).

Equations (25) offer the possibility of estimating the model parameter f based on recession observations. By imposing a slope of 2 on the data displayed in a log (dQ/dt) versus log Q diagram and by taking a lower envelope excluding 5% of the data, the value of the intercept can be calculated. Through the first of equations (25) a corresponding value of f can then be estimated. In (25) the drainage area plays the role of a scaling factor. A similar technique can be used to determine the parameter f in the numerical model. In future studies, different methods of calibrating both the numerical and conceptual models will be compared.

5. Summary

The evaluation of a conceptual catchment scale water balance model is presented. This evaluation is based on a comparison of simulation results from the conceptual model with results from a three-dimensional physically based numerical model and with field observations. The conceptual model relies on a topographic index to predict saturation excess runoff and on Philip's equation to predict infiltration excess runoff. The numerical model is based on the three-dimensional transient Richards equation. The study is carried out at two basin scales: a 7.2-km^2 catchment and a 0.64-km^2 subcatchment. These catchments are located in the North Appalachian ridge and valley region of eastern Pennsylvania. Detailed hydrologic data were collected for both catchments during the 12-day MACHYDRO 90 experiment.

Simplifying assumptions in the conceptual model concerning the spatial distribution and temporal evolution of water table depth, the distribution of soil moisture and pressure head in the unsaturated zone, and the characteristics of base flow recession are discussed. The hypothesis about the spatial and temporal evolution of local water table depth is tested by comparing the distribution of the topographic index with the distributions of the water table depth generated by the numerical model at the end of a 12-day simulation period. It is found that the use of a linear relationship between the local water table depth and the topographic index is reasonable in a basin scale water balance model. To test the effect of initial conditions, longer test runs with the numerical model are performed. Piezometric observations are compared to simulated groundwater dynamics. Close agreement between simulation results and field observations is obtained for shallow well observations. The hydraulic equilibrium assumption for the vertical distribution of soil moisture in the conceptual model is tested by examining the moisture profiles obtained from the numerical model. The results suggest that the conceptual model can be improved by using two layers to model the unsaturated zone. The characteristics of base flow recession for the conceptual and numerical models are compared with analytical solutions to Boussinesq's hydraulic equation and with observations. Based on this comparison we suggest that streamflow recession data can be used to calibrate both the conceptual model and the numerical model.

Further tests are required to confirm some of the findings discussed in this paper. Based on the 12-day simulation period for subcatchment WD-38 we conclude that the distribution of the topographic index is a reasonable measure for the local water table depth in Mahantango Creek. Detailed hydrologic data, as used in this study but for a longer period, are necessary to further justify this conclusion. The effect of catchment topography on the base flow recession characteristics, as suggested in section 4.4, should be further investigated. Other simplifying assumptions in the conceptual model, such as the calculation of soil moisture content, should be tested by comparing the simulation results with field observations and with remotely sensed information. A study comparing simulated soil moisture maps with soil moisture maps generated from remotely sensed information for WE-38 and WD-38 Mahantango Creek and based on MACHYDRO 90 data is in progress. This work will also involve extending some of the numerical simulation tests to WE-38 and to other catchments.

Acknowledgments. The work presented in this paper was supported by NASA (grant NAG 5-1628), U.S. Army Research Office (grant DAAL03-91-G-0165), USDA (grant 58-3K47-0-039), and the Italian NRC (grant 91.02615.PF42); this research support is gratefully acknowledged. The authors wish to thank Dominique Thongs for processing the DEM data used in this study. Comments from three anonymous reviewers are highly appreciated.

References

Band, L. E., Topographic partition of watersheds with digital elevation models, *Water Resour. Res.*, *22*(1), 15–24, 1986.

Beven, K. J., On subsurface stormflow: An analysis of response times, *Hydrol. Sci. J.*, *27*(4), 505–521, 1982.

Beven, K. J., and M. J. Kirkby, A physically based, variable contributing area model of basin hydrology, *Hydrol. Sci. Bull.*, *24*(1), 43–69, 1979.

Binley, A. M., K. J. Beven, and J. Elgy, A physically based model of heterogeneous hillslopes, 2, Effective hydraulic conductivities, *Water Resour. Res.*, *25*(6), 1227–1234, 1989.

Boussinesq, J., Recherches théoriques sur l'écoulement des nappes d'eau infiltrées dans le sol et sur le débit des sources, *J. Math. Pures Appl.*, *10*, 5–78, 1904.

Brooks, R. H., and A. T. Corey, Hydraulic properties of porous media, *Hydrol. Pap. 3*, Colo. State Univ., Fort Collins, 1964.

Brutsaert, W., The concise formulation of diffusive sorption of water in a dry soil, *Water Resour. Res.*, *12*(6), 1118–1124, 1976.

Brutsaert, W., and J. L. Nieber, Regionalized drought flow hydrographs from a mature glaciated plateau, *Water Resour. Res.*, *13*(3), 637–643, 1977.

Engman, E. T., Partial area hydrology and its applications to water resources, *Water Resour. Bull.*, *10*, 512–521, 1974.

Engman, E. T., and A. S. Rogowski, A partial area model for storm flow synthesis, *Water Resour. Res.*, *10*(3), 464–472, 1974.

Famiglietti, J. S., Aggregation and scaling of spatially variable hydrological processes: local, catchment scale, and macroscale models of water and energy balance, Ph.D. dissertation, Dep. of Civ. Eng. and Oper. Res., Princeton Univ., Princeton, N. J., 1992.

Famiglietti, J. S., E. F. Wood, M. Sivapalan, and D. J. Thongs, A catchment scale water balance model for FIFE, *J. Geophys. Res.*, *97*(D17), 18,997–19,007, 1992.

Freeze, R. A., Three-dimensional, transient, saturated-unsaturated flow in a groundwater basin, *Water Resour. Res.*, *7*(2), 347–366, 1971.

Freeze, R. A., and J. A. Cherry, *Groundwater*, Prentice-Hall, Englewood Cliffs, N. J., 1979.

Gan, T. Y., and S. J. Burges, An assessment of a conceptual rainfall-runoff model's ability to represent the dynamics of small

hypothetical catchments, 1, Models, model properties, and experimental design, *Water Resour. Res.*, *26*(7), 1595–1604, 1990*a*.

Gan, T. Y., and S. J. Burges, An assessment of a conceptual rainfall-runoff model's ability to represent the dynamics of small hypothetical catchments, 2, Hydrologic responses for normal and extreme rainfall, *Water Resour. Res.*, *26*(7), 1605–1620, 1990*b*.

Gburek, W. J., The Mahantango Creek watershed, General hydrology and research results, in *Proceedings of the Smithsonian Watershed Research Workshop*, edited by D. L. Correll, pp. 227–250, Chesapeake Bay Center for Environmental Studies, Edgewater, Md., 1977.

Gupta, V. K., and E. C. Waymire, On the formulation of an analytical approach to hydrologic response and similarity at the basin scale, *J. Hydrol.*, *65*, 95–123, 1983.

Gupta, V. K., and E. C. Waymire, Statistical self-similarity in river networks parameterized by elevation, *Water Resour. Res.*, *25*(3), 463–476, 1989.

Hillel, D., *Applications of Soil Physics*, Academic, San Diego, Calif., 1980.

Ibrahim, H. A., and W. Brutsaert, Intermittent infiltration into soils with hysteresis, *J. Hydraul. Div. Am. Soc. Civ. Eng.*, *94*(HY1), 113–137, 1968.

Loague, K. M., and R. A. Freeze, A comparison of rainfall-runoff modeling techniques on small upland catchments, *Water Resour. Res.*, *21*(2), 229–248, 1985.

Mesa, O. J., and E. R. Mifflin, On the relative role of hillslope and network geometry in hydrologic response, in *Scale Problems in Hydrology*, edited by V. K. Gupta, I. Rodríguez-Iturbe, and E. F. Wood, pp. 1–17, D. Reidel, Norwell, Mass., 1986.

Paniconi, C., Hydrologic processes in variably saturated porous media: Analysis of numerical methods for solving the nonlinear Richards equation, and application to catchment scale simulations, Ph.D. dissertation, Dep. of Civ. Eng. and Oper. Res., Princeton University, Princeton, N. J., 1992.

Paniconi, C., and E. F. Wood, A detailed model for simulation of catchment scale subsurface hydrologic processes, *Water Resour. Res.*, in press, 1993.

Paniconi, C., A. A. Aldama, and E. F. Wood, Numerical evaluation of iterative and noniterative methods for the solution of the nonlinear Richards equation, *Water Resour. Res.*, *27*(6), 1147–1163, 1991.

Philip, J. R., The theory of infiltration, 1, The infiltration equation and its solution, *Soil Sci.*, *83*, 345–357, 1957*a*.

Philip, J. R., The theory of infiltration, 2, The profile at infinity, *Soil Sci.*, *83*, 435–448, 1957*b*.

Polubarinova-Kochina, P. Y., *Theory of Ground Water Movement*, translated from Russian by R. J. M. De Wiest, Princeton University Press, Princeton, N. J., 1962.

Reeves, M., and E. E. Miller, Estimating infiltration for erratic rainfall, *Water Resour. Res.*, *11*(1), 102–110, 1975.

Rogowski, A. S., E. T. Engman, and E. L. Jacoby, Transient response of a layered, sloping soil to natural rainfall in the presence of a shallow water table, Experimental results, *Rep. ARS-NE-30*, Agric. Res. Serv., U.S. Dep. of Agric., Hyatsville, M. D., 1974.

Sivapalan, M., and E. F. Wood, Spatial heterogeneity and scale in the infiltration response of catchments, in *Scale Problems in Hydrology*, edited by V. K. Gupta, I. Rodriguez-Iturbe, and E. F. Wood, pp. 81–106, D. Reidel, Norwell, Mass., 1986.

Sivapalan, M., K. J. Beven, and E. F. Wood, On hydrologic similarity, 2, A scaled model of storm runoff production, *Water Resour. Res.*, *23*(12), 2266–2278, 1987.

Sloan, P. G., and I. D. Moore, Modeling subsurface stormflow on steeply sloping forested watersheds, *Water Resour. Res.*, *20*(12), 1815–1822, 1984.

Smith, R. E., and R.H.B. Hebbert, Mathematical simulation of interdependent surface and subsurface hydrologic processes, *Water Resour. Res.*, *19*(4), 987–1001, 1983.

Tarboton, D. G., R. L. Bras, and I. Rodriguez-Iturbe, Scaling and elevation in river networks, *Water Resour. Res.*, *25*(9), 2037–2051, 1989.

Troch, P. A., F. P. De Troch, and W. Brutsaert, Effective water table depth to describe initial conditions prior to storm rainfall in humid regions, *Water Resour. Res.*, *29*(2), 427–434, 1993.

Urban, J. B., The Mahantango Creek watershed, Evaluating the shallow groundwater regime, in *Proceedings of the Smithsonian Watershed Research Workshop*, edited by D. L. Correll, pp. 251–274, Chesapeake Bay Center for Environmental Studies, Edgewater, Md., 1977.

van Genuchten, M. T., and D. R. Nielsen, On describing and predicting the hydraulic properties of unsaturated soils, *Ann. Geophys.*, *3*(5), 615–628, 1985.

Wood, E. F., M. Sivapalan, K. J. Beven, and L. E. Band, Effects of spatial variability and scale with implications to hydrologic modeling, *J. Hydrol.*, *102*, 29–47, 1988.

Wood, E. F., M. Sivapalan, and K. Beven, Similarity and scale in catchment storm response, *Rev. Geophys.*, *28*(1), 1–18, 1990.

Zecharias, Y. B., and W. Brutsaert, Recession characteristics of groundwater outflow from mountainous watersheds, *Water Resour. Res.*, *24*(10), 1651–1658, 1988.

M. Mancini, Dipartimento di Ingegneria Idraulica, Ambientale e del Rilevamento, Politecnico di Milano, Piazza Leonardo da Vinci, Milano, Italy.

C. Paniconi, CRS4, Via Nazario Sauro 10, I-09123 Cagliari, Italy.

P. A. Troch, Laboratory of Hydrology and Water Management, Ghent University, Coupure Links 653, B9000 Gent, Belgium.

E. F. Wood, Water Resources Program, Department of Civil Engineering and Operations Research, Princeton University, Princeton, NJ 08544.

(Received July 15, 1992;
revised January 27, 1993;
accepted February 15, 1993.)

WATER RESOURCES RESEARCH, VOL. 29, NO. 6, PAGES 1601–1620, JUNE 1993

A Detailed Model for Simulation of Catchment Scale Subsurface Hydrologic Processes

CLAUDIO PANICONI[1] AND ERIC F. WOOD

Water Resources Program, Department of Civil Engineering and Operations Research, Princeton University, Princeton, New Jersey

A catchment scale numerical model is developed based on the three-dimensional transient Richards equation describing fluid flow in variably saturated porous media. The model is designed to take advantage of digital elevation data bases and of information extracted from these data bases by topographic analysis. The practical application of the model is demonstrated in simulations of a small subcatchment of the Konza Prairie reserve near Manhattan, Kansas. In a preliminary investigation of computational issues related to model resolution, we obtain satisfactory numerical results using large aspect ratios, suggesting that horizontal grid dimensions may not be unreasonably constrained by the typically much smaller vertical length scale of a catchment and by vertical discretization requirements. Additional tests are needed to examine the effects of numerical constraints and parameter heterogeneity in determining acceptable grid aspect ratios. In other simulations we attempt to match the observed streamflow response of the catchment, and we point out the small contribution of the streamflow component to the overall water balance of the catchment.

1. INTRODUCTION

The grid resolution required to obtain acceptable numerical solutions will be an important controlling factor in the computational feasibility of running large-scale catchment simulations. Discretization constraints can arise from physical or numerical considerations. Time steps can be numerically constrained in order to satisfy convergence, stability, or accuracy requirements. A physical constraint would typically be one which is imposed in order to capture the dynamics of a process of interest, for instance, a time step of the order of seconds or minutes if one is interested in the timing and magnitude of surface saturation and runoff responses during a heavy rainstorm. In the spatial domain one of the important constraints for a catchment scale subsurface model is connected to the aspect ratio of the numerical grid, which we define as the ratio of the horizontal mesh size Δx, Δy to the vertical discretization Δz. The horizontal extent of a large catchment will typically be much greater than its vertical length scale (large surface area and comparatively thin soil zone), and often a very fine vertical resolution, especially near the surface, is needed to accurately simulate infiltration and evaporation processes. Numerical catchment simulations are therefore computationally feasible so long as we can use grids with a large aspect ratio. If we are constrained to adopt smaller aspect ratios (decreasing Δx, Δy) in order to overcome numerical difficulties, then the size of the problem (number of degrees of freedom) can quickly exceed the capacity of available computers.

In this paper we describe a physically based three-dimensional finite element model for the simulation of subsurface hydrologic processes at the subcatchment and catchment scales, and we apply the model to a subcatchment of the Konza Prairie Research Natural Area near Manhattan, Kansas. The practical application of our model to actual catchments is demonstrated, and we investigate computational issues concerning the effects of model resolution (discretization, aggregation, and convergence constraints) on large-scale simulation of hydrologic processes.

One of the overriding problems in hydrology is the understanding of responses over the range of scales $O(10^{-1})$ to $O(10^4)$ km^2 [*Wood et al.*, 1988; *Goodrich and Woolhiser*, 1991]. The low end of this range is roughly the size of a small subcatchment and marks a transition from point and hillslope scales, at which physically based hydrologic models are more easily tested and better understood, to catchment or basin scales. The high end corresponds to the horizontal grid scale used in general circulation models for global climate simulations, and a better understanding of hydrologic processes at this scale is required to improve the land surface boundary conditions for these models. The parameterization of hydrologic processes at large scales is made difficult by the high degree of nonlinearity and variability in catchment parameters and inputs, and thus conceptual or idealized models are often used at these scales. Physically based analytical or numerical models can be used to study the validity of simplifying assumptions in conceptual models. Some examples can be found in the works by *Reeves and Miller* [1975] (time compression approximation for partitioning rainfall into runoff and infiltration), *Broadbridge and White* [1987] (time to ponding), *Gan and Burges* [1990*a*, *b*] (catchment rainfall-runoff models), *Shamsai and Narasimhan* [1991] (Dupuit-Forchheimer assumption under seepage face conditions), *Sloan and Moore* [1984] and *Stagnitti et al.* [1986] (subsurface flow models), *Wilcox et al.* [1990] (runoff prediction models), and *Troch et al.* [1993] (catchment scale water balance models).

Other studies using physically based hillslope and catchment scale models include the early work of *Freeze* [1971, 1972*a*, *b*], who used a three-dimensional finite difference variably saturated flow model coupled with a one-dimensional channel flow model to reveal the importance of subsurface flow processes and parameter variability on watershed runoff response. *Smith and Hebbert* [1983] simplified the model used by Freeze and applied it to an experimental hillslope in Western Australia to investigate the effects of rainfall, soil properties, and hillslope geometry

[1]Now at CRS4, Cagliari, Italy.

Paper number 92WR02333.
0043-1397/93/92WR-02333$05.00

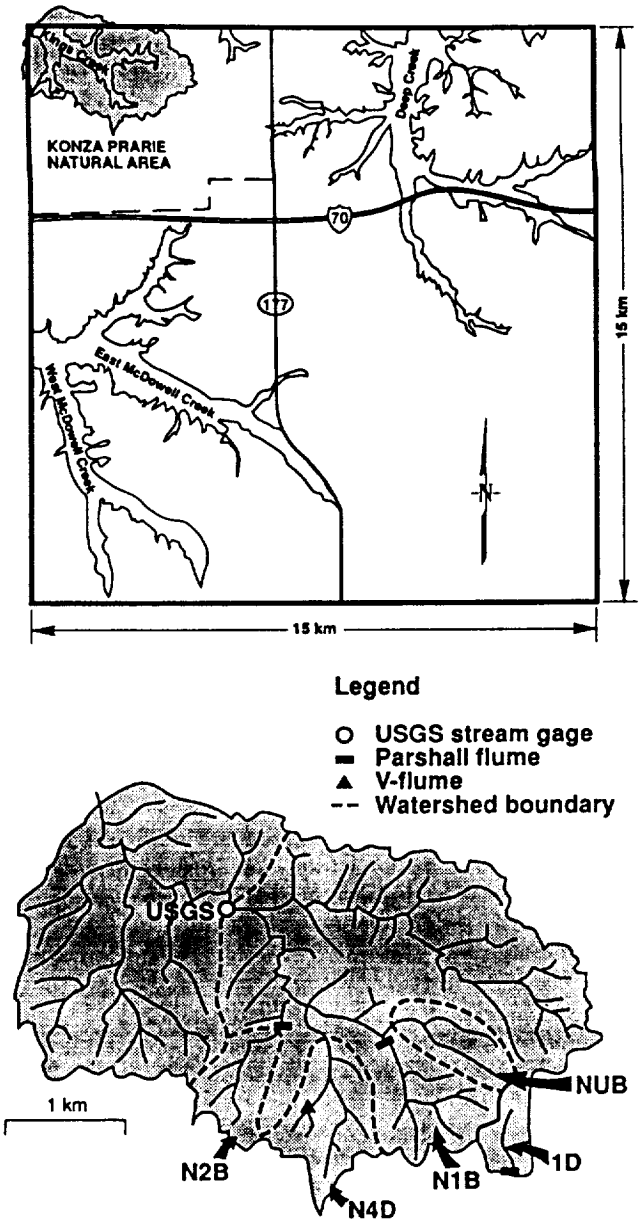

Fig. 1. Map showing location of the Konza Prairie Research Natural Area, the Kings Creek catchment, and the 1D subcatchment.

on runoff. *Loague and Freeze* [1985] and *Loague* [1990] compared the performance of a simple linear regression model, a unit hydrograph model, and a quasi-physically based model in simulating rainfall-runoff response on small catchments. *Beven* [1977], *Bathurst* [1986], and *Govindaraju and Kavvas* [1991] coupled one- or two-dimensional subsurface flow models to physically based models of overland flow and channel flow. *Binley et al.* [1989*a*, *b*] used a three-dimensional model of variably saturated flow to explore the effects of spatially variable hydraulic conductivity and the validity of using an equivalent or effective conductivity value.

The formulation of the numerical model presented here is consistent with one of the long-term objectives of our work, which is to simulate a large catchment such as the Kings Creek catchment shown in Figure 1, containing many distinct subcatchment units and a complex stream network. In this paper we describe simulations of the 1D subcatchment (Figures 1 and 2) located near the Kings Creek catchment (note that "1D" is a site name and bears no relation to the dimensionality of the subcatchment). The primary input to the model is digital topographic data obtained from the U.S. Geological Survey. The original data are in regular grid form, with a resolution of 30 × 30 m, but can be readily interpolated or extrapolated to finer or coarser discretizations. An automated extraction algorithm [*Band*, 1986] is applied to the topographic data to produce a mapping of stream channels, catchment boundaries, and subcatchment partitions. Field observations and remotely sensed data are used for parameterization and calibration of the model. Atmospheric inputs to the model are specified as rainfall and evaporation boundary conditions, and the switching to and from atmosphere- and soil-controlled surface inputs is handled automatically.

The catchment simulation model is based on the three-dimensional Richards equation describing fluid flow in variably saturated porous media. Of the many numerical issues associated with large-scale three-dimensional simulations, some which are specific to catchment subsurface flow modeling include, first, the nonlinearity of Richards's equation, and, at the interface between the saturated and unsaturated zones, possible discontinuities in the nonlinear coefficients and a change in type of the governing partial differential equation (parabolic to elliptic). The nonlinear system integrals require numerical evaluation or some other approximation technique, introducing additional error in the model. Moreover convergence of iterative schemes used to solve the nonlinear equation cannot be guaranteed, and the rate of convergence will depend upon many factors (such as the time step, which directly affects the quality of the initial solution estimate used in an iterative procedure). A second issue is naturally occurring spatial and temporal variability in soils, topography, vegetation, rainfall, and evaporation, requiring complex boundary conditions and a high degree of heterogeneity in the model parameterization. This can produce ill-conditioned system matrices and adversely affect the convergence behavior of linear and nonlinear iterative solvers. A third issue is the irregular geometry of catchments, resulting in sparse system matrices which are not regularly structured. A final issue to note is the large horizontal extent of a catchment compared to its vertical range and vertical discretization requirements, producing distorted elements.

A series of test simulations on three small hypothetical catchments was conducted to evaluate the performance of the numerical code [*Paniconi*, 1991]. The simulations involved alternating episodes of rainfall and evaporation, and generated significant amounts of discharge, infiltration, and saturation excess runoff. The tests included a comparison of lumped and distributed mass matrix versions of the code and a comparison of direct and iterative solvers for the linearized system of equations in the model. Various storage schemes for the system matrices and for the Jacobian coordinate transformation components were also examined.

In the next section we introduce the catchment simulation model and describe in detail the generation of the numerical grid and the representation of various hydrologic processes. This is followed by a description of the Konza Prairie 1D catchment and observation data. The simulation model is then applied to a 17-day rainfall-interstorm sequence where

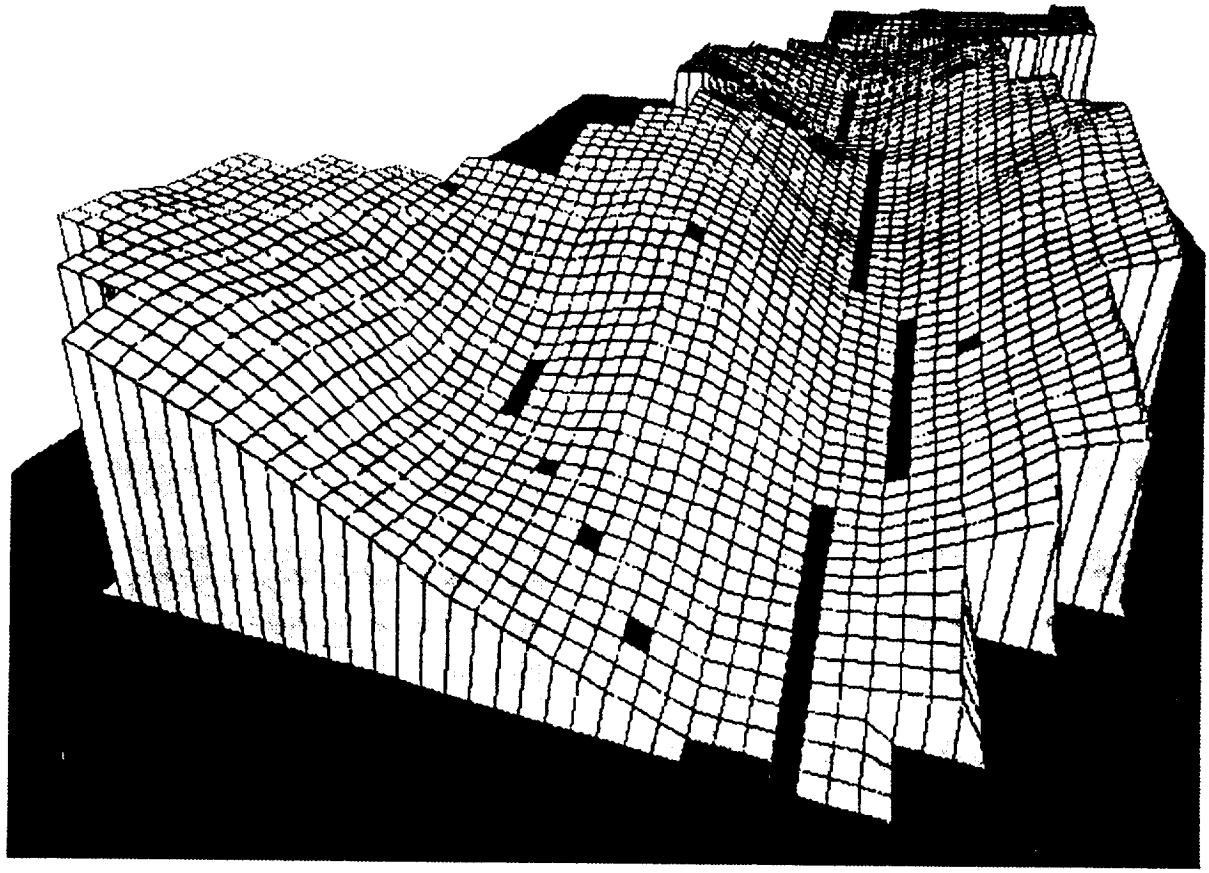

Fig. 2. Elevation image of subcatchment 1D-10 (10 × 10 m grid resolution) showing stream (solid pixels) and location of three surface nodes selected for vertical profile output (shaded pixels).

we discuss some calibration results. We use detailed and averaged rainfall rates for the 17-day simulation to illustrate temporal aggregation effects. Model resolution effects are discussed in more detail in section 4, where we use a 9-day interstorm simulation to examine aspect ratio and convergence constraints.

2. Description of the Model

2.1. *Assumptions and Limitations*

Basing our numerical model for flow in variably saturated porous media on Darcy's law and Richards's equation, we adopt the usual set of assumptions: Flow is laminar and isothermal, inertial forces and chemical gradients are neglected, and the air phase is continuous and at atmospheric pressure [e.g., *Freeze and Cherry*, 1979; *Hillel*, 1980*a*; *Sposito*, 1986]. In addition, we do not account for hysteresis, we assume that the porous medium is isotropic, and we consider only flow within the "soil matrix," neglecting flow through "macropores." Anisotropy can be easily incorporated with a generalization of the hydraulic conductivity term in the model equations. Since our model treats both precipitation and evaporation inputs, it will be important to consider hysteresis effects in future versions of the code. *Mualem* [1974], *Parlange* [1976], and *Kool and Parker* [1987] discuss some conceptual models of hysteresis for soil moisture characteristic equations.

Whereas anisotropy and hysteresis can be readily incorporated into our catchment simulation model, treating nonisothermal effects and macropore flow would require significant extensions or generalizations of the model. Several recent studies suggest that macropore flow (also described as bypass flow, channeling, pipe flow, or preferential flow) may contribute significantly to the transport of water through hillslopes and catchments [e.g., *McDonnell*, 1990; *Pearce*, 1990]. The term macropore generally refers to continuous pore structures which can exhibit nonequilibrium channeling flow, and it may not be appropriate to model this type of flow based on Darcy's law [*Beven and Germann*, 1982]. Two-domain models have been proposed for describing the flow and interactions in a soil matrix/macropore system, and kinematic wave models have also been introduced [e.g., *Germann*, 1990].

Subsurface heat transport and temperature-induced soil moisture flow are important not only for long-term simulations which need to account for seasonal changes in temperature, but also for short-term simulations when one considers the effects of diurnal fluctuations in solar and atmospheric radiation on near-surface soil moisture processes such as evaporation. *Milly* [1982] presents a physically based one-dimensional coupled moisture and heat flow model based on studies of nonisothermal flow in porous media by *Philip and de Vries* [1957] and *de Vries* [1958]. The model treats moisture flow in both the liquid and vapor phases and latent and sensible heat transport by conduction and advection.

The limitations described above pertain to the physics of flow processs within a porous medium. In a realistic basin

scale model one must consider not only the coupling of processes in the saturated and unsaturated zones (soil matrix and macropores, air and liquid phases, heat and moisture flows), but also the coupling between subsurface, surface, and atmospheric hydrologic processes. Surface processes which affect and are affected by subsurface moisture and energy states include overland flow and streamflow [*Eagleson*, 1970; *Freeze*, 1974] and vegetation growth and transpiration [e.g., *Federer*, 1979]. The coupling with atmospheric processes takes us into the realm of large-scale water and energy balance models [e.g., *Eagleson*, 1978, 1979] which can become a component of general circulation models. *Avissar and Verstraete* [1990] discuss some of the difficulties involved in representing small-scale surface processes (such as albedo, stomatal response, momentum transfer, surface roughness, and soil moisture flow) in large-scale atmospheric models.

2.2. *Governing Equations and Numerical Procedures*

The three-dimensional Richards equation with pressure head ψ as the dependent variable can be written as

$$S(\psi)\frac{\partial \psi}{\partial t} = \nabla \cdot [K_s K_r(\psi)\nabla(\psi + z)] \tag{1}$$

where t is time, z is the vertical coordinate, positive upward, and the hydraulic conductivity K is expressed as a product of the conductivity at saturation, K_s, and the relative conductivity, K_r. We use an extension of the van Genuchten characteristic equations [*van Genuchten and Nielsen*, 1985] to describe the nonlinear dependencies of volumetric moisture content θ, specific moisture capacity S, and relative hydraulic conductivity K_r on pressure head [*Paniconi et al.*, 1991]:

$$\begin{aligned} \theta(\psi) &= \theta_r + (\theta_s - \theta_r)[1 + \beta]^{-m} \qquad \psi \le \psi_0 \\ \theta(\psi) &= \theta_r + (\theta_s - \theta_r)[1 + \beta_0]^{-m} + S_s(\psi - \psi_0) \\ & \qquad \psi \ge \psi_0 \end{aligned} \tag{2}$$

$$\begin{aligned} S(\psi) &= \frac{d\theta}{d\psi} = \frac{(n-1)(\theta_s - \theta_r)|\psi|^{n-1}}{|\psi_s|^n(1+\beta)^{m+1}} \qquad \psi \le \psi_0 \\ S(\psi) &= \frac{d\theta}{d\psi} = S_s \qquad \psi \ge \psi_0 \end{aligned} \tag{3}$$

$$\begin{aligned} K_r(\psi) &= (1+\beta)^{-5m/2}[(1+\beta)^m - \beta^m]^2 \qquad \psi \le 0 \\ K_r(\psi) &= 1 \qquad \psi \ge 0 \end{aligned} \tag{4}$$

where θ_r is the residual saturation, θ_s is the saturated moisture content, ψ_s is the capillary or air entry pressure head value, S_s is the specific storage, $m = 1 - 1/n$, $\beta = (\psi/\psi_s)^n$, $\beta_0 = \beta(\psi_0) = (\psi_0/\psi_s)^n$, ψ_0 is a continuity parameter, and n can be interpreted as a pore size distribution index. The exponential relationship

$$K_s = K_s(z) = K_{s_0}\exp[-f(L - z)] \tag{5}$$

is used to model vertical heterogeneity of saturated hydraulic conductivity [*Beven*, 1982, 1984], where K_{s_0} is the saturated conductivity at the surface, f is a fitting parameter, and L is the elevation at the surface above the datum $z = 0$.

To solve (1) numerically we use a finite element Galerkin discretization in space and a finite difference discretization of the time derivative term [e.g., *Ames*, 1977; *Huyakorn and Pinder*, 1983]. The problem domain is discretized into M hexahedral elements and an approximating function is introduced:

$$\psi(x, y, z, t) \approx \hat{\psi}(x, y, z, t) = \sum_{e=1}^{M} \hat{\psi}^{(e)}(x, y, z, t) \tag{6}$$

In local coordinate space (ξ, η, ζ) the approximating function for each element (e) is written as

$$\begin{aligned} \hat{\psi}^{(e)}(\xi, \eta, \zeta, t) &= \sum_{i=1}^{8} N_i^{(e)}(\xi, \eta, \zeta)\psi_i^{(e)}(t) \\ &= (\mathbf{N}^{(e)}(\xi, \eta, \zeta))^T \boldsymbol{\Psi}^{(e)}(t) \end{aligned} \tag{7}$$

where $\psi_i^{(e)}$ are undetermined nodal values of ψ and $N_i^{(e)}$ are trilinear Lagrange basis functions which define, in local coordinate space, a cubic element with eight nodes at $(\pm 1, \pm 1, \pm 1)$. The basis functions have the general form $N_i(\xi, \eta, \zeta) = (1 \pm \xi)(1 \pm \eta)(1 \pm \zeta)/8$. The finite element formulation used is isoparametric, with the mapping from local (ξ, η, ζ) to global (x, y, z) coordinate space given by

$$\begin{aligned} (x, y, z) = \Bigg(& \sum_{i=1}^{8} N_i(\xi, \eta, \zeta)x_i, \\ & \sum_{i=1}^{8} N_i(\xi, \eta, \zeta)y_i, \sum_{i=1}^{8} N_i(\xi, \eta, \zeta)z_i \Bigg) \end{aligned} \tag{8}$$

where (x_i, y_i, z_i), $i = 1, \cdots, 8$ are the global coordinates of the eight corner nodes of element (e).

The finite element spatial discretization yields the system of ordinary differential equations

$$\mathbf{A}(\boldsymbol{\Psi})\boldsymbol{\Psi} + \mathbf{F}(\boldsymbol{\Psi})\frac{d\boldsymbol{\Psi}}{dt} = \mathbf{q}(t) - \mathbf{b}(\boldsymbol{\Psi}) \tag{9}$$

where $\boldsymbol{\Psi}$ is the vector of undetermined coefficients representing the value of pressure head at each node. The system components for each element (e) are

$$\begin{aligned} \mathbf{A}^{(e)} = \int\int\int_{\Omega^{(e)}} & K_s^{(e)} K_r(\hat{\psi}^{(e)})[\mathbf{N}_{,x}^{(e)}(\mathbf{N}_{,x}^{(e)})^T \\ & + \mathbf{N}_{,y}^{(e)}(\mathbf{N}_{,y}^{(e)})^T + \mathbf{N}_{,z}^{(e)}(\mathbf{N}_{,z}^{(e)})^T]\, d\Omega^{(e)} \end{aligned} \tag{10}$$

$$\mathbf{b}^{(e)} = \int\int\int_{\Omega^{(e)}} K_s^{(e)} K_r(\hat{\psi}^{(e)})\mathbf{N}_{,z}^{(e)}\, d\Omega^{(e)} \tag{11}$$

$$\mathbf{F}^{(e)} = \int\int\int_{\Omega^{(e)}} S(\hat{\psi}^{(e)})\mathbf{N}^{(e)}(\mathbf{N}^{(e)})^T\, d\Omega^{(e)} \tag{12}$$

$$\mathbf{q}^{(e)} = \int\int_{\Gamma_N^{(e)}} q_{\Gamma_N^{(e)}}\mathbf{N}^{(e)}\, d\Gamma_N^{(e)} \tag{13}$$

where $q_{\Gamma_N^{(e)}}$ is the specified Darcy flux on the natural boundary $\Gamma_N^{(e)}$. We use the notation $\mathbf{N}_{,x}$ to denote differentiation with respect to x, and $\mathbf{N}^T$ to denote the transpose of N. A lumped form of the mass matrix $\mathbf{F}^{(e)}$ is used:

$$\mathbf{F}^{(e)} = \int\int\int_{\Omega^{(e)}} S(\hat{\psi}^{(e)})\mathbf{N}^{(e)}\, d\Omega^{(e)} \qquad (14)$$

where now $\mathbf{N}^{(e)}$ is taken to be a diagonal matrix rather than a vector.

The system integrals are nonlinear and must be evaluated numerically. We use order 2 Gaussian quadrature with weights of 1.0 and Gauss points at $(\xi, \eta, \zeta) = (\pm 1/\sqrt{3}, \pm 1/\sqrt{3}, \pm 1/\sqrt{3})$. The saturated hydraulic conductivity K_s is assumed constant over each element.

To evaluate the system integrals in local coordinate space we need to compute the determinant of the Jacobian of the global to local coordinate transformation. For the integrals (10) and (11) we also need the inverse of the Jacobian to compute the derivatives of the basis functions (for instance, $\partial N_i/\partial x = (\partial N_i/\partial \xi)(\partial \xi/\partial x) + (\partial N_i/\partial \eta)(\partial \eta/\partial x) + (\partial N_i/\partial \zeta)(\partial \zeta/\partial x)$). The components of the Jacobian and inverse Jacobian will be spatially dependent due to the quadratic and cubic terms in the basis functions. The cost of computing and storing the Jacobian determinant and inverse Jacobian at each Gauss integration point for each element can be quite high for a three-dimensional simulation. For our particular model we could have taken advantage of special features of our catchment discretization to simplify the transformation of (8), thereby minimizing the storage and CPU expenses associated with the Jacobians. For instance, some of the spatial dependencies in (8) can be eliminated when using rectangular elements with the element edges aligned with the global coordinate axes. Furthermore, there are similarities in the Jacobian components from element to element which can be exploited if we use grid spacing in any of the coordinate directions. In the current implementation of the model we use the most general form of the mapping from local to global coordinates, as given by (8), without taking advantage of particular features of our grid geometry.

The Crank-Nicolson finite difference scheme is used to discretize (9) in time. The resulting equation is

$$\mathbf{A}(\Psi^{k+(1/2)})\Psi^{k+(1/2)} + \mathbf{F}(\Psi^{k+(1/2)})\frac{\Psi^{k+1} - \Psi^k}{\Delta t} = \mathbf{q}(t^{k+(1/2)}) - \mathbf{b}(\Psi^{k+(1/2)}) \qquad (15)$$

where superscript k represents time level and $\Psi^{k+(1/2)} = (\Psi^{k+1} + \Psi^k)/2$.

Equation (15) is linearized using Picard iteration, which we can write as

$$\left(\frac{1}{2}\mathbf{A}^{k+(1/2),(m)} + \frac{1}{\Delta t}\mathbf{F}^{k+(1/2),(m)}\right)(\Psi^{k+1,(m+1)} - \Psi^{k+1,(m)}) = -\mathbf{f}(\Psi^{k+1,(m)}) \qquad (16)$$

where superscript (m) denotes iteration level and

$$\mathbf{f}(\Psi^{k+1}) \equiv \frac{1}{2}\mathbf{A}^{k+(1/2)}(\Psi^{k+1} + \Psi^k) + \mathbf{F}^{k+(1/2)}\frac{\Psi^{k+1} - \Psi^k}{\Delta t} - \mathbf{q}^{k+(1/2)} + \mathbf{b}^{k+(1/2)} = \mathbf{0} \qquad (17)$$

To solve the linear system of equations represented in (16) we use a conjugate gradient algorithm from ITPACK [*Kincaid et al.*, 1982] with a symmetric successive overrelaxation preconditioner and a compact nonsymmetric storage scheme. The structure of the system matrix resulting from (16) is sparse and symmetric with a maximum of 27 (3^3) nonzero entries per row. For irregular catchment geometries such as shown in Figure 2 the bandwidth will not be constant over the matrix and can become quite large for some rows.

2.3. *Model Inputs and Representation of Hydrologic Processes*

The catchment simulation model comprises two programs: a grid generator which constructs the finite element mesh and initializes various parameters, and the actual simulation program which numerically solves the three-dimensional Richards equation over a specified time period for a given set of boundary and initial conditions.

The design and structure of the mesh generation and simulation programs were motivated in large part by the availability of digital elevation models (DEMs) of topography from the U.S. Geological Survey. These data bases provide topographic information for extensive geographic regions at high resolution and in regular grid form (30 × 30 m pixels). An automated extraction algorithm [*Band*, 1986] is applied to the DEM data to produce a mapping of stream channels, ridges, and drainage basins and subbasins. Based on this mapping we can define the boundaries of a catchment, obtain elevation, stream, and distance-to-stream data, and subdivide the catchment into physically consistent subcatchments. Figure 2 is a subcatchment image produced using some of the output from the extraction algorithm. The three shaded pixels in this image show the location of three surface nodes selected for detailed vertical profile output during the numerical simulation and the solid pixels outline the stream network.

The finite element mesh generator was developed to take advantage of the regular grid structure of the digital elevation data and to use the information provided by the extraction algorithm. The mesh generation algorithm discretizes a catchment or subcatchment into hexahedral elements, numbers and connects the nodes and elements, initializes the pointer arrays for storing the system matrices, and sets up the boundary and initial conditions for ensuring simulation. A compact storage scheme is used for the sparse system matrices.

The simulation program takes the information from the grid generator, and for each time step of the simulation period it performs the iterations on the nonlinear equation, sets up and solves the linearized system of equations, calculates mass balance errors, and computes the hydrograph contributions. The simulation program is an extension of the model by *Binley et al.* [1989*a*, *b*].

The geometry of a catchment as defined by the DEM extraction algorithm is based on the location of naturally occurring ridges. The finite element method allows us to model irregular domains so there is no smoothing or transformation applied to redefine the catchment boundaries. The ridges are assumed to represent vertical walls which we consider to be impermeable lateral boundaries, and we also define the base of the catchment as a no-flux boundary. The only boundary conditions which need to be explicitly input

are those at the surface (precipitation and evaporation rates). This method of treating nonsurface boundaries is a simplification of the acutal physical processes, and its validity needs to be examined in more detail. In principle the model can handle any type of boundary condition, but there is often a lack of knowledge and data concerning flow processes across nonsurface boundaries. If we define the vertical extent of a catchment deep enough so as not to affect processes (infiltration, runoff, evaporation) occurring near the surface, or if we know the location of an underlying low-permeability layer, then an impermeable boundary condition at the base of the catchment is justified. Defining a deep catchment and analyzing, for example, the simulated flow behavior near the water table could be one method of determining more suitable boundary conditions when a no-flux condition is inappropriate at the catchment base. A similar method for assessing the validity of the zero-flux condition along lateral boundaries would be to simulate a catchment and examine the computed flow patterns across the ridge boundaries of each of the subcatchments which make up the catchment.

The catchment topography is heterogeneous, with elevation inputs obtained directly from the DEM data. The data are in regular grid form, and we retain this uniform grid structure in defining the x and y (horizontal) dimensions of each element of our numerical grid. The size of each DEM pixel is $\Delta x \times \Delta y = 30 \times 30$ m, and it is an easy matter to interpolate these data to a finer grid or to aggregate it to a coarser resolution. In our simulations of the 1D catchment we used linear interpolation to obtain a range of catchment discretizations from 30×30 m to 1×1 m. Although we use uniform grid spacing horizontally ($\Delta x = \Delta y$, constant), the vertical discretization Δz can be variable. This allows us to define, for instance, thinner layers closest to the surface. The mesh generation program has the option of making the thickness of each layer uniform horizontally (this results in a staggered catchment base), or of making the base of the catchment flat (resulting in horizontally nonuniform layer thicknesses).

To treat flow processes occurring on the catchment surface and in streams we need to couple Richards's equation governing subsurface flow, the shallow water equations for channel flow, and a kinematic or shallow water model for overland flow [*Eagleson*, 1970; *Freeze*,1974]. In the current version of our model we use a simple linear transformation to distribute overland flow. Surface runoff generated at a point on the catchment is routed to the stream via a time delay determined from the overland flow velocity (currently assumed constant for the catchment) and the shortest distance from the point to the stream. The location of the stream and values for the shortest overland paths to the stream ("delay distances") are obtained from the DEM extraction algorithm. We note that this approach does not allow for downslope reinfiltration of overland runoff. This simple treatment of overland flow routing is a reasonable approximation when partial contributing areas are the main source of surface runoff. These saturated regions will typically grow as an expanded stream network during a rainfall event [*Dunne and Black*, 1970] so that downslope reinfiltration will not occur and the distances for overland travel will remain relatively short. Streams can be modeled as specified head boundaries (permanent streams), or we can assign stream nodes initially high levels of saturation (ephemeral streams). Channel flow is not considered in the model. Seepage faces and stream banks can be handled numerically [*Neuman*, 1973; *Cooley*, 1983; *Huyakorn et al.*, 1986] but are somewhat complicated to discretize in the case where the stream is internal to the catchment rather than being situated along a lateral boundary. Wide internal streams require a dual stream bank configuration, with the location of stream banks and seepage faces automatically generated from analysis of the DEM data. The current implementation of the model does not have this feature.

In addition to heterogeneities in topography it is important to account for variability in the catchment soils and in the atmospheric inputs to the model. At present the model considers only spatial variability in saturated hydraulic conductivity K_s and spatial and temporal variability in evaporation and precipitation rates. Other parameters, namely f, θ_r, θ_s, ψ_s, n, S_s, and $\psi_{\min}$ described below, are kept constant over the catchment. The extension to spatially variable representation of these parameters is straightforward to implement in the model, although high levels of parameter heterogeneity may adversely affect numerical performance [*Ababou et al.*, 1989]. Values for the soil hydraulic parameters θ_r, θ_s, ψ_s, n, and S_s can be obtained by fitting (2) and/or (4) to observed data or by using other information about the catchment soils. Saturated conductivities are input for each node on the catchment surface, and relationship (5) is used to assign K_s values vertically. The value of parameter f can be estimated by fitting observed K_s data to (5), as shown later. By allowing spatial and temporal variability in precipitation and evaporation it is possible to simulate alternating periods of soil wetting and drying, and to have rainfall and evaporation occurring simultaneously over different portions of the catchment. For the simulations described in this paper we used spatially homogeneous rainfall and evaporation since the 1D catchment is quite small.

At any surface node the simulation program automatically switches from a specified flux (Neumann) to a constant head (Dirichlet) boundary condition when the node becomes saturated or its pressure head becomes smaller than the "air-dry" pressure head value $\psi_{\min}$ [*Hillel*, 1980*b*, p. 121]. The boundary condition switches back to a Neumann type when the magnitude of the flux across the soil surface (computed) exceeds the magnitude of the atmospheric (specified) flux, or when the atmospheric event switches from rainfall to evaporation or evaporation to rainfall. For Dirichlet nodes the flux across the surface is computed by back solving (16) for $\mathbf{q}$ after having solved for the pressure heads. Surface boundary conditions are updated in this manner after each nonlinear iteration.

The initial conditions required for a transient simulation are input as nodal pressure head values. The initial head distribution can be obtained by solving a steady state problem, for example. Alternatively, we can generate the initial heads based on knowledge of the initial water table distribution or initial soil saturation deficits. One method of calculating water table depths or saturation deficits uses a topographic index (computed from the digital elevation data) together with surface K_s values, the exponential parameter f, and a base flow parameter [*Sivapalan et al.*, 1987]. A water table depth or soil moisture deficit can be converted into a vertical pressure head distribution using, for instance, a hydrostatic assumption.

The final group of input parameters to the simulation program are for dynamic time step control, back stepping, monitoring convergence of the nonlinear iterations, and controlling the generation of output for postprocessing. The specified convergence tolerance is *tol*, and the maximum number of nonlinear iterations allowed during a time step is *maxit*. In our simulations we used the convergence test $\|\Psi^{k+1,(m+1)} - \Psi^{k+1,(m)}\|_\infty \leq tol$. The simulation begins with a time step of Δt_0 and proceeds until time T_{max}. The current time step is increased by a factor of Δt_{mag} (to a maximum of Δt_{max}) if convergence of the nonlinear system is achieved in fewer than $maxit_2$ iterations, whereas the time step is decreased by a factor of Δt_{red} (to a minimum of Δt_{min}) if convergence required more than $maxit_2$ iterations. We back step with a reduced time step (factor Δt_{red}, to a minimum of Δt_{min}) if convergence is not attained (*maxit* exceeded).

2.4. *Model Outputs*

Catchment simulation output is processed to produce plots, images, and summary statistics. Vertical profiles of pressure head and moisture content are plotted at various times to show, for instance, the water table response during the simulation. Shaded or color images of surface saturation can show the different mechanisms contributing to surface runoff on various portions of the catchment and the growth of partial contributing areas. Surface images of moisture content, pressure head, and flux values can also be easily produced, as can images along nonsurface cross sections of the catchment.

Hydrograph plots of actual and potential catchment inflows and outflows are produced. The potential inflow in a hydrograph plot consists of the precipitation (positive) and evaporation (negative) flux inputs supplied to the model. When the potential flux is positive, the difference between potential and actual soil inflow is the total runoff. Surface runoff is produced when the surface becomes saturated, either due to a rising water table (saturation excess mechanism) or to the infiltration capacity of the soil's falling below the rainfall rate (infiltration excess mechanism) [*Freeze*, 1974]. In both cases the boundary condition at the node on the surface where saturation occurs switches from a Neumann type (atmosphere-controlled inflow) to a Dirichlet type (soil-controlled inflow). Subsurface runoff in our model is only produced when the soil moisture flux becomes negative across the surface during a rainfall event, that is, when subsurface water exits the soil matrix from a saturated region on the surface. This type of subsurface runoff is sometimes called "return flow" [*Dunne and Black*, 1970]. The path of return flow to the stream is initially subsurface and becomes overland flow when it emerges at the surface. Without stream banks there is no way to treat seepage face subsurface flow. The stream discharges in a hydrograph plot are the surface and subsurface runoff components routed to the stream via the time delays computed from the overland flow velocity and shortest overland paths to the stream. There is no routing along the stream channel to the catchment outlet.

The convergence behavior (for both the nonlinear iterative scheme and the linear solver) and mass balance errors (absolute and normalized) are plotted for each catchment simulation. These plots can help pinpoint trouble spots in a simulation, which often occur during transition periods between rainfall and evaporation, during heavy rainfall episodes, or when the catchment or catchment surface become highly saturated. Absolute mass balance errors are computed at each time step as the difference between the change in moisture storage in the catchment soil and the net boundary influx (amount of water entering or leaving the catchment at the boundaries). The moisture storage is calculated by integrating the $\theta(\psi)$ (equation (2)) over each element and summing over all elements. In the current version of the model, nonzero boundary fluxes occur only at the catchment surface, so the net influx is obtained using the specified atmospheric rates (for Neumann nodes) or the back solved fluxes (for Dirichlet nodes). Normalized or relative mass balance errors are obtained by dividing the absolute mass balance errors by the net influx (and multiplying the result by 100 for a percentage error).

3. SIMULATION OF THE KONZA PRAIRIE 1D CATCHMENT

We apply our three-dimensional numerical model to simulate a subcatchment (catchment "1D") of the Konza Prairie Research Natural Area in northeastern Kansas. Observation data collected during a 1987 field experiment are used to parameterize and calibrate the model.

Whereas extensive streamflow, evaporation (actual rates), and rainfall data were available for the simulation periods of interest, very little soil data specific to the 1D subcatchment were collected, and in some cases parameter estimates were made using generic soil characteristics for the region. Parameterization of the model is therefore adequate for the atmospheric boundary conditions but less than satisfactory for the saturated conductivity distribution, soil zone depths, characteristic equations, and initial conditions. Due to lack of data some degree of calibration is needed even though the model is physically based. Moreover, the streamflow component of the 1D catchment water balance is of much smaller magnitude than water losses due to evaporation, so that model calibration based on observed streamflow hydrographs alone is of limited use. For these reasons a comprehensive and rigorous model assessment, according to procedures such as those described by *James and Burges* [1982], will not be our focus. Evaluation of possible model errors and a more detailed calibration should be conducted using potential evaporation measurements and soil moisture content data in addition to streamflow observations. Data and measurement error would also need to be quantified and taken into account.

3.1. *Description and Discretization of the Catchment*

The Kings Creek catchment and 1D subcatchment are in the Konza Prairie Research Natural Area near Manhattan, Kansas, in the northeastern part of the state (Figure 1). The Konza site, part of the Flint Hills Upland geologial region, is a 34.87 km^2 area of native tallgrass (blue stem) prairie and is one of 11 sites selected for the Long-Term Ecological Research (LTER) program of the National Science Foundation [*Bhowmik*, 1987]. The Konza area has a temperate midcontinental climate with average annual precipitation of about 835 mm. Streamflow is ephemeral with high flows during the winter and late spring but dry in the summer and

TABLE 1. Discretization of 1D Catchment

Catchment	Grid Resolution	Number of Nodes	Number of Elements	Sparsity, %	Storage, $\times 10^6$ words
1D-30	30 × 30 m	1,570	1,064	98.280	0.148
1D-15	15 × 15 m	5,795	4,256	99.534	0.549
1D-10	10 × 10 m	12,680	9,576	99.787	1.20
1D-06	6 × 6 m	34,430	26,600	99.922	3.28
1D-05	5 × 5 m	49,295	38,304	99.945	4.70
1D-03	3 × 3 m	135,355	106,400	99.980	12.91

late fall except during heavy rainstorms [*Engman et al.*, 1989]. The 1D subcatchment has a surface area of 0.24 km^2 and is situated in the southeast corner just off the Kings Creek catchment. The U.S. Geological Survey digital elevation data for the 1D catchment contain 314 pixels at 30 × 30 m resolution.

Soil, streamflow, rainfall, and evaporation data at the Konza site were collected during summer 1987, from late May to mid-October, as part of an international field experiment (the First International Satellite Land Surface Climatology Project Field Experiment, or FIFE) to study land-atmospheric interactions for global climate modeling [*Sellers et al.*, 1990]. Using the observation data we applied our catchment model to simulate the 1D subcatchment for a 9-day interstorm sequence (May 29 to June 6, 1987) and for a 17-day period of alternating rainfall and evaporation (June 25 to July 11, 1987).

To study aspect ratio constraints we interpolated the 30 × 30 m elevation data for the 1D subcatchment to obtain a range of discretizations from 30 × 30 m to 3 × 3 m, shown in Table 1. We label the 30 × 30 m discretized catchment 1D-30, the 15 × 15 m 1D-15, and so on. Figure 2 is an image of the 1D catchment at a horizontal grid discretization of 10 × 10 m. The vertical discretization of catchment 1D was kept fixed at four layers for all simulations, and the number of nodes and elements in the three-dimensional finite element mesh using the different horizontal grid resolutions ranges from $O(10^3)$ to $O(10^5)$. We also interpolated the original elevation data to 2 × 2 m and 1 × 1 m resolution (yielding finite element grids of approximately 300,000 and 1,200,000 nodes, respectively), but these grids could not be simulated as the amount of memory needed to run the code exceeded the 25 million word capacity (64-bit words) of the Pittsburgh Supercomputing Center Cray Y-MP computer. The degree of sparsity shown in Table 1 is calculated as $100(1 - 27/N)$, where N is the number of nodes and 27 is the maximum number of nonzero entries per row in the system matrices.

3.2. *Observation Data and Parameter Fitting*

The catchment and model parameter values used for the 1D catchment simulations are given in Tables 2 and 3. The coordinates of three surface nodes designated for detailed vertical profile output are (x = 150 m, y = 360 m), (300, 360), and (450, 360) and correspond, from left to right, to the three shaded pixels shown in Figure 2.

The values of ψ_s, n, f, and surface K_s were obtained by least squares fits of (2) and (5) to observation data, as shown in Figure 3. The soils in part of the Kings Creek catchment are identified as Florence silty clay loams and Benfield silt loams, and we used moisture retention and saturated hydraulic conductivity data from the Soil Conservation Service of the United States Department of Agriculture (T. Demetriades-Shah et al. unpublished report, 1989) corresponding to Florence and Benfield soils at the FIFE sites. The values for residual moisture content θ_r and porosity θ_s were taken from the estimates for a silty clay loam published by *Rawls et al.* [1982]. The curve and data in Figure 3*b* suggest that even at extremely high suction values the soil moisture content does not fall below 20%. The measurements from the Soil Conservation Service shown in this plot were obtained from soil cores taken at depths of 5–10 cm and 30–70 cm. From near-surface remotely sensed measurements of soil moisture made for the catchment, on the other hand, we do obtain moisture contents below 20% [*Engman et al.*, 1989]. Aside from measurement error, the discrepancies between the observations made by remote sensing and those obtained from soil cores may indicate differences in the characteristics of the soil near the surface and at depth, in which case these differences should be taken into account in the parameterization of the model.

No measurements of relative hydraulic conductivity, specific storage, or overland flow velocity were made for the 1D catchment, and little information for estimating initial conditions or the horizontal distribution of saturated conductivites was available. The $K_r(\psi)$ relationship was obtained from (4) using the parameter values from the $\theta(\psi)$ fit shown in Figure 3*b*. We note that $n = 1.176$ is just outside the range $1.25 < n < 6$ suggested by *van Genuchten and Nielsen* [1985] for the validity of (4) and of the relationship $m = 1 - 1/n$, so it will be important to validate the $K_r(\psi)$ relationship with experimental data. The horizontal distribution of saturated hydraulic conductivities was assumed to be spatially homogeneous. For the 17-day precipitation-evaporation simula-

TABLE 2. Soil and Grid Parameter Values for 1D Catchment Simulations

Parameter	Value
θ_r	0.04
θ_s	0.471
ψ_s, m	−0.741
n	1.176
S_s, m^{-1}	0.001
ψ_{min}, m	"−999.9"
Surface elevation range, m	[417.0, 442.0]
Δx, Δy, m	3.0, 5, 6, 10, 15, 30.0 (1D-03, 1D-05, ···, 1D-30)
L, m	1.0
Δz, m	
Top two layers	0.2
Bottom two layers	0.3
Overland flow velocity, m/h	4.0

TABLE 3. Saturated Conductivity, Time Step, and Convergence Parameter Values for 1D Catchment Simulations

Parameter	17-Day Precipitation-Evaporation Simulation	9-Day Evaporation Simulation	12-Hour Evaporation Simulation
Surface K_s, m/h	0.2180	0.0218	0.0218
f, m^{-1}	3.526	3.526	3.526
T_{max}, hours	408.0 (17 days)	216.0 (9 days)	12.0 (0.5 days)
Δt_0, hours	0.05	0.10	0.10
Δt_{min}, hours	0.0005	0.01	0.0001
Δt_{max}, hours	1.0*, 2.0†	12.0	3.0
Δt_{rad}	0.5	0.5	0.5
Δt_{mag}	1.2	1.2	1.2
tol, m	0.005	0.05	0.0005
maxit	8	12	12
$maxit_2$	5	6	6

*Simulation using 15-min rainfall rates.
†Simulation using daily-averaged rainfall rates.

tion we assumed fairly wet antecedent moisture conditions and tried various distributions of initial conditions. Varying the initial conditions, however, did not have as great an effect on the simulated catchment discharge rates as variations in surface K_s. For the 9-day evaporation simulation we assumed the catchment was completely saturated at the start (based on high streamflows observed in the days just prior to the interstorm period, with a peak rate of approximately 26 m^3/h), and we used a vertically hydrostatic initial pressure head distribution. We used values of 0.001 m^{-1} for specific storage and 4.0 m/h for overland flow velocity, which will require verification. The average soil depth of the 1D catchment has been estimated to be 0.76 m [*Blain*, 1989], although we used a uniform value of 1.0 m in our simulations. We discretized the catchment vertically into four layers with two thin layers (0.2 m) near the surface and two thicker layers (0.3 m) at the base of the catchment.

Since catchment 1D is quite small we assumed spatial homogeneity for the atmospheric inputs to the model. Precipitation data were collected at 32 rain gauges on the Kings Creek FIFE site, and we averaged the data from the two gauges closest to the 1D catchment. Evaporation measurements were made during four separate periods over the summer and represent actual rather than potential soil moisture losses to the atmosphere. In the absence of potential evaporation rates it was necessary to set the air-dry pressure

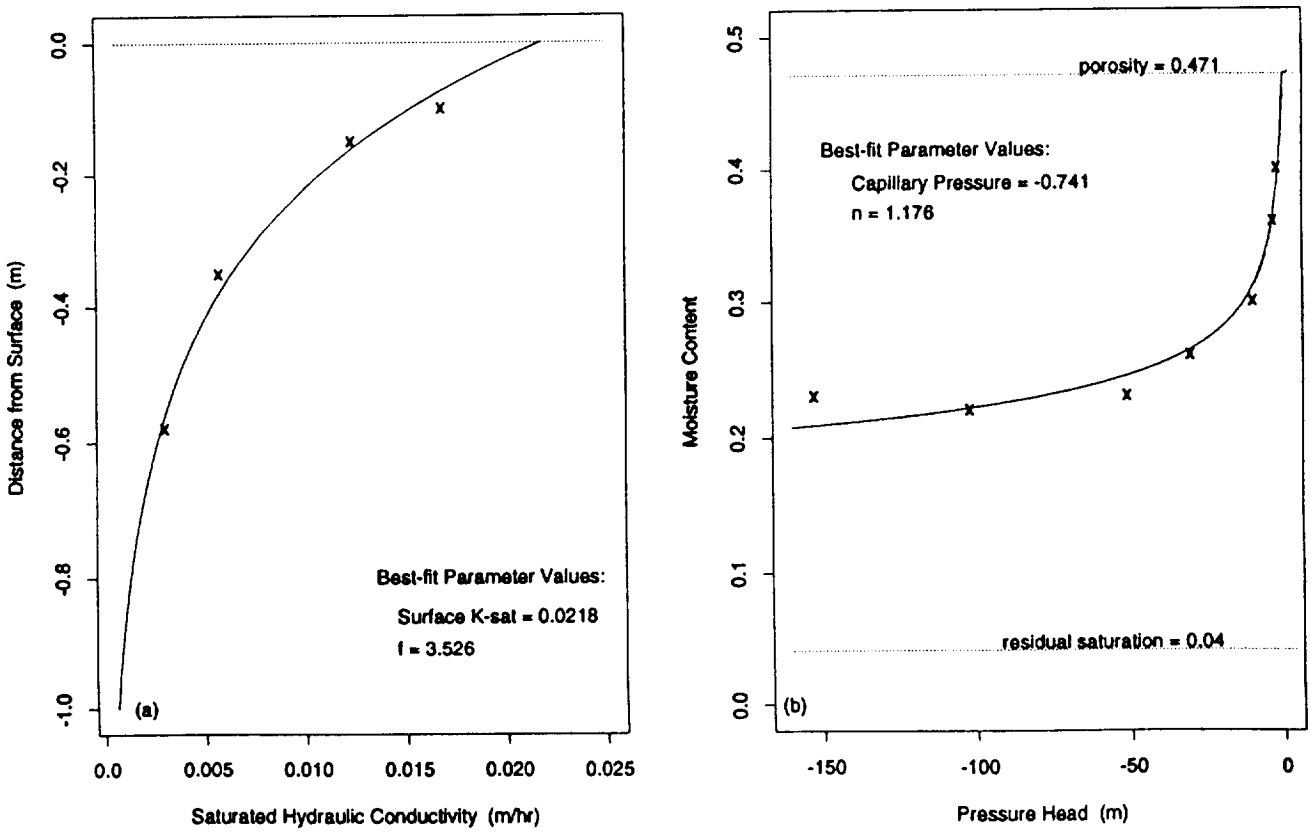

Fig. 3. Least squares fits (solid lines) of the (*a*) $K_s(z)$ and (*b*) $\theta(\psi)$ relationships to observed data (crosses).

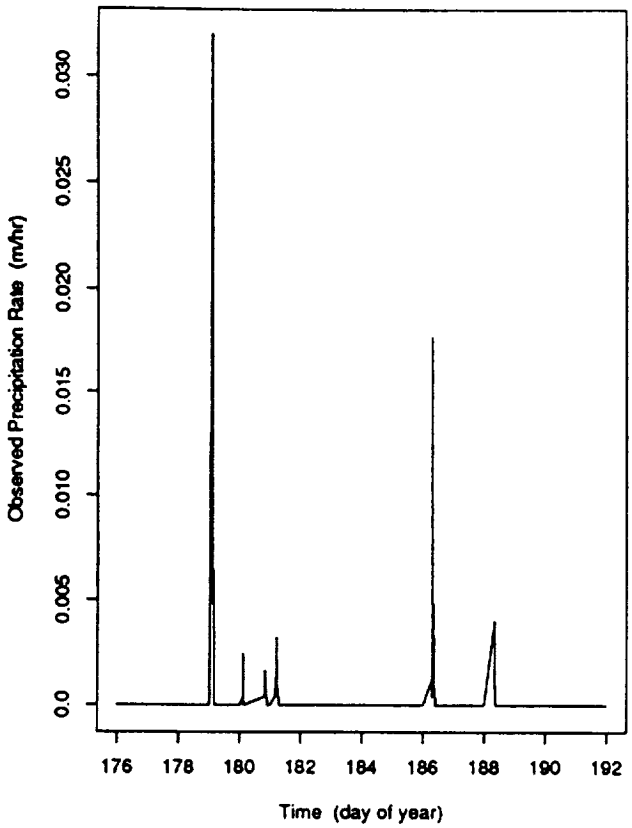

Fig. 4. Observed precipitation data for the 17-day rainfall-interstorm period June 25, 1987 (day 176) to July 11, 1987 (day 192).

head value ψ_{min} to an arbitrarily small value (indicated as "−999.9" in Table 2) to ensure that evaporation remained atmosphere controlled throughout the simulation period, with the atmospheric evaporation rate equal to the actual (observed) rate. If potential evaporation data were available and an estimate of ψ_{min} could be made, an important check on the performance of the model would be to run a simulation using the potential rates as input boundary conditions and allowing the model to switch from atmosphere- to soil-controlled evaporation, so that the computed actual evaporation rates could be compared with the observed actual rates.

3.3. *Simulation of 17-Day Rainfall-Interstorm Sequence*

The precipitation, evaporation, and streamflow observation data used for the 17-day rainfall-interstorm simulation (June 25 to July 11, 1987) is shown in Figures 4 and 5. We used daily-averaged evaporation rates (Figure 5*b*) and had to interpolate the average rates for days 179 and 180 due to insufficient observation data for these two days. There were two major rain events during the 17-day period (Figure 4), on June 28 (17.14 mm) and July 5 (10.23 mm). In addition, between 2.3 and 3.5 mm of rain was recorded for three smaller precipitation events which occurred on June 29, June 30, and July 7. Several storms also occurred during the week ending June 25, delivering 11.5, 21.2, 7.2, and 21.5 mm of rain on June 18, 20, 22, and 24 respectively. These large rainstorms immediately prior to June 25 enabled us to assume fairly wet initial soil conditions for the simulation.

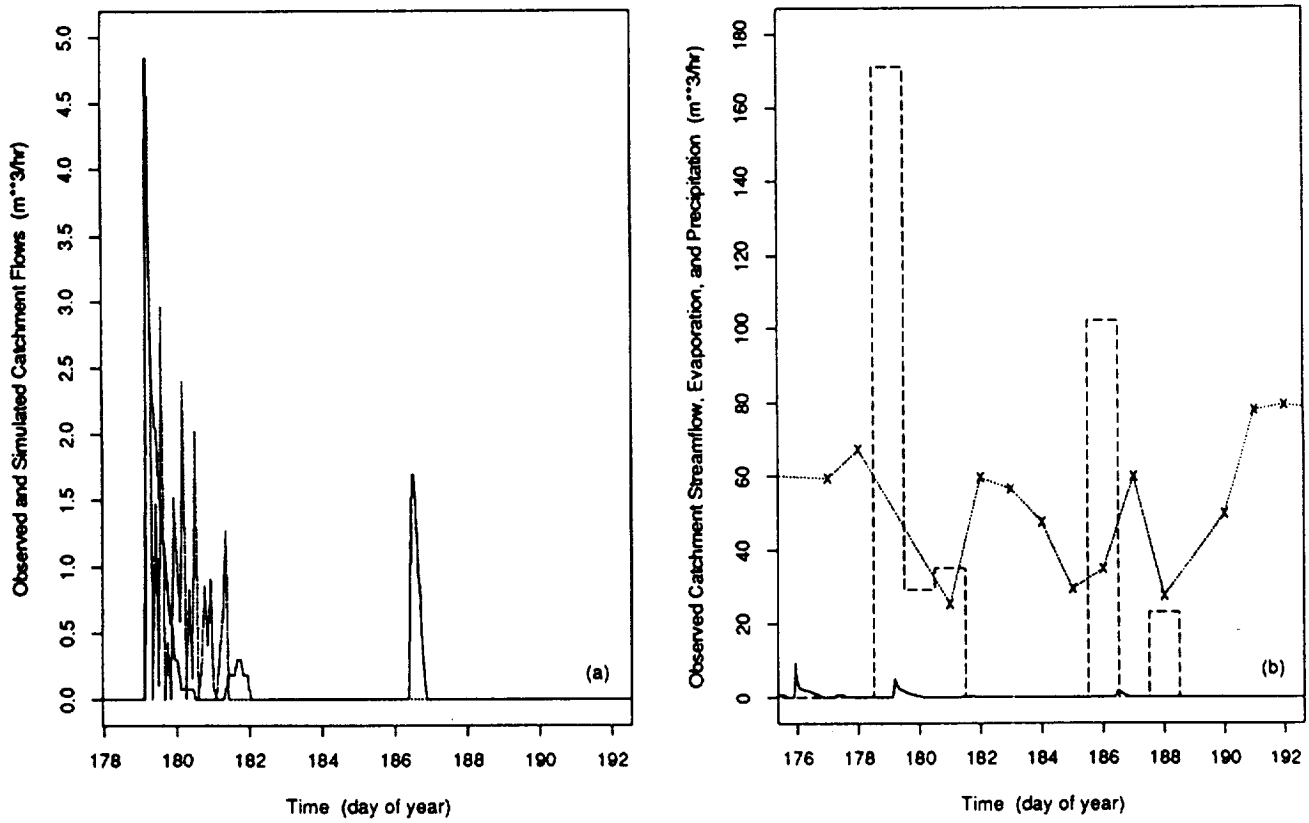

Fig. 5. (*a*) Observed streamflow (solid line) and simulated discharge (dotted line), and (*b*) comparison of streamflow (solid line), evaporation (dotted line with crosses), and precipitation (dashed line) components of the catchment water balance for the 17-day rainfall-interstorm period ending July 11, 1987 (day 192).

There were no observation data to verify the initial pressure head distributions used for the simulations, so the initial conditions can be considered somewhat arbitrary. We found, however, that varying the initial conditions did not have as great an effect on the simulated catchment discharge rates as variations in other model parameters.

We ran two series of simulations using the 17-day rainfall-evaporation data. In the first series we used detailed, 15-min rainfall rates (Figure 4) and attempted to match the observed streamflow record. There are two distinct discharge events in the streamflow hydrograph (Figure 5*a*), in response to large storms on June 28 and July 5. Since the two discharge events appear to be responses to independent storms, we calibrated the model to match the June 28 event and then used these calibration results to attempt a match of the July 5 event. We remark that for proper model calibration and verification we should use additional observation sequences, encompassing a wide range of scenarios, though given the field data limitations described earlier we were unable to conduct more extensive tests. Furthermore, calibration based on streamflow observations alone is of limited use, as can be ascertained when we examine the relative contributions of the various components of the catchment water balance. We see in Figure 5*b* that the rainfall and evaporation components are at least an order of magnitude larger than the streamflow component for the 17-day period of interest. It is apparent that almost all of the rainfall occurring during this period infiltrates the soil and only a small part reaches the stream as overland flow or rapid subsurface flow.

The simulations of the 17-day period enabled us to examine the sensitivity of model response to variations in parameters and inputs. In particular, some preliminary tests on time aggregation effects were conducted in a second series of simulations. In these tests we used daily-averaged rainfall rates (Figure 5*b*), and we compared the hydrologic and numerical behavior with results from the simulations using detailed 15-min rain rates. We obtained significant discrepancies in surface saturation response during the storm events, but overall the simulated hydrologic responses using the averaged and detailed rain rates were quite similar. The advantage of using averaged rates for atmospheric inputs is that larger time steps can be used, making the simulation cheaper to run. Averaged rates also produce smoother boundary conditions which can reduce numerical difficulties. On the other hand, the high degree of variability in atmospheric fluxes may make it necessary to use detailed inputs, depending on the hydrologic responses of interest. For instance, large discharge events triggered by infiltration excess overland flow will be very sensitive to small-scale fluctuations in precipitation rates.

The results from the first series of simulations are shown in Figure 5*a*. We were able to approximately match the observed peak, volume, and duration of streamflow response for the June 28–30 rainfall events, but the model produced no discharge for the July 5 storm. Note that the model result shown is total discharge, which is surface runoff routed to the stream. The model does not consider channel flow, and thus we could not compute streamflow rates at the catchment outlet. The lack of a channel flow component, along with the linear and discrete method used in the model to route and delay overland flow (surface runoff produced on 30 × 30 m grid blocks is accumulated without downslope reinfiltration into 2-hour hydrograph intervals), may account for the fluctuations in the computed discharge shown in Figure 5*a*. The results for the first two days of the 17-day simulation are not shown in Figure 5*a*. There is streamflow activity on these first two days in response to the rain events which occurred during the week ending June 25, but we do not explicitly account for these rain events in the 17-day simulation.

The model was first run using the parameter values obtained from observation data (Figure 3 and Tables 2 and 3), but this produced an excessive amount of surface runoff. To calibrate the model we systematically altered the values of some of the parameters: soil depth L, vertical discretization Δz, overland flow velocity, saturated conductivity K_s at the surface, fitting parameter f for vertical exponential K_s, time steps, and initial conditions. We found that only overland flow velocity and surface K_s had significant effects on the simulated discharge: overland flow velocity on the duration of the discharge response and surface K_s on the peak rate and total volume of discharge. Vertical discretization will have some effect on simulated discharge in the case where infiltration excess runoff production is dominant. This type of runoff is controlled by surface K_s, and in the model we evaluate relationship (5) at the midpoint of each element so that a thin surface layer will have a higher saturated conductivity than a thicker surface layer, thereby potentially reducing infiltration excess runoff. We found, however, that even using a 19-layer vertical discretization with the layer nearest to the surface 0.02 m thick (compared to 0.2 m for the four-layer discretization), the model still produced too much runoff. To reduce the amount of runoff it was necessary to increase surface K_s from its fitted value of 0.0218 m/h. We obtained best results using a value of 0.218 m/h (for the four-layer discretization). This higher value may be justified considering the remarks made earlier regarding the discrepancies between near-surface remotely sensed soil moisture observations and deeper measurements obtained from soil core analyses, since these discrepancies suggest that the soil near the catchment surface may be very porous. With surface K_s = 0.218 m/h, an overland flow velocity of 0.4 m/h, and all other parameter values as determined from observation data, we obtained the match shown in Figure 5*a*. To match the streamflow response for July 5 it was necessary to run a separate simulation using surface K_s = 0.06 m/h. The need for different surface K_s values to match separate discharge events suggests that it may be important to collect and incorporate information on the spatial distribution of hydraulic conductivity for the 1D catchment. Note that since we altered surface K_s from the value obtained by parameter fitting (Figure 3*a*) we should have refit parameter f to the observation data using the modified value of surface K_s. This was not done for the simulations reported here.

The surface runoff which generated discharge during the 17-day simulation was initially of the infiltration excess type, in response to peak rainfall rates on June 28, and later of the saturation excess variety, in response to declining rates but continued rainfall on June 29 and 30. This can be seen in Figure 6, where infiltration excess saturation is shown by heavily shaded areas, saturation excess by solid areas, and unsaturated portions of the catchment surface by lightly shaded areas. Note the high degree of surface saturation at the start of the simulation (day 176.0) owing to the wet initial conditions which were used. The initial conditions were

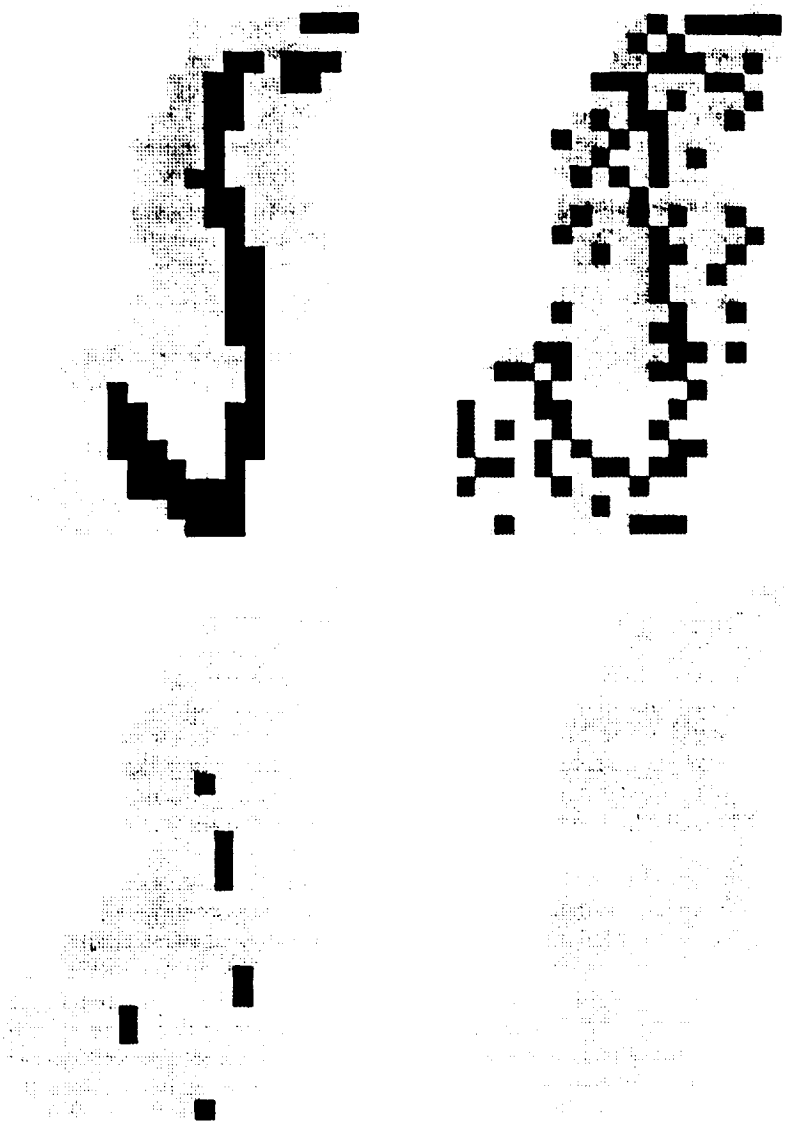

Fig. 6. Surface saturation response for the 17-day precipitation-evaporation simulation, using 15-min rainfall rates: (Top left) day 176.0 (June 25, 1987, initial conditions); (top right) day 179.103; (bottom left) day 181.280; and (bottom right) day 193.0. Light shading indicates unsaturated; heavy shading, infiltration excess; and solid regions, saturation excess.

generated using a topographic index method as described previously, producing the wettest soils closest to the stream channel and catchment outlet. Since rainfall rates and saturated hydraulic conductivities were horizontally homogeneous, infiltration excess runoff occurred first where near-surface pressure head gradients were lowest, corresponding roughly to the wetter near-stream regions. The patchiness in the infiltration excess pattern seen in Figure 6 is probably due to oscillations in the surface boundary condition switching mechanism from one iteration to the next, oscillations which were caused by approximation errors in the back solved surface flux values. Saturation excess runoff occurred where water table levels were closest to the surface, corresponding once again to near-stream regions. These partial contributing areas then expanded upslope from the catchment outlet and outward from near-stream areas in response to continued rainfall.

It is not surprising that we found high sensitivity to surface K_s in the simulated discharge given that infiltration excess is a dominant mechanism for surface runoff generation. In fact, when we used daily-averaged rainfall rates we failed to generate any infiltration excess runoff, and consequently the simulated discharge hydrograph had a smaller peak and less volume and was of shorter duration than the observed streamflow hydrograph. The simulation with daily-averaged rates also produced less saturation excess overland flow. The different responses during periods of heavy rainfall can be seen in the vertical profiles of presssure head and moisture content shown in Figure 7. These vertical profiles are taken at the three selected surface nodes of Figure 2. In these plots we can see that the daily-averaged rainfall rates yielded drier soils during the storm on day 179. (The time value for the profiles labeled 179.1 in Figure 7 is actually 179.105 for the 15-min rainfall rate case and 179.162 for the daily-averaged case; for the profiles labeled 188.5 the actual time is 188.461 for the 15-min case and 188.496 for the

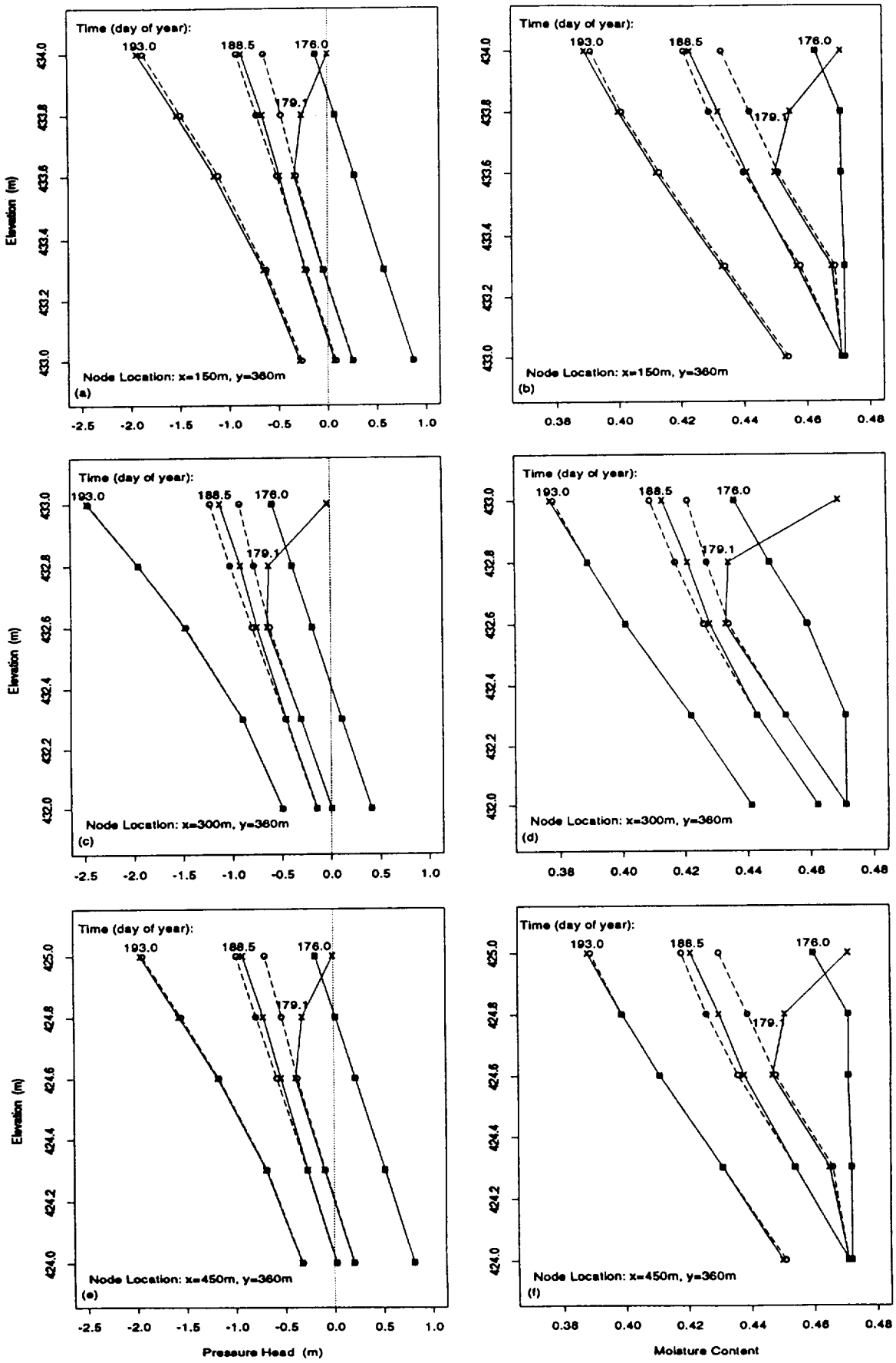

Fig. 7. Vertical profiles for the 17-day precipitation-evaporation simulation, using 15-min (solid lines) and daily-averaged (dashed lines) rainfall rates. (Day 176 is June 25, 1987.)

daily-averaged case.) Aside from discrepancies in surface saturation results during heavy rainfall periods, the hydrologic responses were generally quite similar between the simulations using averaged and detailed precipitation rates. This can be seen in Figure 7 for the profiles at day 188.5 and at the end of the simulation (day 193.0).

The main difference in numerical behavior between the averaged and detailed simulations was that the simulation using 15-min rates required significantly more CPU time, since smaller time steps had to be used to resolve the detailed rainfall rates. The numerical results are shown in the convergence and mass balance plots of Figure 8 and are summarized in the second and third columns from the left in Table 4. The simulation using detailed rainfall rates had some difficulty during the peak rainfall/saturation periods on June 28 and July 5, as evidenced by the slower convergence and higher mass balance errors seen in Figure 8. Outside of these two periods the number of nonlinear (Picard) iterations remained roughly constant at two or three and the number of linear (conjugate gradient) iterations decreased steadily as the simulation progressed. The 17-day rainfall-interstorm simulation of the 1D catchment required 19 min of CPU using 15-min rainfall rates and 6.5 min using daily-averaged rates.

4. Sensitivity to Model Resolution

4.1. *Statement of the Problem*

In this section we examine the feasibility of using a detailed physically based model for catchment scale simulations. In particular, we will investigate computational issues related to model resolution by simulating the 1D subcatchment over a range of grid sizes and convergence tolerance values. In a study of discretization effects for a two-dimensional hillslope model, *Calver and Wood* [1989] recommended using $\Delta x/\Delta z \leq 20$ for successful numerical simulations. In the results presented below we obtained satisfactory results using aspect ratios as high as 150 ($\Delta x = \Delta y = 30$ m, $\Delta z = 0.2$ m). However, when we imposed a stricter convergence criterion on the nonlinear iterations, simulations with different aspect ratios produced different mass balance and convergence results.

The 1D subcatchment is small enough that it was not necessary to extrapolate the 30 × 30 m digital topographic data to coarser horizontal discretizations, but for larger catchments it will be necessary to examine whether aspect ratios even greater than 150 can be used. Large aspect ratios will also arise when a very fine vertical resolution is required to accurately reproduce runoff and moisture front responses from rainfall and evaporation events. Small vertical grid sizes may in turn lead to stability-related restrictions on time step, further increasing the cost of running large-scale catchment simulations.

The effect of heterogeneities on numerical and physical grid constraints also needs to be investigated. For instance, while a fine grid may be needed to resolve hydrologic responses to highly variable inputs, a large problem size and high parameter variability may lead to ill-conditioned model equations which may adversely affect numerical convergence. *Ababou et al.* [1989] discuss related heterogeneity effects in the context of a three-dimensional finite difference model applied to steady state saturated flow problems.

4.2. *Simulation of 9-Day Interstorm Sequence*

In Figure 9 we show the evaporation and streamflow observation data for the 9-day interstorm period from May 29 (day 149) to June 6, 1987 (day 157). There was no rainfall on the Kings Creek catchment during this period, except for a very small amount (1 mm) on May 29. There was high streamflow just prior to day 149, and although we had no rainfall observation data prior to May 29 we assumed that there was significant rainfall immediately prior to this date, and we therefore started the 9-day simulation from saturated conditions. We used daily-averaged evaporation rates rather than detailed, diurnally fluctuating rates. This allowed us to use large time steps (up to 12.0 hours), although we observe that the streamflow record in Figure 9 is oscillatory with a periodicity of approximately 1 day, which may be a response to the diurnal fluctuations in evaporation. Due to insufficient data for days 149, 153, and 154 we interpolated average evaporation rates for these days from the observed rates on surrounding days.

We ran two series of simulations using the evaporation data. In the first series we simulated the entire 9-day period for a range of mesh discretizations from 1D-30 to 1D-03. This was done to study the effects of aspect ratio on catchment simulation responses, in particular to determine whether we can successfully run a catchment scale simulation using aspect ratios as large as 150 (corresponding to catchment 1D-30). In the second series of tests we used only the first 12 hours of the 9-day interstorm record and ran simulations of catchments 1D-30 and 1D-05 using a strict convergence criterion for the nonlinear iterations ($tol = 0.0005$ m compared to $tol = 0.05$ m used for the 9-day simulations).

The results from the first series of simulations are presented in Figures 10 and 11 and summarized in the fourth, fifth, and six columns from the left in Table 4. In the figures we compare the 1D-30 and 1D-03 catchment simulations, and in the table we include also statistics from the 1D-10 simulation. Similar results were obtained for catchments 1D-15, 1D-06, and 1D-05.

In Figure 10 we show vertical profiles of pressure head and moisture content at the three selected surface nodes of Figure 2. There is reasonable agreement between the results obtained using a 30 × 30 m grid discretization (aspect ratio of 150) and the results using a grid resolution of 3 × 3 m (aspect ratio of 15). We note also the similarities in the profiles at the three different locations owing to the spatial uniformity of atmospheric input rates, initial conditions, and parameter distributions.

The differences in aspect ratio did not have significant effects on the numerical performance of the model. In the fourth, fifth, and sixth columns from the left in Table 4 we observe close agreement for the 1D-30, 1D-10, and 1D-03 simulations. All three simulations were successfully completed in 40 time steps, and none of the runs encountered difficulties severe enough to require back stepping. All simulations required between two and four nonlinear iterations to converge and an average of about 14 iterations to solve the linearized system of equations. In each case, convergence of the linear solver was slowest at the start of the simulation (20–25 iterations) and much more rapid by the end of the simulation (three to five iterations). Similar mass balance results were obtained for each of the simulations, with the largest discrepancies occurring during the first few

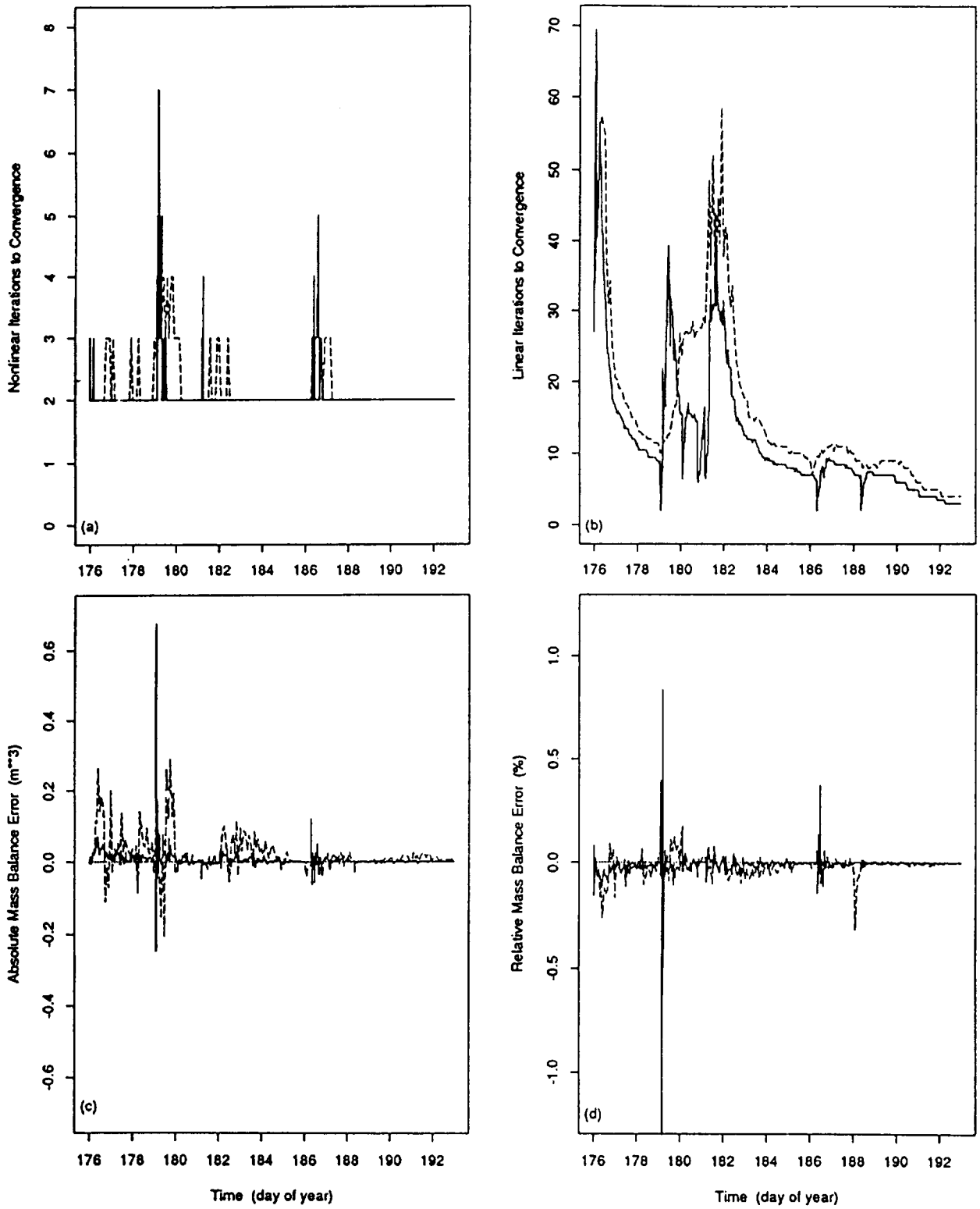

Fig. 8. Convergence and mass balance results for the 17-day precipitation-evaporation simulation, using 15-min (solid lines) and daily-averaged (dashed lines) rainfall rates. In Figure 8*d* the peak value for the solid curve is −3.47%. (Day 176 is June 25, 1987.)

time steps. These discrepancies at the start of the simulation, which can be seen in Figure 11, account in large part for the differences in average mass balance errors reported in Table 4. High relative mass balance errors were obtained at the third time step (238% for catchment 1D-03 and −40.5% for 1D-30), values much larger than the errors computed at all other time steps. We note that average mass balance errors were significantly lower for the 17-day rainfall-interstorm

TABLE 4. Summary of 1D Catchment Simulation Results

	17-Day Precipitation-Evaporation Simulation (Catchment 1D-30)		9-Day Evaporation Simulation			12-Hour Evaporation Simulation	
	15-min Averaged Rainfall Rates	Daily-Averaged Rainfall Rates	Catchment 1D-30	Catchment 1D-10	Catchment 1D-03	Catchment 1D-30	Catchment 1D-05
Number of nodes	1,570	1,570	1,570	12,680	135,355	1,570	49,295
Number of time steps	663	223	40	40	40	81	201
Number of back steps	1	1	0	0	0	16	50
CPU, s	1,150.3	391.4	66.84	583.9	6,452.6	215.5	19,597.0
CPU/time step/node	0.00111	0.00112	0.00106	0.00115	0.00119	0.00169	0.00198
Nonlinear iterations/time step	2.26	2.17	2.40	2.48	2.53	2.56	2.64
Linear iterations/nonlinear iteration	11.08	18.39	13.92	13.69	14.78	8.91	7.47
Average |absolute MBE|, m^3	0.012	0.031	2.927	3.044	3.284	0.00764	0.00081
Average |relative MBE|, %	0.038	0.034	2.021	5.960	7.255	0.233	0.070

Convergence parameter *tol* = 0.0005 m. MBE denotes mass balance error.

simulation than for the 9-day interstorm simulation (compare the second and third columns from the left in Table 4), owing to a smaller value of *tol* and smaller time steps used for the 17-day simulation.

The importance of not being limited by aspect ratio constraints in a catchment scale simulation is suggested by the storage requirements shown in Table 1 and by the CPU results shown in the fourth, fifth, and sixth columns, from the left in Table 4. With a grid resolution of 30 × 30 m we were able to simulate the 9-day evaporation sequence in slightly more than 1 min of computer time, requiring $O(10^5)$ words of memory. The same 9-day simulation with grids of 3 × 3 m required over 100 min of CPU and similarly 100 times more memory.

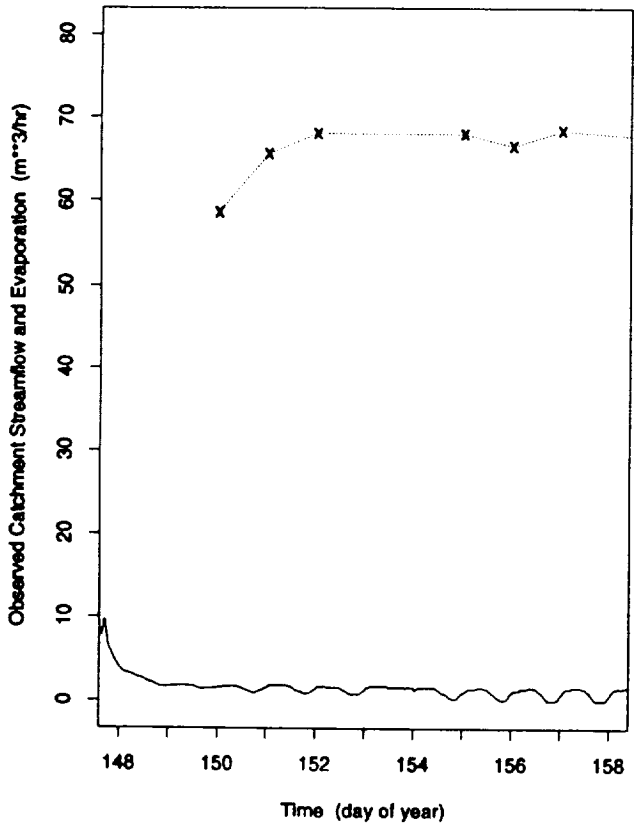

Fig. 9. Evaporation (dotted line with crosses) and streamflow (solid line) observation data for the 9-day interstorm period May 29, 1987 (day 149) to June 6, 1987 (day 157).

The results from the second series of simulations, using *tol* = 0.0005 m and the first 12 hours of the evaporation period, are summarized in the two rightmost columns in Table 4. These results can be roughly compared to the results in the fourth, fifth, and sixth columns from the left in Table 4 for the 9-day, *tol* = 0.05 m simulation. In reducing *tol* we have increased the accuracy of the simulations, decreasing by about 2 orders of magnitude the resulting mass balance errors. However, this gain is achieved at the expense of a substantial increase in CPU. For catchment 1D-30 we simulated the 9-day evaporation period in 40 time steps and 67 s of CPU s with no occurrences of back stepping, while the 12-hour simulation required twice as many time steps, frequent back stepping, and over 200 s of CPU. For catchment 1D-05 the 12-hour simulation required 5.5 hours of CPU.

We observe from the two rightmost columns in Table 4 that catchment 1D-05 has more trouble converging than catchment 1D-30 (201 time steps and 50 back stepping occurrences compared to 81 steps and 16 back steps for 1D-30) and that it achieves smaller mass balance errors than 1D-30. In this case the differences in aspect ratio (150 for catchment 1D-30 and 25 for 1D-05) had an effect on the convergence of the nonlinear iterations and on the accuracy of the simulation results (as reflected in the mass balance errors).

5. Summary and Concluding Remarks

We have described a three-dimensional physically based numerical model for the simulation of hydrologic processes at the subcatchment and catchment scales. The simulation model consists of a grid generator and a finite element code. The grid generator makes use of catchment information extracted from digital topographic data, and the numerical code is based on the nonlinear Richards equation for flow in variably saturated porous media. The model can be applied to catchments of arbitrary geometry and topography. Nonsurface boundaries are considered impermeable, and grid spacing is uniform horizontally but can be variable along the

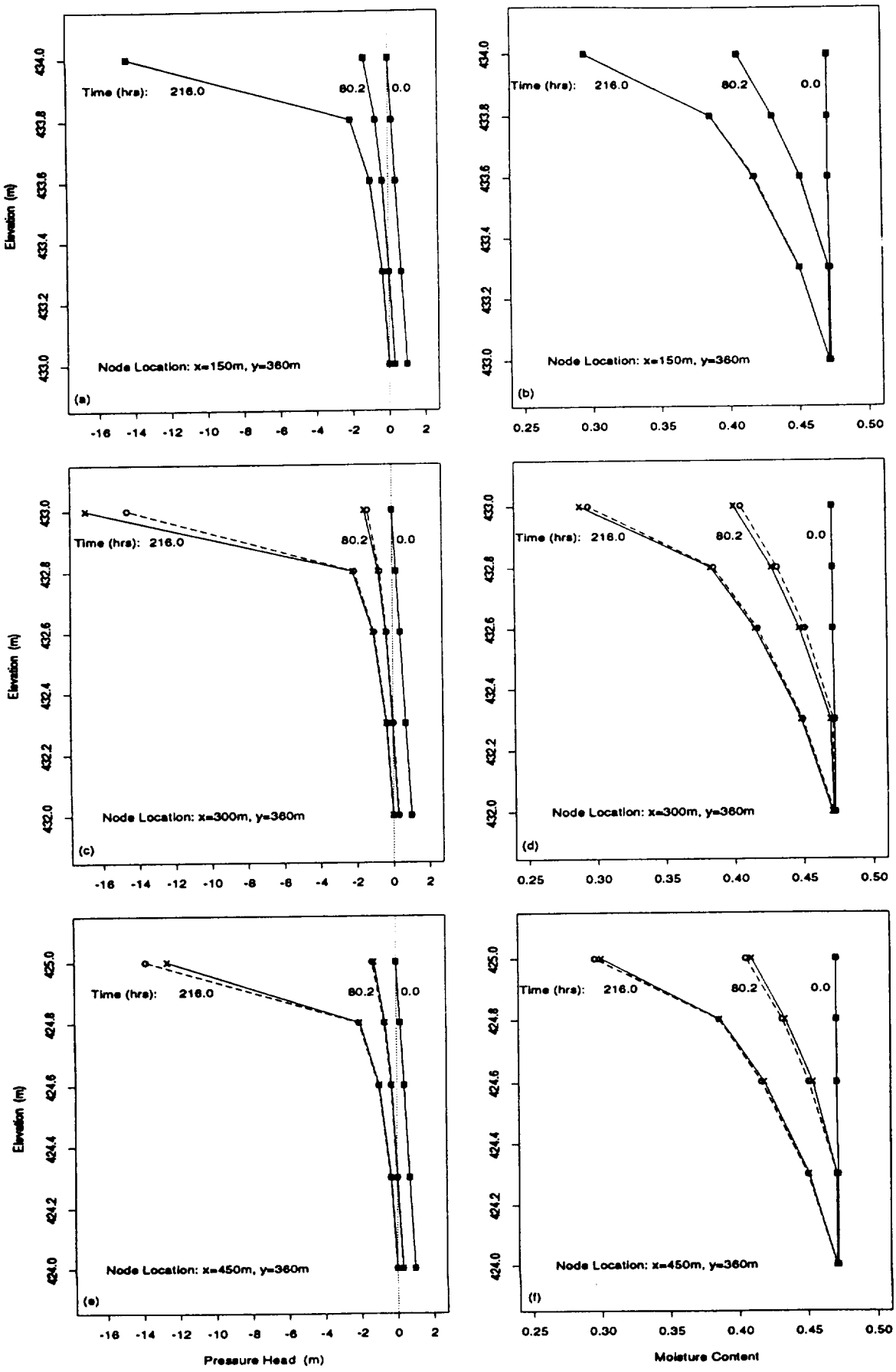

Fig. 10. Vertical profiles for the 9-day evaporation simulation, using 3 × 3 m (solid lines) and 30 × 30 m (dashed lines) grid discretizations. (Hour 0 is May 29, 1987, 0000 hours.)

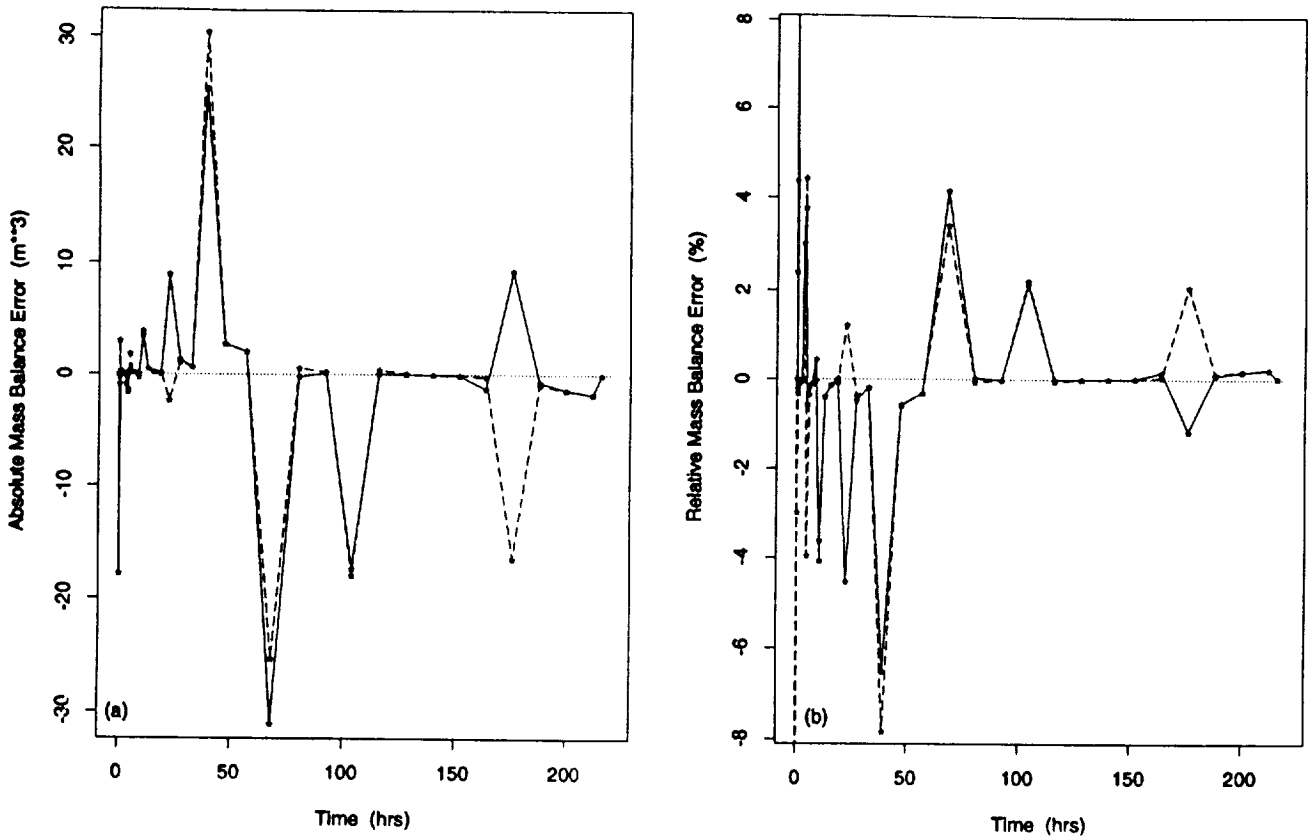

Fig. 11. Mass balance results for the 9-day evaporation simulation, using 3 × 3 m (solid lines) and 30 × 30 m (dashed lines) grid discretizations. (Hour 0 is May 29, 1987, 0000 hours.)

vertical coordinate. The model automatically handles both soil-driven and atmosphere-driven inflows and outflows, and both saturation excess and infiltration excess runoff production. Atmospheric inputs can be spatially and/or temporally variable, and heterogeneities in hydraulic conductivity are also considered. Initial conditions can be generated from elevation and surface conductivity data, and extended van Genuchten equations are used to describe the nonlinear soil hydraulic characteristics. Simplifying assumptions are made to handle flow processes occurring on the catchment surface and in streams. Time stepping is adaptive and based on the convergence behavior of the nonlinear iterative scheme.

The simulation model was applied to subcatchment 1D of the Konza Prairie Research Natural Area in northeastern Kansas. Observation data collected during a 1987 field experiment were used to parameterize and calibrate the model.

In simulations of a 17-day rainfall and interstorm sequence we attempted to match discharge produced by the model with observed streamflow. It was necessary to increase the fitted value of surface saturated conductivity to match the largest of two distinct streamflow events, but with this higher value of surface K_s we were unable to match the smaller streamflow peak. Matching both discharge events simultaneously may require information on the spatial variability of saturated conductivity for the 1D catchment. The 17-day simulations were performed using both detailed 15-min rainfall rates and daily-averaged rainfall rates. The detailed rates are necessary if we want to capture the surface saturation response of the catchment during periods of heavy rainfall, but in other respects the use of detailed and averaged rates produced similar hydrologic and numerical results.

Simulations of a 9-day evaporation period were performed using a wide range of spatial grid discretizations in order to study model resolution effects. We obtained satisfactory results using a nonlinear convergence tolerance of 0.05 m and a grid aspect ratio as large as 150, indicating that horizontal grid dimensions may not be unreasonably constrained by the typically much smaller vertical length scale of a catchment and by vertical discretization requirements. This is an encouraging result, although tests using heterogeneous parameter distributions and even larger aspect ratios are recommended. Constraints on grid aspect ratios dictated by numerical stability, accuracy, and convergence requirements also need to be investigated.

Much of the work described in this paper is in preliminary stages. In future work we would like to extend the model to handle hysteresis and seepage faces, and improve on the simplifying assumptions used in runoff routing. For a more comprehensive model of catchment scale hydrologic processes, it will be necessary to couple the three-dimensional subsurface flow model to a physically based model of overland flow and channel flow, and to incorporate vegetation, transpiration, macropore flow, and nonisothermal effects. With more detailed and extensive observation data for the 1D catchment (e.g., potential evaporation rates, surface soil moisture readings, and surface conductivity measurements) we will be able to run rigorous model assessment tests, including an evaluation of errors in the model formulation.

It would appear that catchment scale simulations can be feasibly performed using a detailed physically based model. The 9-day evaporation simulation of the 0.24-km^2 1D catchment required only 67 s of Cray Y-MP comuter time using a finite element grid of 1570 nodes, and 180 min of CPU using a 135,355-node mesh. From the fourth, fifth, and sixth columns from the left in Table 4 we estimate the CPU requirement for our simulation model to be 0.001 s (2.78×10^{-7} hours) per time step per node, using a relatively weak convergence tolerance (tol = 0.05 m) and using the ITPACK routine SSORCG vectorized for the Cray Y-MP to solve the linearized system of equations. The U.S. Geological Survey digital elevation data for the entire King's Creek catchment contain 12,913 pixels at 30 × 30 meter resolution. The surface area of this catchment is 11.62 km^2. A finite element discretization of the Kings Creek catchment using nine vertical layers would yield a 129,130-node mesh. A single 100–time step simulation with this grid would require 3.6 hours of CPU. The mesh for a horizontal discretization of 15 × 15 m with four layers vertically would contain approximately 258,260 node, and would require just over 7 hours of CPU, again for a simulation of 100 time steps. Aside from the vectorized SSORCG solver, the numerical model was executed in scalar mode. Significant efficiency gains can be expected from vectorization and parallelization of other components of the model. One possibility would be to assign to each processor of a parallel computer the task of simulating one subcatchment of a large catchment such as Kings Creek.

Acknowledgments. This work was supported in part by the Andrew W. Mellon Foundation and by U.S. NASA grants NAG-1392 and NAG5-899. We would also like to acknowledge support from the John von Neumann Center for use of the Cyber 205 (grant NAC 1249) and from the Pittsburgh Supercomputing Center for use of the Cray Y-MP (grant EAR900004P).

REFERENCES

Ababou, R., D. McLaughlin, L. W. Gelhar, and A. F. B. Tompson, Numerical simulation of three-dimensional saturated flow in randomly heterogeneous porous media, *Transp. Porous Media*, *4*, 549–565, 1989.

Ames, W. F., *Numerical Methods for Partial Differential Equations*, 2nd ed., Academic, San Diego, Calif., 1977.

Avissar, R., and M. M. Verstraete, The representation of continental surface processes in atmospheric models, *Rev. Geophys.*, *28*(1), 35–52, 1990.

Band, L. E., Topographic partition of watersheds with digital elevation models, *Water Resour. Res.*, *22*(1), 15–24, 1986.

Bathurst, J. C., Physically-based distributed modelling of an upland catchment using the Système Hydrologique Européen, *J. Hydrol.*, *87*, 79–102, 1986.

Beven, K. J., Experiments with a finite element model of hillslope hydrology—The effect of topography, in *Surface and Subsurface Hydrology: Proceedings of the Fort Collins Third International Hydrology Symposium, on Theoretical and Applied Hydrology*, edited by H. J. Morel-Seytoux, J. D. Salas, T. G. Sanders, and R. E. Smith, pp. 37–51, Water Resources Publications, Fort Collins, Colo., 1977.

Beven, K. J., On subsurface stormflow: An analysis of response times, *Hydrol. Sci. J.*, *27*(4), 505–521, 1982.

Beven, K. J., Infiltration into a class of vertically non-uniform soils, *Hydrol. Sci. J.*, *29*(4), 425–434, 1984.

Beven, K. J., and P. Germann, Macropores and water flow in soils, *Water Resour. Res.*, *18*(5), 1311–1325, 1982.

Bhowmik, N. G., Hydrologic research at LTER sites, *Eos Trans. AGU*, *68*(37), 745, 750, 756, 1987.

Binley, A. M., J. Elgy, and K. J. Beven, A physically based model of heterogeneous hillslopes, 1, Runoff production, *Water Resour. Res.*, *25*(6), 1219–1226, 1989*a*.

Binley, A. M., K. J. Beven, and J. Elgy, A physically based model of heterogeneous hillslopes, 2, Effective hydraulic conductivities, *Water Resour. Res.*, *25*(6), 1227–1234, 1989*b*.

Blain, C. A., Development of a physically based numerical soil moisture flow model which has applications to the soil matrix and macropore domains, M.S. thesis, Dep. of Civ. Eng. and Oper. Res., Princeton Univ., Princeton, N. J., 1989.

Broadbridge, P., and I. White, Time to ponding: Comparison of analytic, quasi-analytic, and approximate predictions, *Water Resour. Res.*, *23*(12), 2302–2310, 1987.

Calver, A., and W. L. Wood, On the discretization and cost-effectiveness of a finite element solution for hillslope subsurface flow, *J. Hydrol.*, *110*, 165–179, 1989.

Cooley, R. L., Some new procedures for numerical solution of variably saturated flow problems, *Water Resour. Res.*, *19*(5), 1271–1285, 1983.

de Vries, D. A., Simultaneous transfer of heat and moisture in porous media, *Eos Trans. AGU*, *39*(5), 909–916, 1958.

Dunne, T., and R. D. Black, Partial area contributions to storm runoff in a small New England watershed, *Water Resour. Res.*, *6*(5), 1296–1311, 1970.

Eagleson, P. S., *Dynamic Hydrology*, McGraw-Hill, New York, 1970.

Eagleson, P. S., Climate, soil, and vegetation, 1, Introduction to water balance dynamics, *Water Resour. Res.*, *14*(5), 705–712, 1978.

Eagleson, P. S., The annual water balance, *J. Hydraul. Div. Am. Soc. Civ. Eng.*, *105*(HY8), 923–941, 1979.

Engman, E. T., G. Angus, and W. P. Kustas, Relationships between the hydrologic balance of a small watershed and remotely sensed soil moisture, in Remote Sensing and Large-Scale Global Processes: Proceedings of the IAHS Third International Assembly, edited by A. Rango, *IAHS Publ. 186*, 75–84, 1989.

Federer, C. A., A soil-plant-atmosphere model for transpiration and availability of soil water, *Water Resour. Res.*, *15*(3), 555–562, 1979.

Freeze, R. A., Three-dimensional, transient, saturated-unsaturated flow in a groundwater basin, *Water Resour. Res.*, *7*(2), 347–366, 1971.

Freeze, R. A., Role of subsurface flow in generating surface runoff, 1, Base flow contributions to channel flow, *Water Resour. Res.*, *8*(3), 609–623, 1972*a*.

Freeze, R. A., Role of subsurface flow in generating surface runoff, 2, Upstream source areas, *Water Resour. Res.*, *8*(5), 1272–1283, 1972*b*.

Freeze, R. A., Streamflow generation, *Rev. Geophys.*, *12*(4), 627–647, 1974.

Freeze, R. A., and J. A. Cherry, *Groundwater*, Prentice-Hall, Englewood Cliffs, N. J., 1979.

Gan, T. Y., and S. J. Burges, An assessment of a conceptual rainfall-runoff model's ability to represent the dynamics of small hypothetical catchments, 1, Models, model properties, and experimental design, *Water Resour. Res.*, *26*(7), 1595–1604, 1990*a*.

Gan, T. Y., and S. J. Burges, An assessment of a conceptual rainfall-runoff model's ability to represent the dynamics of small hypothetical catchments, 2, Hydrologic responses for normal and extreme rainfall, *Water Resour. Res.*, *26*(7), 1605–1620, 1990*b*.

Germann, P. F., Preferential flow and the generation of runoff, 1, Boundary layer flow theory, *Water Resour. Res.*, *26*(12), 3055–3063, 1990.

Goodrich, D. C., and D. A. Woolhiser, Catchment hydrology, *U.S. Natl. Rep. Int. Union Geod. Geophys. 1987–1990, Rev. Geophys.*, *29*(Suppl.), 202–209, 1991.

Govindaraju, R. S., and M. L. Kavvas, Dynamics of moving boundary overland flows over infiltrating surfaces at hillslopes, *Water Resour. Res.*, *27*(8), 1885–1898, 1991.

Hillel, D., *Fundamentals of Soil Physics*, Academic, San Diego, Calif., 1980*a*.

Hillel, D., *Applications of Soil Physics*, Academic, San Diego, Calif., 1980*b*.

Huyakorn, P. S., and G. F. Pinder, *Computational Methods in Subsurface Flow*, Academic, San Diego, Calif., 1983.

Huyakorn, P. S., E. P. Springer, V. Guvanasen, and T. D. Wadsworth, A three-dimensional finite-element model for simu-

lating water flow in variably saturated porus media, *Water Resour. Res.*, *22*(13), 1790–1808, 1986.
James, L. D., and S. J. Burges, Selection, calibration, and testing of hydrologic models, in *Hydrologic Modeling of Small Watersheds*, edited by C. T. Haan, H. P. Johnson, and D. L. Brakensiek, pp. 437–472, American Society of Agricultural Engineers, St. Joseph, Mich., 1982.
Kincaid, D. R., J. R. Respess, D. M. Young, and R. G. Grimes, ITPACK 2C: A FORTRAN package for solving large sparse linear systems by adaptive accelerated iterative methods, *ACM Trans. Math. Software*, *8*(3), 302–322, 1982.
Kool, J. B., and J. C. Parker, Development and evaluation of closed-form expressions for hysteretic soil hydraulic properties, *Water Resour. Res.*, *23*(1), 105–114, 1987.
Loague, K., R-5 revisited, 2, Reevaluation of a quasi-physically based rainfall-runoff model with supplemental information, *Water Resour. Res.*, *26*(5), 973–987, 1990.
Loague, K. M., and R. A. Freeze, A comparison of rainfall-runoff modeling techniques on small upland catchments, *Water Resour. Res.*, *21*(2), 229–248, 1985.
McDonnell, J. J., A rationale for old water discharge through macropores in a steep, humid catchment, *Water Resour. Res.*, *26*(11), 2821–2832, 1990.
Milly, P. C. D., Moisture and heat transport in hysteretic, inhomogeneous porous media: A matric head–based formulation and a numerical model, *Water Resour. Res.*, *18*(3), 489–498, 1982.
Mualem, Y., A conceptal model of hysteresis, *Water Resour. Res.*, *10*(3), 514–520, 1974.
Neuman, S. P., Saturated-unsaturated seepage by finite elements, *J. Hydraul. Div. Am. Soc. Civ. Eng.*, *99*, 2233–2250, 1973.
Paniconi, C., Hydrologic processes in variably saturated porous media: Analysis of numerical methods for solving the nonlinear Richards equation, and application to catchment scale simulations, Ph.D. dissertation, Dep. of Civ. Eng. and Oper. Res., Princeton Univ., Princeton, N. J., 1991.
Paniconi, C., A. A. Aldama, and E. F. Wood, Numerical evaluation of iterative and noniterative methods for the solution of the nonlinear Richards equation, *Water Resour. Res.*, *27*(6), 1147–1163, 1991.
Parlange, J.-Y., Capillary hysteresis and the relationship between drying and wetting curves, *Water Resour. Res.*, *12*(2), 224–228, 1976.
Pearce, A. J., Streamflow generation processes: An austral view, *Water Resour. Res.*, *26*(12), 3037–3047, 1990.
Philip, J. R., and D. A. de Vries, Moisture movement in porous materials under temperature gradients, *Eos Trans. AGU*, *38*(2), 222–232, 1957.
Rawls, W. J., D. L. Brakensiek, and K. E. Saxton, Estimation of soil water properties, *Trans. ASAE*, *25*(5), 1316–1320, 1328, 1982.
Reeves, M., and E. E. Miller, Estimating infiltration for erratic rainfall, *Water Resour. Res.*, *11*(1), 102–110, 1975.
Sellers, P. J., F. G. Hall, D. E. Strebel, E. T. Kanemasu, R. D. Kelly, B. L. Blad, B. J. Markham, and J. R. Wang, Experiment design and operations, in *Symposium on FIFE*, pp. 1–5, American Meteorological Society, Boston, Mass., 1990.
Shamsai, A., and T. N. Narasimhan, A numerical investigation of free surface-seepage face relationship under steady state flow conditions, *Water Resour. Res.*, *27*(3), 409–421, 1991.
Sivapalan, M., K. J. Beven, and E. F. Wood, On hydrologic similarity, 2, A scaled model of storm runoff production, *Water Resour. Res.*, *23*(12), 2266–2278, 1987.
Sloan, P. G., and I. G. Moore, Modeling subsurface stormflow on steeply sloping forested watersheds, *Water Resour. Res. 20*(12), 1815–1822, 1984.
Smith, R. E., and R. H. B. Hebbert, Mathematical simulation of interdependent surface and subsurface hydrologic processes, *Water Resour. Res.*, *19*(4), 987–1001, 1983.
Sposito, G., The "physics" of soil water physics, *Water Resour. Res.*, *22*(9), 83S–88S, 1986.
Stagnitti, F., M. B. Parlange, T. S. Steenhuis, and J.-Y. Parlange, Drainage from a uniform soil layer on a hillslope, *Water Resour. Res.*, *22*(5), 631–634, 1986.
Troch, P. A., M. Mancini, C. Paniconi, and E. F. Wood, Evaluation of a distributed catchment scale water balance model, *Water Resour. Res.*, in press, 1993.
van Genuchten, M. T., and D. R. Nielsen, On describing and predicting the hydraulic properties of unsaturated soils, *Ann. Geophys.*, *3*(5), 615–628, 1985.
Wilcox, B. P., W. J. Rawls, D. L. Brakensiek, and J. R. Wright, Predicting runoff from rangeland catchments: A comparison of two models, *Water Resour. Res.*, *26*(10), 2401–2410, 1990.
Wood, E. F., M. Sivapalan, K. J. Beven, and L. E. Band, Effects of spatial variability and scale with implications to hydrologic modeling, *J. Hydrol.*, *102*, 29–47, 1988.

C. Paniconi, CRS4, Via Nazario Sauro 10, I-09123 Cagliari, Italy.
E. F. Wood, Water Resources Program, Department of Civil Engineering and Operations Research, Princeton University, Princeton, NJ 08544.

(Received January 30, 1992;
revised September 15, 1992;
accepted September 28, 1992.)

Effects of Spatial Variability and Scale on Areal-Average Evapotranspiration

J.S. FAMIGLIETTI and E.F. WOOD
Water Resources Program
Department of Civil Engineering and Operations Research
Princeton University
Princeton, New Jersey

Submitted to:
Water Resources Research
February 5, 1993

J. S. Famiglietti and E. F. Wood
Water Resources Program
Department of Civil Engineering and Operations Research
Princeton University
Princeton, New Jersey, 08544

ABSTRACT

This paper explores the effect of spatial variability and scale on areally-averaged evapotranspiration. A spatially-distributed water and energy balance model is employed to determine the effect of explicit patterns of model parameters and atmospheric forcing on modeled areally-averaged evapotranspiration over a range of increasing spatial scales. The analysis is performed from the local scale to the catchment scale. The study area is King's Creek catchment, an 11.7 km ^{2} watershed located on the native tallgrass prairie of Kansas. The dominant controls on the scaling behavior of catchment-average evapotranspiration are investigated by simulation, as is the existence of a threshold scale for evapotranspiration modeling, with implications for explicit versus statistical representation of important process controls. It appears that some of our findings are fairly general, and will therefore provide a framework for understanding the scaling behavior of areally-averaged evapotranspiration at the catchment and larger scales.

1. Introduction

The hydrologic cycle has a significant effect on land-atmosphere interaction over a range of scales. At the catchment or regional scale, this interaction determines the frequency of flooding and drought, as well as the quantity and quality of the water supply. At the grid scale of a general circulation model (GCM), the hydrology at the land surface determines important boundary conditions for climate simulations such as soil moisture and evapotranspiration. Globally, the distribution of atmospheric water has a major impact on climate, weather, and biogeochemical cycles. To better understand the role of hydrology in these interactions, improved land surface water and energy balance models are required, particularly at the larger scales.

Two of the major problems associated with the development of larger scale (catchment scale and greater) water and energy balance models are related to scaling and aggregation of hydrological processes. The scale problem addresses the relationship between spatial variability, scale, and the proper representation of hydrologic response at a particular scale. The second problem is related to aggregating process representations known at various space-time scales up to larger scales. What is the proper way to aggregate spatially-variable hydrologic processes whose dynamics occur at different space-time scales? Is the method of aggregation related to the scale of interest?

The second and third papers in this series investigated methods of aggregating a local water and energy balance model (Famiglietti and Wood, 1992a) up to larger scales. Famiglietti and Wood (1992b) presented a deterministic approach to spatial aggregation, utilizing digital elevation models (DEMs) and geographic information systems (GIS) to represent spatial variability explicitly. This model was proposed for use at the catchment scale due to the computational expense associated with applying the spatially-distributed model structure at larger scales. Famiglietti and Wood (1992c) utilized a statistical aggregation approach, in which the local model was aggregated with respect to a statistical distribution of a combined topographic-soils index (Beven, 1986). This model was proposed for use at larger scales with the implicit assumption that a statistical representation of actual patterns of topography, soils, and soil moisture is adequate to accurately model the water and energy fluxes at these scales, and that spatial variability in these variables dominates the spatial variability in the fluxes.

This paper investigates the validity of such assumptions by analyzing the relationship between spatial variability, spatial scale, areally-averaged evapotranspiration rates, and methods of aggregation. Specifically, we will explore the dynamics of areally-averaged evapotranspiration as spatial scale increases. For consistency with the previous papers in this series, the largest scale of application is the catchment scale. However, with adequate water and energy balance data, the analysis can be extended to much larger scales. The study area is the King's Creek catchment, an 11.7 km ^{2} watershed located on the native tallgrass prairie of Kansas. This area was the site of the First ISLSCP Field Experiment (FIFE) in 1987 and 1989 (Sellers et al., 1988). During FIFE, multiscale water and energy balance data were collected using ground-based and remote equipment. Thus the FIFE data afford unique opportunities to study the scaling behavior of hydrological processes.

The spatially-distributed water and energy balance model of Famiglietti and Wood (1992b) is used to explore the sensitivity of catchment-scale evapotranspiration rates to explicit patterns of model parameters and atmospheric forcing. Areally-averaged evapotranspiration computed with spatially-distributed fields of model parameters will be systematically compared to areally-averaged evapotranspiration computed with catchment-average parameter values. The analysis will be performed over a range of spatial scales, where increasing scale is represented by progressively larger subcatchments within the King's Creek catchment. We expect that at small scales, actual patterns of model parameters and inputs (e.g. root zone moisture content, soil properties, vegetation, solar radiation) are important factors governing catchment-scale evapotranspiration rates. However, as catchment scale increases, more of the variability in the distributions underlying these patterns is sampled. We suspect that at scales larger than some threshold scale, the mean evapotranspiration rate will no longer depend on the actual patterns of variability, but rather on the statistical characteristics representing the underlying distributions. Wood et al. (1988) termed this threshold scale a Representative Elementary Area (REA), analogous to the REV for porous media. They defined the REA as a "critical area at which continuum assumptions can be used without knowledge of the patterns of parameter values, although some knowledge of the underlying distributions may still be necessary." Using a simulation approach, they found that the REA exists at spatial scales on the order of 1 km ^{2} for catchment rainfall-runoff response.

In this study we wish to further analyze and probe the REA concept in the context of catchment-scale evapotranspiration. For evapotranspiration modeling, the existence of a

REA implies that at scales greater than the REA, exact patterns of spatially-variable model parameters and inputs need not be represented explicitly. However, it may still be necessary to account for the underlying variability of these parameters through distributional functions rather than representing an area in terms of uniform parameters.

In the next section an overview of the simulation analysis and a discussion of the simulation experiments is presented. The scope of the paper is then outlined, followed by a presentation of results, a discussion and summary of this work.

2. Overview of the Analysis

Wood et al. (1988) listed three requirements for this type of simulation experiment. First, a disaggregation scheme must exist for the study catchment so that it can be partitioned into a number of smaller subcatchments. Second, a local model of hydrologic processes must exist whose scale of application is much smaller than the smallest subcatchment, so that the average response of any subcatchment is equivalent to the average of the local responses within it. Third, spatially-distributed model inputs and parameters must exist so that the local model can be applied throughout the study catchment.

The first requirement is satisfied by the FIFE data set. A 30 m U. S. Geological Survey DEM is available for the King's Creek catchment area. Topographic analysis of the DEM yielded the 4 levels of discretization shown in Figure 1. The first level of disaggregation partitions the catchment into 66 subcatchments. The second level yields 39 subcatchments, the third 13, and the fourth 5 subcatchments.

The second requirement is satisfied by the spatially-distributed water and energy balance model. This model partitions the catchment into a number of 30 m grid elements which are coregistered with the local DEM and the FIFE GIS. The local water and energy balance model of Famiglietti and Wood (1992a) is applied at each grid element of the catchment.

The third requirement is also satisfied by the FIFE dat set. The local topographic-soils index was determined for each grid element in the catchment using the local DEM and FIFE GIS (see Famiglietti and Wood, 1992b). The various soils within the catchment were determined from the FIFE GIS and the corresponding soil parameters are given in Table 3 of Famiglietti and Wood (1992b). Some allowance for spatially-variable vegetation parameters was made in this study that was not made by Famiglietti and Wood (1992b). A 5 m tall vegetation was modeled along the stream channels (roughly 5 percent of the

catchment surface area). In these locations, the measurement height, z_a, was set equal to 7 m; the roughness length, z_0, was assumed equal to 0.8 m; the zero plane displacement, d, was assumed equal to 3.35 m; and a value of 5 x 10^{9} s/m was assumed for R_u, the root resistance. Spatially-distributed clear-sky solar radiation was provided by Dubayah (personal communication) for the FIFE site for October 5, 1987. The remaining model parameters are summarized by Famiglietti and Wood (1992b) in Tables 1, 2, and 4 for FIFE intensive field campaign IFC4.

The spatially-distributed model was applied at the King's Creek catchment for the first 5 days of IFC4 (October 5-9, 1987). Simulations were run using the spatially-variable topographic, soil, moisture content, vegetation, and solar radiation data described above. Since this is primarily a sensitivity study and not a validation study, the spatially-distributed solar radiation data of October 5 were also used to force model simulations of October 6-9. Spatially-variable initial root and transmission zone moisture contents were also employed (see Figure 2). This simulation will be referred to as the control run in future sections. Additional simulations were run in which these spatially-distributed data were systematically held at catchment-average values. These simulations will be referred to as the sensitivity runs.

For a particular simulation, the local (grid-element) evapotranspiration fluxes were averaged over the various subcatchments shown in Figure 1 at selected times during the simulation. The average evapotranspiration rate for each of the subcatchments was plotted versus subcatchment area to analyze the effect of spatial variability on catchment-average evapotranspiration with increasing spatial scale. To determine the sensitivity of catchment-average evapotranspiration to spatial-variability in the various model parameters and inputs, plots of catchment-average evapotranspiration rate versus catchment area were compared for the control and sensitivity runs at different times during the simulations.

3. Scope of the Paper

This paper will focus on two sets of questions regarding the relationship between spatial heterogeneity, scale, and areally-averaged evapotranspiration:

1.) What is the effect of spatial heterogeneity on areally-averaged evapotranspiration rates as spatial scale increases? Does a REA exist for evapotranspiration modeling? This threshold scale would represent a fundamental building block for larger-scale evapotranspiration modeling. At scales larger than the REA it should be possible to simplify the representation of areally-averaged evapotranspiration response, while still retaining the important effects of heterogeneity in land-atmosphere interaction. For regions larger than the REA scale, actual patterns of important model variables such as soil moisture need not be considered; rather, their spatial variability can be considered statistically through their means and variances.

2.) To which spatially-variable model parameters is the scaling behavior of areally-averaged evapotranspiration most sensitive? (Note that the term 'scaling behavior' is defined here as the relationship between areally-averaged evapotranspiration rate and spatial scale.) Are there conditions under which evapotranspiration rates scale up? (The term 'scaling up' is defined here as an insignificant bias between evapotranspiration computed with spatially-variable versus spatially-constant model parameters and inputs.) These results will have important implications for modeling areally-averaged evapotranspiration at the catchment and larger scales. Relevant issues include which model parameters will require a statistical representation of spatial variability at scales greater than the REA scale, and which can be represented by simple areally-averaged or effective values.

As stated previously, this analysis was conducted for the King's Creek catchment at the FIFE site. The King's Creek catchment has little spatial variability in soil properties (predominantly silty clay loam), vegetation (predominantly native tallgrass) and topography (roughly 100 meters of elevation difference). Consequently, we expect spatial variability in root zone moisture content to be an important control on areally-averaged evapotranspiration rates. We expect this to be particularly true during periods of moisture stress, when evapotranspiration frequently occurs at soil or vegetation-controlled rates. Figure 3 shows the general form of the transpiration capacity-moisture content and exfiltration capacity-moisture content relationships used in the spatially-distributed model. These relationships

suggest that when soil and vegetation controls of evapotranspiration are active, and the spatial distribution of root zone moisture content includes the nonlinear portions of the curves, evapotranspiration will not scale up at King's Creek. Under these atmospheric and land surface conditions, we expect that a statistical representation of root zone moisture content will be required to adequately model evapotranspiration at spatial scales greater than the REA scale. In this study, we explore this hypothesis by simulating our control and sensitivity runs using data from FIFE IFC4, a period during which soil and vegetation-controls of evapotranspiration were active. The spatial distribution of initial root zone moisture content shown in Figure 2 was also employed in the simulations. This distribution yields significant spatial variability in transpiration and exfiltration capacities, so that the nonlinearity shown in Figure 3 is well represented within the catchment.

4. Results

Figure 4 shows simulated catchment-average evapotranspiration for the control run. To analyze the effect of spatial variability and scale on catchment-average evapotranspiration, the procedure outlined above was applied at numerous times during the simulation. The results for three times – 1245, 1415, and 1815 GMT, October 7, 1987 (0745, 0915 and 1315 local time; times 56, 57.5 and 61.5 in Figure 4) – are shown in Figure 5a. For comparison, Figure 5b shows catchment average evapotranspiration versus catchment area for a sensitivity run in which all model parameters and inputs were held at catchment-average values. Figure 5a shows that the effect of spatial variability has been in general, to increase the variability in the catchment-average evapotranspiration rate at small scales, and to increase the mean rate at all scales. Figure 5a suggests that a threshold (REA) scale does in fact exist which marks the transition from highly variable mean behavior at small scales, to stable mean behavior at larger scales. This figure also shows that the variability in the mean evapotranspiration rate at small scales, and thus the REA scale, is greater at mid-day than in the morning. It is inferred that for areas larger than the REA, most of the variability in model parameters and inputs has been sampled, so that at larger scales, the mean evapotranspiration rate stabilizes.

Note that the times shown in Figure 5 should be considered representative time steps for the simulation. Similar scaling behavior was observed throughout the simulation at the

corresponding times each day (i.e. an increase in the REA scale from local scales in the morning to 1 - 2 km ^{2} at mid-day, and decreasing back to local scales in the late afternoon).

The significant bias between evapotranspiration computed with and without spatially-variable model parameters indicates that spatial heterogeneity in land surface-atmosphere interaction plays a major role in the simulation of catchment-average evapotranspiration. To elucidate fundamental relationships between spatial variability, scale, and evapotranspiration fluxes, the scaling analysis described above was applied to the three components of simulated evapotranspiration – evaporation from the wet canopy, transpiration from the dry canopy, and evaporation from bare soils – at the same times as in Figure 5. In each case an attempt was made to determine the spatially-variable model parameters to which the component was most sensitive, and whether this sensitivity changed diurnally. This analysis should result in a better understanding of the important process controls on areally-averaged evapotranspiration, and thus the scaling behavior shown in Figure 5a, with implications for how these controls should be represented within land surface parameterizations.

The results of the scaling analysis are described in detail for bare soil evaporation, since evaporation from bare soils was the primary component of evapotranspiration during FIFE IFC4 due to senescence of the native tallgrass (see Figure 6). The results for wet canopy evaporation and dry canopy transpiration are analogous to those for bare soil evaporation. These results are presented in detail by Famiglietti (1992) and are only briefly described here.

4.1 Bare-Soil Evaporation

The actual rate of evaporation from bare soils, e_{bs}, is given by Famiglietti and Wood (1992b) as

$$e^i_{bs} = min[e^{*i}, e^i_{pe}] \tag{1}$$

where i is the grid element index, e^* is the local exfiltration capacity and e_{pe} is the local potential evaporation rate. When the exfiltration capacity is less than the potential evaporation rate, the actual evaporation rate is equal to the exfiltration capacity. Evaporation under these conditions is known as soil-controlled evaporation. In this section the scaling behavior of bare-soil evaporation is investigated in terms of its two components, the exfiltration capacity and the potential evaporation.

4.1.1 *Potential Evaporation*

Figure 7 shows the computed catchment-average potential evaporation rate versus catchment scale for the three representative time steps during the control simulation (1245, 1415, and 1815 GMT, October 7, 1987). In each case, the catchment-average potential evaporation shows more variability at small scales than at large scales. Figure 7 suggests that a threshold (REA) scale exists which marks this transition in mean behavior. This figure also shows that the variability in catchment average potential evaporation at small scales, and thus the REA scale, is greater at mid-day than in the morning.

To better understand the sources of variation in computed catchment-average potential evaporation with scale, two sensitivity runs were simulated. Of the parameters assumed spatially variable in this report, those that affect potential evaporation most significantly are solar radiation and soil properties. The two sensitivity runs utilized the following combinations of model inputs: spatially-constant solar radiation and spatially-constant soil properties (crcs); and spatially-constant solar radiation and spatially-variable soil properties (crvs). These were compared to the control run, which was generated with spatially-variable solar radiation data and spatially-variable soil properties (vrvs). Spatially-constant model inputs were held at their catchment-average values.

Figure 8 shows computed catchment-average potential evaporation rates versus catchment scale at 1815 GMT for the control and sensitivity runs. The solid line represents catchment-average potential evaporation for the case of spatially-constant solar radiation and soil properties. The inclusion of spatially-variable soil properties has a minor effect on catchment-average potential evaporation rates at all scales. The inclusion of spatially-variable solar radiation has a significant impact on the catchment-average potential evaporation, yielding a high degree of variability at small scales. At larger scales however, spatial variability in solar radiation has less of an effect on catchment-average potential evaporation rates. Figure 8 also shows that the REA scale for the potential evaporation rate at this time is 1.0 - 2.0 km ^{2}. We believe that at this scale, most of the spatial variability in the solar radiation has been sampled, so that at larger scales the mean potential evaporation rate stabilizes.

4.1.2 *Exfiltration Capacity*

To better understand the scaling behavior of catchment-average exfiltration capacity, three sensitivity runs were simulated and compared to the control run (vmvrvs). Of the

parameters that are assumed spatially variable in this work, those with the most significant impact on exfiltration capacities include root zone moisture content, soil properties, and solar radiation. We systematically held these parameters at their catchment-average values in the sensitivity runs. In the first simulation, spatially-constant soil moisture, solar radiation and soil properties were employed (cmcrcs). The second simulation maintained constant solar radiation and soil properties, but was initialized with the spatial distribution of root zone moisture content shown in Figure 2 (vmcrcs). The third simulation added spatially-variable soil properties to the list of model inputs used in the second simulation (vmcrvs).

Figure 9 shows catchment-average exfiltration capacity versus catchment scale at 1815 GMT, October 7, 1987, for the control and sensitivity runs described above. The lower line (cmcrcs) represents catchment-average exfiltration capacity for spatially-constant soil moisture, solar radiation and soil properties. The upper line (vmcrcs) shows the impact of including spatially-variable moisture content to the simulation. The mean exfiltration capacity has increased over all scales, and its variability has increased significantly at small scales. The inclusion of spatially-variable soil properties has lowered the mean exfiltration capacity over all scales. The inclusion of spatially-variable solar radiation has little impact on the mean exfiltration capacity over all scales. Figure 9 implies that, for the parameter combinations tested, the dominant control on the scaling behavior of the catchment-average exfiltration capacity is the spatial distribution of moisture content. Figure 9 also shows that the REA scale for exfiltration capacity at this time step is roughly 1.0 - 2.0 km ^{2}. At this scale, most of the spatial variability in the moisture content, solar radiation and soil properties has been sampled, so that at larger scales the mean exfiltration capacity stabilizes.

These results are best understood by considering the relationship of the spatial distribution of root zone moisture content (see Figures 2 for the distribution used to initialize the simulations) to the exfiltration capacity - soil moisture relationship shown in Figure 3. When the moisture content distribution lies on a linear portion of this curve, spatial variability in moisture content has little effect on the catchment-average exfiltration capacity. However, when the moisture content distribution includes the nonlinear portion of the curve, spatial variability in moisture content has a significant impact on the catchment-average exfiltration capacity.

4.1.3 Actual Bare-Soil Evaporation

The effect of including spatially-variable soil moisture and other model inputs in a spatially-distributed catchment simulation is that different catchment locations evaporate

at different rates during the same time step. At any time, all bare-soil locations within the catchment fall into two groups – those evaporating at the potential rate and those evaporating at soil-controlled exfiltration capacities. Thus, variability in the catchment-average actual evaporation rate with scale is a function of the relative amounts of land surface evaporating at potential or soil-controlled rates and the scaling behavior of these two components. (See Famiglietti and Wood (1992c), who compute the amount of land surface evaporating at potential or soil-controlled rates for each time step during IFC4). If the REA scale differs for the potential and capacity components of evaporation, then the REA scale for the actual evaporation rate should vary according to the amount of land surface evaporating under either condition. To explore these interactions, actual bare-soil evaporation was computed for the first five days of IFC4 for the control run. The catchment-average potential evaporation rate, exfiltration capacity, and actual evaporation rate were plotted versus catchment scale for 1245, 1415, and 1815 GMT, October 7, 1987.

Figure 10a shows the results at 1245 GMT. In the early morning, the potential evaporation rate is low, as shown by the lower line, and the simulation results indicates that most of the catchment evaporates at this low rate. The catchment-average actual evaporation rate should nearly equal the catchment-average rate of potential evaporation. Figure 10a shows that in fact the two are essentially equal. In the morning, when most of the catchment is evaporating at the potential rate, the dominant controls on the scaling behavior of the catchment-average actual evaporation rate (and thus its REA) are those associated with the potential evaporation rate.

Figure 10b presents the results for 1415 GMT (mid-morning). As the potential evaporation rate increases (middle line), more of the catchment evaporates at soil-controlled rates. Thus, the degree of variability in the catchment-average actual evaporation (lower line) at small scales is greater than that of the potential evaporation, but less than that of the exfiltration capacity. Both the potential and capacity components are contributing to the variability in catchment-average actual evaporation at small scales, and to the mean actual evaporation rate over all scales.

The results for 1815 GMT (mid-day) are displayed in Figure 10c. At mid-day, the potential evaporation rate (middle line) exceeds the exfiltration capacity (upper line) over much of the catchment. Thus the catchment-average actual evaporation rate reflects more of the variability of the catchment-average exfiltration capacity. More bare-soil locations within the catchment have switched from evaporation at potential rates to soil-controlled

rates. Consequently, the dominant controls of the scaling behavior of catchment-average actual evaporation have switched from those associated with the potential evaporation rate to those associated with the exfiltration capacity.

Figure 11 shows the catchment-average actual evaporation rate versus catchment scale for 1245, 1415, and 1815 GMT. This figure clearly shows the increase in variability of the catchment-average actual evaporation rate at small scales with time. Figure 11 also suggests that the REA scale increases with time, from very small scales in the morning, to 1.0 - 2.0 km ^{2} at mid-day. Both the increased variability at small scales and the increase in the REA scale reflect the change in evaporation modes within the catchment, from predominantly potential rates in the morning, to predominantly soil-controlled rates at mid-day.

4.2 Dry Canopy Transpiration and Wet Canopy Evaporation

Famiglietti (1992) observed scaling behavior similar to that of bare soil evaporation for the cases of dry canopy transpiration and wet canopy evaporation. As in the case of bare-soil evaporation, an increase in the REA scale was noted, from local scales in the early morning to 1.0 - 2.0 km ^{2} at mid-day. Figure 12 shows these dynamics for the catchment-average actual transpiration rate. Both the increased variability at small scales and the increase in the REA scale correspond to the change of transpiration modes within the catchment, from primarily unstressed rates in the morning, to predominantly vegetation-controlled rates at mid-day. As the mechanisms of transpiration switch from those associated with unstressed rates to those associated with increased stomatal control, the dominant controls on the scaling behavior of catchment-scale transpiration switch accordingly. The dominant spatially-variable model parameters for the various components of evapotranspiration are summarized in Table 1 for the King's Creek catchment during FIFE IFC4.

4.3 Evapotranspiration

Famiglietti and Wood (1992a) compute local rate of evapotranspiration, e^i, as

$$e^i = f^i_{bs} e^i_{bs} + f^i_v [e^i_{wc} + e^i_{dc}] \tag{2}$$

where f_{bs} is the local fraction of bare soil, f_v is the local fraction of vegetated soil, e_{wc} is rate of evaporation from the wet-canopy, and e_{dc} is rate of transpiration from the dry canopy. The

catchment-average evapotranspiration rate is simply the average of the local rates, or the sum of the average bare-soil, wet canopy, and dry canopy components of evapotranspiration.

Figure 13 shows the catchment-average evapotranspiration rate versus catchment scale at 1415 GMT, October 7, 1987. The catchment-average bare-soil, dry canopy and wet canopy evaporation components are plotted as well. The weighted sum of these components yields the catchment-average evapotranspiration rate at any scale. The variability in the catchment-average evapotranspiration rate with scale is therefore a function of the variability of its components.

The catchment-average evapotranspiration rate versus catchment scale is shown in Figure 5a for 1245, 1415, and 1815 GMT, October 7, 1987. The scaling behavior of catchment-average evaptranspiration reflects that of its components, described above. The variability at small scales increases with time until mid-day. The REA scale shows a corresponding increase with time, from small scales in the morning, to 1.0 - 2.0 km ^{2} at mid-day. Both the increased variability at small scales and the increase in the REA scale reflect the change in the dominant controls on the catchment-average evapotranspiration rate, from those associated with potential rates in the morning, to those associated with soil and vegetation-controlled rates at mid-day.

5. Discussion

5.1 Effects of Spatial Variability and Scale on Areal-Average Evapotranspiration

The previous sections have shown that for the simulations conducted in this study, the dominant controls on the scaling behavior of catchment-average evapotranspiration depend on the dominant controls on its components – evaporation from the wet canopy, transpiration from the dry canopy, and evaporation from bare soils. The controls on these components depend in turn on whether evapotranspiration is occurring at potential rates or soil and vegetation-controlled rates.

In general, when root-zone moisture content levels are relatively high, or the potential evapotranspiration rates are low, evapotranspiration will occur at predominantly potential rates. The scaling behavior of catchment-average evapotranspiration under these conditions is largely determined by the controls on the potential evapotranspiration rates. When

root zone moisture content levels are low, or potential evapotranspiration rates are high, evapotranpiration will occur at soil and vegetation-controlled rates. The scaling behavior of catchment-average evapotranspiration is dominated by the controls on the soil and vegetation-controlled rates.

The interaction between the land surface and the atmosphere will have both seasonal and diurnal time scales. For example, during wetter periods, evapotranspiration will occur at predominantly potentential rates. However, the space-time variability in atmospheric forcing and moisture content, as well as the spatial variability in vegetation and soils, will result in portions of the catchment evaporating at soil or vegetation-controlled rates if the potential evapotranspiration rate is too high (e.g. at mid-day), or if moisture content levels fall too low (e.g. during an extended interstorm period). Conversely, during dry periods, more evapotranspiration will occur at moisture-stressed rates, but some or all of the catchment may evaporate at potential rates when the potential rates are low (e.g. in the early morning), or if root zone moisture contents rise to high levels (e.g. after a storm). The seasonal and diurnal dynamics of land-atmosphere interaction will be reflected in the scaling behavior of catchment-average evapotranspiration.

5.2 Implications for Hydrologic Modeling

This study outlines a methodology for assessing the importance of spatial variability in land surface and atmospheric variables for modeling evapotranspiration at the catchment scale. The existence of an REA scale for simulated evaptranspiration indicates how spatial variability in important variables can be incorporated into hydrological models. At scales greater than the REA scale, much of the variability in the underlying distributions of land surface parameters and atmospheric forcing has been sampled. At these scales, a statistical representation of spatial variability in important model parameters and inputs is adequate for evapotranspiration modeling (i.e. a statistically-aggregated model of land hydrologic processes is an appropriate representation for catchment evapotranspiration modeling). At scales less than the REA scale, explicit patterns of important spatially-variable model parameters and inputs have a significant impact on simulated evapotranspiration. At these scales a spatially-explicit aggregation approach is required to model catchment-average evapotranspiration at scales less than the REA scale.

One example of a statistical aggregation procedure is given by Famiglietti and Wood (1992c). They present a statistical-dynamical hydrological model, in which the local water

and energy balance model is aggregated with respect to a probability density function of combined topographic and soil properties. The spatial variability in topographic and soil properties results in spatial variability in modeled moisture content and the water and energy fluxes related to moisture content, such as runoff and evapotranspiration. All other model parameters and inputs in the statistical model are represented by catchment-average values. However, when spatial variability in these other parameters is correlated to the spatial distribution of the topographic-soils index (e.g. vegetation parameters), it can easily be incorporated into the model framework.

Figure 14 compares catchment-average evapotranspiration computed for the King's Creek catchment (for October 5-9, 1987) using the spatially-distributed model, the statistically-aggregated model, and the one-dimensional local model. The middle line in Figure 14 represents the control simulation of evapotranspiration computed using the spatially-distributed model with all model inputs and parameters varying spatially. The upper line represents evapotranspiration computed with the statistically-aggregated model. The difference between these two simulations results from the combined effect of representing spatially-variable moisture content statistically and all other model inputs and parameters with catchment-average values (e.g. solar radiation, vegetation, soil properties). The lower line represents evapotranspiration computed with the one-dimensional model. The one-dimensional simulation represents the effect of holding all model inputs and parameters, including initial root zone moisture content and the topography, at catchment-average values. At the catchment scale there is little difference between explicitly and statistically- aggregated evapotranspiration at the King's Creek catchment. However, there is a significant difference between the simulations run with spatially-constant and spatially-variable initial root zone moisture content.

Figure 14 clearly indicates that at the King's Creek catchment, during IFC4, a period when soil and vegetation controls of evapotranspiration were active, modeled evapotranspiration does not scale up during mid-day hours. The considerable bias between evapotranspiration computed with spatially-variable root zone moisture content and catchment-average moisture content indicates further that some representation of spatial variability in root zone moisture content (and in this case, the topographic-soil index, which is employed to model topographic redistribution of subsurface soil moisture and thus spatial variability in root zone moisture content) more so than other model parameters, is required for realistic simulation of evapotranspiration during this time period. Figure 14 also shows that at the scale of the

King's Creek catchment, which is greater than the REA scale, a statistical representation of the spatial variability in topography, and thus root zone moisture content, is an adequate representation of the actual patterns represented within the spatially-distributed model.

As previously mentioned, our choice to simulate evapotranspiration during IFC4 at the King's Creek catchment was made to investigate the role of spatial variability in root zone moisture content. Consequently, these results may be in part site, model, and time dependent. For example, a site with greater spatial variability in vegetation may show a stronger dependence on vegetation parameters than root zone soil moisture content. Or, if the comparison shown in Figure 14 were repeated during IFC3 (August 6-21, 1987), a period during which root zone moisture content was relatively wet and evapotranspiration occurred at potential rates, then spatial variability in moisture content may not be the dominant control on the scaling behavior of areally-averaged evapotranspiration. Under these land and atmospheric conditions, evapotranspiration may scale up more readily. Similarly, we suggest that later in the year, or in general when the spatial distribution of root zone moisture content is relatively dry with little spatial variability, even though evapotranspiration may occur under active soil and vegetation control, it may again scale up readily.

However, we believe that the findings presented here provide a framework for understanding and modeling areally-averaged evapotranspiration at the catchment and larger scales. The concept that the dominant controls on areally-averaged evapotranspiration vary with the amount of land surface evaporating at potential rates versus soil or vegetation-controlled rates, is, we propose, site independent and applicable at larger scales. At these larger scales ($O(10000\ km^2)$), the variability in the various components of areally-averaged evapotranspiration may be a function of large scale controls that are not evident at the catchment scale. For example, topographic, soil, and vegetation properties may vary on the scale of regional geology and climate. Soil moisture may vary on the scale of storm systems. Potential evapotranspiration may vary with synoptic-scale weather patterns and variations in vegetation and soil properties. The behavior of areally-averaged evapotranspiration from the catchment scale to the scale of a GCM grid square, and the land surface-atmosphere conditions under which evapotranspiration will scale up, are the subjects of ongoing research.

6. Summary

In this paper we explored the effect of spatial variability and scale on areally-averaged evapotranspiration. We employed a spatially-distributed model to determine the effect of explicit patterns of model parameters and atmospheric forcing on modeled areally-averaged evapotranspiration over a range of increasing spatial scales, from the local scale to the catchment scale. The study catchment was the King's Creek catchment, an 11.7 km ^{2} watershed located on the native tallgrass prairie of Kansas.

This report shows that an REA scale exists for catchment-scale evapotranspiration modeling at the King's Creek catchment. We believe that at scales greater than this threshold scale, a statistically-aggregated model of land hydrologic processes is an appropriate representation for catchment evapotranspiration modeling. At scales less than the REA scale, we believe that a spatially-explicit aggregation approach is required to model catchment-average evapotranspiration.

The simulations conducted for the King's Creek catchment showed that the dominant controls on the scaling behavior of catchment-average evapotranspiration depend on the dominant controls on its components – evaporation from the wet canopy, transpiration from the dry canopy, and evaporation from bare soils. The controls on these components depend in turn on whether evapotranspiration is occurring at potential rates or soil and vegetation-controlled rates. During FIFE IFC4, a period of significant soil and vegetation control of evapotranspiration, spatial variability in root zone moisture content was shown to be the dominant control on areally-averaged evapotranspiration for the catchment. It was shown by example that some representation of spatial variability in root zone moisture content was required to avoid significant bias in computed evapotranspiration during IFC4. It was also shown that a statistical representation of this spatial variability was adequate at the catchment scale.

Although this work was performed for a specific location at the catchment scale, we believe that the some of the concepts outlined here are fairly general. Therefore, we believe that these findings will provide a framework for understanding the scaling behavior of areally-averaged evapotranspiration at the catchment and larger scales.

Acknowledgements. This work was supported by NASA grants NAGW-1392 and NGT-

60153; this research support is gratefully acknowledged. We thank Ralph Dubayah for providing spatially-distributed solar radiation data for the FIFE site. We thank Dominique Thongs for providing the spatial averaging software and for his help in processing other spatially-distributed FIFE data. This work benefited greatly from discussions with Robert Gurney.

TABLE 1. Dominant Spatially-Variable Model Parameters

	wet canopy evaporation	dry canopy transpiration	bare soil evaporation
potential/unstressed rates	vegetation	vegetation	-
soil/vegetation controlled rates	-	root zone moisture content	root zone moisture content

7. References

1. BEVEN, K., 1986: Runoff production and flood frequency in catchments of order n: An alternative approach. *Scale problems in hydrology*, V. K. Gupta et al. Eds., D. Reidel Publishing Company, 107-131.
2. BROOKS, R. H. AND A. T. COREY, 1964: Hydraulic properties of porous media. *Hydrology Paper No. 3*, Colorado State Univ., Ft. Collins, Colorado.
3. FAMIGLIETTI, J. S., 1992: Aggregation and scaling of spatially-variable hydrological processes: Local, Catchment-Scale, and Macroscale Models of Water and Energy Balance. Ph. D. dissertation, Department of Civil Engineering and Operations Research, Princeton University, Princeton, NJ.
4. FAMIGLIETTI, J. S. AND E. F. WOOD, 1992a: Aggregation and scaling of spatially-variable hydrological processes, 1, A local model of water and energy balance. Submitted to
5. FAMIGLIETTI, J. S. AND E. F. WOOD, 1992b: Aggregation and scaling of spatially-variable hydrological processes, 2, A catchment-scale model of water and energy balance. Submitted to *Wat. Resour. Res.*
6. FAMIGLIETTI, J. S. AND E. F. WOOD, 1992c: Aggregation and scaling of spatially-variable hydrological processes, 3, A macroscale model of water and energy balance. Submitted to *Wat. Resour. Res.*
7. SELLERS, P. J., F. G. HALL, G. ASRAR, D. E. STREBEL, AND R. E. MURPHY, 1988: The first ISLSCP field experiment (FIFE). *Bull. Amer. Meteor. Soc.*, **69**, 22-27.
8. SIVAPALAN, M., K. BEVEN AND E. F. WOOD, 1987: On hydrologic similarity, 2. A scaled model of storm runoff production. *Water Resour. Res.* **23**, 2266-2278.
9. WOOD, E. F., M. SIVAPALAN, K. BEVEN, AND L. BAND, 1988: Effects of spatial variability and scale with implications to hydrologic modeling. *J. Hydrol.* **102**, 29-47.

Figure Captions List

Fig. 1. Disaggregation of the King's Creek catchment into subcatchments. From left to right and top to bottom: 66, 39, 13, and 5 subcatchments.

Fig. 2. Spatial distribution of root zone moisture content used to initialize simulations of IFC4. The scale black to white represents 45 percent by volume to less than 10 percent by volume.

Fig. 3. General form of transpiration capacity and exfiltration capacity versus moisture content utilized in Famiglietti and Wood (1992a).

Fig. 4. Evapotranspiration computed for the King's Creek catchment during FIFE IFC4, October 5-9, 1987 (control run). Time 0 corresponds to 445 GMT, October 5.

Fig. 5. Computed catchment-average evapotranspiration rate versus catchment area for 1245, 1415, and 1815 GMT, October 7, 1987: a.) control run; b.) all parameters spatially-averaged.

Fig. 6. Evapotranspiration computed for the King's Creek catchment during FIFE IFC4, October 5-9, 1987 (control run): a.) for bare soil (ebs), dry canopy (edc), and wet canopy (ewc) components, and total evapotranspiration (et); b.) for each component weighted by the fraction of bare soil (fbs) or the fraction of vegetated surface (fv). Time 0 corresponds to 445 GMT, October 5.

Fig. 7. Computed catchment-average potential evaporation versus catchment area for three 1245, 1415, and 1815 GMT, October 7, 1987.

Fig. 8. Computed catchment-average potential evaporation versus catchment area at 1815 GMT, October 7, 1987 for spatially-constant solar radiation and spatially-constant soil properties (crcs); spatially-constant solar radiation and spatially-variable soil properties (crvs); and spatially-variable solar radiation and spatially-variable soil properties (vrvs).

Fig. 9. Computed catchment-average exfiltration capacity versus catchment area at 1815 GMT, October 7, 1987 for the following combinations of model inputs: spatially-constant moisture content, solar radiation, and soil properties (cmcrcs); spatially-variable moisture content and spatially-constant solar radiation and soil properties (vmcrcs); spatially-variable soil moisture and soil properties and spatially-constant solar radiation (vmcrvs); spatially-variable moisture content, solar radiation and soil properties (vmvrvs).

Fig. 10. Computed catchment-average potential evaporation, exfiltration capacity, and actual evaporation versus catchment area for October 7, 1987: a.) 1245 GMT; b.) 1415 GMT; and c.) 1815 GMT.

Fig. 11. Computed catchment-average actual evaporation rate versus catchment area for 1245, 1415, and 1815 GMT, October 7, 1987.

Fig. 12. Computed catchment-average actual transpiration rate versus catchment area for 1245, 1415, and 1815 GMT, October 7, 1987.

Fig. 13. Computed catchment-average evapotranspiration rate, catchment-average wet canopy evaporation rate, catchment-average dry canopy transpiration rate, and catchment-average bare soil evaporation rate versus catchment area for 1415 GMT, October 7, 1987.

Fig. 24. Computed catchment-average evapotranspiration using the spatially-distributed model (explicit), the statistically-aggregated model (statistical), and the one-dimensional local model (1-d), October 5-9, 1987.

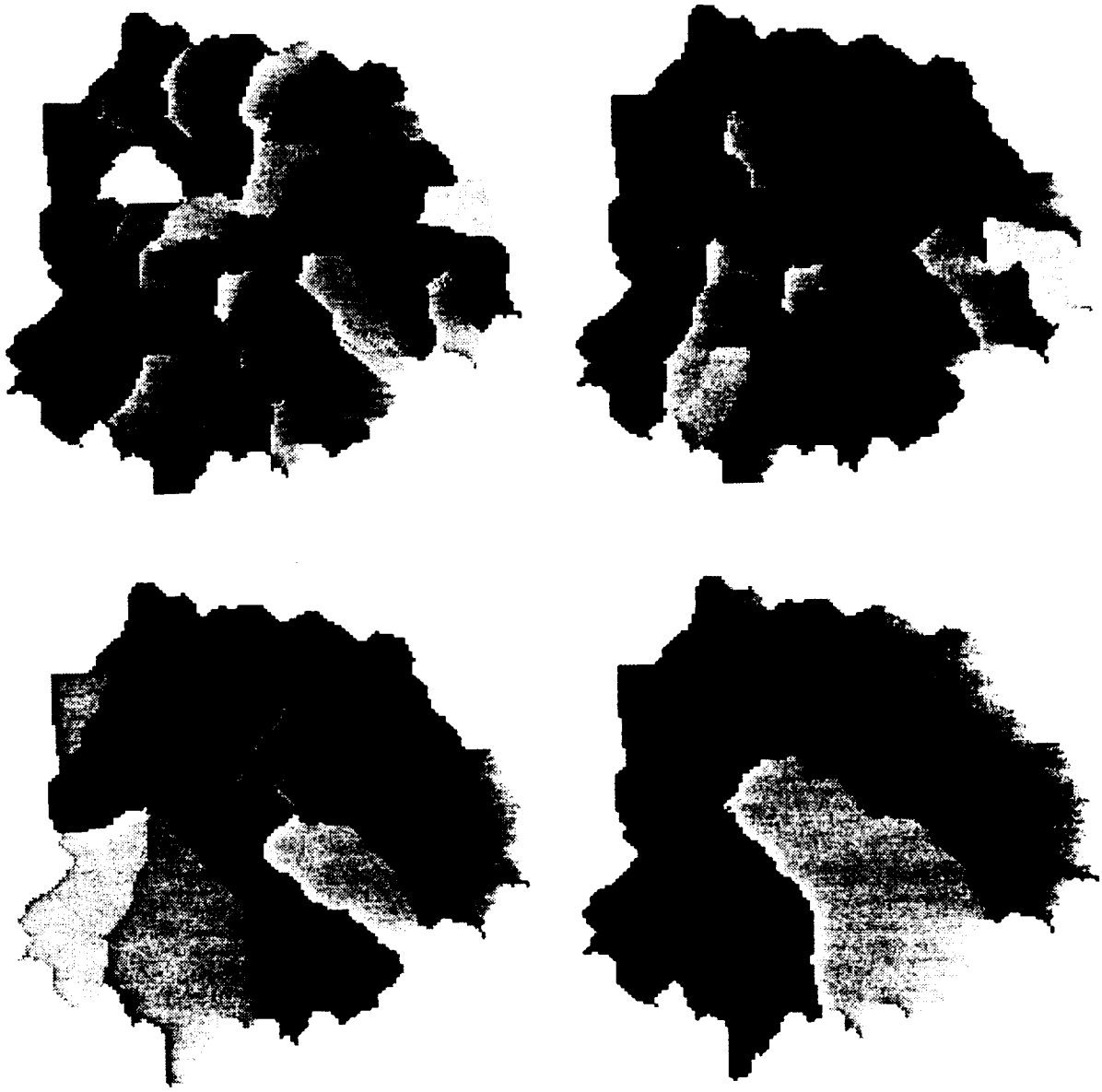

Figure 1. Disaggregation of the King's Creek catchment into subcatchments. From left to right and top to bottom: 66, 39, 13, and 5 subcatchments.

Figure 2. Spatial distribution of root zone moisture content used to initialize simulations of IFC4. The scale black to white represents greater thean 45 percent by volume to less than 10 percent by volume.

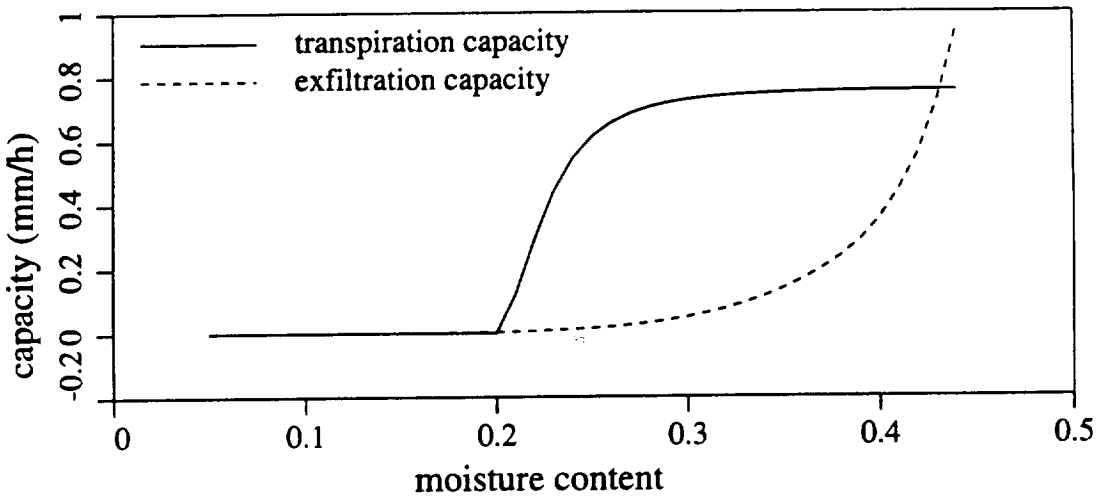

Figure 3. General form of transpiration capacity and exfiltration capacity versus moisture content utilized in Famiglietti and Wood (1992a-c).

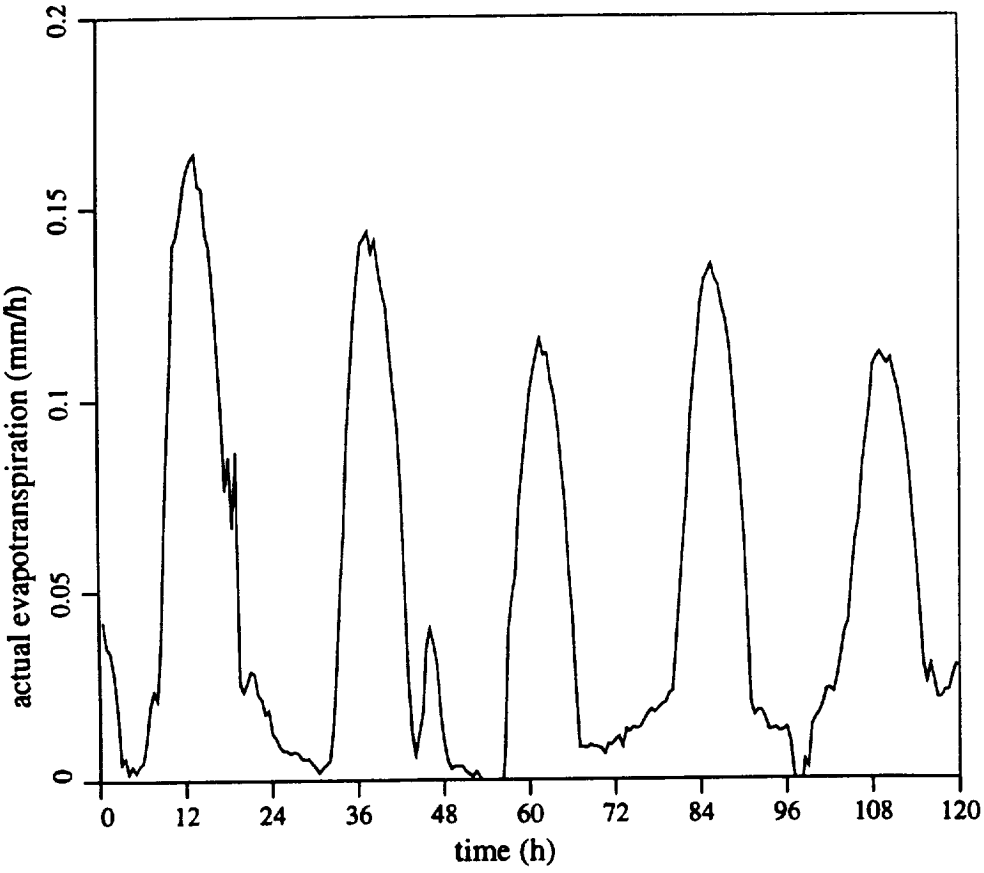

Figure 4. Evapotranspiration computed for the King's Creek catchment during FIFE IFC4, October 5-9, 1987 (control run). Time 0 corresponds to 445 GMT, October 5.

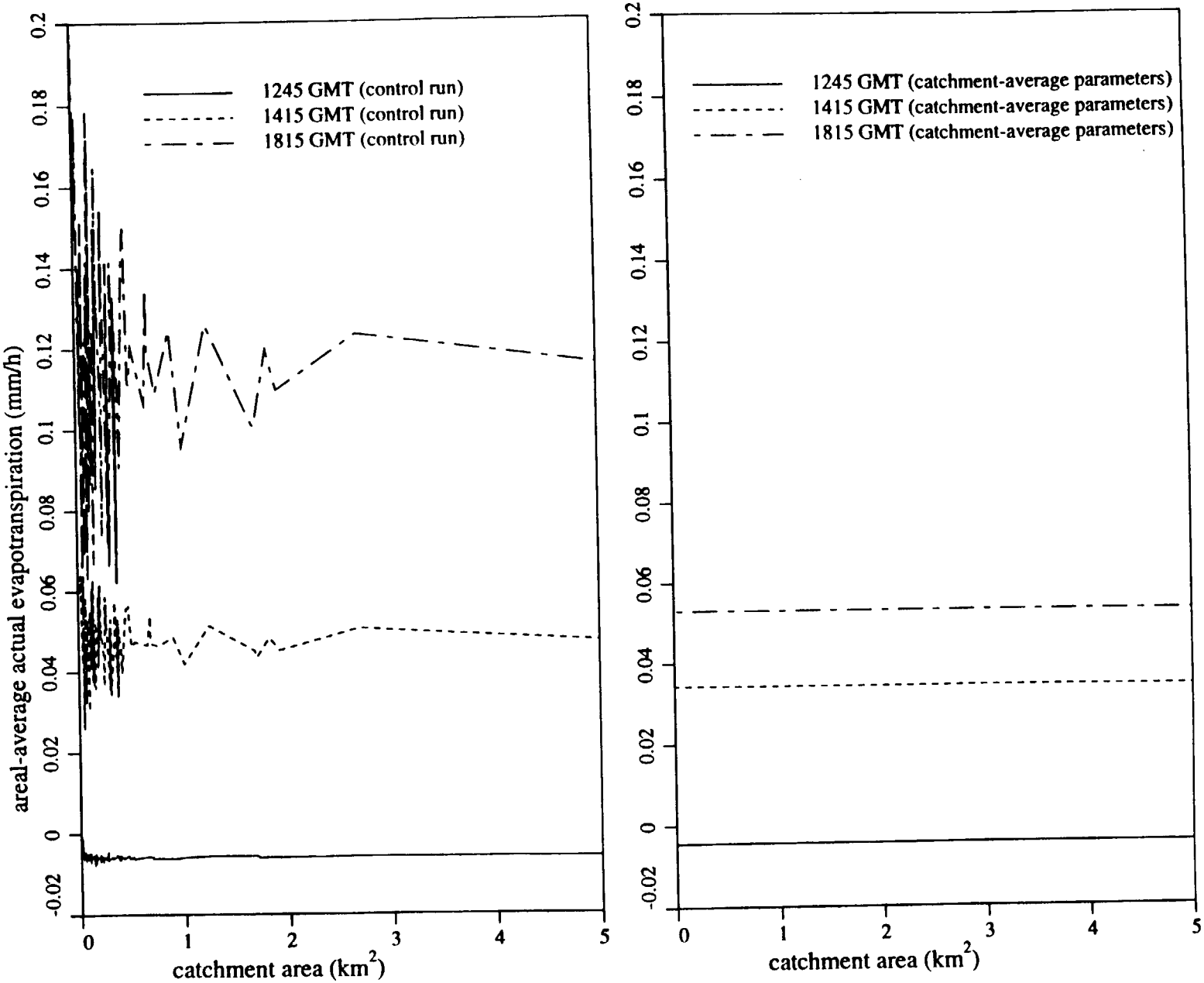
areal-average actual evapotranspiration (mm/h)
0.2
0.18
0.16
0.14
0.12
0.1
0.08
0.06
0.04
0.02
0
-0.02
1245 GMT (control run)
1415 GMT (control run)
1815 GMT (control run)
0
1
2
3
4
5
catchment area (km^2)
1245 GMT (catchment-average parameters)
1415 GMT (catchment-average parameters)
1815 GMT (catchment-average parameters)
catchment area (km^2)

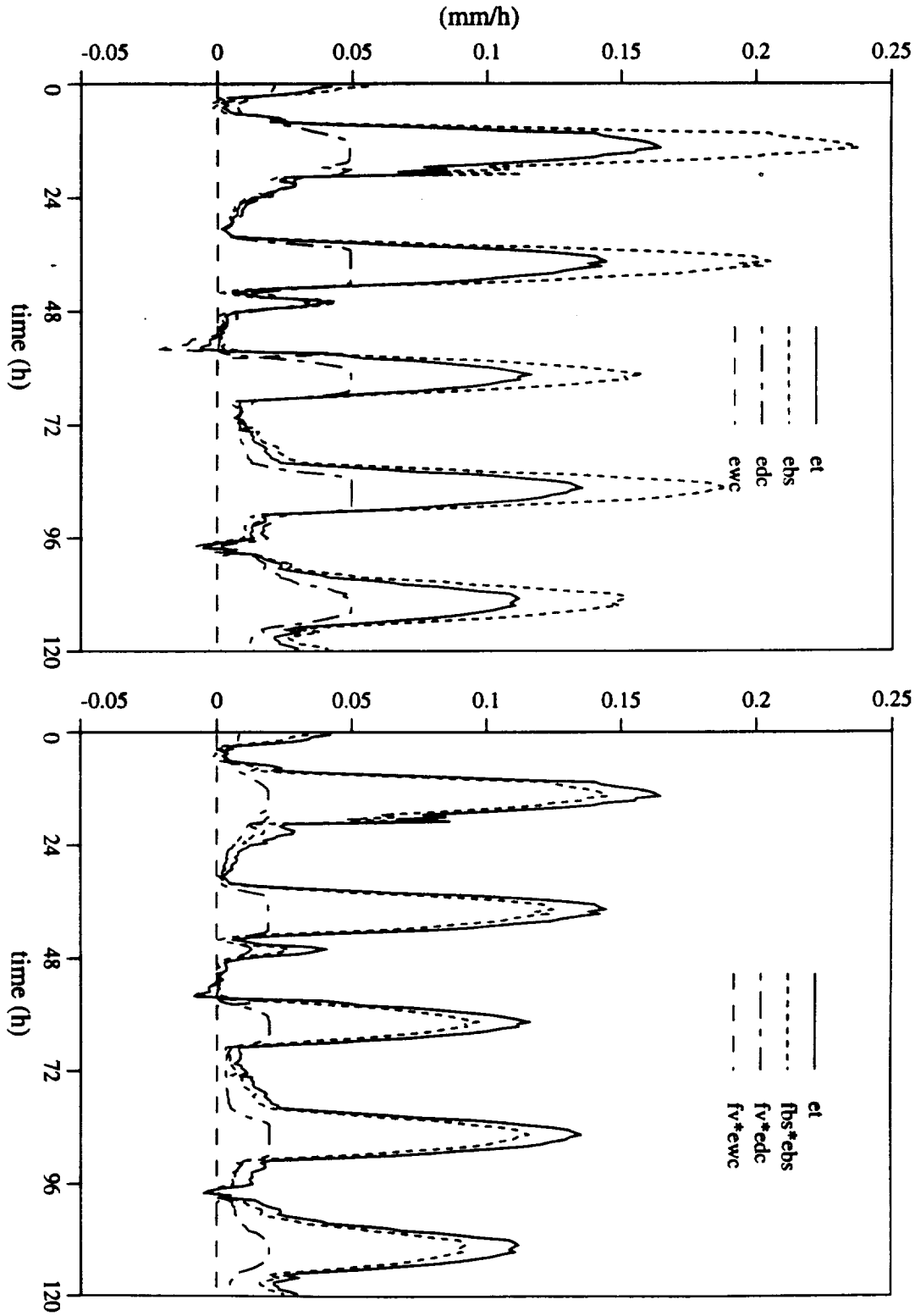
(mm/h)
-0.05
0
0.05
0.1
0.15
0.2
0.25
time (h)
0
24
48
72
96
120
et
ebs
edc
ewc
et
fbs*ebs
fv*edc
fv*ewc

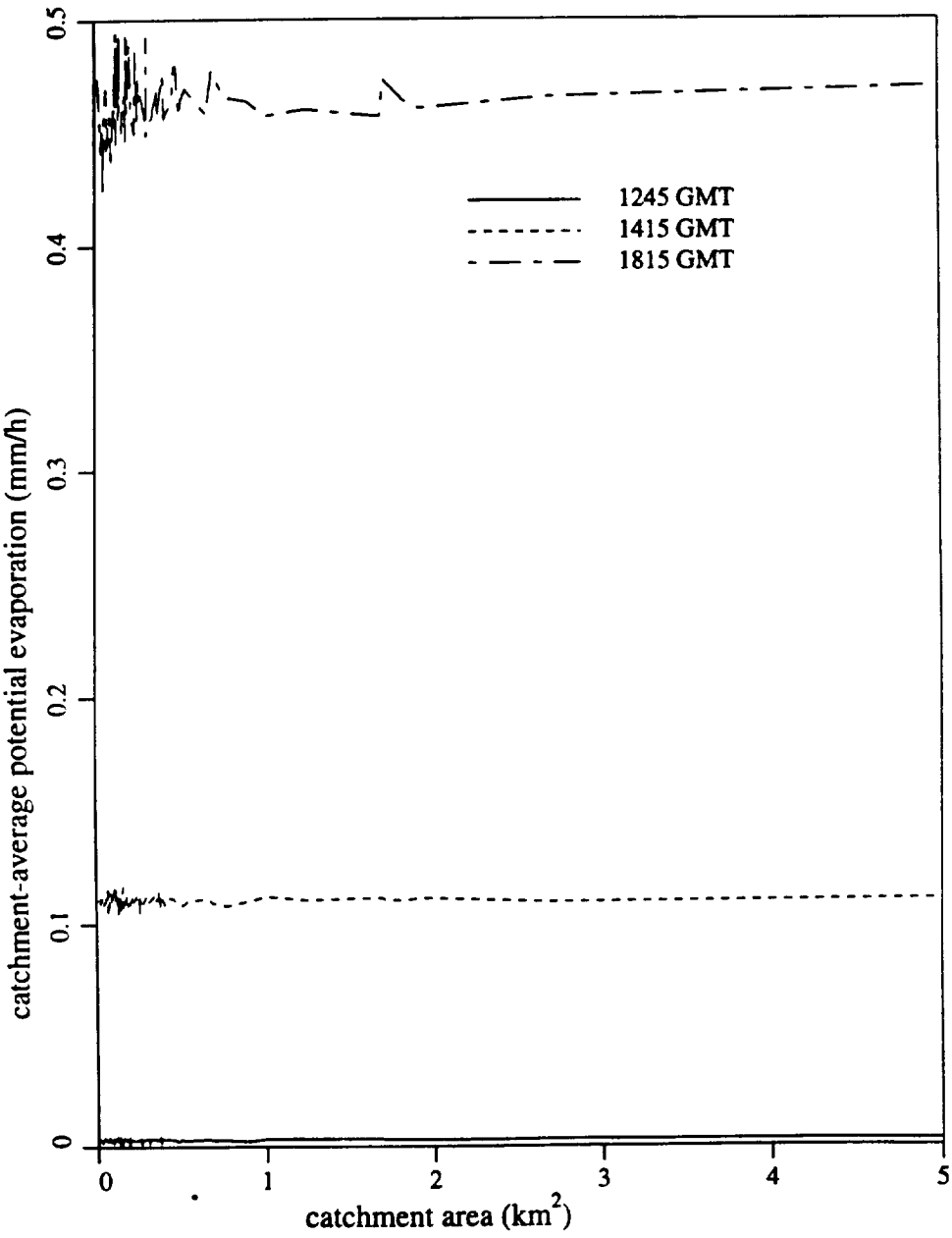

Figure 7. Computed catchment-average potential evaporation versus catchment area for three 1245, 1415, and 1815 GMT, October 7, 1987.

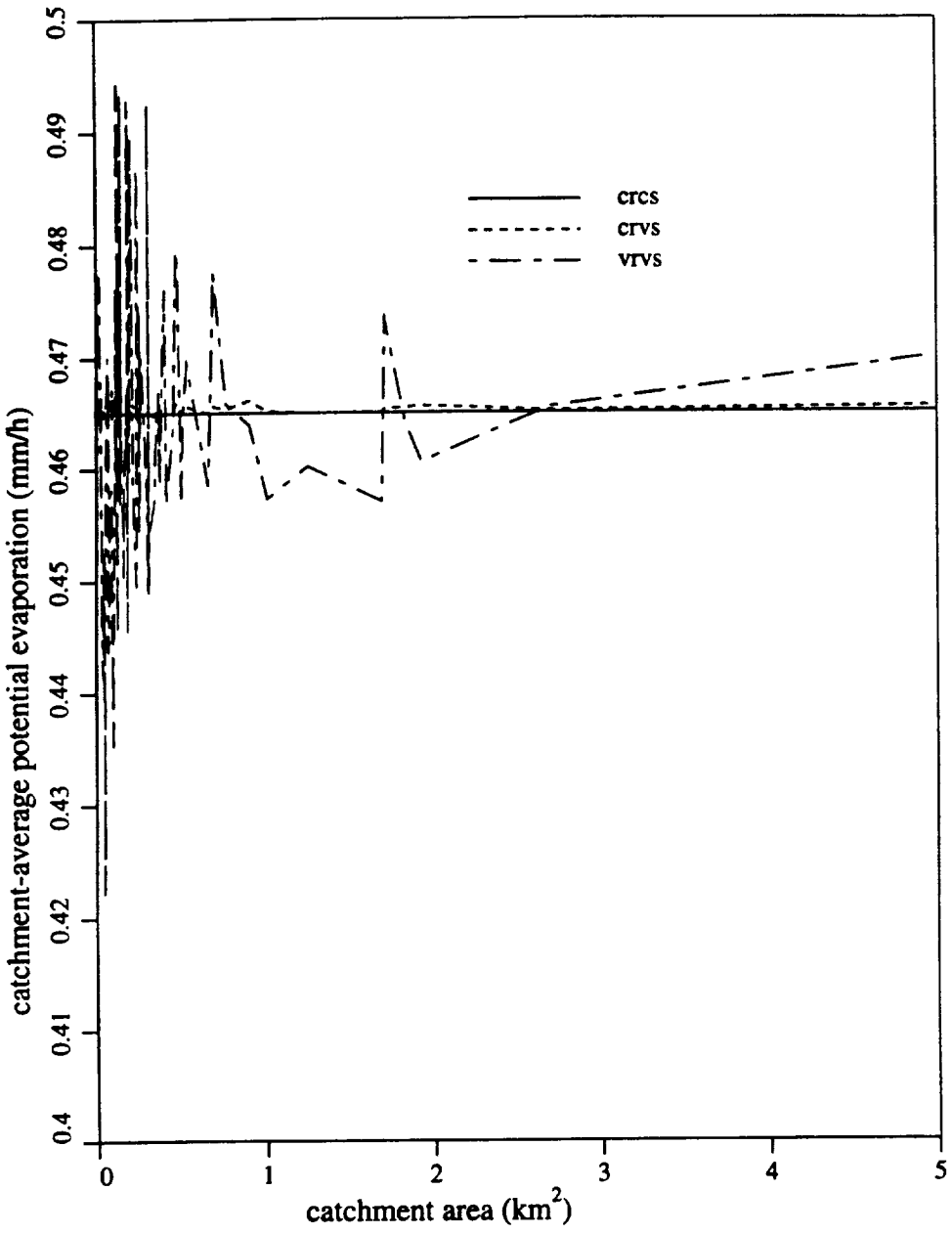

Figure 8. Computed catchment-average potential evaporation versus catchment area at 1815 GMT, October 7, 1987 for spatially-constant solar radiation and spatially-constant soil properties (crcs); spatially-constant solar radiation and spatially-variable soil properties (crvs); and spatially-variable solar radiation and spatially-variable soil properties (vrvs).

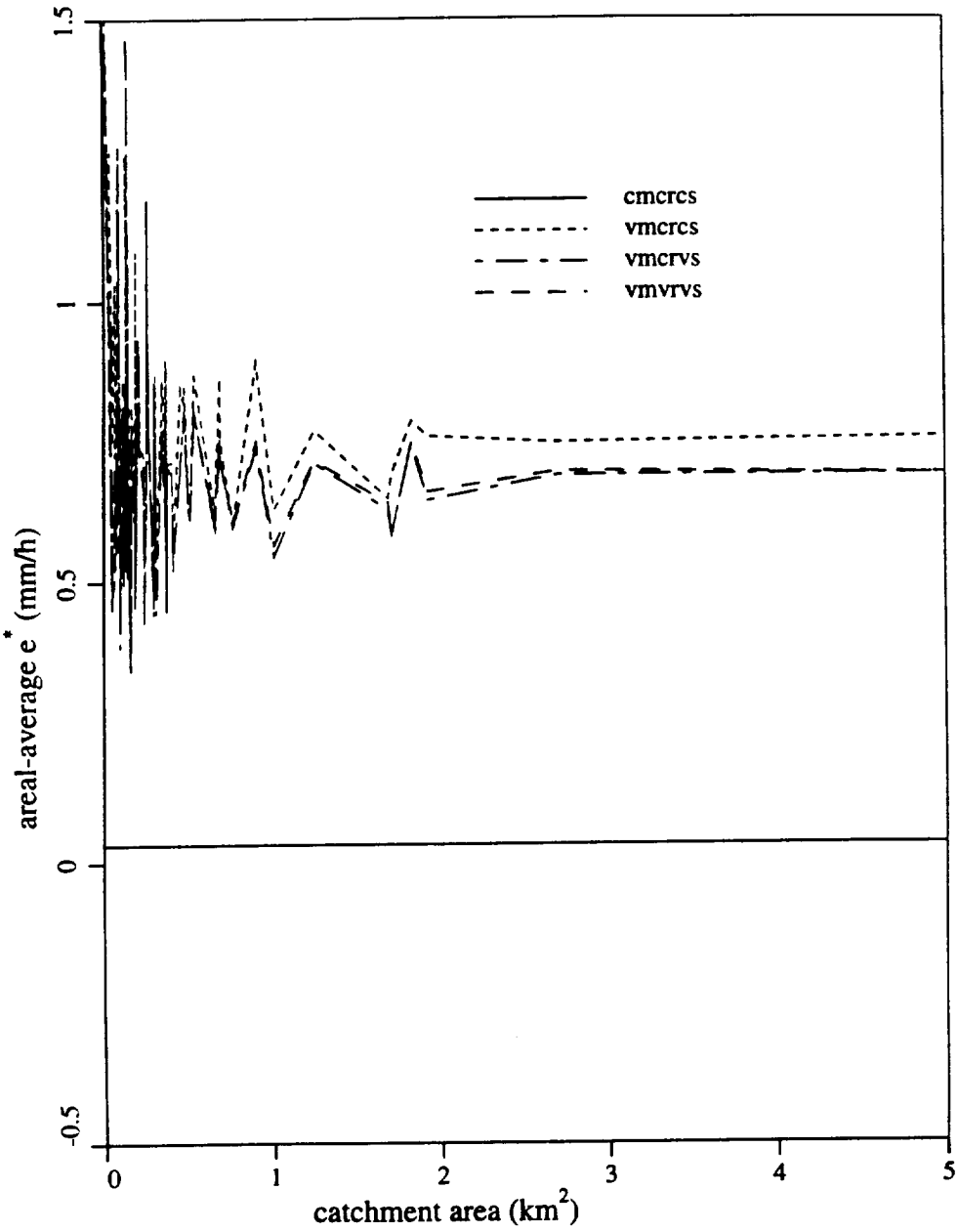

Figure 9. Computed catchment-average exfiltration capacity versus catchment area at 1815 GMT, October 7, 1987 for the following combinations of model inputs: spatially-constant soil moisture, solar radiation, and soil properties (cmcrcs); spatially-variable soil moisture and spatially-constant solar radiation and soil properties (vmcrcs); spatially-variable soil moisture and soil properties and spatially-constant solar radiation (vmcrvs); spatially-variable soil moisture, solar radiation and soil properties (vmvrvs).

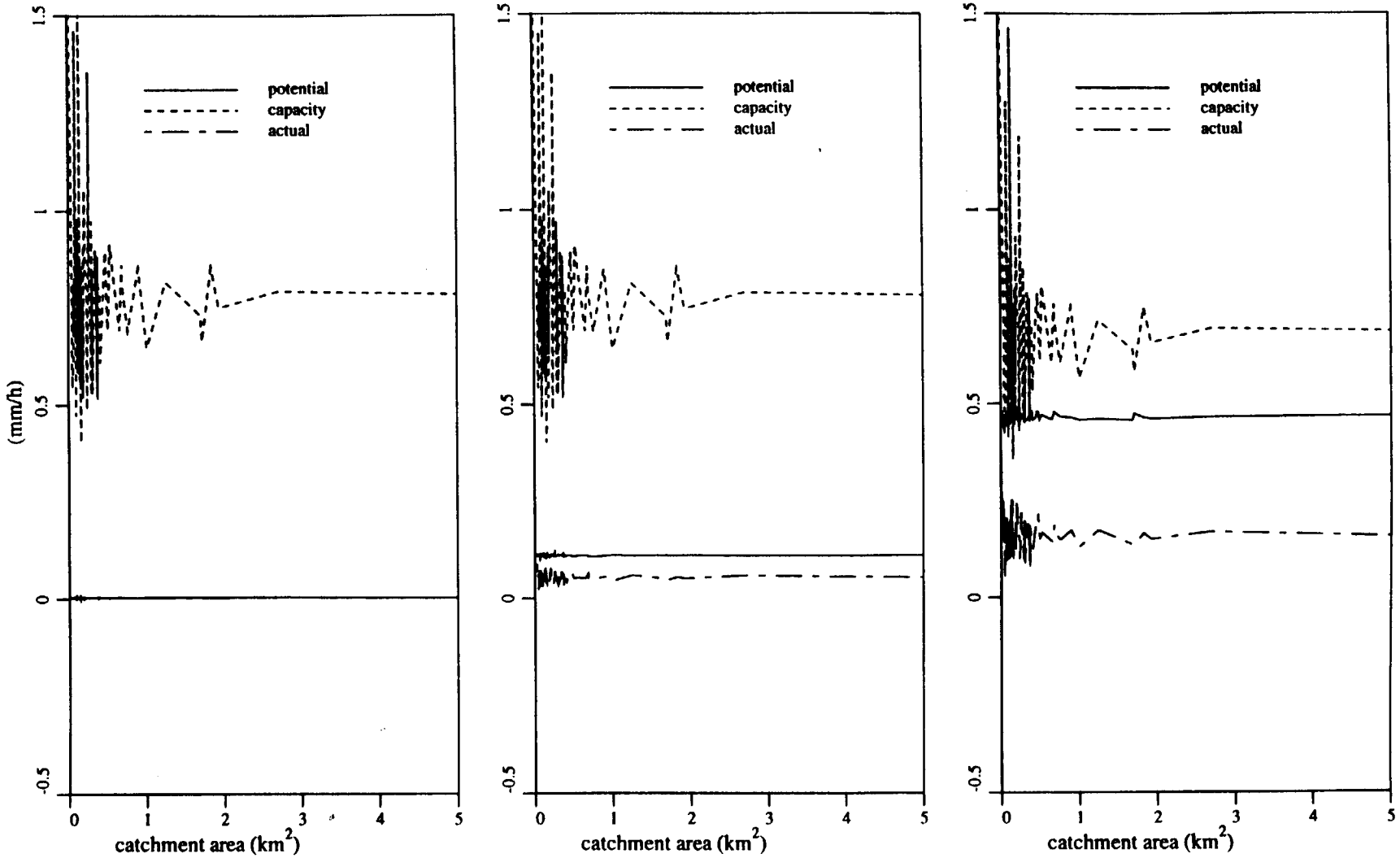
potential
capacity
actual
(mm/h)
1.5
1
0.5
0
-0.5
0
1
2
3
4
5
catchment area (km2)

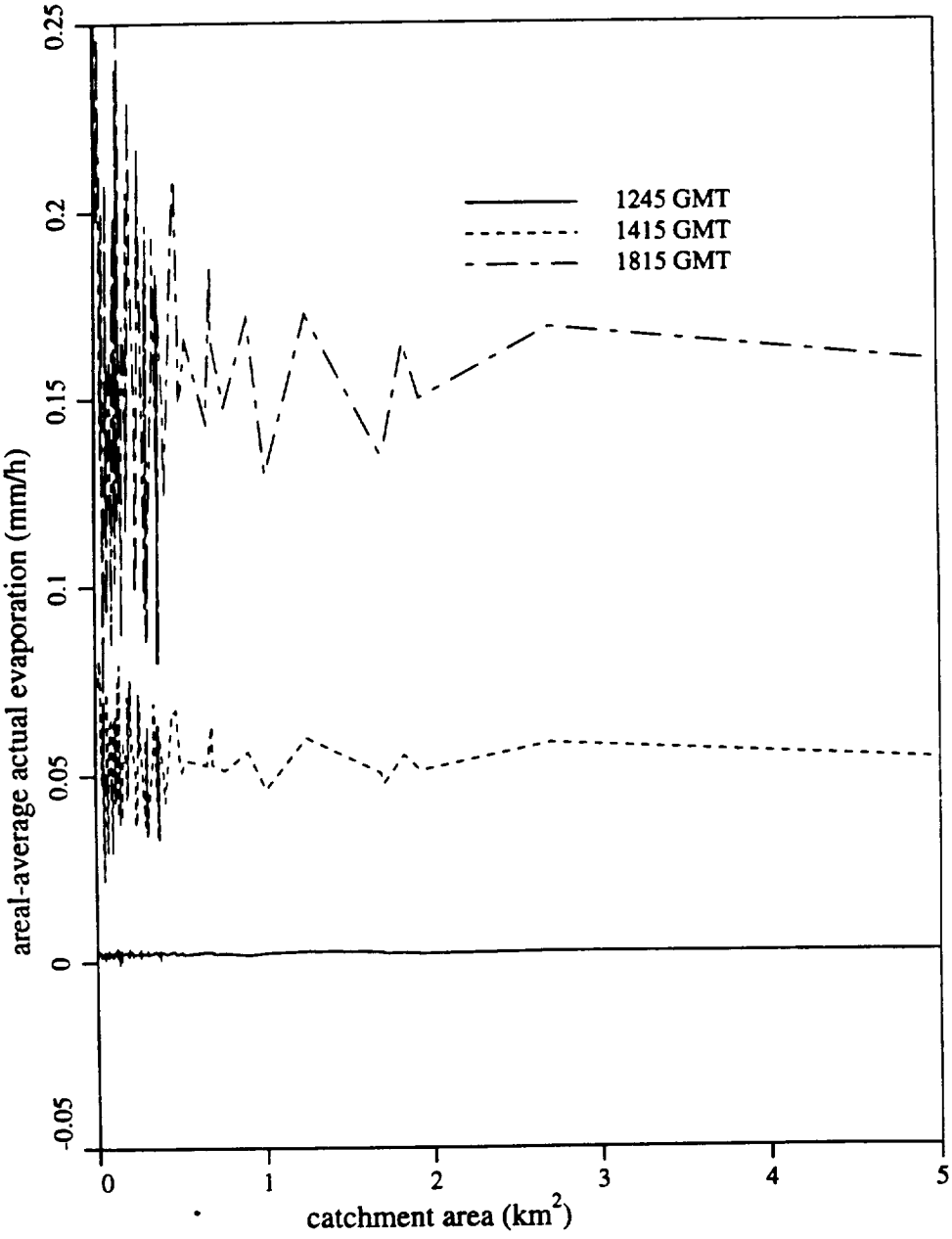

Figure 11. Computed catchment-average actual evaporation rate versus catchment area for 1245, 1415, and 1815 GMT, October 7, 1987.

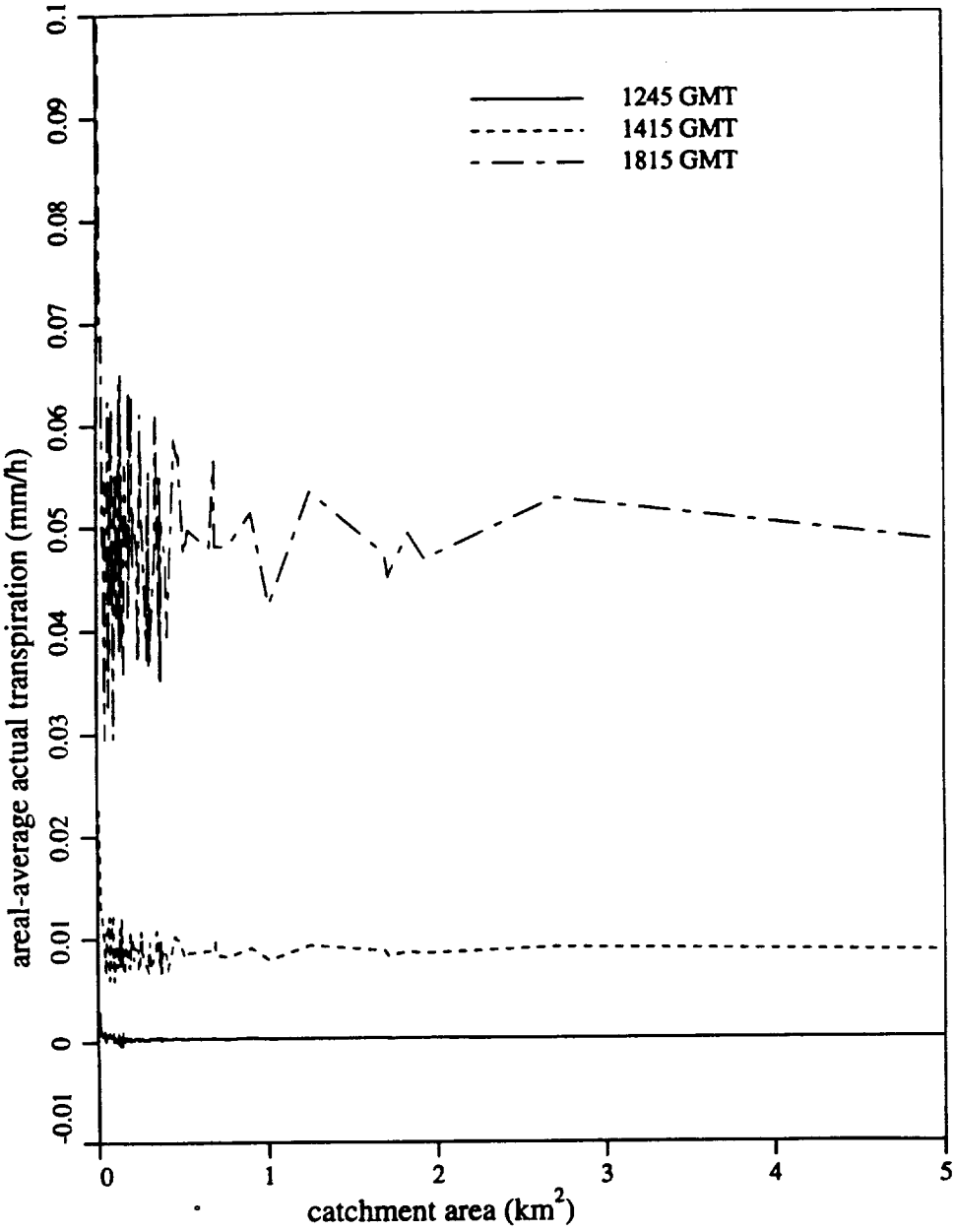

Figure 12. Computed catchment-average actual transpiration rate versus catchment area for 1245, 1415, and 1815 GMT, October 7, 1987.

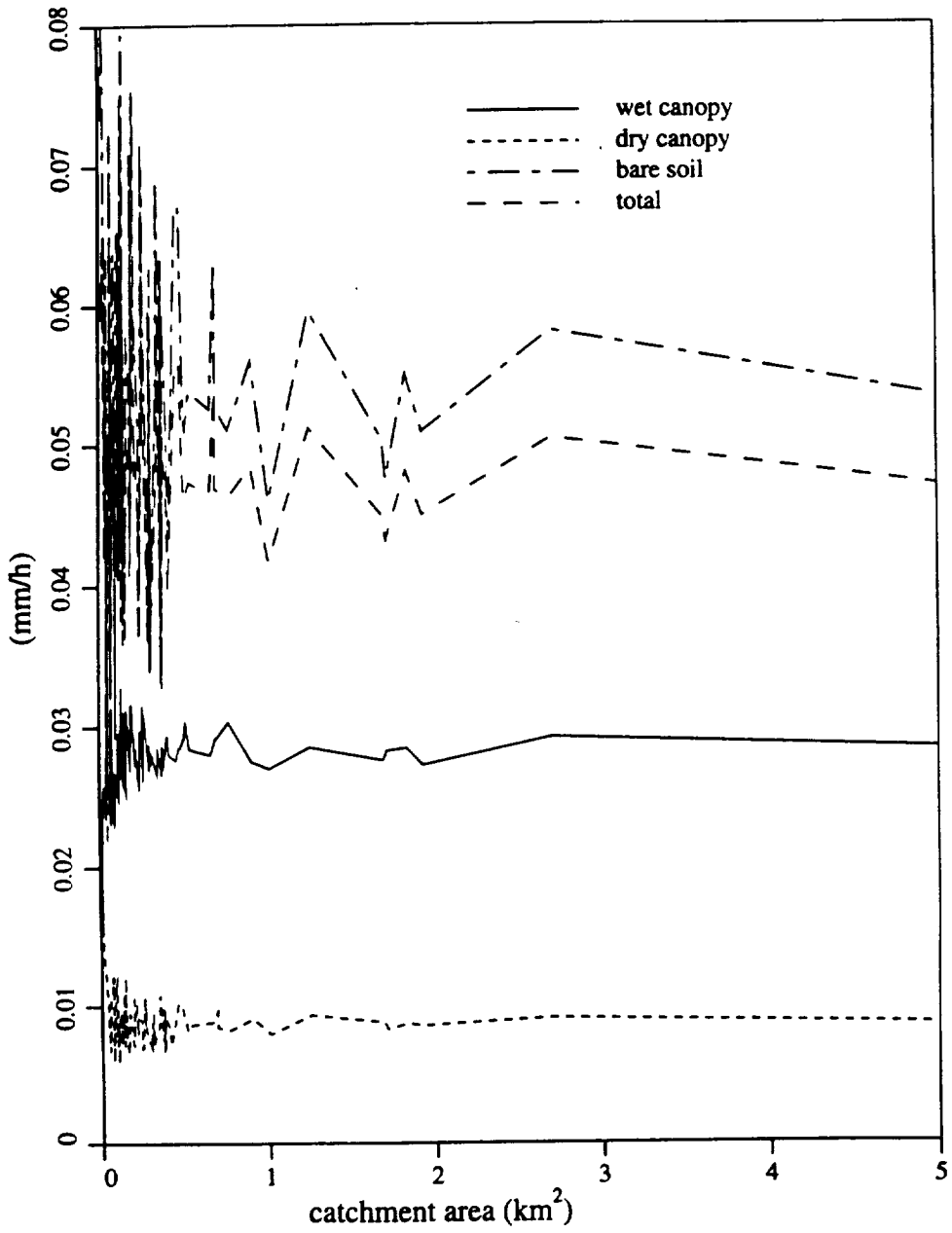

Figure 13. Computed catchment-average evapotranspiration rate, catchment-average wet canopy evaporation rate, catchment-average dry canopy transpiration rate, and catchment-average bare soil evaporation rate versus catchment area for 1415 GMT, October 7, 1987.

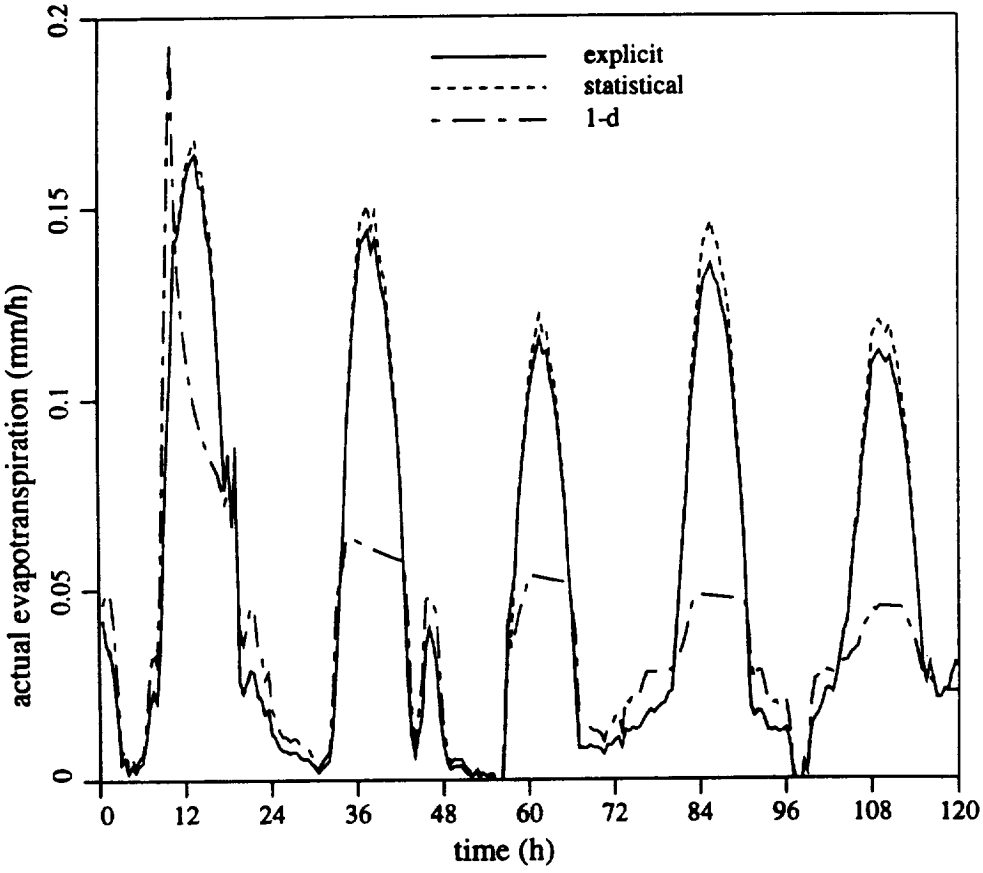

Figure 14. Computed catchment-average evapotranspiration using the spatially-distributed model, the statistically-aggregated model, and the one-dimensional local model, October 5-9, 1987.

Scaling, Soil Moisture and Evapotranspiration in Runoff Models

Eric F. Wood

Water Resources Program
Princeton University
Princeton, NJ 08544

Accepted:
Special Issue on Hydroclimatology
Advances in Water Resources
October, 1993

Abstract.

The effects of small-scale heterogeneity in land surface characteristics on the large-scale fluxes of water and energy in the land-atmosphere system has become a central focus of many of the climatology research experiments. The acquisition of high resolution land surface data through remote sensing and intensive land-climatology field experiments (like HAPEX and FIFE) has provided data to investigate the interactions between microscale land-atmosphere interactions and macroscale models. One essential research question is how to account for the small scale heterogeneities and whether 'effective' parameters can be used in the macroscale models. To address this question of scaling, the probability distribution for evaporation is derived which illustrates the conditions for which scaling should work. An correction algorithm that may appropriate for athe land parameterization of a GCM is derived using a 2nd order linearization scheme. The performance of the algorithm is evaluated.

Introduction.

Research into land-atmospheric interactions suggest a strong coupling between land surface hydrologic processes and climate (Charney et al., 1977; Walker and Rowntree, 1977; Shukla and Mintz, 1982; and Sud et al.,1990.) Due to this coupling, the issue of 'scale interaction' for land surface-atmospheric processes has emerged as one of the critical unresolved problems for the parameterization of climate models. To help resolve this issue, the understanding of the scaling properties of water and energy fluxes with their corresponding storage terms (especially soil moisture) has been an important scientific objective of land-climatology experiments like FIFE (see Sellers etal, 1988) and GCIP (see WCRP, 1992).

In fact, the acquisition of high resolution land surface data through remote sensing and intensive land-climatology field experiments (like HAPEX and FIFE) has provided data to investigate the interactions between microscale land-atmosphere interactions and macroscale models. One essential research question is how to account for the small scale heterogeneities and whether 'effective' parameters can be used in the macroscale models. The current scientific thinking on this issue is mixed. For example Sellers et al. (1992) claim that analysis of the FIFE data supports that land-atmospheric models are almost scale invariant, a conclusion also reached by Noilhan (personal communication) using HAPEX-MOBILHY data. Counter arguments have been made by Avissar and Pielke (1989) who found that heterogeneity in land characteristics resulted in sea-breeze like circulations, and significant differences in surface temperatures and energy fluxes across the patches. The results of analyses presented later in this paper suggest that soil moisture is the critical variable that controls the

non-linear behaviour of land-atmospheric interactions, and the effect is most pronounced when soil moisture heterogeneity is such that part of the domain is under soil-vegetation control and part is under atmospheric control.

The understanding of the scale problem is critical for new climate projects such as the Global Energy and Water Experiment (GEWEX) or the Earth Observing System (Eos). It is also important for the parameterization of the macroscale land-surface hydrology in climate models, and crucial in our understanding in how to represent sub-grid variability in such macroscale models.

From a modeling perspective, it's important to establish the relationship between spatial variability in the inputs and model parameters, the scale being modeled and the proper representation of the hydrologic processes at that scale. Figure 1 presents a schematic for modeling over a range of scales. Let us consider this figure in light of the terrestrial water balance, which for a control volume may be written as:

$$\left\langle \frac{\partial S}{\partial t} \right\rangle = \langle P \rangle - \langle E \rangle - \langle Q \rangle \qquad (1)$$

where S represents the moisture in the soil column, E evaporation from the land surface into the atmosphere, P the precipitation from the atmosphere to the land surface, and Q the net runoff from the control volume. The spatial average for the control volume is noted by $\langle \cdot \rangle$.

Equation (1) is valid over all scales and only through the parameterization of individual terms does the water balance equation become a 'distributed' or 'lumped' model. By 'distributed' model, we mean a model which accounts for spatial variability in inputs, processes or parameters.

Lumped Versus Distributed Models.

Figure 1 presented a framework for considering the relationship between distributed and lumped models. Wood et al. (1988), Wood et al. (1990), Wood and Lakshmi (1993) studied the behaviour of aggregated inputs and the resulting hydrologic responses which lead to the concept of the representative elementary area, a scale where a statistical representation can replace actual patterns of variability. In this paper we compare the output between a macroscale, distributed model and a lumped model to try and determine when the macroscale model provides an accurate response when compared to the average of the distributed model.

Two distributed model are used in latter sections: one is based on the model described in Famiglietti and Wood (1992) (referred to as TOPLATS - Topgraphic-Land-Atmospheric-Transfer-Scheme) and is an extension of the model described in Famiglietti et al. (1992); these models have been applied to the intensive field campaign periods (IFCs) during FIFE of 1987. TOPLATS can include variability in topography, soils, net radiation and vegetation. The first two, topography and soils, leads to variations in soil moisture under the TOPMODEL framework; the latter two lead to variations in potential and actual transpiration. The second model (Wood et al., 1992) described here has variations in infiltration capacities across a catchment of GCM grid square and is referred to as the VIC model. This model has been used in GCM climate simulations (see Stamm et al, 1993) and is the model used in this paper to demenstrate the impact of a second order correction term to the lumped model to account for sub-grid heterogeniety.

Derived Distribution of Soil Moisture and Evaporation.

The concept of the representative elementary area leads to a statistical description of the sub-grid variability in water table depths,

soil moisture, evapotranspiration, and so forth. Models at this scale are referred to as macroscale, distributed models. For TOPLATS, the distribution in the soil-topographic index leads to a distribution in water table depths (see Beven and Kirkby, 1979; Wood et al., 1990; or Famiglietti et al., 1992). From the distribution of water table depths z, and the soil characteristic relations which relates the soil matrix head, ψ, to soil moisture θ as a function of soil properties, the statistical distribution for surface soil moisture can be derived. Certain assumptions are usually applied, for example a steady state vertical flow which leads to $\partial\psi/\partial z = 1$. Actual evaporation e_a (or transpiration from vegetation) depends on the availability of soil moisture (i.e. a soil controlled rate) and the atmospheric demand for moisture; the actual evaporation being the minimum of the two rates. Thus given the atmospheric demand and the the statistical distribution of soil moisture, the distribution of the actual evaporation can be derived. For simple functional forms the mapping of $z \rightarrow \theta \rightarrow e_a$ can be done analytically; in any case it can be done through simulation. Figure 2 provides some results using TOPLATS for two conditions: Figure 2a is for quite dry conditions - low water table - for two times during the day. Figure 2b is for the same dirurnal times but for a wetter (but not extremely wet) condition. The parameters for the curves are taken from Famiglietti and Wood (1992) and represent conditions for Kings Creek area of FIFE in Kansas. The figures have been divided into four panels that show the derivation of the bare soil evaporation distribution. Panel (i) in the lower right corner gives the probability distribution for water table depths derived from the soil-topographic index of TOPLATS, and soilwater table depth to surface soil moisture as discussed ewater table depth to surface soil moisture as discussed earlier in this section. These two figures could gewater table depth to surface soil moisture as discussed earlier in this section. These

two figures could generate a derived probability distribution for surface soil moisture. This is not shown here. The upper left portion of the figure (iii) gives the relationship between surface soil moisture and actual evaporation for the two times during the day. The maximum evaporation rate is the potential rate, which is lower during the early morning and late afternoon. For portions of the catchment where surface soil mositure is high, the actual evaporation rate is equal to the potential rate. For drier areas, the rate is lower. The resulting probability distribution for the actual evaporation is shown in the lower left portion of the figure. This panel is divided into two, the top giving the distribution for the time related to the lower potential evaporation rate.

Inspection of the derived distributions for the two times and two conditions reveals that for the very dry conditions the distribution for evaporation is narrow and the average water table depth can be used to estimate the average evaporation rate. This is because the soil moisture - evaporation function is essentially linear in the range of soil moistures representing the dry conditions. For the wetter condition, the function is non-linear and the range of soil moistures contain areas which are very dry (having low evaporation rates) and wet (having rates at potential.) If the conditions were even wetter, then the distribution of evaporation rates would be at the potential rate. It is at these intermediate conditions where the non-linearities appear to have the greatest impact.

Comparisons between the average bare soil evaporation and that estimated using the average depth to the water table are given in Table 1 for both conditions and the two times. From Figure 2 and Table 1 it is clear that dry conditions during periods of high atmospheric demands result in

evaporation rates that are biased low. During periods with high soil moisture (or extremely low soil moisture) or during early or late times during the day when the atmospheric demands are low, the bias from using the average water table depth is minimal.

To test the sensitivity due to dry soil conditions and to compare the distributed water-energy balance model (TOPLATS) to a lumped representation (one-dimensional model or a first order model), comparisions were made between the models for 5 days during the October 1987 FIFE intensive field campaign, IFC-4. This period had the driest conditions observed during the 1987 experiment. Figure 3 shows the simulations for October 5 - 9, 1987. The models were run at a 0.5 hour time step to capture the diurnal cycle in potential evapotranspiration. Three models are compared: a fully distributed model, a macroscale model in which the spatial variability is considered statistically and a lumped one-dimensional model in which parameters and inputs are spatially constant.

The one-dimensional model predicts well the evapotranspiration during the morning and late afternoon when the atmospheric demand is low, but fails to accurately predict this flux during the middle portion of the day when soil and vegetation controls limit the actual evapotranspiration. It is during this period that the sensitivity is high and by ignoring the spatial variability in soil moisture the lumped model serverely underestimates the catchment-scale evapotranspiration. During wet periods, the one-dimensional model may work quite well. This complicates the linkage between a distributed and lumped representation since the appropriateness of the simpler representation varies with the state of the system.

Linearized, 2nd Order Model for Sub-grid Variability.

While these results imply that distributed models are needed to accurately account for sub-grid variability in soil moisture and the resulting evapotranspiration, such models may be computationally burdensome when incorporated within a GCM. An alternative approach would be to develop correction schemes for the often used 'lumped' models. Such a scheme should have correction terms that vary with soil moisture conditions.

A lumped representation (or what will also be referred to as a one-dimensional representation) is obtained by using spatially constant values for 'state' variables; in the case of TOPLATS this would be the soil-topographic index and vegetation parameters; in the case of VIC the soil moisture. The effect of representing the distributed model by a lumped model, or equivalently by replacing the spatially variable parameters and inputs by average values, will depend on nonlinearities in the model. Conceptually this can be seen by considering a second order Taylor's series expansion about the mean for the function $y = g[x,\theta]$ where θ are fixed parameters and x variable with mean $\mu(x)$ and variance $\sigma(x)$. A first order approximation for y is $\mu_1(y) \simeq g[\mu(x),\theta]$, while a second order approximation would be

$$\mu_2(y) \simeq g[\mu(x),\theta] + \frac{1}{2} \left|\frac{d^2g}{dx^2}\right|_{\mu(x)} \sigma(x) \qquad (3)$$

Differences between $\mu_1(y)$ and $\mu_2(y)$ depend on the magnitude of the second term in equation (3) -- the sensitivity term. As an illustrative example, consider the estimation of downslope subsurface flows, q_i, within TOPLATS with and without considering variability in the local water table z_i. TOPLATS relates q_i to z_i by $q_i = T_i \tan\beta \exp(-f\ z_i)$. Thus a first order approximation of the mean subsurface flow would be

$$\mu_1(q_i) = T_i \tan\beta \exp(-f\ \bar{z}) \tag{4}$$

while a second order approximation would be

$$\mu_2(q_i) = T_i \tan\beta \exp(-f\ \bar{z}) + \frac{1}{2} \{\ T_i \tan\beta\ f\ \}^2 \exp(-f\ \bar{z})\ \sigma(z_i) \tag{5}$$

If we scale $\mu_2(q_i)$ by $\mu_1(q_i)$ and recognize that

$$\sigma(z_i) = f^2\ \sigma(\ln \frac{\alpha T_e}{T_i \tan\beta}) \tag{6}$$

we obtain

$$\frac{\mu_2(q_i)}{\mu_1(q_i)} = 1 + 0.5\ \sigma(\ln \frac{\alpha T_e}{T_i \tan\beta}) \tag{7}$$

Analysis of the soil-topographic index for Kings Creek yields a variance of 3.25. This results in the first order estimate for q_i of being biased low by approximately 65%. Since the subsurface flows and the local water table are related and since the local water table depth effects the surface soil moisture which subsequently determines the soil evaporation and infiltration rates, it's clear that the lumped model may very well lead to significant biases in the water balance fluxes.

For the more complex functions used for bare soil evaporation and transpiration, the sensitivities can be determined through simulation. For these functions the sensitivities will change with the state of the catchment (wet or dry). For example Figure 4 gives the vegetation transpiration and soil exfiltration capacities used to model the FIFE data (Famiglietti and Wood, 1992). Notice that at low and high soil moisture values the transpiration capacity function is essentially linear and the sensitivity would be low to soil moisture variations in these ranges. For volumetric moisture contents in the range 0.2 - 0.3, the sensitivity of the transpirtaion capacity function is high. As can be seen from Figure 4, sensitivity characteristics for soil exfiltration capacity would be high for soil moisture values greater than about 0.3.

moisture, which for any fractional area with capacity i greater than i_o can be estimated as $\theta = i_o\eta/i$, where η is the soil porosity. Using the results for a Beta distribution between $[i_o, i_m]$ results in a mean and variance for i conditional upon $i>i_o$ of

$$\bar{i} = i_o + (i_m - i_o)/(1+B) \tag{11}$$

$$Var(i) = (i_m - i_o)^2 \frac{B}{(1+B)^2(2+B)} \tag{12}$$

A second order mean soil moisture can be estimated using (7) as

$$\bar{\theta} = \frac{i_o\eta}{\bar{i}} + \frac{i_o\eta}{\bar{i}^3} Var(i) \tag{13}$$

$$Var(\theta) = \frac{(i_o\eta)^2}{\bar{i}^4} Var(i) \tag{14}$$

To estimate bare soil evaporation we can use a Philip's form of the exfiltration capacity (Eagleson, 1978) which is of the form $E = 0.5\, S_e\, t^{-1/2}$, where S_e is a desorptivity term that can be written in the form $S_e = K(\theta-\theta_r)^{C/2}$. Here K and C are parameters which depends on soil characteristics. Using the mean and variance of θ will yield a second order model for the mean soil evaporation rate whose sensitivity will depend on the variance of θ and the sensitivity term for the evaporation function. After some simple algebra, the sensitivity term $d^2E/d\theta^2$ can be written as

$$\frac{d^2E}{d\theta^2} = \left(\frac{C}{2}\right)\left(\frac{C}{2} - 1\right) \frac{E}{(\bar{\theta} - \theta_r)^2} \tag{15}$$

where E is evaluated at $\bar{\theta}$, and θ_r is the residual soil moisture.

To test the algorithm and compare it with the distributed VIC model, simulations were run varying the initial soil water capacity (W_o) and

for different shape parameters for the distribution of infiltration capacities. (see equation 8). The simulations used potential evaporation data from IFC-4 of FIFE'87. The following initial parameters were used: a maximum infiltration capacity, i_m = 30.5 cm and a shape parameter of B = 0.3. Using an initial wetness corresponding to i_o = 10 cm yield the results shown in Figure 7. The solid line represents the distributed VIC model in which evaporation is estimated using 100 slices of the soil moisture distribution. The dotted line is the solution using the average value of soil moisture for where $i > i_o$ (i.e. a 1st order linear model) and the dashed line is the 1st order model plus the correction term (i.e. the 2nd order, linearized model.) For this case, the correction term is about 50% of the estimate using just the average soil moisture. If the conditions are wetter than Figure 7, i.e. have i_o = 15 cm, then we get the results shown in Figure 8. Here the lumped model does very well. If conditions drier than Figure 7 prevail, i.e. i_o = 5 cm (which is very dry) then the linearized model does very poorly; as shown in Figure 9.

The results do depend on the value of B, the shape parameter. For example having B = 1.3 and i_o = 10 cm (the conditions of Figure 7) resulted in much better performance of the correction algorithm as can be seen in Figure 10. As shown in Stamm et al. (1993), the distribution of B ranges globally from about 0.3 to 2.5 suggesting that the applicability of such a correction algorithm may be widespread. Furthermore, it can be determined before hand where the algorithm should work, and under what soil moisture conditions. This suggests that for those GCM grid squares with sufficient moisture or favorable infiltration capacity shape parameters, the simple 2nd order algorithm can be implemented. For condition too dry, the distributed model can be run for those particular time steps. This approach would lead to the most efficient and accurate computational effort.

Conclusions

The effect of subgrid variability in soil moisture on evaporation has been investigated with the aim of resolving whether effective (or average) values for soil moisture can replace the distribution found within a catchment or GCM grid square. It appears that there is a critical range of intermediate values for which the subgrid variability has a significant impact of grid total evaporation (and transpiration). This arises from the non-linearity between soil moisture and evaporation within this critical range, and the essentially linear behavoiour outside this range.

This lead to an initial attempt in developing a 2nd order, linearized, model for evaporation that could be incorporated with GCMs. Initial performance of this algorithm is encouraging with the correction term representing about 50% of the evaporation predicted based on only using the average soil moisture value. For extremely dry conditions the linearized model still under estimates evaporation which may result in using the fully distributed model in these conditions.

Acknowledgements

I would like to thank J. Famiglietti and V. Lakshmi with their help in running some of the examples used in this paper, and D. Thongs and J. Stamm with some of the graphics. The research was supported in part from NASA grants NAG-5-899 and NAGW-1392; this research support is gratefully acknowledged.

References

Abbott, M.B., J.C. Bathurst, J.A. Cunge, P.E. O'Connell, and J. Rasmussen, "An Introduction to the European Hydrological System-Systeme Hydrologique Europeen SHE, 1, History and Philosophy of a Physically-Based, Distributed Modelling System", Journal of Hydrology, 87, 45-59, 1986a.

Abbott, M.B., J.C. Bathurst, J.A. Cunge, P.E. O'Connell, and J. -Rasmussen, "An Introduction to the European Hydrological System-Systeme Hydrologique European SHE, 2, Structure of a Physically-Based, Distributed Modelling System", Journal of Hydrology, 87, 61-77, 1986b.

Beven, K. and M. J. Kirkby, "A Physically Based, Variable Contributing Area Model of Basin Hydrology, Hydrol. Sci. Bull., 24(1), 43-69, 1979.

Binley, A.M., J. Elgy and K.J. Beven, "A Physically-Based Model of Heterogeneous Hillslopes", Water Resources Research , 25, 1219-1226, 1989.

Charney, J., W. Quirk, S. Chow and J. Kornfield, "A Comparative Study of the Effects of Albedo Change on Drought in Semi-Arid Regions", Journal of the Atmospheric Sciences, 34, 1366-1385, 1977.

Eagleson, P.S., "Climate, Soil and Vegetation", Water Resources Research, 14(5), 705-776, October, 1978.

Famiglietti, J.S., and Eric F. Wood, "Aggregation and Scaling of Spatially-Variable Hydrological Processes, 1. A Local Model of Water and Energy Balance; 2, A Catchment-Scale Model of Water and Energy Balance; 3, A Macroscale Model of Water and Energy Balance", submitted to Water Resources Research, October, 1992.

Famiglietti, J.S. and Eric F. Wood, "Aggregation and Scaling of Spatially-Variable Hydrological Processes, 4, Effects of Spatial Variability and Scale on Areal-Average Evapotranspiration", submitted to Water Resources Research, January, 1993.

Famiglietti, J.S., Eric F. Wood, M. Sivapalan and D.J. Thongs, "A Catchment Scale Water Balance Model for FIFE", Journal of Geophysical Research, November, 1992a.

Moore, I.D., E. M. O'Laughlin and G.J. Burch, "A Contour-Based Topographic Model for Hydrological and Ecological Applications", Earth Surf. Processes Landforms, 13, 305-320, 1988.

Paniconi, C. and Eric F. Wood, "A Detailed Model for Simulation of Catchment Scale Subsurface Hydrologic Processes", Water Resources Research, in press (1992).

Sellers, P.J., F.G. Hall, G. Asrar, D.E. Strebel and R.E. Murphy, "The First ISLSCP Field Experiment (FIFE)", Bulletin of the American Meteorological Society, 69, 22-27, 1988.

Sellers, P. J., M. Heiser and F. G. Hall "Relations Between Surface Conductance and Spectral Vegetation Indices and Intermediate (100 m^2 to 15 km^2) Length Scales", J. Geophys. Res., 97(D17), 19033-19059, November 30, 1992.

Shukla, J. and Y. Mintz, "The Influence of Land-Surface Evapotranspiration on Earth's Climate", Science, 215, 1498-1501, 1982.

Stamm, J., E. F. Wood, and D. Lettenmaier "Sensitivity of a GCM Simulation of Global Climate to the Representation of Land Surface Hydrology", submitted J. Climate (1992).

Sud, Y. C., P. Sellers, M. D. Chow, G. K. Walker and W. E. Smith "Influence of Biosphere on the Global Circulation and Hydrologic Cycle - A GCM Simulation Experiment", Agricultural and Forestry Meteorology, 52, 133-188, 1990.

Walker, J.M. and P.R. Rowntree, "The Effect of Soil Moisture on Circulation and Rainfall in a Tropical Model", Quart. J.R. Meteor. Soc., 103, 29-46.

Wood, Eric F. and V. Lakshmi, "Scaling Water and Energy Fluxes in Climate Systems: Three Land-Atmospheric Modeling Experiments", J. of Climate, 6(5), 839-857, 1993.

Wood, Eric F., K. Beven, M. Sivapalan and L. Band, "Effects of Spatial Variability and Scale with Implication to Hydrologic Modeling", Journal of Hydrology, 102, 29-47, 1988.

Wood, Eric F., M. Sivapalan and K.J. Beven, "Similarity and Scale in Catchment Storm Response", Reviews in Geophysics, 28(1), 1-18, February 1990.

Wood, Eric F., D.-S. Lin, M. Mancini, D. Thongs, P.A. Troch, T.J. Jackson and E.T. Engman, "Intercomparisons Between Passive and Active Microwave Remote Sensing, and Hydrological Modeling for Soil Moisture", Symposium A.3, Progress in Scientific Hydrology and Water Resource Management using Remote Sensing, Proceedings of the 29th Plannery Meeting of the Committee on World Space Research, (COSPAR), Washington, D.C.August 28-September 5, 1992.

Wood, Eric F., D.P. Lettenmaier and V.G. Zartarian, "A Land Surface Hydrology Parameterization with Sub-Grid Variability for General Circulation Models", Journal of Geophysical Research, 97/D3, 2717 - 2728, February 28, 1992.

World Climate Research Programme "The Scientific Plan for the GEWEX Continental-Scale International Project", WCRP-67 WMO/TD-No. 461, Geneva, Switzerlamnd, February 1992, 65pp.

Table 1. Average Evaporation Rates

Soil Condition	Average based on the Variable Evaporation		Average based on using average $\bar{z}$	
	Potential Evaporation (mm/hr)		Potential Evaporation (mm/hr)	
	Low	High	Low	High
Dry	0.051	0.037	0.054	0.046
Wet	0.11	0.088	0.12	0.097

Figure 4: Vegetation transpiration capacity and bare soil evaporation capacities as functions of soil moisture (from Famiglietti and Wood, 1992).

Figure 5: (a) Actual soil evaporation for five different times during a day, notice that the actual level is the minimum of the capacity (figure 4) and the potential. (b) The evaporation sensitivity term $\partial^2 E_s/\partial\theta^2$ for the same times as in (5a).

Figure 6: The vegetation transpiration sensitivity term $\partial^2 T_v/\partial\theta^2$.

Figure 7: Comparisons of model derived latent heat estimates using the distributed VIC model for medium dry conditions, a 1st order linear model and a 2nd order linear model. Pamameters for the simulation are given in the text.

Figure 8: Comparisons of model derived latent heat estimates using the distributed VIC model for wet conditions, a 1st order linear model and a 2nd order linear model. Pamameters for the simulation are given in the text.

Figure 9: Comparisons of model derived latent heat estimates using the distributed VIC model for very dry conditions, a 1st order linear model and a 2nd order linear model. Pamameters for the simulation are given in the text.

Figure 10: Comparisons of model derived latent heat estimates using the distributed VIC model for the moisture conditions used in figure 7 and a modified soil capacity shape parameter. Also shown are a 1st order linear model and a 2nd order linear model. Pamameters for the simulation are given in the text.

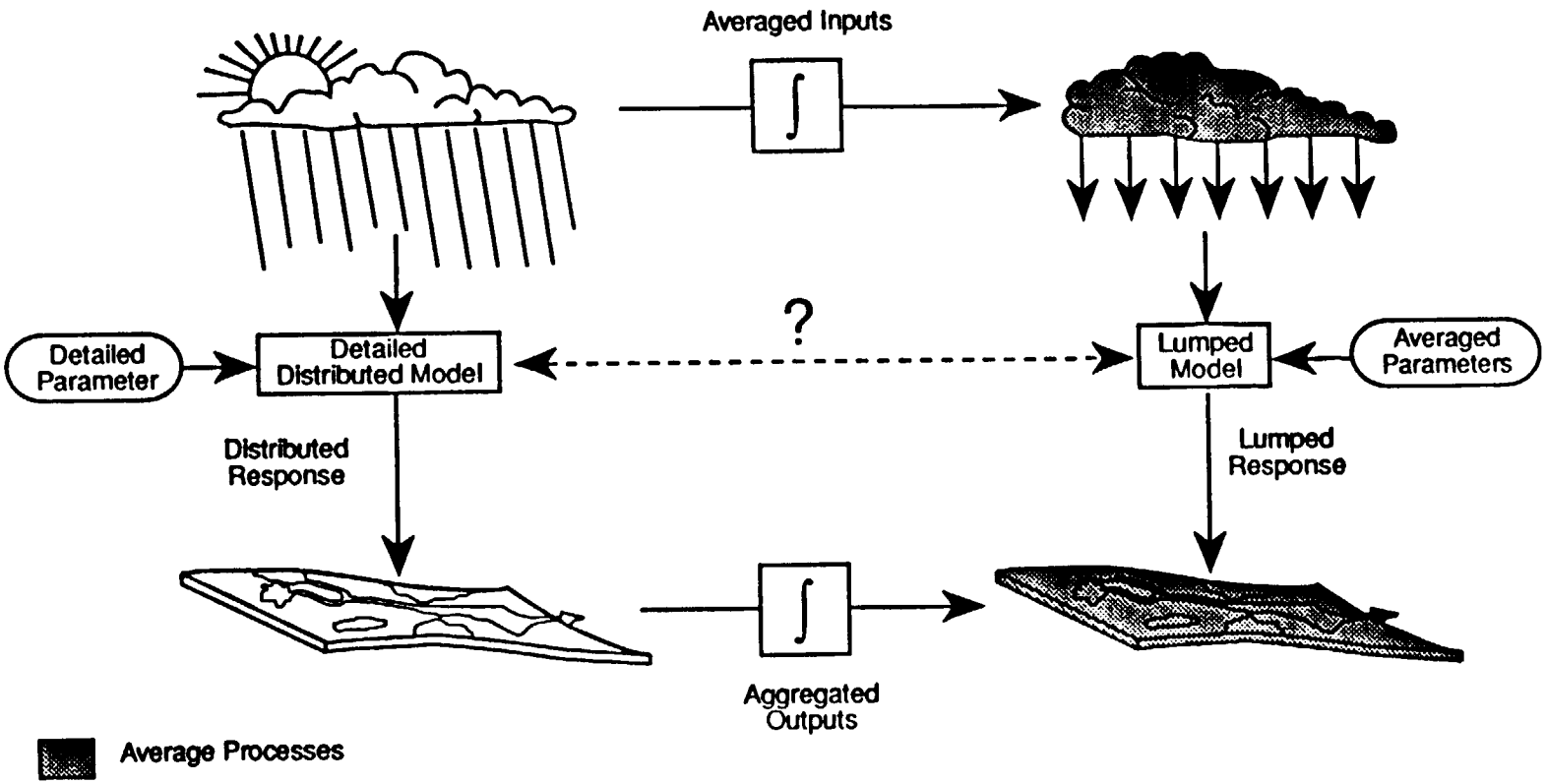
Averaged Inputs
?
Detailed Parameter
Detailed Distributed Model
Lumped Model
Averaged Parameters
Distributed Response
Lumped Response
Aggregated Outputs
Average Processes

Fig. 1

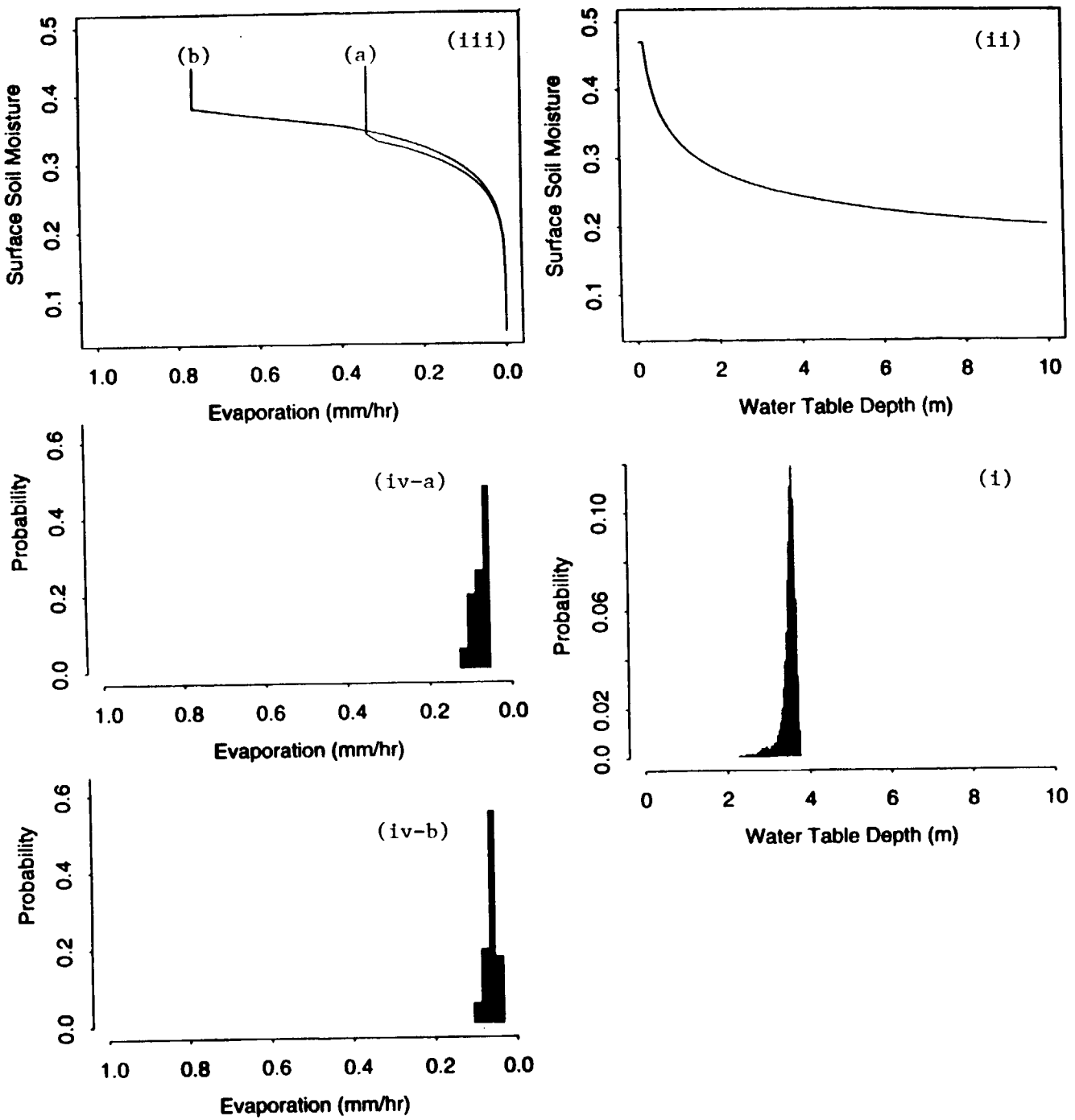
(iii)
(b)
(a)
Surface Soil Moisture
0.1
0.2
0.3
0.4
0.5
1.0
0.8
0.6
0.4
0.2
0.0
Evaporation (mm/hr)
(ii)
Surface Soil Moisture
0.1
0.2
0.3
0.4
0.5
0
2
4
6
8
10
Water Table Depth (m)
(iv-a)
Probability
0.0
0.2
0.4
0.6
1.0
0.8
0.6
0.4
0.2
0.0
Evaporation (mm/hr)
(i)
Probability
0.0
0.02
0.06
0.10
0
2
4
6
8
10
Water Table Depth (m)
(iv-b)
Probability
0.0
0.2
0.4
0.6
1.0
0.8
0.6
0.4
0.2
0.0
Evaporation (mm/hr)

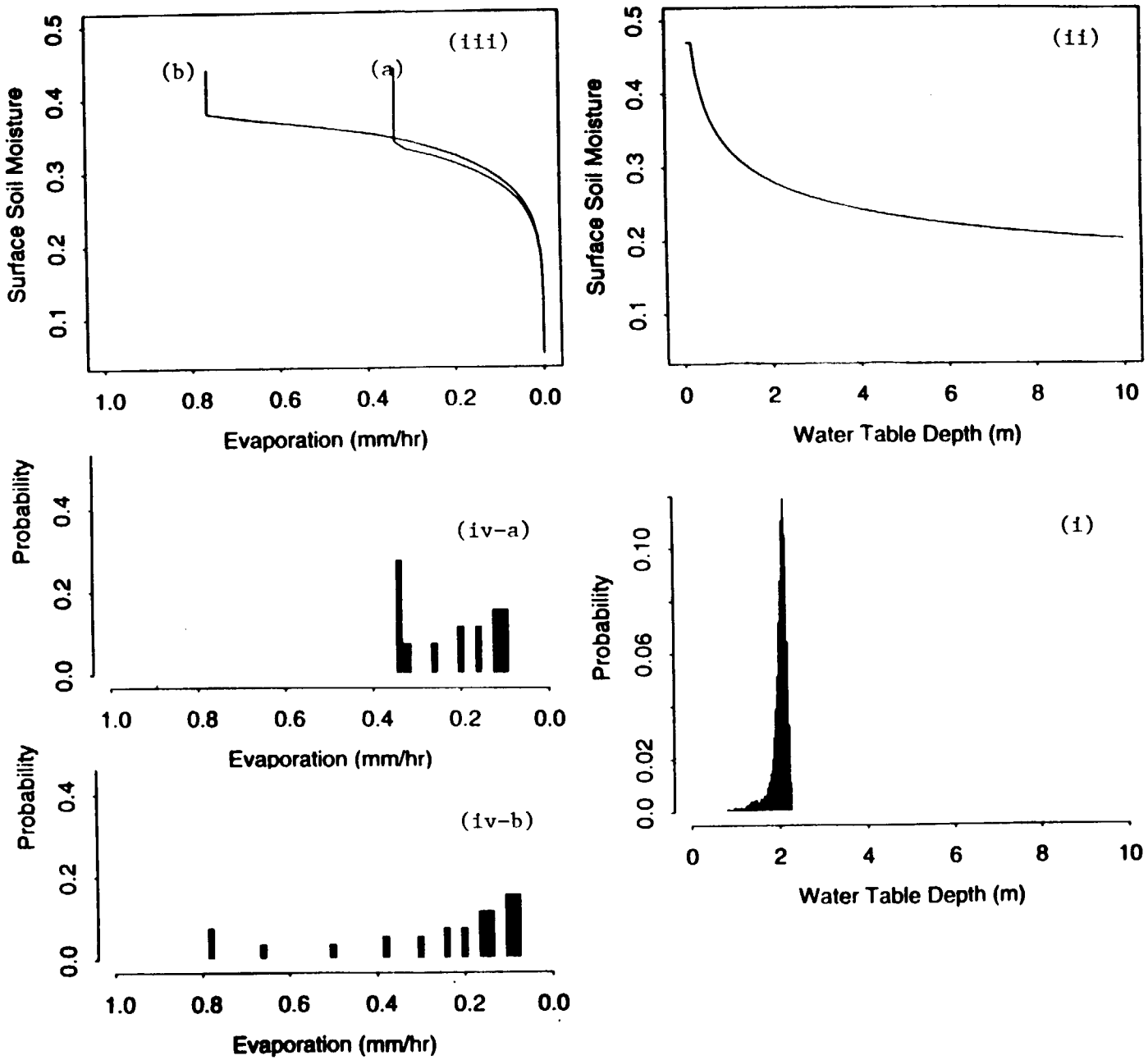
(iii)
(b)
(a)
Surface Soil Moisture
0.1
0.2
0.3
0.4
0.5
1.0
0.8
0.6
0.4
0.2
0.0
Evaporation (mm/hr)
(ii)
Surface Soil Moisture
0.1
0.2
0.3
0.4
0.5
0
2
4
6
8
10
Water Table Depth (m)
(iv-a)
Probability
0.0
0.2
0.4
1.0
0.8
0.6
0.4
0.2
0.0
Evaporation (mm/hr)
(i)
Probability
0.0
0.02
0.06
0.10
0
2
4
6
8
10
Water Table Depth (m)
(iv-b)
Probability
0.0
0.2
0.4
1.0
0.8
0.6
0.4
0.2
0.0
Evaporation (mm/hr)

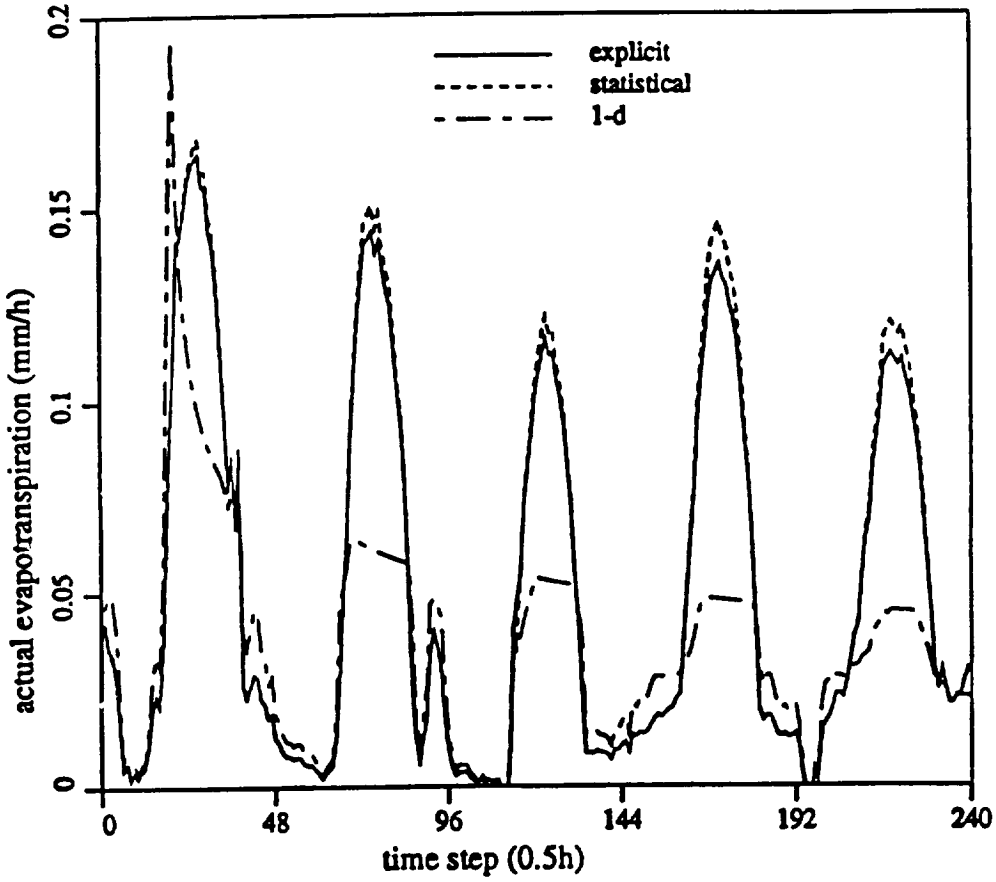
explicit
statistical
1-d
actual evapotranspiration (mm/h)
0
0.05
0.1
0.15
0.2
0
48
96
144
192
240
time step (0.5h)

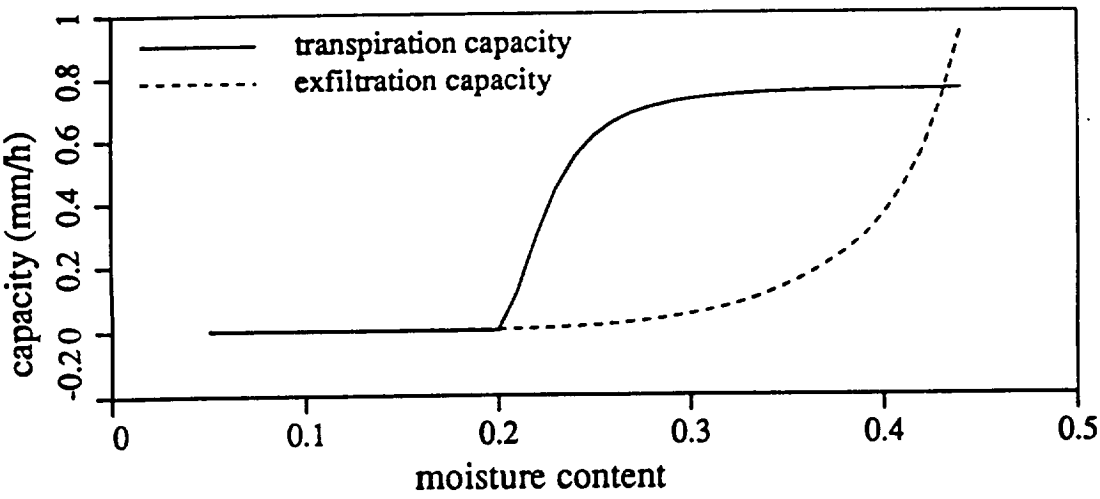
transpiration capacity
exfiltration capacity
capacity (mm/h)
-0.2
0
0.2
0.4
0.6
0.8
1
0
0.1
0.2
0.3
0.4
0.5
moisture content

F. 4

Bare Soil

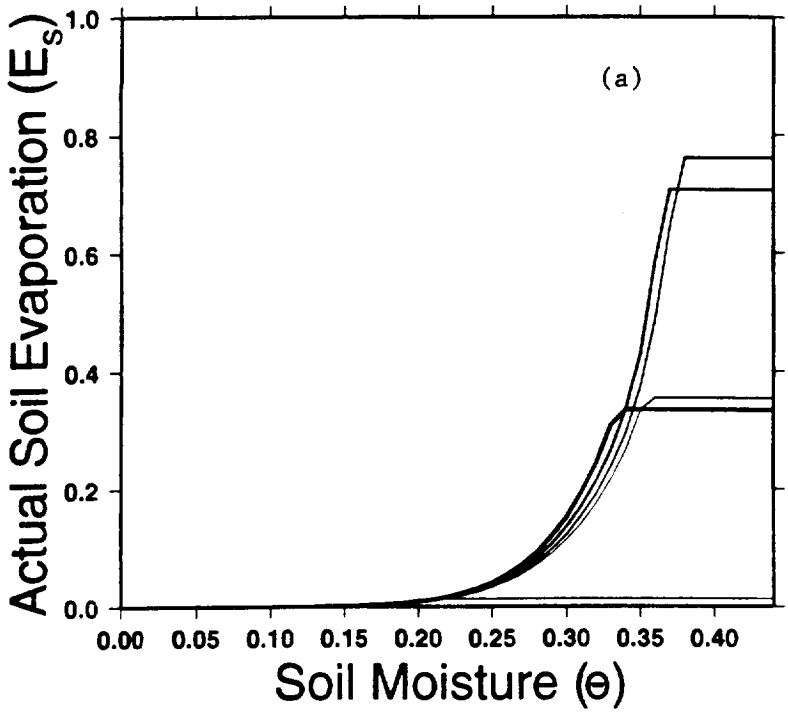

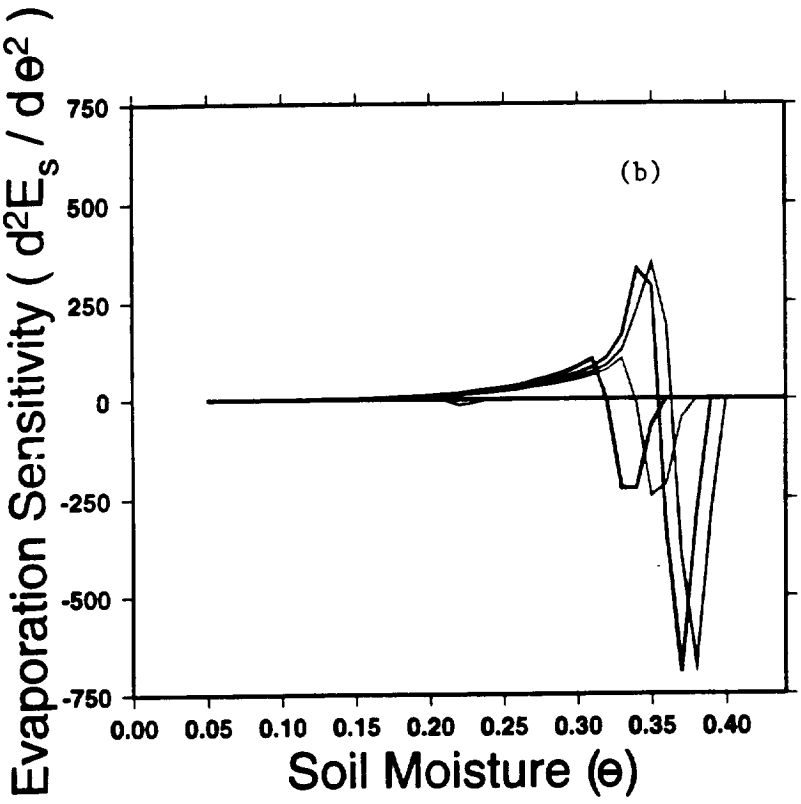

Fig 5

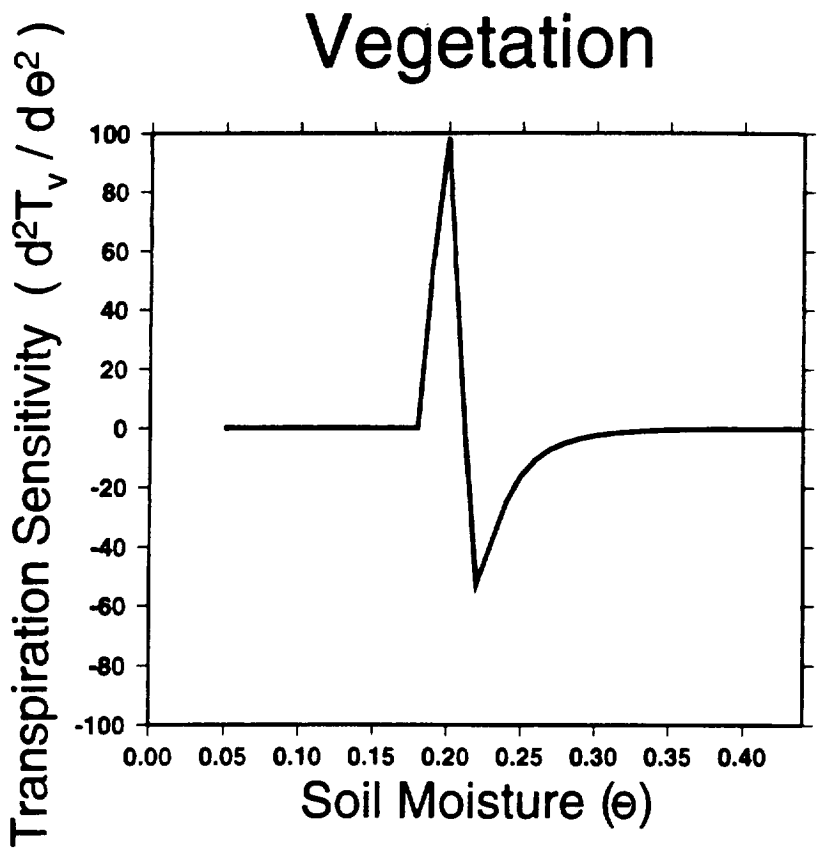
Vegetation
Transpiration Sensitivity ($d^2T_v / d\theta^2$)
100
80
60
40
20
0
-20
-40
-60
-80
-100
0.00
0.05
0.10
0.15
0.20
0.25
0.30
0.35
0.40
Soil Moisture (θ)

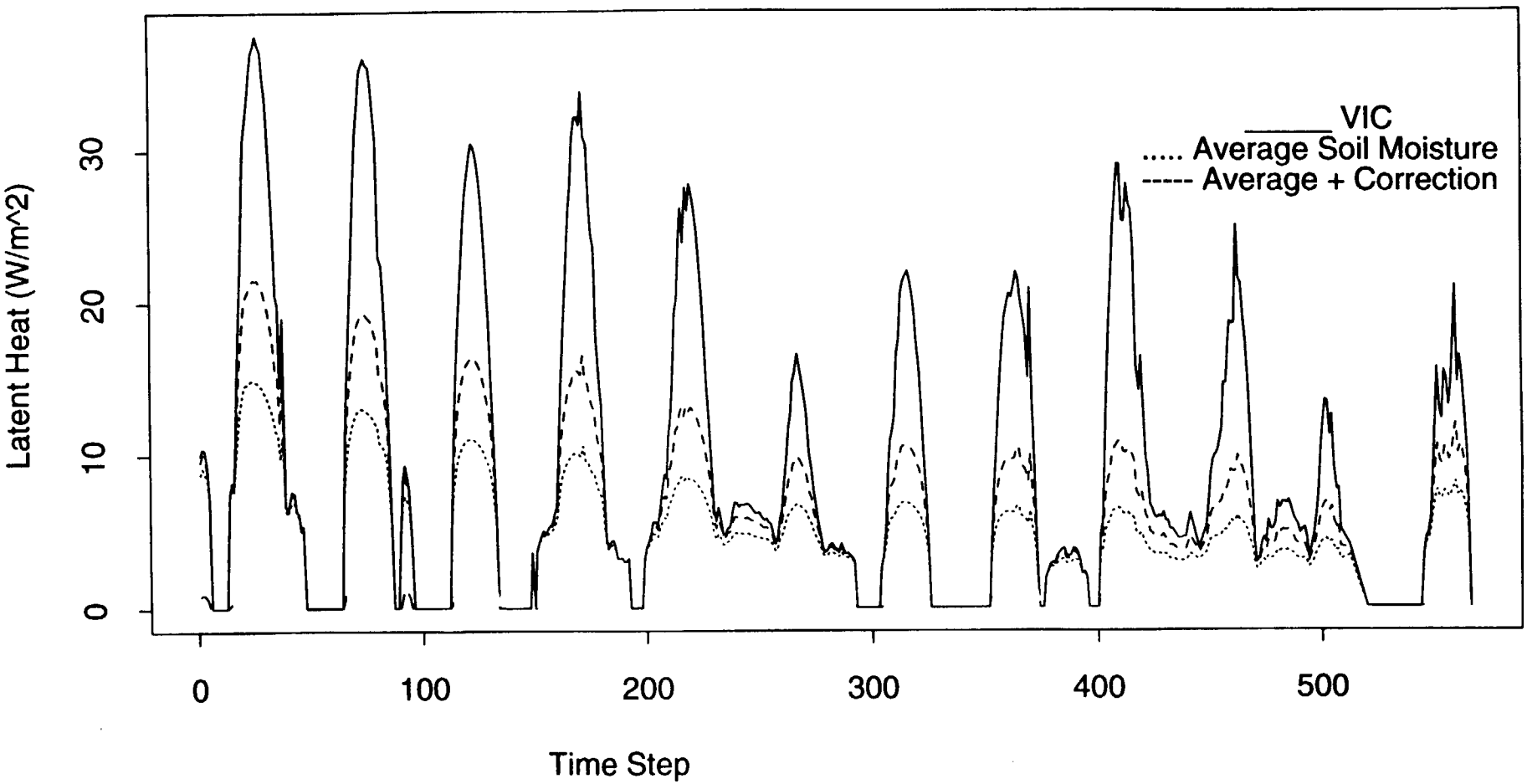
Latent Heat (W/m^2)
0
10
20
30
0
100
200
300
400
500
Time Step
VIC
Average Soil Moisture
Average + Correction

Fig 7

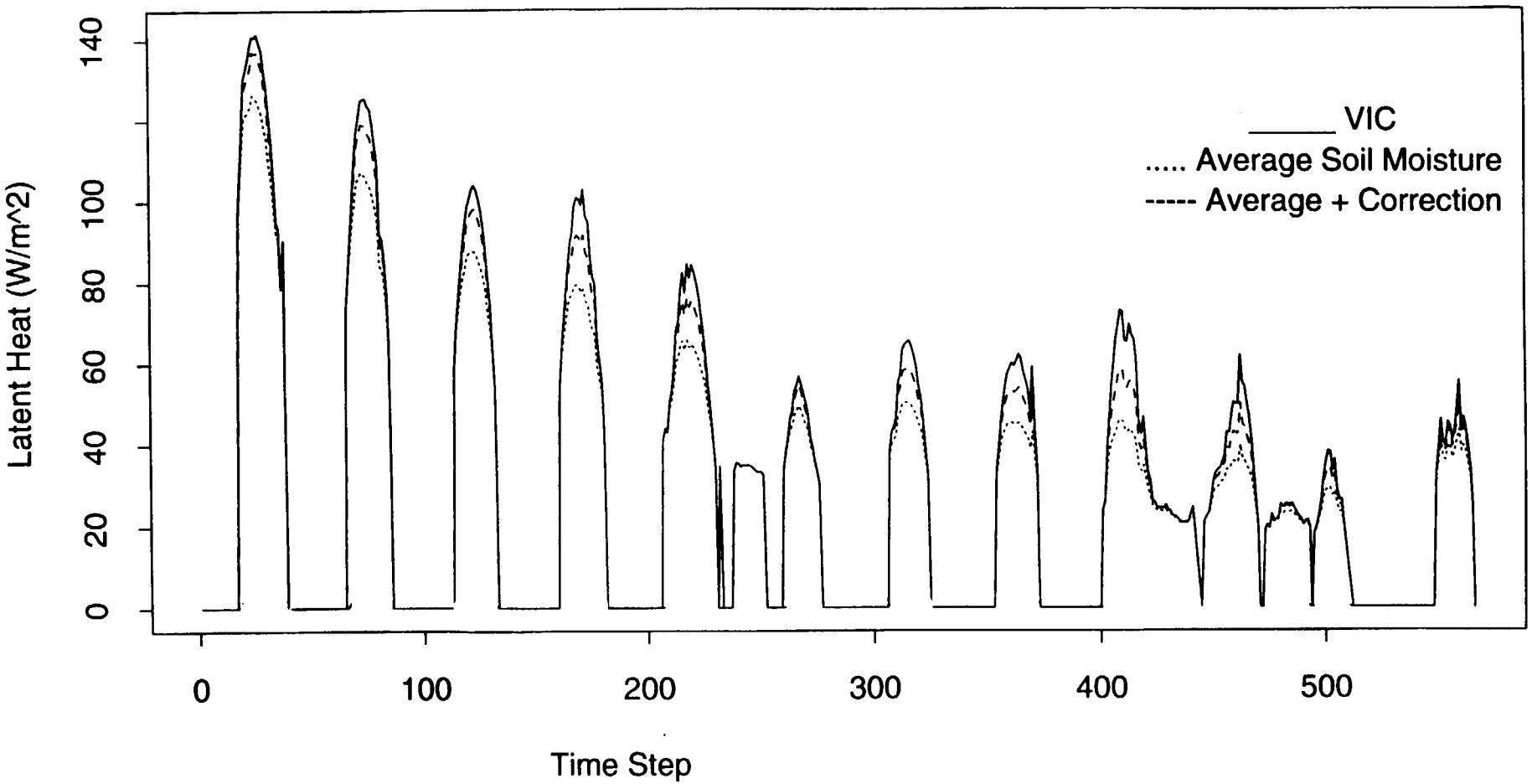
Latent Heat (W/m^2)
0
20
40
60
80
100
140
0
100
200
300
400
500
Time Step
_____ VIC
..... Average Soil Moisture
----- Average + Correction

Fig. 9

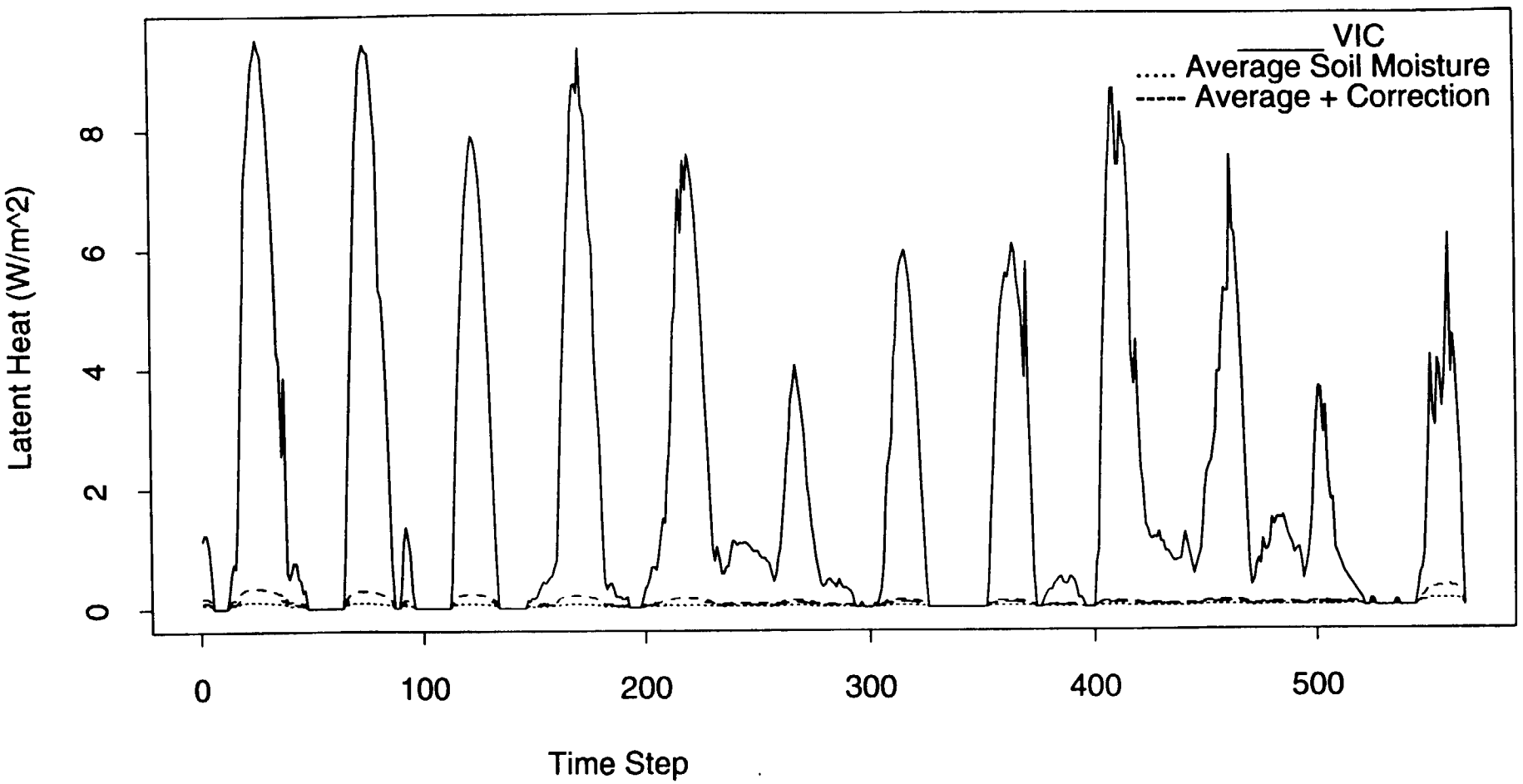
VIC
..... Average Soil Moisture
----- Average + Correction
Latent Heat (W/m^2)
0
2
4
6
8
0
100
200
300
400
500
Time Step

Fig 5

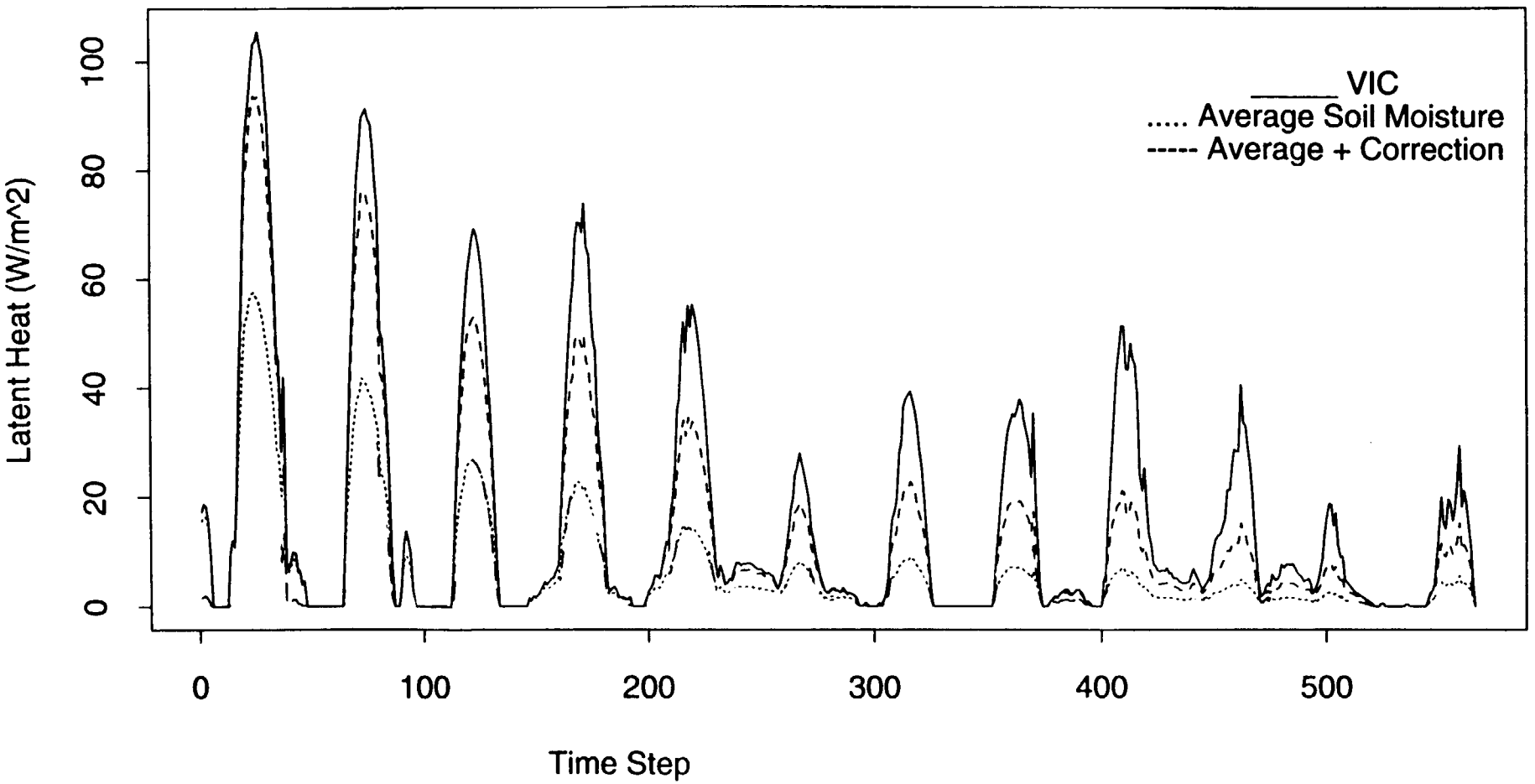
Latent Heat (W/m^2)
0
20
40
60
80
100
0
100
200
300
400
500
Time Step
VIC
..... Average Soil Moisture
----- Average + Correction

Fig 10